

# AMYLOID $\beta$ -DERIVED SWITCH-PEPTIDES AS TOOL TO STUDY CONFORMATIONAL CHANGES RELEVANT IN DEGENERATIVE DISEASES

THÈSE N° 3992 (2008)

PRÉSENTÉE LE 25 JANVIER 2008

À LA FACULTÉ DES SCIENCES DE BASE  
LABORATOIRE DE CHIMIE BIOMIMÉTIQUE ET DES PEPTIDES  
PROGRAMME DOCTORAL EN CHIMIE ET GÉNIE CHIMIQUE

ÉCOLE POLYTECHNIQUE FÉDÉRALE DE LAUSANNE

POUR L'OBTENTION DU GRADE DE DOCTEUR ÈS SCIENCES

PAR

Marie-Stéphanie CAMUS

M.Sc. in Chemistry and Chemical Engineering, Royal Institute of Technology, Stockholm, Suède  
et de nationalité française

acceptée sur proposition du jury:

Prof. G. Dietler, président du jury  
Prof. M. Mutter, directeur de thèse  
Prof. A. Beck-Sickinger, rapporteur  
Prof. P. Dumy, rapporteur  
Prof. K. Johnsson, rapporteur



ÉCOLE POLYTECHNIQUE  
FÉDÉRALE DE LAUSANNE

Suisse  
2008



*À mes parents*



## *Remerciements*

Je tiens à exprimer ma profonde reconnaissance à mon directeur de thèse, le professeur Manfred Mutter, pour m'avoir accueillie au sein de son groupe de recherche et permis de travailler sur le sujet passionnant de la maladie d'Alzheimer. Ses conseils, sa confiance et ses encouragements m'ont été d'une aide précieuse tout au long de ce travail.

Je remercie également la docteur Gabriele Tuchscherer pour son coaching et ses conseils toujours très judicieux.

J'aimerais également remercier les membres de mon jury, le prof. G. Dietler, président du jury, ainsi que les professeurs A. Beck-Seckinger, P. Dumy et K. Johnsson d'avoir accepté d'évaluer ce travail.

J'adresse aussi mes remerciements au Professeur Hilal Lashuel pour m'avoir accueillie dans son laboratoire lors de notre collaboration et pour m'avoir fait découvrir le monde passionnant des neurosciences. Je remercie aussi l'équipe des sciences de la vie, le LMNN, le LEN et le LNGF, plus particulièrement Véréne, Samareh, Valérie, David et Diego pour leur accueil chaleureux et les bons moments partagés ensemble.

Un grand merci à Adrian pour la microscopie électronique, la relecture de ce manuscrit ainsi que pour toute l'aide et le soutien qu'il a m'apportés durant cette thèse.

Je souhaite remercier tous les membres du groupe Mutter et plus particulièrement, Mandal, Robert, Karine, Sonia, Arunan, Arnaud, Lydiane, Enrico, Richard, John et Lyvinka pour leur amitié et leur soutien.

Je remercie aussi l'équipe du LCA pour les pauses déjeuner toujours très conviviales.

Un grand merci à toute l'équipe du magasin ainsi qu'aux équipes techniques (services de masse, atelier mécanique, service informatique) pour leur bonne humeur et leur disponibilité.

Merci à Christine et Anne Lene pour leur aide précieuse dans les tâches administratives et pour leur disponibilité.

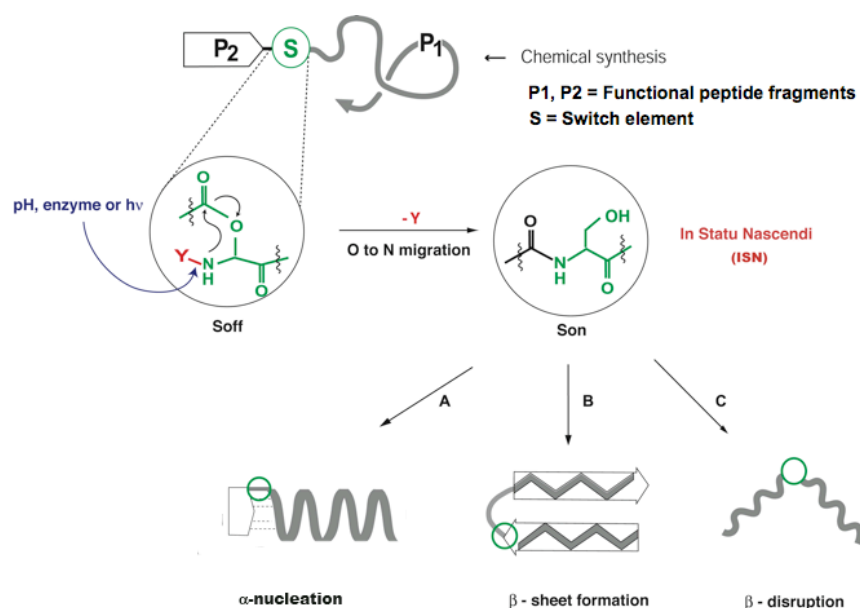
Merci à toutes les personnes qui me sont proches et à ma famille, surtout à mes parents, qui m'ont toujours encouragée dans mes projets et qui ont toujours cru en moi.

Enfin, "Merci viu mau" Manuel pour ton soutien et ta patience, merci d'être toujours là pour moi et d'illuminer ma vie.



## Abstract

The rapid growing number of patients diagnosed with a neurodegenerative disease and more particularly with Alzheimer's disease (AD) has stimulated intensive research in determining and understanding biological phenomena causing such devastating diseases and hence allowing for the elaboration of adapted therapeutic treatments. These diseases are also commonly called "conformational" diseases because they result from the misfolding of a protein leading to the formation of self-associated  $\beta$ -sheets, which in turn give rise to the formation of oligomers, protofibrils as well as insoluble fibrils characterizing the plaques found in the brain of affected patients. Consequently, the investigation of such proteins, in particular of Amyloid  $\beta$  ( $A\beta$ ) in the case of AD, is a limited and difficult task to achieve, which often leads to contradictory results. To overcome these difficulties and to be able to study the key steps of conformational transitions and misfolding of such peptides and proteins, our research group has developed a new tool, called switch-peptides, enabling to block ( $S_{\text{off}}$  state) and trigger ( $S_{\text{on}}$  state) peptide folding at will (Figure).



The introduction of a switch element S built from Ser, Thr or Cys residues disrupts the regular polypeptide chain by the insertion of an ester and a flexible C-C bond resulting in a conformational disconnection of P<sub>1</sub> and P<sub>2</sub> (Figure), i.e. in an unordered (random coil), non-folded conformation. Each S element is protected by a protecting group Y ( $S_{\text{off}}$  state) that can be cleaved independently by adding a base, an enzyme or by light, depending on the chemical nature of Y. The cleavage of the different protecting groups Y triggers a spontaneous O to N

acyl migration, re-establishing the regular amide backbone of the peptide chain, hence enabling the peptide to fold “*in statu nascendi*” and to adopt a well-defined secondary structure.

The present thesis explores the potential of this novel concept for the example of conformational transitions relevant in amyloid  $\beta$  misfolding.

In the first part we investigate the chemical stability of the **S** element in aqueous media, exposing a number of switch-peptides to various experimental conditions. Most notably, the ester bond proved to be stable at acidic as well as physiological conditions for several hours, opening a broad range of biological applications.

The second part of the work is dedicated to the study of conformational transitions of switch-peptides derived from  $A\beta(1-42)$ . By incorporating one or several switch elements disposing orthogonal protecting groups **Y**, the impact of different fragments of the peptide as nucleation site for the process of  $\beta$ -sheet formation, self-assembly and aggregation has been revealed as monitored by CD, TEM studies and ThT (pathway B, Figure). For the first time, the orthogonal triggering of the two switch elements, i.e.  $S^{26}$  and  $S^{37}$  allowed to delineate the important role of the C-terminal part of  $A\beta$  in the early step of misfolding.

Subsequently, one of the nucleation sites for aggregation, i.e. segment  $A\beta(14-24)$  was excised from the native sequence and transformed to a switch-peptide applying the host-guest technique. Detailed CD studies were applied for investigating conformational transitions of type random-coil ( $S_{\text{off}}$ ) to  $\beta$ -sheet structure ( $S_{\text{on}}$ ), serving as proof of concept for the use of  $A\beta$ -derived nucleation sites as guest sequence in combination with  $\beta$ -sheet promoting host peptides for the screening of potential inhibitors of fibril formation as early molecular event in the context of AD.

This has been demonstrated in applying the elaborated host-guest peptides to evaluate the  $\beta$ -sheet breaking potential of pseudo-proline ( $\psi$ Pro)-containing switch-peptides derived from  $A\beta$  (pathway C, Figure). Preliminary results indicate that the in situ formation of kink-conformations may exert a  $\beta$ -sheet destabilizing effect, confirming previous observations from the Soto group.

Finally, the use of switch-peptides as  $\beta$ -sheet and fibril breaking molecules by in situ  $\alpha$ -helix nucleation (pathway A, Figure) has been explored. To this end, the potentially  $\beta$ -sheet forming segment  $A\beta(14-24)$  was linked via **S** element to a helix nucleating peptidomimetic (“N-Cap”). In the  $S_{\text{off}}$  state ( $\text{pH} \leq 4$ ), CD and TEM studies point to the onset of a  $\beta$ -sheet, fibril forming structure. In triggering O,N-acyl migration ( $\text{pH} \approx 7$ ), a so far unprecedented transition of type  $\beta$ -



sheet to  $\alpha$ -helix is observed, paralleled by a drastic increase in solubility and a complete disappearance of fibrils.

The reversibility of  $\beta$ -sheet and fibril formation by  $\alpha$ -helix nucleation in situ represents a most interesting observation and deserves further exploration as potential tool in the study of folding processes.

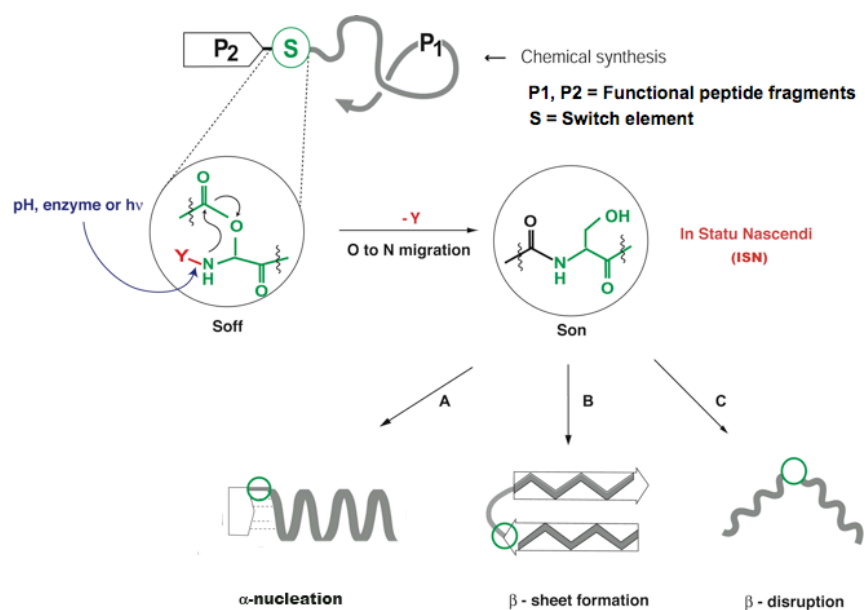
In conclusion, the concept of “switch-peptides” has been successfully applied to biologically relevant molecular events of utmost therapeutical interest.

**Keywords:** Amyloid  $\beta$ -derived switch-peptides; multiple O,N-acyl migration; conformational transitions; fibril disruption; neurodegenerative diseases; reversal of  $\beta$ -sheet formation.



## Résumé

Le nombre croissant de patients atteints de maladies neurodégénératives et plus particulièrement de la maladie d'Alzheimer a stimulé la recherche ayant pour but de déterminer et comprendre les phénomènes biologiques causant ces maladies dévastatrices afin de permettre l'élaboration de traitements thérapeutiques adaptés. Ces maladies sont aussi communément appelées maladies "conformationnelles" car elles résultent principalement du mauvais repliement d'une protéine conduisant à la formation de feuillets  $\beta$  s'associant entre eux pour donner naissance à des oligomères, des protofibrilles ainsi que des fibrilles insolubles qui caractérisent les plaques retrouvées dans le cerveau des patients atteints. Par conséquent, l'étude de ces protéines, plus particulièrement de l'Amyloide  $\beta$ , est limitée et difficile, donnant souvent lieu à des résultats contradictoires. Afin de contourner ces difficultés pour pouvoir plus facilement étudier les étapes clés du changement de conformation et du repliement incorrect de l'A $\beta$ , notre groupe de recherche a développé un nouvel outil, appelé les « switch-peptides », permettant de bloquer (état  $S_{off}$ ) puis de déclencher (état  $S_{on}$ ) le repliement du peptide à souhait (Figure).



L'introduction d'un élément switch **S** construit à partir des résidues Ser, Thr ou Cys interrompt la chaîne polypeptidique par l'insertion d'une liaison ester et d'une liaison C-C flexible résultant dans une déconnection conformationnelle de P<sub>1</sub> et P<sub>2</sub> (Figure), c-à-d dans une conformation désordonnée de type pelote statistique. Les éléments **S** sont protégés par des groupes protecteurs **Y** (état  $S_{off}$ ) pouvant être clivés de manière indépendante par l'ajout d'une base, d'une enzyme ou par la lumière, dépendant de la nature chimique de **Y**. Le clivage de **Y** déclenche une

migration acylique spontanée qui rétablit la liaison amide et la chaîne peptidique, ce qui permet au peptide de se replier « *in statu nascendi* » et d'adopter une structure secondaire définie.

Le travail décrit dans cette thèse explore le potentiel de ce nouveau concept pour l'exemple des transitions conformationnelles de grande importance dans le repliement incorrect de l'amyloïde  $\beta$  (A $\beta$ ).

Dans un premier temps, nous avons étudié la stabilité de l'élément S en milieu aqueux, exposant plusieurs « switch-peptides » à différentes conditions expérimentales. Nous avons notamment démontré que dans des conditions acides et physiologiques, la liaison ester reste stable pour plusieurs heures, donnant accès à un large éventail d'applications biologiques.

Nous nous sommes ensuite consacrés à l'étude des changements conformationnels de « switch-peptides » dérivés de l'amyloïde  $\beta$  1-42. Par l'incorporation d'un ou plusieurs éléments switch disposants de groupes protecteurs orthogonaux Y, l'impact de différents fragments du peptide comme site de nucléation dans le processus de formation des feuillets  $\beta$ , de l'auto-assemblage et l'aggrégation (voie B, Figure) a été révélé grâce à l'utilisation de plusieurs techniques complémentaires telles que CD, TEM et ThT. Pour la première fois, le déclenchement orthogonal de deux éléments switch, c-à-d S<sup>26</sup> et S<sup>37</sup> a permis de déterminer le rôle majeur de la partie C-terminale de l'A $\beta$  dans les premières étapes du repliement incorrect du peptide.

Ensuite, un des sites de nucléation de l'aggrégation, le segment A $\beta$ (14-24) fut excisé de la séquence native et transformé en un « switch-peptide » appliquant la technique host-guest. Des études détaillées par CD furent utilisées afin d'examiner les transitions conformationnelles de type pelote statistique (S<sub>off</sub>) à feuillet  $\beta$  (S<sub>on</sub>), servant de preuve du concept dans l'utilisation de sites de nucléation dérivés de l'A $\beta$  comme séquence guest en combinaison avec des peptides host promoteurs de feuillets  $\beta$  pour le screening d'inhibiteurs potentiels de la formation des fibrilles, événement moléculaire majeur survenant tôt dans le contexte de la maladie d'Alzheimer.

Ceci fut démontré en appliquant les peptides host-guest élaborés à l'évaluation de « switch-peptides » dérivés de l'amyloïde  $\beta$  comprenant une pseudo-proline ( $\psi$ Pro) comme potentiels briseurs de feuillets  $\beta$  (voie C, Figure). Les résultats préliminaires indiquent que la formation in situ de conformations en coude peut exercer un effet déstabilisant sur les feuillets  $\beta$ , confirmant ainsi de précédentes observations faites par C. Soto et al.

Enfin, l'utilisation de « switch-peptides » comme molécules capables de briser feuillets  $\beta$  et fibrilles par la nucléation in situ d'une hélice  $\alpha$  (voie A, Figure) a été explorée. A cette fin, le

segment A $\beta$ (14-24) formant des feuillets  $\beta$  a été lié via un élément **S** à un peptidomimétique nucléateur d'hélices (« N-Cap »). À l'état  $S_{\text{off}}$  (pH  $\leq$  4), les études CD et TEM pointent vers le commencement d'une structure de type feuillet  $\beta$  formant des fibrilles. Par le déclenchement de la migration acylique (pH  $\approx$  7), une transition de type feuillet  $\beta$  à hélice  $\alpha$  jamais observée jusqu'à présent a pu être démontrée. Parallèlement, une augmentation extrême de la solubilité et la disparition complète des fibrilles furent observées.

La réversibilité de la formation des feuillets  $\beta$  et des fibrilles par nucléation in situ d'hélice  $\alpha$  représente une observation extrêmement importante et mérite une exploration plus approfondie comme outil potentiel dans l'étude des processus du repliement des protéines.

En conclusion, le concept des « switch-peptides » fut appliqué avec succès dans l'étude des événements biologiques moléculaires d'intérêt thérapeutique majeur.

**Mots clés:** “switch-peptides” dérivés de l'amyloïde  $\beta$  ; multiple O,N-acyl migration ; transitions conformationnelles ; déstabilisation de fibrilles ; maladies neurodégénératives ; réversibilité de la formation de feuillets  $\beta$ .



Acknowledgements

Abstract

Abbreviations

---

**CHAPTER I. INTRODUCTION** **1**

---

<b>1. GENERAL NOTIONS ON PEPTIDE AND PROTEIN STRUCTURE AND FUNCTION</b>	<b>1</b>
1.1. THE PEPTIDE BOND	2
1.2. TORSION ANGLES AND RAMACHANDRAN PLOT	3
1.3. PEPTIDE AND PROTEIN STRUCTURES	4
1.4. THE RANDOM COIL	5
1.5. THE $\beta$ -SHEET	5
1.6. THE $\alpha$ -HELIX	6
1.7. INITIATING $\alpha$ -HELICES USING NCAP TEMPLATES	7
<b>2. PROTEIN FOLDING AND MISFOLDING</b>	<b>9</b>
<b>3. ALZHEIMER'S DISEASE</b>	<b>11</b>
3.1. NEUROFIBRILLARY TANGLES IN AD	12
3.2. FROM AMYLOID PRECURSOR PROTEIN TO AMYLOID $\beta$	13
3.3. UNDERSTANDING AMYLOID $\beta$ MISFOLDING AND ITS TOXICITY	14
3.4. THERAPEUTIC STRATEGIES: STATE-OF-THE-ART	18
<b>4. THE CONCEPT OF SWITCH-PEPTIDES</b>	<b>22</b>
4.1. THE SWITCH ELEMENT S	23
4.2. O, N-ACYL MIGRATION	25
<b>5. AIM OF THIS WORK</b>	<b>28</b>

---

**CHAPTER II. RESULTS AND DISCUSSION** **31**

---

<b>1. OVERVIEW</b>	<b>31</b>
<b>2. STUDY OF THE STABILITY OF THE SWITCH ELEMENT S IN THE <math>S_{OFF}</math> STATE</b>	<b>33</b>
2.1. STABILITY TOWARDS HYDROLYSIS AT PH 4.6	34
2.2. STABILITY TOWARDS HYDROLYSIS AT PH 7.4	35
2.3. STABILITY TOWARDS HYDROLYSIS AT PH 8	37
2.4. CONCLUSION	39
<b>3. STUDYING THE FOLDING MECHANISM OF THE FULL LENGTH AMYLOID <math>\beta</math> PEPTIDE USING SWITCH-PEPTIDES</b>	<b>41</b>
3.1. BACKGROUND AND DESIGN	41
3.2. SYNTHESIS AND ANALYTICAL DATA	44
3.3. STABILITY STUDIES	45
3.4. FOLDING AND AGGREGATION STUDIES	48
3.5. THT KINETIC COMPARISON	55
3.6. DISCUSSION	57
<b>4. HOST-GUEST SWITCH-PEPTIDES DERIVED FROM A<math>\beta</math> AS A MODEL FOR STUDYING FIBRILLOGENESIS AND FOR SCREENING AMYLOID <math>\beta</math> INHIBITORS IN VITRO.</b>	<b>59</b>
4.1. BACKGROUND	59
4.2. DESIGN OF HOST-GUEST SWITCH-PEPTIDES	60
4.3. DISCUSSION	80
<b>5. DESIGN AND SYNTHESIS OF SWITCH-PEPTIDES OF AMYLOID <math>\beta</math> FIBRIL DISRUPTING POTENTIAL</b>	<b>81</b>
5.1. BACKGROUND	81
5.2. DESIGN AND SYNTHESIS	83
5.3. KINETIC STUDIES	87
5.4. STUDY OF THE INHIBITION POTENTIAL OF AMYLOID-DERIVED SWITCH-PEPTIDES	93

5.5. DISCUSSION	98
<b>6. DISRUPTION OF AMYLOID-DERIVED PEPTIDE ASSEMBLIES THROUGH THE CONTROLLED INDUCTION OF A <math>\beta</math>-SHEET TO <math>\alpha</math>-HELIX TRANSFORMATION: APPLICATION OF THE SWITCH-CONCEPT</b>	<b>99</b>
6.1. DESIGN	101
6.2. SYNTHESIS	102
6.3. N-CAP INDUCED $\beta$ TO $\alpha$ REVERSAL OF A $\beta$ (14-25)	103
6.4. CONCLUSION AND PERSPECTIVE	109
<b>CHAPTER III. EXPERIMENTAL PART</b>	<b>111</b>
<b>1. INSTRUMENTATION AND GENERAL METHODS</b>	<b>111</b>
<b>2. SOLID-PHASE PEPTIDE SYNTHESIS</b>	<b>114</b>
<b>3. SYNTHESIS</b>	<b>116</b>
3.1. BUILDING BLOCK SYNTHESIS	116
3.2. SYNTHESIS OF SWITCH-PEPTIDES OF AMYLOID B FIBRIL DISRUPTING POTENTIAL	120
3.3. SWITCH-PEPTIDE 7	126
3.4. HOST-GUEST SWITCH-PEPTIDE 8	129
3.5. HOST-GUEST SWITCH-PEPTIDE 9	131
3.6. SYNTHESIS OF AMYLOID- $\beta$ (1-42) DERIVED SWITCH-PEPTIDE 22	133
3.7. SYNTHESIS OF AMYLOID- $\beta$ (1-42) DERIVED SWITCH-PEPTIDE 23	136
PRODUCT INDEX	139
BIBLIOGRAPHY	145
CURRICULUM VITAE	158



## Abbreviations

---

A $\beta$	Amyloid $\beta$
Abs	Absorbance
Ac	Acetyl
AcN	Acetonitrile
AcOEt	Ethyl acetate
AD	Alzheimer's disease
APP	Amyloid precursor protein
Boc	<i>tert</i> -Butyloxycarbonyl
Boc <sub>2</sub> O	Di- <i>tert</i> -butyl dicarbonate
Bzl	Benzoyl
CD	Circular dichroism
CDCl <sub>3</sub>	Deuteriochloroform
DCC	<i>N,N'</i> -Dicyclohexylcarbodiimide
DIC	<i>N,N'</i> -Diisopropylcarbodiimide
DCM	dichloromethane
DEA	diethylamine
DIPEA	<i>N,N</i> -Ethyl-diisopropylamine
DPPIV	Dipeptidyl aminopeptidase IV
DMAP	Dimethylaminopyridine
DMF	Dimethylformamide
DMSO	Dimethylsulfoxide
D <sub>2</sub> O	Deuterium oxide
EDT	Ethanedithiol
EDCI	1-(3-Dimethylaminopropyl)-3-ethylcarbodiimide
EM	Electron microscopy
ESI-MS	Electrospray Ionisation Mass Spectroscopy
Et <sub>2</sub> O	Diethylether
EtOH	Ethanol
Fmoc	9-Fluorenylmethyloxycarbonyl
HATU	O-(7-Azabenzotriazol-1-yl)- <i>N,N,N',N'</i> -tetramethyluronium hexafluorophosphate
HCl	Hydrochloric acid

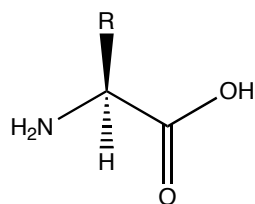
## Abbreviations

---

HOBt	1-Hydroxybenzotriazole
HPLC	High Pressure Liquid Chromatography
MALDI-TOF	Matrix assisted laser desorption ionization time of flight
MeOH	Methanol
MSNT	1-(2-Mesitylenesulfonyl)-3-nitro-1 <i>H</i> -1,2,4-triazole
MeIm	N-Methylimidazole
NMDA	N-methyl-D-aspartic acid
NMR	Nuclear Magnetic Resonance
NVoc	6-nitroveratroyloxycarbonyl
PBS	Phosphate buffer solution
Pd/C	Palladium on charcoal
PyBOP	(Benzotriazol-1-yloxy)-tripyrrolidinophosphonium hexafluorophosphate
R <sub>t</sub>	Retention time
SPPS	Solid phase peptide synthesis
<sup>t</sup> Bu	<i>Tert</i> -butyl
TFA	Trifluoroacetic acid
TFE	Trifluoroethanol
THF	Tetrahydrofuran
ThT	Tioflavin T
Tris	Tris(hydroxymethyl)aminomethane
TIS	Triisopropylsilane
Trt	Trityl

Amino Acids

General structure of L-amino acids:



Name	Side Chain R
Alanine (Ala, A)	CH <sub>3</sub> -
Arginine (Arg, R)	H <sub>2</sub> N-C(NH)-NH-CH <sub>2</sub> CH <sub>2</sub> CH <sub>2</sub> -
Asparagine (Asn, N)	H <sub>2</sub> NCO-CH <sub>2</sub> -
Aspartic acid (Asp, D)	HO <sub>2</sub> C-CH <sub>2</sub> -
Cysteine (Cys, C)	HS-CH <sub>2</sub> -
Glutamic acid (Glu, E)	HO <sub>2</sub> C-CH <sub>2</sub> CH <sub>2</sub> -
Glutamine (Gln, Q)	H <sub>2</sub> NCO-CH <sub>2</sub> CH <sub>2</sub> -
Glycine (Gly, G)	H-
Histidine (His, H)	
Isoleucine (Ile, I)	CH <sub>3</sub> CH <sub>2</sub> (CH <sub>3</sub> )CH-
Leucine (Leu, L)	(CH <sub>3</sub> ) <sub>2</sub> CH-CH <sub>2</sub> -
Lysine (Lys, K)	H <sub>2</sub> NCH <sub>2</sub> CH <sub>2</sub> CH <sub>2</sub> CH <sub>2</sub> -
Methionine (Met, M)	H <sub>3</sub> C-S-CH <sub>2</sub> CH <sub>2</sub> -
Phenylalanine (Phe, F)	
Proline (Pro, P)	
Serine (Ser, S)	HO-CH <sub>2</sub> -
Threonine (Thr, T)	CH <sub>3</sub> CH(OH)-
Tryptophane (Trp, W)	
Tyrosine (Tyr, Y)	
Valine (Val, V)	(CH <sub>3</sub> ) <sub>2</sub> CH-



## Chapter I. Introduction

### 1. General notions on peptide and protein structure and function

Peptides and proteins are fundamental molecules characterizing living organisms. Their structure and function are both very essential in every process within living cells. Conventionally, proteins are polypeptide chains comprising more than 50 amino acids. Their size is extremely variable and goes from several hundred to several thousand kilo Daltons depending on the protein. They possess a wide range of functions, for example they function as catalysts, transport and store other molecules such as oxygen, provide mechanical support and immune protection, generate movement, transmit nerve impulses, and or control growth and differentiation. Peptides have also very relevant physiological functions, acting in particular as hormones, neurotransmitters, cytokines and growth factors.

Proteins are the most abundant macromolecules in living cells, representing more than half of their dry weight. For that reason, in 1838, the chemist Gerardus Mulder proposed to call them proteins from the greek *proteios*, meaning “of primary importance”. At that time, the extraordinary properties of those macromolecules were totally unknown since their structure and composition remained a mystery.

A century later, L. Pauling and R. Corey<sup>1</sup> deduced by x-ray crystallography the two main structural features of proteins: the  $\alpha$ -helix and  $\beta$ -sheet, now known to form the backbones of tens of thousands of proteins.

Proteins and peptides are linear polymers built of monomer units, the amino acids, forming covalent bonds called peptide bonds (Figure 1).

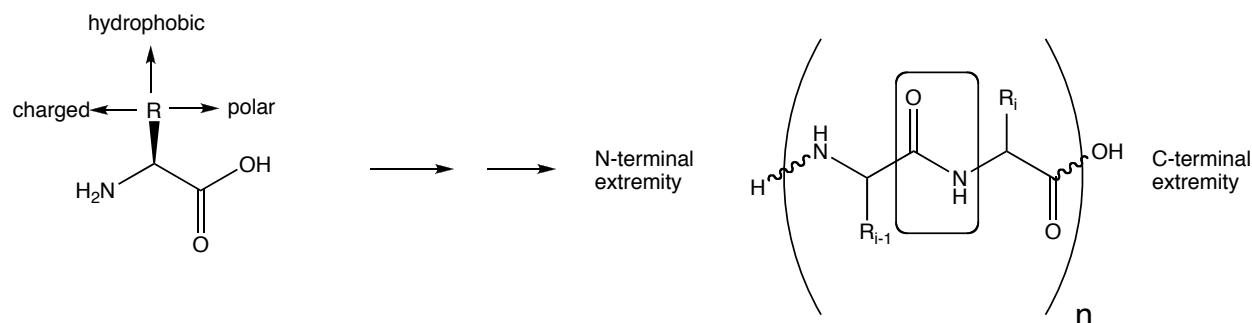


**Figure 1.** General structure of an L-amino acid (left). General formula of a protein formed by  $n$  peptide bonds (right).

Remarkably, proteins and long peptides spontaneously fold up into three-dimensional structures that are determined by the sequence of amino acids in the polymer.

Proteins and peptides are built from a repertoire of 20 amino acids. Each amino acid is an  $\alpha$ -amino acid, containing both amine and carboxyl functional groups, where the amine function is in  $\alpha$  position of the acid function.

Each amino acid varies from one another by its side chain (R), which gives to amino acids distinctive chemical specificities that can be classified in three different groups owing to their chemical reactivity:

(a) polar

Uncharged polar amino acids are: Serine, Threonine, Cysteine, Tyrosine, Asparagine and Glutamine residues.

(b) charged

Charged amino acids are: Aspartic acid, Glutamic Acid, Lysine, Arginine, and Histidine.

(c) hydrophobic

Hydrophobic uncharged and non-polar amino acids are: Glycine, Alanine, Valine, Leucine, Isoleucine, Proline, Phenylalanine, Tryptophane and Methionine.

Among those amino acids, proline is a particular residue because its ring structure makes it more conformationally restricted than the other amino acids.

In naturally occurring amino acids, the stereochemical configuration of the chiral center is exclusively L. The D forms of amino acids are extremely rare.

### 1.1. The peptide bond

A peptide bond (or amide bond) is formed when two amino acids react together via a condensation reaction with the loss of a water molecule. In this bond, the non-linking electron pair of nitrogen is conjugated with the double bond of the carbonyl oxygen group to give rise to two mesomeric forms (Figure 2). The planarity of the peptide bond reduces the geometry around the bond to only two conformers: *trans* and *cis*. In the *trans* configuration, the two  $\alpha$ -carbon atoms are on the opposite sides of the peptide bond. In the *cis* configuration, these groups are on the same side of the peptide bond. Almost all peptide bonds in proteins are *trans* because the steric hindrance of amino acid side chains clearly penalizes the *cis* conformation in comparison

to the *trans* conformation. Only amide bonds followed by a proline residue present 10% of *cis* conformation.

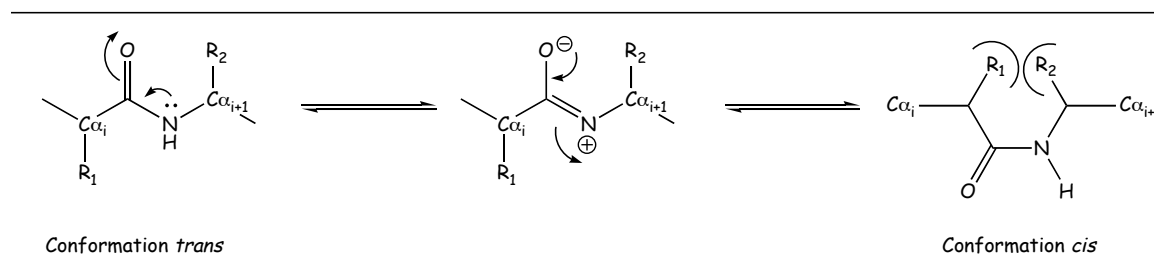


**Figure 2.** *Cis-trans isomerization of the peptide bond.*

## 1.2. Torsion angles and Ramachandran plot

Contrary to amide bonds, which can only adopt *cis* or *trans* conformations, the phi ( $\phi$ ) (between N-C $\alpha$ ) and psi ( $\Psi$ ) (between C-C $\alpha$ ) torsion angles are relatively flexible (Figure 3). Nevertheless, because of steric interferences between atoms only some of the possible combinations of  $\phi$  and  $\Psi$  angles are allowed.

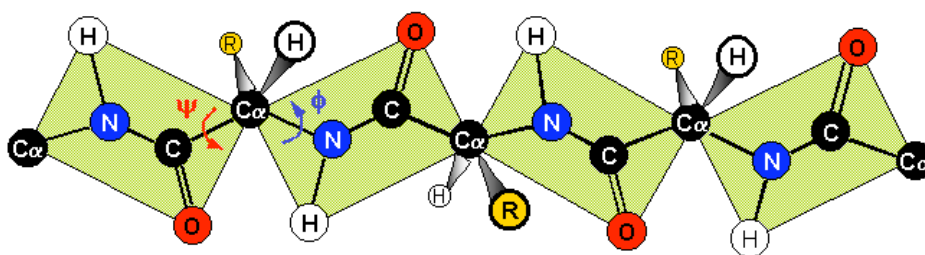


**Figure 3.** *Spatial representation of a polypeptide chain to demonstrate the torsion freedom of a peptide unit. Only the N-C $\alpha$  and C $\alpha$ -C bonds can rotate, with bond angles designated  $\phi$  and  $\Psi$ .*

This was analyzed by Ramachandran and Sasisekharan<sup>2</sup>, who used solid sphere models of amino acids to determine the range of allowed values for  $\phi$  and  $\Psi$  and reported the results in the so-called Ramachandran plot as depicted in the figure below.

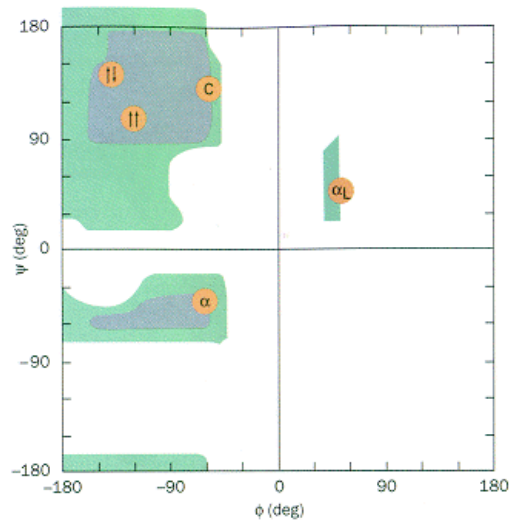


**Figure 4.** Ramachandran plot. The gray and green regions indicate the allowed combinations of  $\phi$  and  $\Psi$  angles for all residues except Gly and Pro.  $\beta$ -sheet conformation is found for  $90 < \Psi < +180$  and  $-180 < \phi < -60$ , right handed helix is found for  $-60 < \Psi < +30$  and  $-120 < \phi < -30$ , left handed helix is found for  $0 < \Psi < +60$  and  $-45 < \phi < +90$ .

### 1.3. Peptide and protein structures

➤ The primary structure of a peptide or a protein corresponds to the linear arrangement of the amino acid residues in the polypeptide chain. The position of each amino acid in the sequence will determine how the chain will fold and adopt its secondary structure.

➤ The secondary structure is the local conformation of a polypeptide chain and corresponds to the first level of organization of the polypeptide chain in the space. It results from the tendency of each amino acid residue to adopt defined combinations of dihedral angles  $\phi$  and  $\Psi$  and also from the establishment of hydrogen-bonding patterns between the carbonyls and amide protons along the chain. The two most frequent secondary structures are the  $\alpha$ -helices and the  $\beta$ -sheets.

➤ The tertiary structure refers to the spatial arrangement of the secondary structure units; it is the complete three-dimensional structure of a polypeptide chain.

Proteins, which are built of several polypeptide chains, exhibit a fourth structural level, called the quaternary structure.



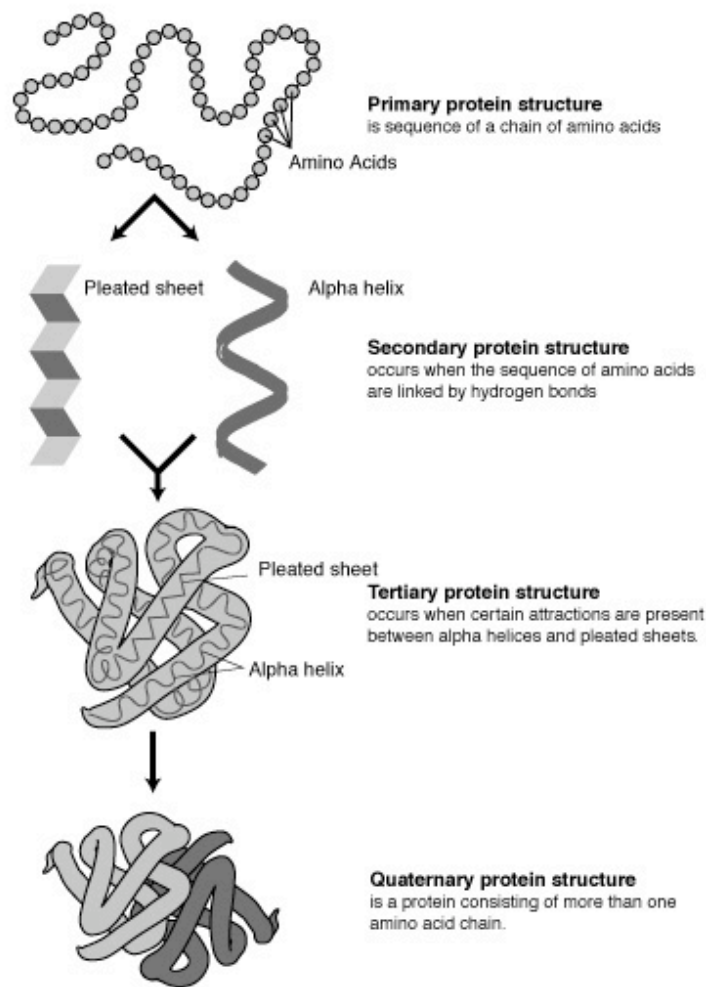


**Figure 5.** *The four levels of protein structure.*

#### 1.4. The random coil

Proteins fold into a well-defined structure after their synthesis on a ribosome. However, small peptides and some polypeptide segments of proteins do not adopt a specific conformation due to a lack of amino acid side-chain interactions and because free rotation can take place around every bond of the backbone. This absence of specific interactions and the rotation freedom generates randomly oriented subunits, resulting in an unfolded state, called random coil.

#### 1.5. The $\beta$ -sheet

One of the major components found in proteins is the  $\beta$ -sheet. The basic unit is the  $\beta$ -strand, with the polypeptide almost fully extended. The dihedral angles' region corresponding to  $\beta$ -strands in the Ramachandran plot is between  $\phi, \Psi = -120^\circ, +130^\circ$ . This extended conformation is

stable only when incorporated into a  $\beta$ -sheet, where hydrogen bonds with close to optimal geometry are formed between the peptide groups on adjacent  $\beta$ -strands. Adjacent strands can be either parallel or antiparallel, and the stereochemistry of the strands in the two cases are slightly different, such as the hydrogen bonding pattern between the two strands (Figure 6).

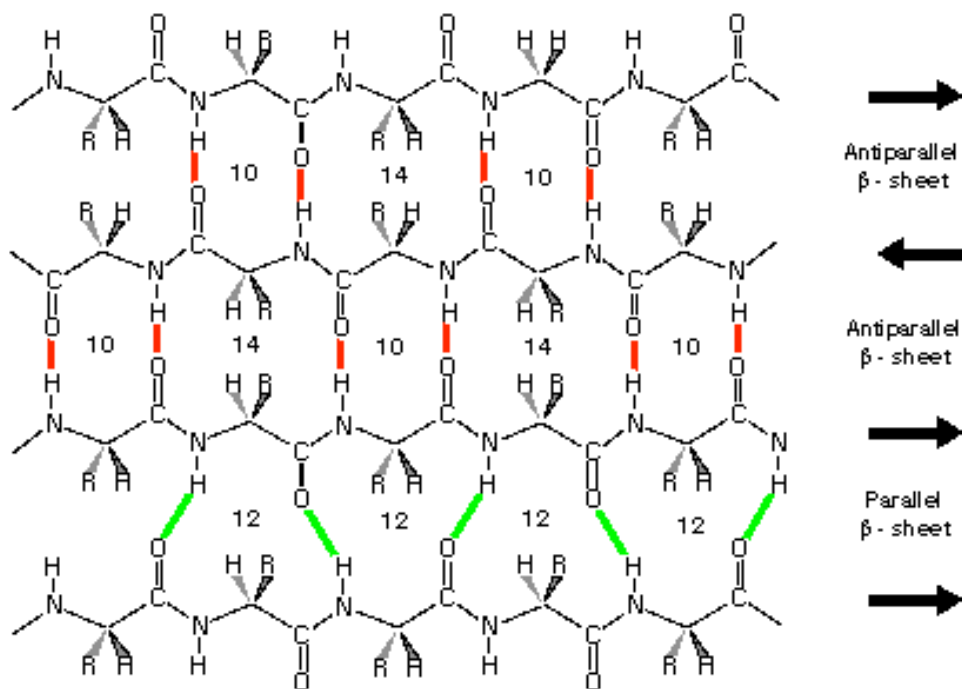


**Figure 6.** Antiparallel and parallel  $\beta$ -sheet bonding patterns.

### 1.6. The $\alpha$ -helix

The  $\alpha$ -helix is the major element of secondary structure in proteins. It was first described by Linus Pauling in 1951<sup>1</sup>.  $\alpha$ -helices are formed when a stretch of consecutive residues have a  $\phi$ ,  $\Psi$  angle pair approximately  $-60^\circ$  and  $-50^\circ$  (Ramachandran plot). The  $\alpha$ -helix is right-handed in Nature because of the natural occurrence of L-amino acids. It has 3.6 residues per turn with hydrogen bonds between C=O of residue  $n$  and NH of residue  $n+4$ ; the vertical distance between each turn is 5.4 Å. Each peptide unit in an  $\alpha$ -helix has a dipole moment arising from the different polarity of NH and CO groups, these dipole moments are also aligned along the helical axis, which results in a partial positive charge at the amino end and a partial negative charge at the carboxy end of the  $\alpha$ -helix<sup>3</sup> (Figure 7).

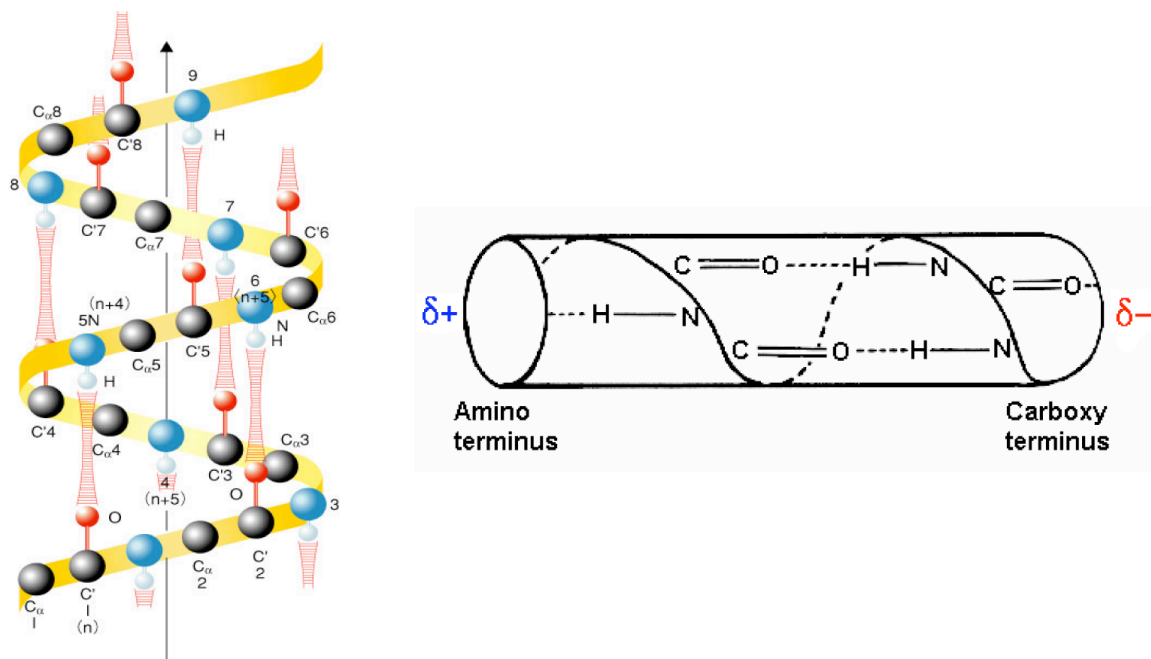


**Figure 7.** Secondary structure of an  $\alpha$ -helix (left) and its dipole moment.

It is worth mentioning that  $\alpha$ -helical motifs play a key role in many biological processes; for example, the key receptor-binding component in peptide hormones, such as neuropeptide Y<sup>4</sup> or calcitonin<sup>5</sup>, have a bioactive helical conformation; furthermore, sequence specific DNA-binding proteins often employ  $\alpha$ -helical motifs as the DNA recognition element<sup>6</sup>; eventually, the hemolytic activity of melittin and alamethicin peptides are believed to be linked to their helical structure<sup>7</sup>.

### 1.7. Initiating $\alpha$ -helices using Ncap templates

As we have previously seen, the two most common arrangements in proteins are helices and sheets. However, the  $\alpha$ -helix is not a stable conformation in short polypeptides of fewer than 20 residues because it lacks specific stabilizing interactions<sup>8</sup>. In 1959, Zimm and Bragg<sup>9</sup> (and Lifson and Roig shortly afterwards) defined two parameters, the helix initiation constant ( $\sigma$ ) and the propagation constant ( $s$ ), to assess  $\alpha$ -helix stability in peptides. The Zimm-Bragg equation gives  $K = [\text{helix}]/[\text{random coil}] = \sigma s^{n-1}$ , where  $n$  corresponds to the number of residues in the sequence. The initiation constant reflects the probability of aligning the first three residues in an  $\alpha$ -helical conformation. Without stabilizing hydrogen bonds, this is a highly disfavored process, due to the repulsive interactions between the aligned dipoles and the loss of entropy. The propagation constant  $s$  reflects the likelihood of an amino acid residue adopting  $\alpha$ -helical torsion

angles, when added to the end of a pre-existing helix. And while initiating the helix is paid only once for each helix, propagating it multiplies the statistical weight by one additional  $s$ -value for each hydrogen bond.

To overcome the problem of initiating helices, Baldwin and coworkers<sup>10-12</sup> added conformational constraints like salt bridges or charged groups at both termini of the sequence to force the peptide into  $\alpha$ -helical conformation. Shortly after Kemp<sup>13</sup> (and several other groups afterwards) developed rigid synthetic templates known as N-caps providing hydrogen bonding acceptors for the first four amide protons in the sequence that normally lack them (Figure 8). One difficulty in the design and synthesis of such N-Caps lies in the requirement to align H-bond acceptors in the correct geometry for helix initiation.

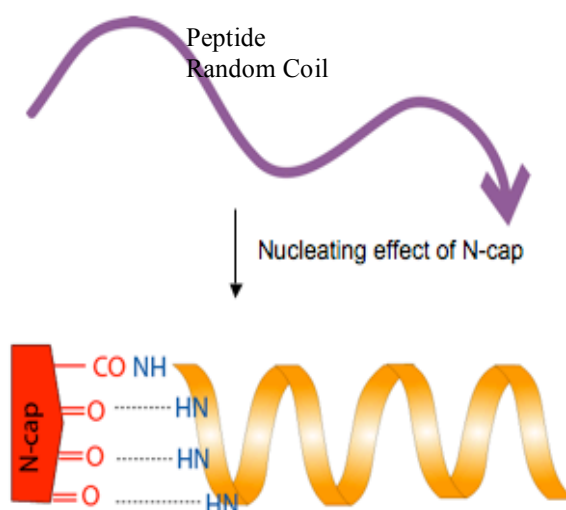


**Figure 8.** A short peptide has a random coil conformation in aqueous solution and once an N-cap nucleating template is added to the sequence, the peptide adopts an  $\alpha$ -helical structure.

## ***2. Protein folding and misfolding***

The complex machinery of protein folding is an amazing and fascinating process. How a protein, after its synthesis on ribosome, will fold and adopt its well-defined three-dimensional structure, essential for its precise function in the cell, is still today not completely understood. Many parameters have to be taken into account in protein folding, most notably, its amino acid sequence and the cellular environment surrounding the polypeptide chain. The amazing recognition and catalytic characteristics of proteins are deeply rooted in their three-dimensional structure. Whether they are involved in enzymatic catalysis, immune response, reception and emission of stimuli or in the expression and organization of genetic information, their particular shape is the key of their success. The stability of the defined structure of a protein is the result of the sum of covalent bonds, like disulphur bridges, and a full set of non-bonding interactions like Van der Waals interactions, hydrogen bonds, dipolar interactions and hydrophobic packing. The latter results from the tendency of hydrophobic residues to form a compact core in the middle of the entity while hydrophilic ones tend, in contact with water, to face outwards, creating a dense complex surface.

If most proteins spontaneously fold into their native state, some require the help of enzymes called chaperones to assist them to achieve their proper folding. However, if the folding is unsuccessful, the polypeptide is directed to the proteasome – a large multisubunit protease - for degradation.

Ensuring accuracy in protein folding is crucial for maintaining proper cellular function. Protein misfolding can have dramatic effects on health.

Several diseases are caused by a loss of protein function because the misfolded proteins have been degraded by the proteasome. Other misfolding diseases are caused by conformational changes coupled to the aggregation of misfolded proteins outside the cell, beyond the influence of intracellular quality control systems. The major representatives of these disorders are the amyloidoses, characterized by insoluble extracellular deposits of protein aggregates occurring in the post-mitotic environment of the neuron and they include Alzheimer's and Parkinson's disease.

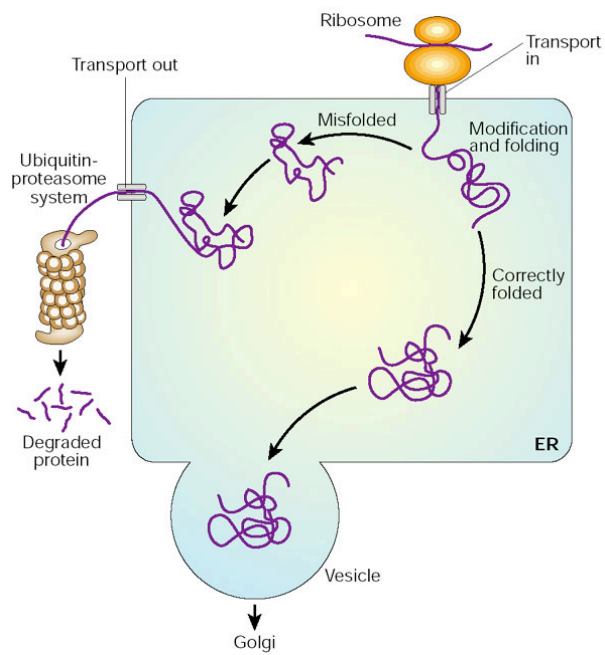


**Figure 9.** Regulation of protein folding in the Endoplasmic Reticulum (ER).

### 3. Alzheimer's disease

Dementia is among the most feared consequences of growing old, and with the aging of the populations, its prevalence is expected to increase in most industrialized countries in the coming decades. Indeed, Alzheimer's disease (AD), which is a devastating neurodegenerative disorder affecting millions of individuals and for which, 100 years after its discovery, there is still no cure, accounts for more than 60% of cases of dementia<sup>14, 15</sup>.

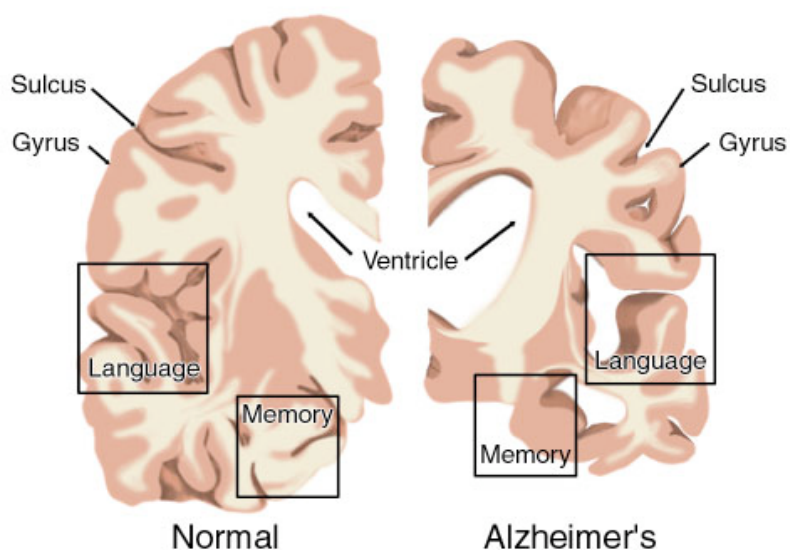


**Figure 10.** Brain cross-section as seen from the front. The cross-section on the left represents a brain from a normal individual and the one on the right represents a brain with Alzheimer's disease.

The disease is named after a Bavarian neuropsychiatrist, the Dr. Alois Alzheimer, who first encountered in 1901 Auguste D., a 51 years old woman, who was suffering from progressive changes in her personality. She suffered notably from reduced comprehension and memory, aphasia, disorientation, unpredictable behaviour, and paranoia. Dr. Alzheimer, who had never encountered a patient with such symptoms before, was fascinated by Auguste D.'s case and decided to examine her more closely<sup>16</sup>. Over time, her state generally worsened, and in her final year, she became completely apathetic and spent most of her time hunched up in bed. After her death in 1906, Alzheimer autopsied her brain and discovered dense deposits outside and around the nerve cells called senile plaques, composed of deposits of Amyloid- $\beta$  peptide and found to be common in the brains of people with senile dementia. But he also observed the presence of twisted bands of fibers, inside the nerve cells, known as the neurofibrillary tangles. These tangles

are composed of hyperphosphorylated Tau protein. Those findings were first presented and published 1906 and in 1911 and still remain today the key diagnostic features of AD<sup>17-19</sup>.

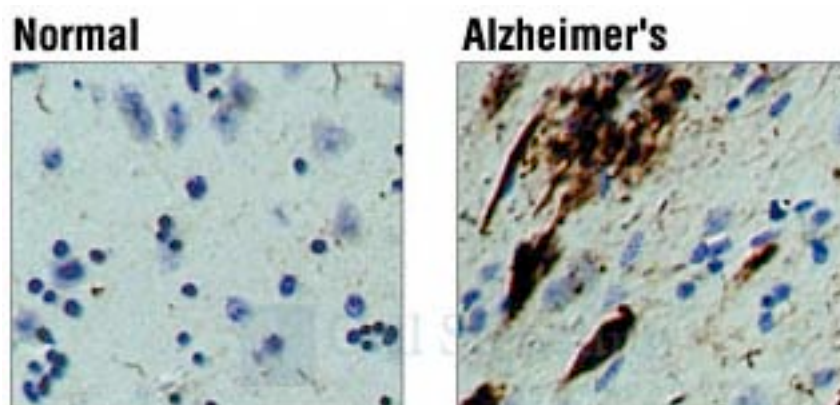


**Figure 11.** Hippocampus from a neurologically normal individual and an individual with confirmed Alzheimer's disease.

### 3.1. Neurofibrillary tangles in AD

Neurofibrillary tangles (NFT) are one of the pathologic hallmarks of Alzheimer's disease<sup>20, 21</sup> and many other neurological diseases, such as, amongst others, amyotrophic lateral sclerosis, corticobasal degeneration and supranuclear progressive paralysis.

Neurofibrillary tangles are intracellular fibrillar aggregates of the microtubule-associated protein tau that exhibit hyperphosphorylation and oxidative modifications. Microtubules are strongly involved in intracellular transport processes and are essential in the development of cell processes and establishment of cell polarity<sup>22, 23</sup>.

Under physiological conditions, tau is a microtubule-associated protein (MAP) regulating the formation of axonal microtubules<sup>23</sup>, signal transduction<sup>24</sup> and neurite outgrowth<sup>25</sup>. The state of phosphorylation of MAPs, balanced by protein kinases and phosphatase, plays a pivotal role in modulating microtubule networks<sup>26</sup>. However, abnormally hyperphosphorylated Tau protein accumulates and aggregates to paired helical filaments (PHFs) finally leading to neurodegeneration<sup>27</sup> (see Figure 12). Interestingly, hyperphosphorylation of tau also blocks APP trafficking, suggesting that this tau and elevated levels of A $\beta$  might be linked<sup>28</sup>. However, a recent study carried out by Goldsbury et al. demonstrated that inhibition of APP trafficking by tau protein did not increase the generation of Amyloid- $\beta$  peptides<sup>28</sup>.



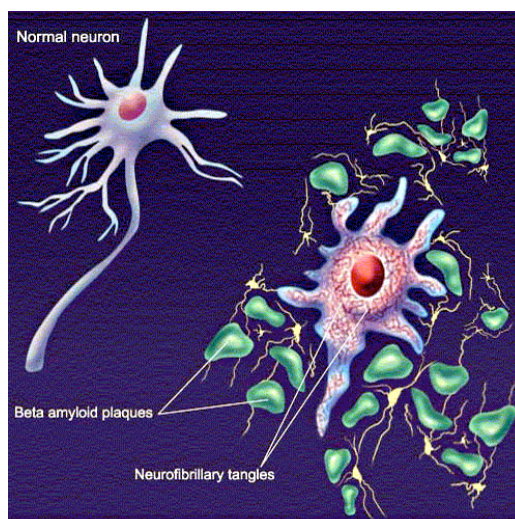


**Figure 12.** Comparison between a healthy neuron and a dead neuron comprising amyloid plaques and neurofibrillary tangles.

### 3.2. From Amyloid Precursor Protein to Amyloid $\beta$

The Amyloid Precursor Protein (APP) is localized to chromosome 21 and is expressed in many cell and tissue types including endothelia, glia and neurons of the brain. Within its polypeptide chain it bears the sequence of amyloid  $\beta$  ( $A\beta$ ) 40 and 42, thought to play a key role in the pathology of AD. Three major isoforms of the protein exist,  $APP_{770}$ ,  $APP_{751}$  and  $APP_{695}$ . The brain seems to produce predominantly the 695 amino acid isoform and thus this isoform has received the most attention in research on AD<sup>29</sup>.

This transmembrane protein with a large extracellular amino-terminal domain and a small cytoplasmic domain can be localized to many membranous structures in the cell such as endoplasmic reticulum and Golgi compartments, as well as to the cell membrane. Although its exact role is not fully understood, it seems to have an important function in cell adhesion, intercellular communication and membrane-to-nucleus signaling<sup>30</sup>.

Unlike most receptors, APP is sensitive to proteolytic cleavage. Three main proteolytic cleavage sites (the  $\beta$ ,  $\alpha$  and  $\gamma$  sites) have been identified: two close to the membrane and one within the transmembrane domain. The full-length  $A\beta$  is generated by the  $\beta$ -secretase cleavage at the  $\beta$ -cleavage site, between residues 596 and 597. It releases a sAPP (the sAPP $\beta$ ) and a membrane bound peptide (C99) containing the  $A\beta$  domain. C99 undergoes further cleavage by  $\gamma$ -secretase resulting in the two forms of  $A\beta$ ,  $A\beta_{40}$  and  $A\beta_{42}$  (Figure 13).

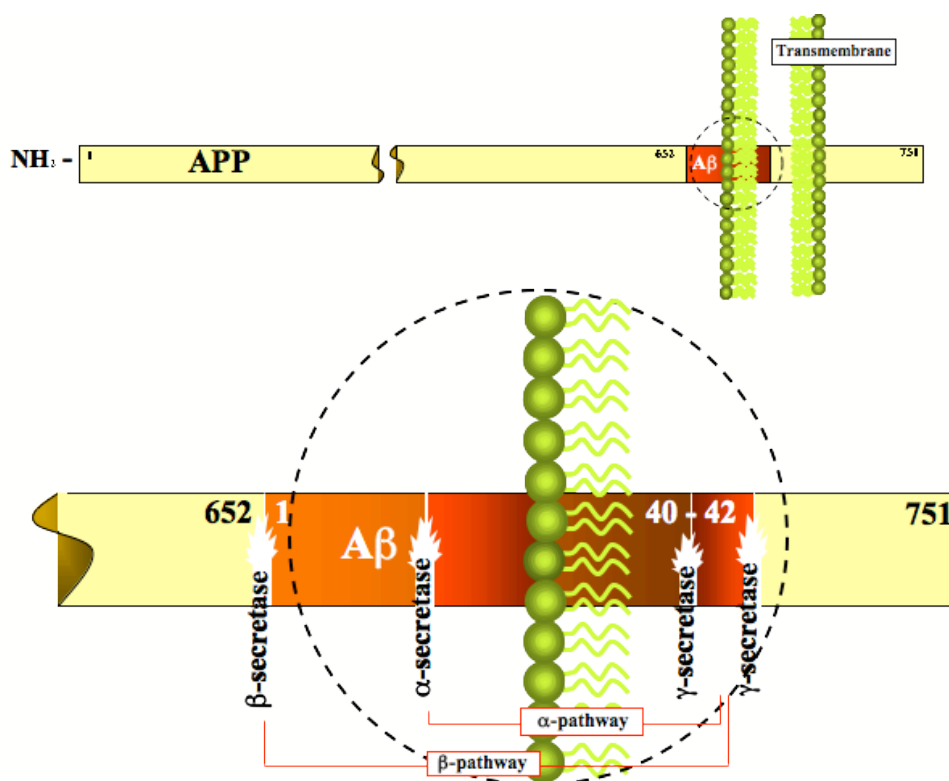


**Figure 13.** Diagram of the cleavage of Amyloid Precursor Protein (APP) by the sequential events of different secretases, which result in the metabolic products of A $\beta$  peptide. Above: representation of full length APP spanning the membrane. Below: enlarged, transmembrane segment of APP showing site action of secretases<sup>31</sup>.

It was formerly thought that A $\beta$  formation was a result of aberrant APP processing, but it is now clear that A $\beta$  is a normal product of APP metabolism since it is also found in normal human cerebrospinal fluid and is believed to play a role in axonal transport of APP<sup>32</sup>.

However, the mechanism by which A $\beta$  accumulates and becomes toxic to neuronal cells leading to AD is still the subject of massive international research efforts. Today, there are increasing evidences suggesting that there is a link between induced oxidative stress and conformational changes occurring in A $\beta$ , leading to neurotoxicity<sup>33-35</sup>.

### 3.3. Understanding Amyloid $\beta$ misfolding and its toxicity

Hundred years after the discovery by Dr. Alois Alzheimer of amyloid plaques in the brain of Auguste D suffering from dementia, the mechanism of amyloid formation and toxicity still

remains elusive. However, the clinical importance of AD has boosted intensive research in the mechanisms of A $\beta$  folding and self-assembly.

Early studies clearly demonstrated that aggregation of A $\beta$  was essential for toxicity, but characterization of the assemblies that formed *in vitro* was limited, and it was assumed that since amyloid fibrils were detectable, these assemblies mediated the observed toxicity. Yet, it is known that there is a relatively weak correlation between the severity of dementia and the density of fibrillar amyloid plaques<sup>36-38</sup>.

Moreover, there is growing evidence suggesting that early, diffusible oligomers (for example, dimers, trimers, and tetramers) of A $\beta$  could themselves be toxic to synapses<sup>39-42</sup>, whereas the abundant fibrils of mature amyloid plaques represent a relatively inert reservoir of amyloid  $\beta$  protein that is in equilibrium with the smaller, biologically active oligomers<sup>43-45</sup>. Those  $\beta$ -sheet-rich oligomeric intermediates exist as a heterogeneous mixture of aggregates of various sizes and morphologies (globular, chainlike, and annular structures) and are collectively called protofibrils<sup>46-48</sup>.

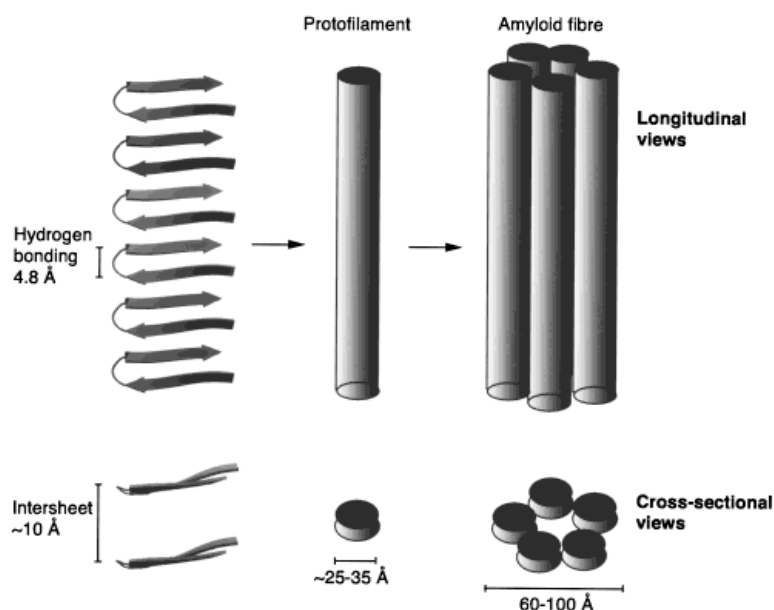


**Figure 14.** Schematic diagram showing the different levels of structure, from the continuous, hydrogen-bonded  $\beta$ -sheet within a protofilament to the organization of the protofilaments in the amyloid fibril<sup>49</sup>.

There is also considerable evidence that the effects of an A $\beta$  protein-initiated inflammatory and neurotoxic process include excessive generation of free radicals and oxidative injury to proteins and other macromolecules in neurons<sup>43</sup>.

Although significant progress has been made in the resolution of structural properties of amyloid fibrils, little is known about the events leading to the aggregation process. Several kinetic studies have suggested that fibril formation is a two step process, comprising an initial lag-phase, in which nuclei are formed, followed by an exponential or polymerization phase, in which early protofibrils grow and assemble to render mature amyloid fibrils, which are then in equilibrium with A $\beta$  monomers (Figure 15).

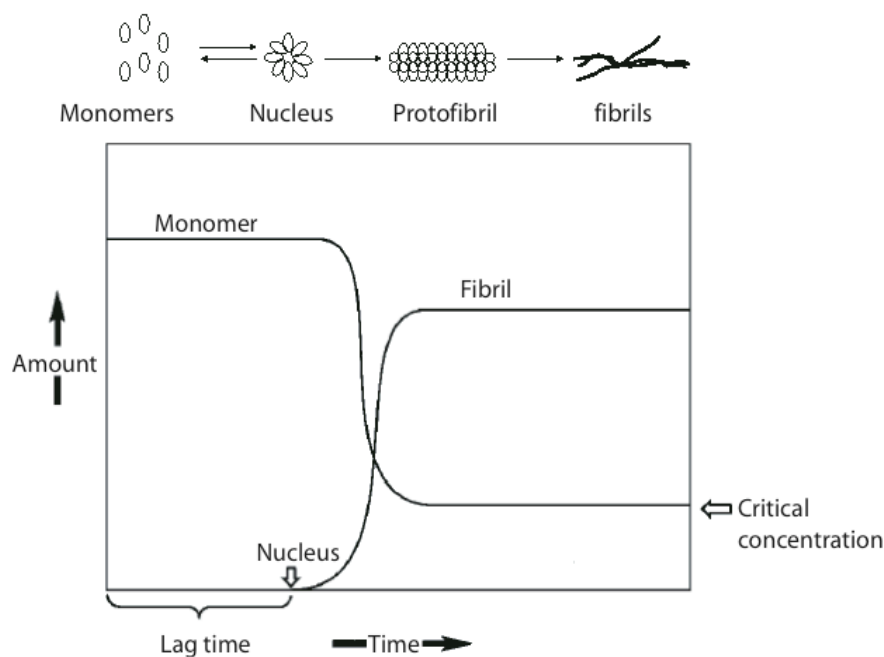


**Figure 15.** Amyloid fibril formation by nucleation-polymerization.

The nucleation step is the rate-limiting step in the process of amyloid formation. The addition of pre-formed fibrils to the solution reduces substantially the length of the lag phase in a concentration dependent manner. This phenomenon is known as seeding. Addition of small amounts of seed can have dramatic effects in speeding up the process of amyloid formation. After nucleation occurs, various assemblies exhibiting structural and morphological characteristics of an increasingly complex nature (micelle-like aggregates or spheroids, protofibrils, protofilaments) populate sequentially to finally render mature amyloid fibrils.

In 2006, Lansbury and Lashuel<sup>50</sup> published a state-of-the-art review on the protein aggregation issue. They explain that due to the greater understanding of the protein fibrillization process *in vitro*, researchers are now focusing on which species are neurotoxic and are trying to elucidate the pathway by which they cause neuronal dysfunction leading to disease and death. For the last

15 years, the “amyloid cascade hypothesis” has driven most of the research done in AD<sup>51</sup>. It was thought that protein aggregation was the trigger of the cascade of events resulting in neurodegeneration and disease. However, it is difficult to find a correlation between protein deposits, neuronal dysfunction, neuronal loss and severity of symptoms at the time of death. It is also difficult to trace *in vivo* the early stages of the disease during which oligomers and protofibrils forms due to a lack of technical methods. Nevertheless, significant progress has been made in that field and it will soon be possible to track the natural history of protein aggregation and correlate it with disease progression<sup>52, 53</sup>. At present, it is already possible to detect *in vivo* fibrillar amyloid plaques with a positron emission tomography imaging reagent, but since fibrillar amyloid assemblies occur relatively late in the disease, it would be more useful to have analogous reagents targeting early amyloid species.

Furthermore, a large amount of results has emerged from biophysical studies, providing a mechanistic rationale to better explain the effects of disease-causing mutations, but the major issue here is that the idealized experimental systems have poor resemblance to the complexity of the brain.

In the review, Lansbury and Lashuel discuss also various hypotheses on neurodegeneration that have been proposed up-to-now, to find a rational between the results that have emerged from *in vitro* and *in vivo* studies. They ask what can be done to refine and clarify the current models and what needs to be done in order to produce disease-modifying treatments for neurodegenerative diseases and to identify presymptomatic individuals who could benefit from such treatments.

They demonstrate that, although the techniques have significantly evolved, it remains difficult to eliminate any hypothesis since important diagnostic tools are still missing. However, they provide relevant information to confirm that the route of oligomers and protofibrillar aggregates as toxic species, stands heads above the rest.

Furthermore, Lührs et al.<sup>54</sup> published in 2005 a very important finding on the 3D structure of A $\beta$  determined by NMR studies. Their findings suggest that A $\beta$  misfolds by arranging itself into two  $\beta$ -sheets that run along the fibril axis. Sheet  $\beta$ 1 is formed by residues 18-26, and sheet  $\beta$ 2 is formed by residues 31-42 (Figure 16). They demonstrated that intersheet contacts are formed between residues F19/G38 and A21/V36 and a salt bridge between residues D23 and K28.

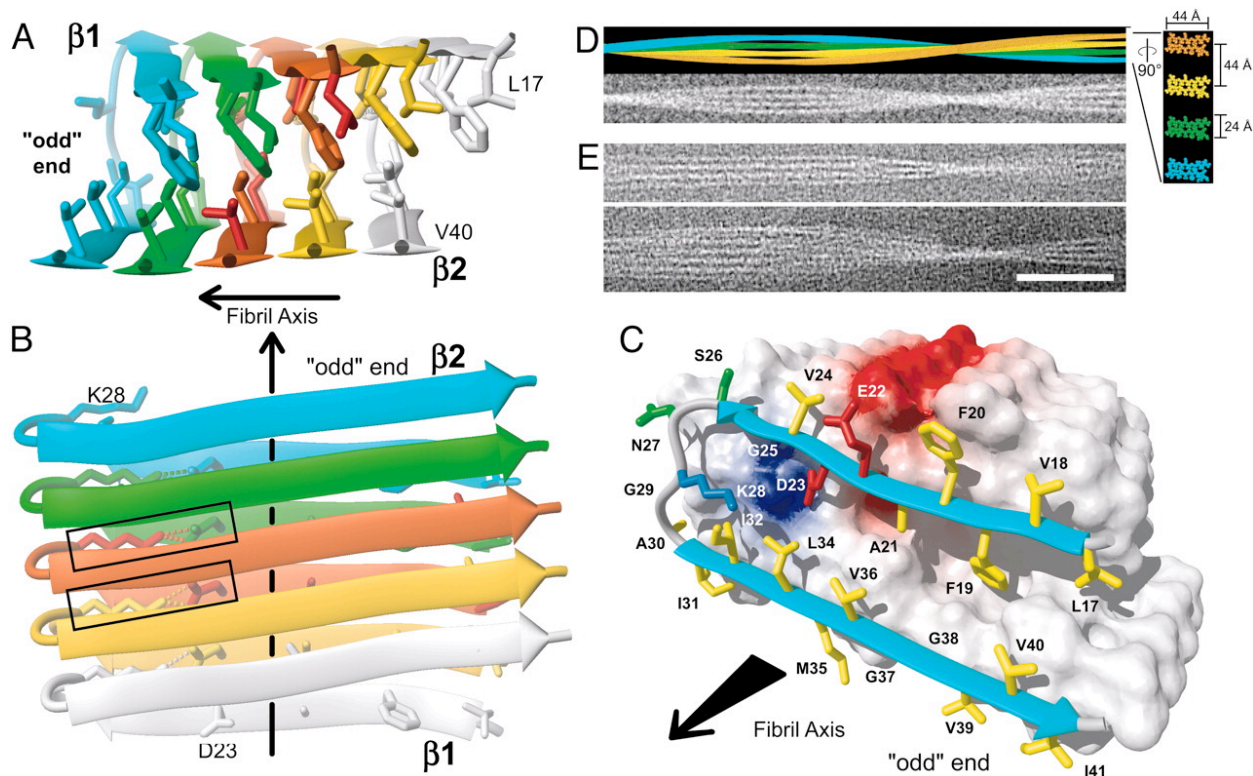


**Figure 16.** 3D structure of  $A\beta(1-42)$  fibril<sup>54</sup>.

The structure of  $A\beta(1-42)$  protofilament explains the sequence selectivity, the cooperativity and the unidirectionality of the fibril growth. It also provides a structural explanation for the working mechanism of current  $A\beta$  fibrillization inhibitors.

This study opens new perspectives in the comprehension of amyloidogenesis and may help in the development of anti-AD drugs.

### 3.4. Therapeutic strategies: state-of-the-art

Over the past 20 years, enormous progress has been made in both the diagnosis and treatment of dementia and in particular AD. However, due to the complexity of the disease, it is still nowadays only possible to slow down the symptoms that accompany the early stages of the disease onset. There is still no efficient remedy able to completely stop the gradual decline in memory, leading to dementia and ultimately to patient's death. The drugs that are on the market aim at improving the patients' life by decreasing symptoms like anxiety, insomnia or depression, they also provide improvement of the patient's memory and concentration. These agents act specifically in regulating the neurotransmitters acetylcholine and glutamate.

Acetylcholine (ACh) is a small neurotransmitter allowing nerve cells to communicate with each other. It is synthesized in neurons of the CNS and PNS by the enzyme choline acetyltransferase

from choline and acetyl-CoA. The successful release and uptake of ACh between neurons is followed by its clearance by the enzyme acetylcholinesterase (ACh E), it re-establishes the sensitivity of neurons and is essential for proper muscle function. Several observations have demonstrated that during the progression of AD, the levels of ACh decline, and thus a therapeutic strategy was to develop compounds capable of inhibiting ACh E degradation in order to keep an appropriate level of ACh in the brain. Those ACh E inhibitors (Donepezil, Rivastigmin and Galantamin) have shown favourable, albeit mild, effects on cognitive impairment<sup>55, 56</sup>.

Glutamate is another important neurotransmitter, which plays a crucial role during the development of dementia. Glutamate found in hippocampal neurons is involved in learning and memory processes. Contrary to acetylcholine, secretion of glutamate is increased during the development of AD, causing calcium ions to enter cells via NMDA receptors channels, leading to neuronal damage and cell death. Memantine, an NMDA receptor antagonist, is the only drug of this type on the market and works by preventing glutamate from binding to the post-synaptic NMDA receptors, thereby decreasing post-synaptic calcium influx through NMDA channels. This treatment as well improves the symptoms but does unfortunately not cure the disease<sup>57-60</sup>.

Several studies also support the fact that statin drugs, widely used cholesterol-lowering drugs, have therapeutic benefits for Alzheimer's disease. It has been demonstrated that taking statin drugs has positive effects on cognition in the elderly and can therefore reduce the risk of developing AD<sup>61</sup>. However, little is known about the mechanism through which the drug works and more intense research needs to be done to confirm those observations.

Considerable evidence shows that oxidative stress is a marker of neurodegeneration and has been recently shown to be also involved in the early stages of the pathogenesis of various neurodegenerative disorders<sup>62-64</sup>. Several lines of evidence implied that oxidative damage to lipid membranes could disrupt normal neuronal and glial cell functioning, leading to the formation of amyloid plaques and to neuronal cell death. Hence, many antioxidants, such as for example, flavonoids, tannic acid, vitamin E and C are tested as potential drugs to prevent AD since they might inhibit the production of free radicals and reactive oxygen species. Moreover, it is recommended for people at risk to have a diet rich in antioxidants.

More recent therapeutic strategies have attempted to target the A $\beta$  overload in different ways. One possibility is to prevent APP proteolytic processing by inhibiting the action of  $\gamma$ -secretase and  $\beta$ -secretase, responsible for A $\beta$  biogenesis<sup>65, 66</sup>. These compounds have shown a significant

lowering of plasma and CSF A $\beta$  levels. The company Myriad genetics is developing such a compound (known as Flurizan<sup>TM</sup>) that has proven to reduce the level of A $\beta$ 42 in cell culture and in animal model of AD by modulating the activity of  $\gamma$ -secretase. It is currently being evaluated in phase III clinical trials in patients with mild AD.

Another strategy uses immunization and immunomodulation of A $\beta$  to promote clearance and inhibit toxicity<sup>67</sup>. The aborted clinical trial with the Elan vaccine (AN1792) due to inflammation of the brain has provided a large amount of information on how antibodies work to clear A $\beta$  from the brain<sup>68, 69</sup>. Novel methods of antigen approaches are now under investigation and are designed to avoid the autoimmune adverse events<sup>70</sup>.

A third approach targets directly A $\beta$  itself. This should have a lower risk of developing unanticipated side effects, as the accumulated A $\beta$  molecule is restricted to Alzheimer's disease. Moreover, inhibiting the formation of A $\beta$  fibrils seems a reasonable therapeutic strategy, because familial mutations that lead to an increase in A $\beta$  concentration result in neuropathology.  $\beta$ -breaker peptidomimetics based on the sequence of A $\beta$ 16-21 have proved to block both A $\beta$  seeding and growth *in vitro*. However, the pharmacological profile of these compounds is not ideal and Soto's peptide showed toxicity in rats in phase I clinical trials<sup>71, 72</sup>.

A new and very promising small molecule from the company Neurochem (Tramiprosate, Alzhemed<sup>TM</sup>) has entered advanced clinical trials<sup>73</sup>. It acts by binding monomeric A $\beta$  and it was shown to cross the blood-brain-barrier as well as to significantly reduce A $\beta$  levels in the brain. It has been demonstrated that Tramiprosate affects the levels of soluble A $\beta$ 40 and A $\beta$ 42 and influences its efflux from the brain and catabolism. To date, Tramiprosate completed phase III clinical trial in the US and Canada and demonstrated safety, efficacy and disease-modifying potential in the treatment of mild-to-moderate AD. It is now under phase III clinical trial in Europe.

Finally, although researchers are focusing mainly on Amyloid  $\beta$ , studies on neurofibrillary tangles have progressed and, as with A $\beta$ , small compounds capable of inhibiting aggregation and fibrillization of tau protein are now under investigation *in vitro*<sup>74, 75</sup>.

Average life expectancy of people suffering from AD has increased in the last few decades thanks to intensive scientific research. It seems now clear that targeting a single mechanism of action or a single class of compound will not be sufficient to treat and cure this complex illness. However, given the scientific and clinical progress that has been made recently, physicians and



scientists strongly believe that it will take only few years for the “drugs of tomorrow”, capable of stabilizing and preventing the disease, to be available on the market.

#### 4. *The concept of switch-peptides*

As discussed in the previous chapter, the protein misfolding problem is extremely difficult to solve, most notably due to the high propensity of the peptide or protein being investigated to self-assemble and aggregate<sup>76-79</sup>. However, it has become very urgent to be able to follow and understand the pathway from the native state of a peptide or protein to its misfolded and aggregated state since there is increasing evidence suggesting that this is the key event leading to neurotoxicity and to a large number of neurodegenerative diseases<sup>50</sup>, including Alzheimer's disease on which we have focused our work.

Our group<sup>80</sup> developed a few years ago a new concept for in situ induction of conformational transitions called the switch-concept. In this concept switch-peptides are folding precursors, which allow not only to induce a defined structure in a peptide but also to study conformational transitions relevant in debilitating diseases.

The designed switch-peptides consist of three segments: a peptide fragment **P1** (which can also be a conformational induction unit  $\sigma$ ), a switch element **S** and another peptide fragment **P2**, which may serve numerous functions such as host sequence, recognition sequence or bioactive sequence (Figure 17). The key conceptual feature of this design is that **P1** and **P2** are separated from each other when the peptide is in the  $S_{\text{off}}$  state rendering the peptide more flexible and if **P1** is a conformational inducing unit  $\sigma$ , the effect of  $\sigma$  is decoupled when the switch is off and its effect is set off only when the switch is triggered to re-establish the regular backbone of the peptide.

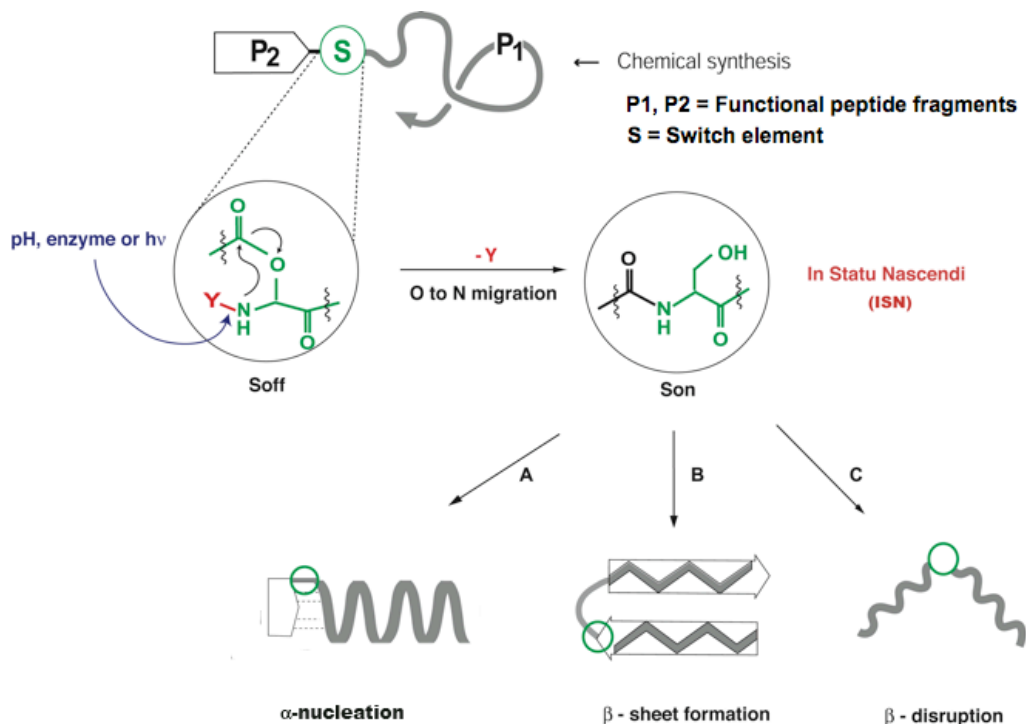


**Figure 17.** ISN-induction of conformational transitions. By removal of  $Y$ , an  $O$  to  $N$  acyl migration occurs, restoring a regular peptide bond between  $P_1$  and  $P_2$  and thus leading to a change in the conformation of the peptide, typically from a flexible  $rc$  ( $S_{off}$ ) to a folded state ( $S_{on}$ ). These conformational changes can be used to study the onset of biological function (A),  $\beta$ -sheet formation (B) and disruption of  $\beta$ -structures (C)<sup>80</sup>.

$Y$  represents the amino-protecting group of the residues Ser or Thr involved in the formation of the switch element  $S$ ; it can be either a  $H^+$ , an enzymatic cleavable group or a photolytically cleavable group. Due to the different nature of the  $Y$  groups, it is possible to introduce in a peptide sequence multiple switch elements, which can be triggered orthogonally and independently. This technique turns out to be very relevant in the investigation and possibly the identification of aggregation “hot spots” in a defined sequence<sup>81</sup>.

#### 4.1. The switch element $S$

The novel class of switch peptides described in the previous paragraph belongs to the family of depsipeptides (depsi means ester in greek). They comprise one or several ester bonds localized to specific residues having a hydroxy group in their side-chain, i.e. Ser or Thr. The structural modification induced by the substitution of the related amide bond by such flexible non-peptidic bonds, leads to a considerable improvement of the solubility (presence of an ionisable amine) and the conformational flexibility of the peptide.

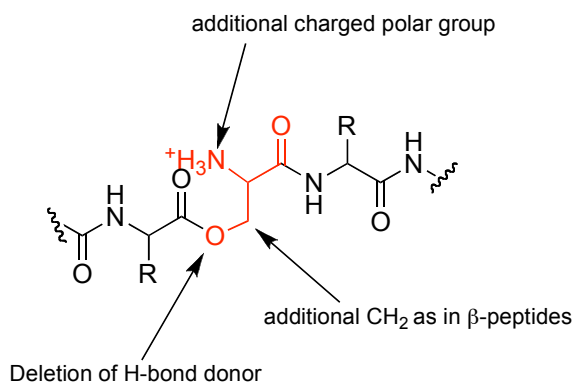


**Figure 18.** A serine derived switch element *S*.

The substitution of the amide bond with an ester bond is fairly conservative since both types of bonds prefer a *trans* conformation, are planar and have similar bond angles and lengths, preferring similar  $\Psi$  and  $\phi$  dihedral angles<sup>82-84</sup>. However, they differ in their capacity of forming hydrogen bonds. The carbonyl group of the ester bond is a weaker hydrogen bond acceptor than the amide bond<sup>85</sup>. Moreover, the nitrogen atom of the amide bond is a hydrogen bond donor contrary to the ester bond (Figure 19).

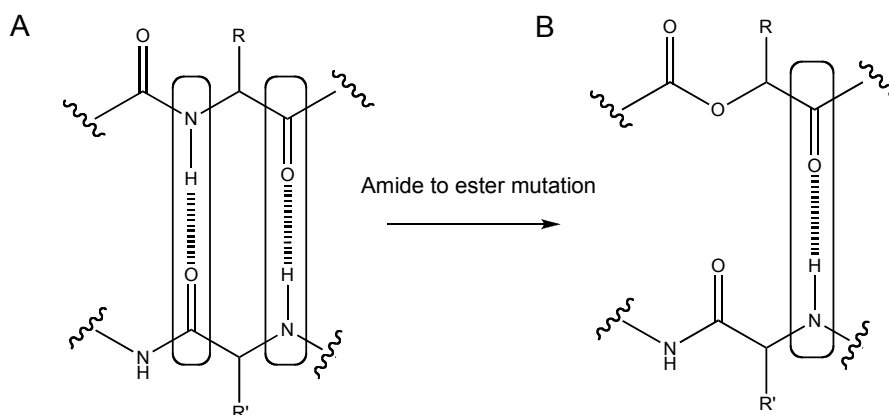


**Figure 19.** Schematic representation of a normal polypeptide backbone hydrogen bonding (A) and the deletion of a hydrogen bond by the incorporation of an ester (B).

The substitution of one or several amide bonds in a peptide or protein results in a decrease of thermodynamic stability. The insertion of ester bonds in secondary structures of type  $\beta$ -sheet or  $\alpha$ -helix gave an estimation of these effects<sup>86</sup>. The obtained values have a large variation scale (0.7 to 24.6 kcal/mol) depending on the number of hydrogen bonds that are suppressed during the incorporation of ester functions in the native protein structure. Schultz and coworkers<sup>87</sup> have examined the contribution of hydrogen bonds in  $\alpha$ -helices to the overall stability of a protein by replacing several backbone amide linkages in  $\alpha$ -helix 39-50 of T4 lysozyme with ester linkages.

It was estimated that a substitution at the N- or C-terminal positions, suppressing a hydrogen bond, has a destabilizing effect of about 0.7 and 0.9 kcal/mol. In the middle of the helix, the removal of two hydrogen bonds destabilizes the helical structure by 1.7 kcal/mol.

Kelly et al.<sup>88</sup> have demonstrated that the introduction of ester bonds in a small  $\beta$ -sheet protein has the strongest destabilizing effect when H-bonds that are enveloped by a hydrophobic cluster are perturbed. Mutations at the extremities of the strands exposed to solvent where water molecules can compete had much weaker effects.

Furthermore, the introduction of a  $\text{CH}_2$  group in the switch-peptide backbone introduces an additional degree of flexibility to the peptide. Indeed, the rotation around the  $\text{C}\alpha\text{-C}\beta$  bond<sup>89</sup> increases the number of possible conformations of the switch-peptides.

Eventually, the charged amino group in the alpha position can also exert a structure destabilizing effect through Coulomb interactions with the polypeptide backbone by interfering with the hydrogen bond network. According to the Chou-Fasman parameters<sup>90</sup>, positively or negatively charged amino acids have a lower  $\beta$ -sheet propensity (for example  $\text{P}\beta_{\text{Glu}} = 0.37$ ;  $\text{P}\beta_{\text{Ile}} = 1.60$ ).

All these modifications introduced by the switch element in a peptide sequence should modify dramatically its structure and function and should result in the disconnection of peptide segments, which allows us to study the impact of specific peptide regions on its folding and aggregation.

#### 4.2. O, N-acyl migration

The concept of switch-peptides is based on the well-known O to N intramolecular migration reaction. The reversible O,N-acyl migration reaction was first investigated by Bergmann<sup>91</sup> in 1923. They demonstrated that the migration is pH-dependent and results in the interconversion between an O-acyl and an N-acyl analogue. Under acidic conditions, the equilibrium is shifted in favor of the O-acyl analogue and, under basic conditions, in favor of the N-acyl analogue. In peptides, the reaction is possible at positions of the sequence containing Ser or Thr residues (Figure 20).

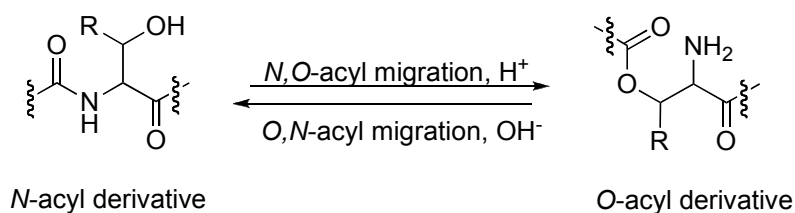


**Figure 20.** Reversible O to N acyl migration in serine and threonine containing peptides.

Today, intramolecular migration reactions find wide applications not only in peptide and protein chemistry but also in the area of protecting groups and prodrugs.

### *Mechanism*

Acyl transfer reactions have been the subject of extensive mechanistic studies and two distinct mechanisms have been proposed for this rearrangement<sup>92, 93</sup>. The key difference between these mechanisms is the resulting stereochemistry of the carbon atom connected with the hydroxyl group.

The first mechanism involves the formation of a hydroxyoxazolidine intermediate and leads to a retention of configuration as no bond with the asymmetric carbon atom is involved. This rearrangement is initiated by the nucleophilic attack of the hydroxyl functionality on the electrophilic amide carbonyl to form the hydroxyoxazolidine intermediate. Subsequent ring opening of this cyclic intermediate gives the O-acyl analogue.

The second mechanism involves the formation of an oxazoline intermediate via nucleophilic attack of the carbonyl oxygen on the hydroxyl group containing carbon atom. Subsequent ring opening results in the O-peptide with a complete inversion of configuration at the chiral carbon.

Depending on the experimental conditions, either mechanism is possible. When a serine is involved, both mechanisms yield the same product, as there are no chiral carbon atoms in the side chain. Experimental evidence suggests that steric factors and the choice of solvent used play a role in controlling the mechanism by which the rearrangement occurs. Moreover, in addition to esters, acyloxy<sup>94</sup> and carbamate<sup>95</sup> groups, and even amides (upon heating)<sup>96</sup> can also undergo intramolecular acyl migration via the same mechanisms.

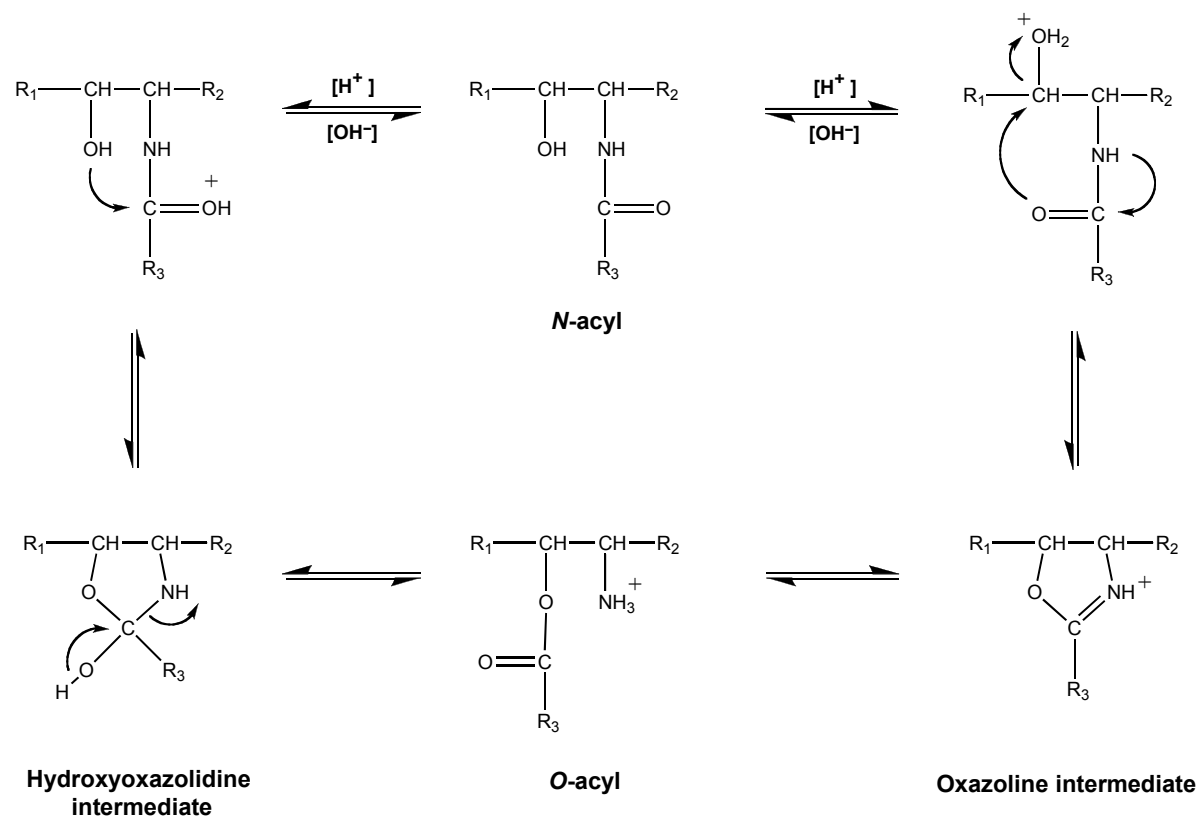


**Figure 21.** Two possible mechanisms of O to N acyl migration.

## 5. Aim of this work

The work presented in this thesis is within the framework of the switch concept, which has been established as a novel tool for the *in situ* induction of structural and functional properties of bioactive peptides (Figure 17). Basically, switch-peptides are used to enable the control and onset of secondary structures in peptides having a high propensity to aggregate spontaneously, making their investigation difficult to achieve.

In a first study, switch-peptides' stability in their  $S_{\text{off}}$  state was explored and gave us important information on the conditions applied in subsequent studies.

This thesis focuses particularly on switch-peptides derived from amyloid  $\beta$ , known to play a key role in the pathology of Alzheimer's disease. The first objective was to synthesize  $A\beta(1-42)$  switch-peptides containing multiple orthogonal switch elements to allow for the observation of folding events in separate and specific regions of the peptide. It was made possible through the sequential activation of orthogonal switch-elements (pathway B, Figure 17). This represents an attractive tool for the identification of sequence "hot-spots" crucial for misfolding and aggregation.

In a next step, the  $A\beta(14-24)$  segment, which has demonstrated to play a key role in  $A\beta$  misfolding process was excised from the whole sequence and was used in the host-guest technique combined with the switch concept in order to study its conformational transition from an unfolded flexible precursor ( $S_{\text{off}}$ ) to its native folded state ( $S_{\text{on}}$ ). Since the handling of aggregation-prone peptides is troublesome, making the investigation for potential aggregation inhibitors difficult, it was thus of particular interest to examine the potential of host-guest switch-peptides for the screening and evaluation of specific  $A\beta$  inhibitors.

This has been demonstrated in applying the elaborated host-guest peptides to evaluate switch-peptides derived from  $A\beta$  capable of preventing or even reversing  $A\beta$  misfolding and aggregation. These peptides are composed of an  $A\beta$  recognition sequence and a structure-disrupting unit containing a pseudoproline, which are linked together via a switch element  $S$ , rendering the molecule more flexible. This dynamic and flexible system, which separates the



recognition and disruption unit should facilitate the insertion of the molecules within A $\beta$  aggregates and thus enhance their therapeutic potential in the treatment of Alzheimer's disease.

Finally, to explore pathway A of the concept (Figure 17), the same sequence of A $\beta$ (14-24) was coupled via a switch element **S** to an  $\alpha$ -helix inducing template  $\sigma$  (Ncap). Using several complementary techniques, like CD, EM, ThT or Congo Red, we examined the impact of the Ncap unit on helix nucleation and its potential as  $\beta$ -sheet destabilizing agent.



## Chapter II. Results and discussion

### 1. overview

As we have already seen in chapter I, switch-peptides are composed of three different fragments: a peptide fragment **P1** (which can also be a conformation induction unit  $\sigma$ ), a switch element **S** and a second peptide fragment **P2** (Figure 17).

Section 2 of this chapter deals with the stability of the switch element (S) over time when the peptide is in the  $S_{\text{off}}$  state and exposed to different conditions.

In section 3, the incorporation of multiple switch elements into the full length  $A\beta(1-42)$  to disrupt its native structure in order to understand its folding mechanism and to examine the folding of specific segments of the peptide is discussed.

Section 4 concentrates on the host-guest switch-peptide technique, where the segment of  $A\beta(14-24)$ , which has proven to be important for  $A\beta$  misfolding, has been excised from the amyloid sequence and is used with the host-guest technique as a model for studying fibrillogenesis and for screening amyloid  $\beta$  inhibitors *in vitro*.

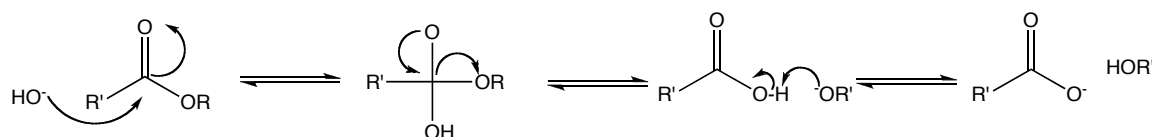
The elaboration of switch-peptides as potential  $A\beta$  aggregation inhibitors and their inhibitory effects on the host-guest switch-peptides studied in the previous section are presented in section 5.

Finally, in section 6, the same  $A\beta(14-25)$  sequence was coupled via a switch element to an Ncap unit to study conformational transitions of type  $\beta$  to  $\alpha$ . it resulted in a drastic increase in solubility and a complete disappearance of fibrils.

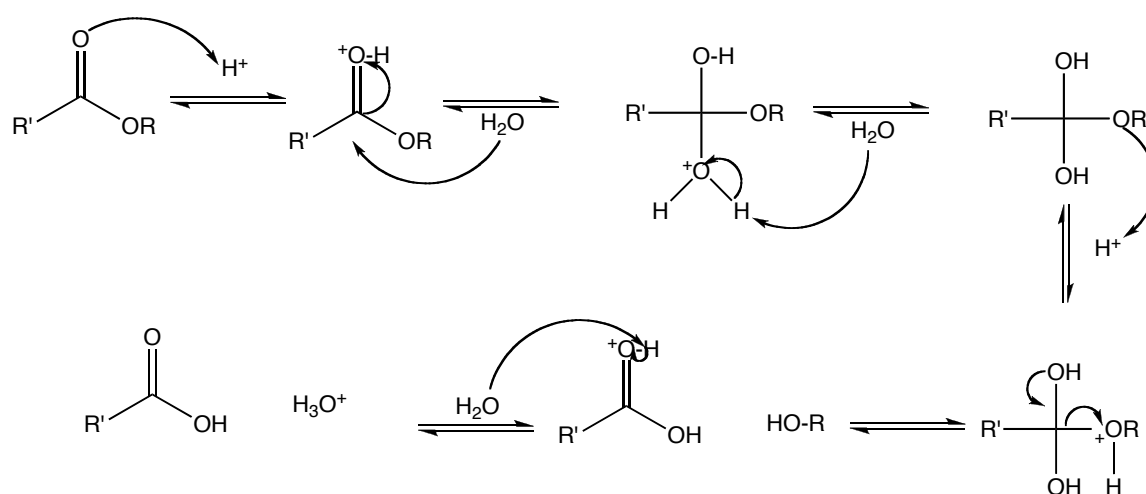


## 2. Study of the stability of the switch element $S$ in the $S_{\text{off}}$ state

Under physiological conditions, the O to N acyl migration is a rather fast process, which can vary depending on the nature of the protecting group Y (Figure 17), on the nature of the residues involved in the switch element and on the conditions that are applied. Here, we discuss the stability of the switch element over time to be certain that the O to N acyl migration occurs before the ester bond undergoes hydrolysis. Indeed, one critical aspect of switch-peptides is that the ester bond constituting the switch element may undergo time dependent hydrolysis. The mechanisms for acid and base hydrolysis are described in the following schemes:



**Scheme 1.** Mechanism of the base ester hydrolysis.



**Scheme 2.** Mechanism of the acid catalyzed hydrolysis.

We investigate the stability of switch-peptides towards hydrolysis in the  $S_{\text{off}}$  state under different conditions, varying the pH of the medium from 4.6 to 8 and the temperature from 25°C to 37°C.

Switch-peptides, with a  $H^+$  as protecting group, have to be dissolved in an acidic medium in order to avoid spontaneous O to N acyl migration and hence to retain the  $S_{\text{off}}$  state of the peptide.

Switch-peptides having a protecting group removable by the enzyme DPPIV are exposed to pH up to 8 as the enzyme's activity is maximal at pH 8.

Furthermore, the side chain of the amino acids involved in the switch as well as the size of the peptide chain can have an effect on its stability. To study all the parameters, investigations are carried out on three different peptides:

- Fmoc-Leu-(Boc)Ser-OH<sup>1</sup> depsidipeptide (peptide **2**)
- Fmoc-Gly-(NVoc)Ser-OH depsidipeptide (peptide **6**)
- Ac-Leu-Cys( $\psi^{\text{Me, Me}}$ pro)-Ala-(Arg-Pro)Ser -(NMe)Phe-Phe-Asp-NH<sub>2</sub> (peptide **19**)

The kinetics of the stability were monitored by RP-HPLC assays at pH 4.6, 7.4 and 8 over a period of one month at two different temperatures (25°C and 37°C).

### 2.1. Stability towards hydrolysis at pH 4.6

When the protecting group of a switch-peptide is a proton (H<sup>+</sup>), the peptide has to be first dissolved in an acidic medium to keep it in its S<sub>off</sub> state and to avoid a spontaneous O to N acyl migration. For this reason, the ester hydrolysis rate of peptides **2** and **6** were monitored under acidic conditions. The peptides were dissolved in 10 mM acetate and 150 mM NaCl buffer, pH 4.6, at a concentration of 0.5 mM and were incubated at 25 °C and 37°C. 50  $\mu$ L aliquots of incubated samples were withdrawn at the indicated time points and analyzed by analytical RP-HPLC.

Figure 22 represents the time dependent hydrolysis of switch-peptides **2** and **6** in the S<sub>off</sub> state at 25°C and 37°C, respectively.

---

<sup>1</sup> We follow the proposed nomenclature for depsipeptides. See: S. V. Filip, F. Cavelier, *J. Pept. Sci.* **2004**, *10*, 115-118.

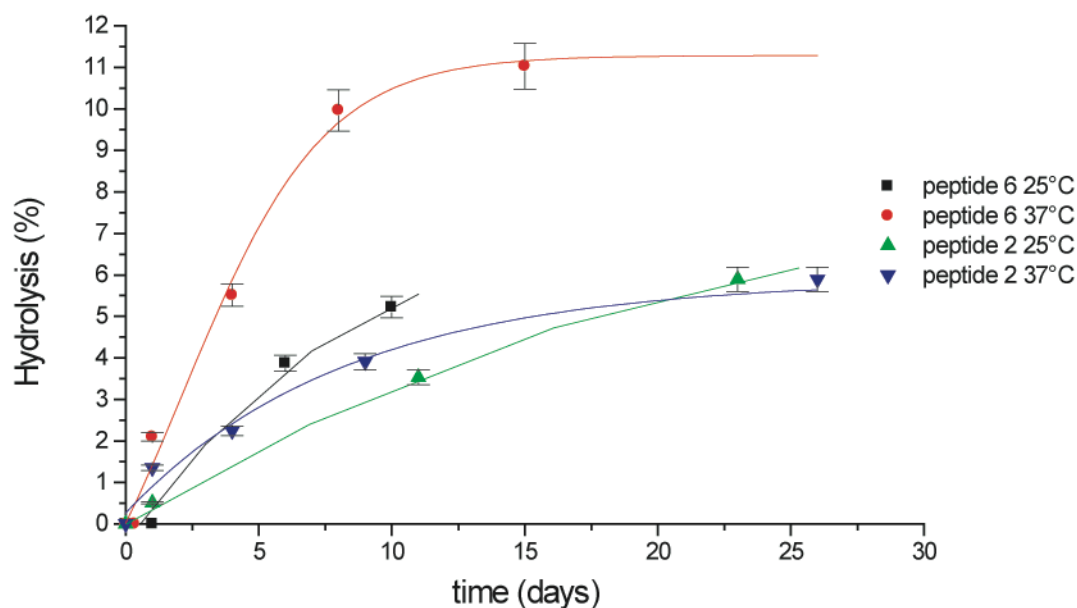


**Figure 22.** Hydrolysis of peptides **2** and **6** over 25 days, at pH 4.6, 25°C and 37°C.

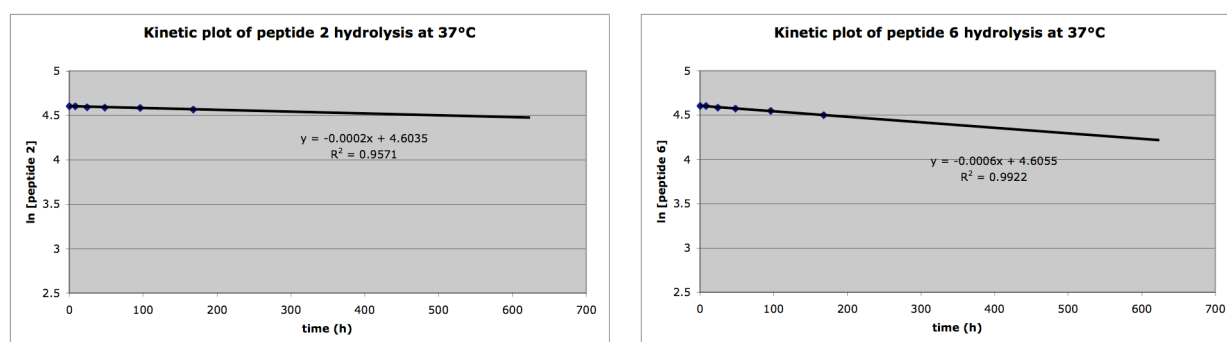


**Figure 23.** pseudo-first order kinetic plot of peptide **2** and **6** at 37°C, pH 4.6.

For peptides **2** and **6** we observe that the degradation of the ester bond follows a pseudo-first-order kinetic (Figure 22 & Figure 23). In all cases, the hydrolysis reaction was found to be very slow under acid conditions at pH 4.6, showing substantial stability over a 48h incubation at 37°C (less than 2% degradation).

## 2.2. Stability towards hydrolysis at pH 7.4

In order to test the stability of peptides **2**, **6** and **19** at physiological conditions, samples were dissolved in 10 mM PBS and 150 mM NaCl buffer, pH 7.4, at a concentration of 0.5 mM and incubated at 25 °C and 37°C. At various intervals, 50  $\mu$ L aliquots were withdrawn and injected

in analytical RP-HPLC. Figure 24 shows the HPLC chromatograms of peptide **6** at time 0 and after 24h at pH 7.4 and 37°C. After 24h the HPLC shows three distinct peaks at  $R_t = 16.3$  min, 22 min, and 24.4 min respectively, two of them corresponding to the degradation products. The peak at  $R_t = 16.3$  min corresponds to the fragment NVoc-Ser-OH and the peak at  $R_t = 22$  min to the fragment Fmoc-Gly-OH of the depsipeptide after hydrolysis. The area of the  $S_{\text{off}}$  peak after 24h at 37°C corresponds to about 87% of the  $S_{\text{off}}$  peak at time 0, which means that the peptide underwent 13% hydrolysis after that incubation period (see also Figure 25).

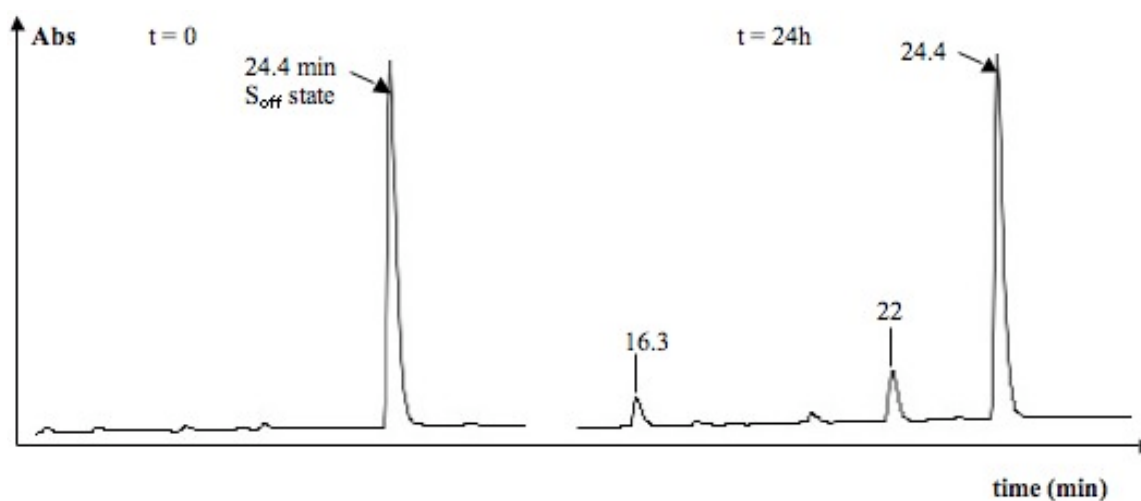


**Figure 24.** HPLC chromatogram of peptide **6** at  $t = 0$  and after 24h at physiological conditions.

For the six different assays, the percentage of hydrolysis of the  $S_{\text{off}}$  state was plotted against time to compare the influence of the temperature on the different switch-peptides (Figure 25).



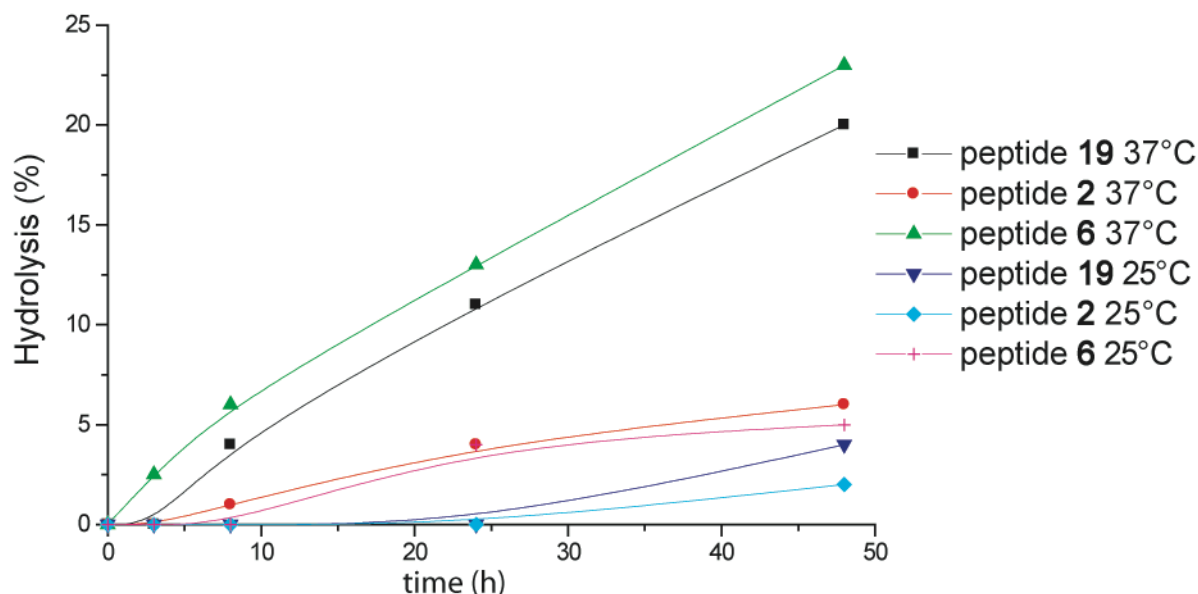


**Figure 25.** Hydrolysis of peptides **2**, **6** and **19** over 48h, at pH 7.4, 25°C and 37°C.

The above kinetics reveal that the fragility of the ester bond clearly depends on the bulkiness of the side chain of the amino acid composing the ester, but does not seem to depend on the chain length of the peptide. Indeed, we observe that peptide **6**, containing a glycine residue, shows increased susceptibility towards hydrolysis compared to peptide **2** containing a leucine (23% for peptide **6** after 48h compared to 5% for peptide **2**). Peptide **19**, the longest peptide chain among the three peptides, having a switch element composed of an alanine residue is more stable than peptide **6** but less than peptide **2** containing the bulky side chain of leucine to protect against degradation.

Increased peptide stability was observed at lower temperature (25°C), showing less than 5% hydrolysis under otherwise identical conditions.

### 2.3. Stability towards hydrolysis at pH 8

0.5 mM of Peptides **2**, **6** and **19** were dissolved in 10 mM Tris and 150 mM NaCl buffer, pH 8 and were incubated at 25 °C and 37°C. Following incubation, the percentage of hydrolysis was determined as outlined above.

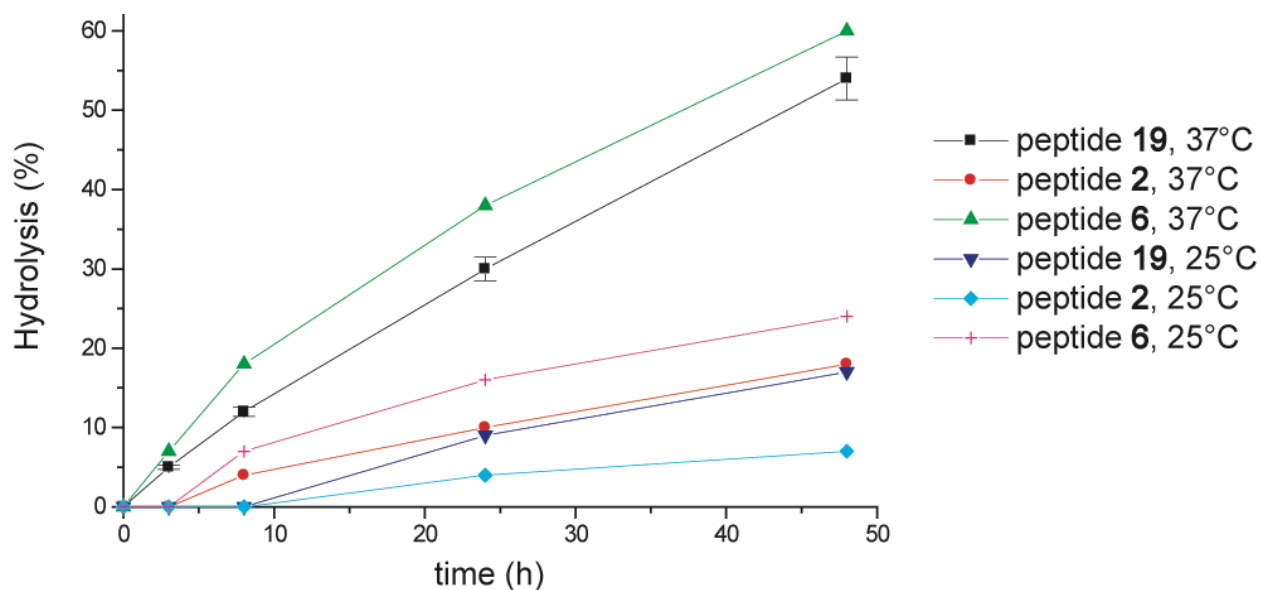


**Figure 26.** Hydrolysis of peptide **2**, **6** and **19** over time, at pH 8, 25°C and 37°C.

The results depicted in Figure 26 show that under alkaline conditions all three peptides were less stable relative to milder or more acidic conditions. Moreover, as previously observed at acidic and neutral pH, peptide **2** having the bulky and hydrophobic side chain of a leucine residue is more stable than peptide **6** containing a glycine and peptide **19** containing an alanine. However, for all three peptides less than 10% hydrolysis was recorded after 5h, and the O to N acyl migration is a fast reaction, which is complete within hours if not minutes. Thus the depsi-peptides are stable long enough to allow for the migration to occur.

## 2.4. Conclusion

The findings on the ester bond stability show that switch-peptides in the  $S_{\text{off}}$  state have a substantial degree of stability in acidic, neutral or basic environments. The obtained data indicate that the optimum pH for maximum stability is in the region of pH 4-5 for the three peptides. With increasing pH, the rate of hydrolysis increases and, depending on the nature of the switch element, relatively significant degradation can be observed at alkaline pH and 37°C.

Moreover, these results indicate that steric hindrance, caused by branched alkyl groups<sup>97-99</sup> in the side chain of the amino acid composing the switch element, significantly decreases the hydrolysis rate of the ester bond at 37°C and to a lesser extent at 25°C.

These results provide significant information on the handling of switch-peptides, information that is of particular importance for the work done in the context of this thesis. Notably, it proves that significant hydrolysis does not occur before O to N acyl migration is complete. It also provides us with valuable information on the time frame in which switch elements in the  $S_{\text{off}}$  state remain stable in solution at various pH and temperature. It is particularly important to know the ability of switch-peptides for remaining in an unfolded conformation in the  $S_{\text{off}}$  state. Finally, these results validate the foundations of the switch concept.



### 3. Studying the folding mechanism of the full length amyloid $\beta$ peptide using switch-peptides

#### 3.1. Background and design

As well known from systematic research on  $\beta$ -sheet forming oligopeptides, a detailed investigation of these processes is strongly hampered by the strong tendency of the involved peptides for spontaneous self-assembly and aggregation, limiting their experimental accessibility<sup>100</sup>. Moreover, Protein folding is a difficult process to simulate with classical dynamics as secondary structures can form in microseconds and because this process involves an ensemble of transition states difficult to monitor with the existing techniques<sup>101-103</sup>. To overcome this intrinsic problems in the preparation and investigation of  $\beta$ -sheet forming peptides, we have seen in the introduction chapter that our laboratory has recently developed a new concept<sup>80, 100, 104</sup>, called the switch concept. Here, we apply this concept to amyloid  $\beta$  1-42 peptide. This new generation of amyloid  $\beta$  switch-peptides enables us to start from a flexible, unfolded precursor (switch-peptide in the  $S_{\text{off}}$  state) *in situ*. Triggering of the switch elements by removal of the protecting group **Y** allows a spontaneous O to N acyl migration, re-establishing the native polyamide backbone and setting off peptide folding ( $S_{\text{on}}$ ) (Figure 27). This versatile method allows to follow via different techniques the early folding events and the structure onset as well as evolution of the molecule “*in statu nascendi*” (ISN).

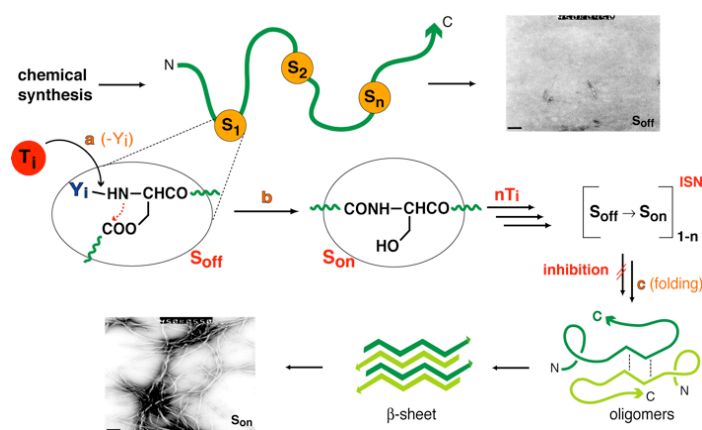


**Figure 27.** Amyloid  $\beta$  switch-peptide as folding precursors: consecutive triggering of O, N acyl migrations in switch-peptides ( $S_{\text{off}}$ ) for the onset ( $S_{\text{on}}$ ) of peptide folding and self-assembly in statu nascendi (ISN) of the folding molecule<sup>104</sup>.

Simultaneously, the use of pH-induced O,N-acyl migrations for accessing “difficult sequences” has been independently described by the groups of Kiso<sup>105</sup> and Bienert<sup>106</sup>.

Our main goal resides in the identification of nucleation sites (“hot spots”) for fibril formation in A $\beta$  sequences as well as to be able to follow its early aggregation steps. To this end, we explore in this chapter four different A $\beta$  switch-peptides containing different orthogonal switch elements for potential applications *in vitro* and *in vivo*.

As A $\beta$  possesses two Serine residues at positions 8 and 26 of its sequence and we know that the Serine at position 8 is far away from the critical part of the sequence, in a first generation, a switch-peptide was designed with one switch at position 26 (peptide **20**). The rationale for choosing this position for the switch element lies in the findings by Telpow et al.<sup>107</sup> and Lührs et al.<sup>54</sup> that residues Val24-Lys28 form a turn nucleating the intramolecular folding of A $\beta$  monomer and from this step, subsequently assemble into A $\beta$  oligomers.

In a second generation of A $\beta$  switch-peptides, an additional switch element was added at the C-terminus of the A $\beta$  sequence by replacing Gly37 with a Ser. It seems very appropriate to place a switch element S at this position since it has been demonstrated recently by the NMR-based 3D structure<sup>54</sup> that the C-terminal segment constitutes the core structure of A $\beta$ (1-42) fibrils (peptide **21** & **22**). This modification should not modify the folding behavior of A $\beta$ , the side chain of residue 37 being oriented outside of the  $\beta$ -strands (Figure 16).

In a third generation, the switch-element at position 26 was replaced by a  $\Psi$ Pro as solubilizing agent during the synthesis and only one switch element was kept at the C-terminus part (S<sup>37</sup>) of the sequence (peptide **23**).

We have explored a series of orthogonal triggering systems using chemical and enzymatic methodologies<sup>81</sup> (Figure 28) for incorporation in A $\beta$  in order to identify nucleation sites for fibrillogenesis in the sequence. Due to their proteinogenic cleavage sites, enzymatic triggering is particularly useful for modulating the O,N-acyl migration step *in vitro*. Similarly, photolytically cleavable N-protecting groups have been explored and have proved their utility in switch-peptides.

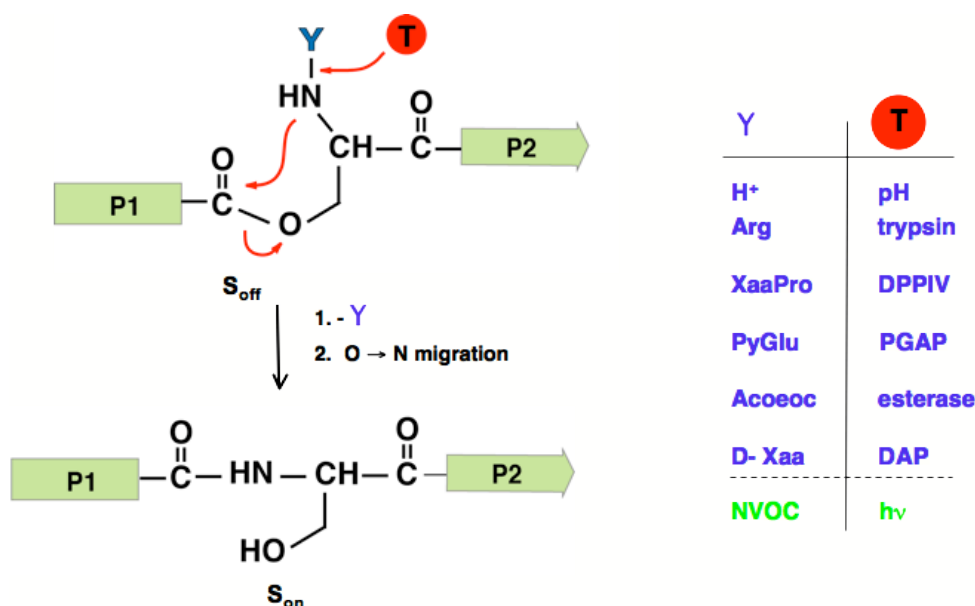
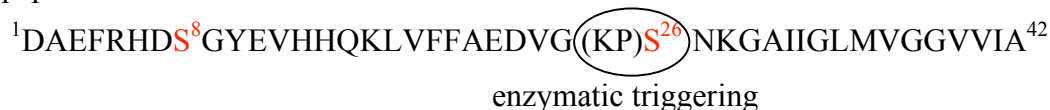


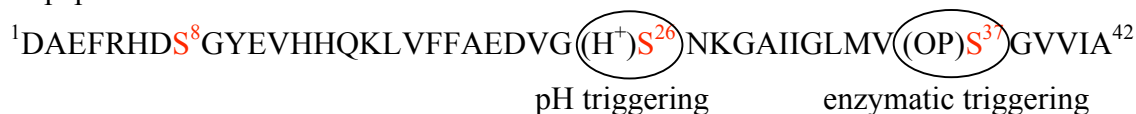
**Figure 28.** Orthogonal triggering systems. The *N*(*Y*)-protected switch-peptide containing an *O*-acyl isoserine (*S<sub>off</sub>* state) as *S*-element is transformed to native state (*S<sub>on</sub>*) by chemical (*hν*, pH) or enzymatic cleavage of *Y*, triggering spontaneous intramolecular acyl migration at physiologic pH<sup>81</sup>.

Using these orthogonal protecting groups, the following four Aβ switch-peptides were synthesized and are investigated in this chapter:

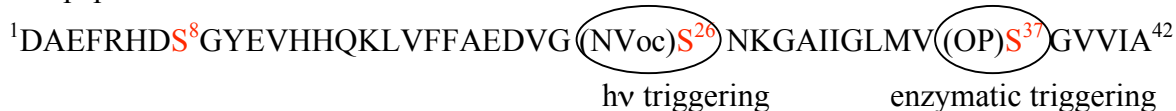
- peptide 20:



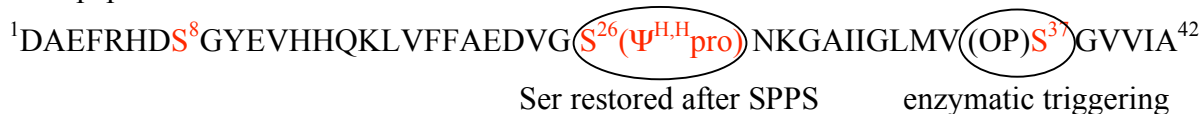
- peptide 21:



- peptide 22:

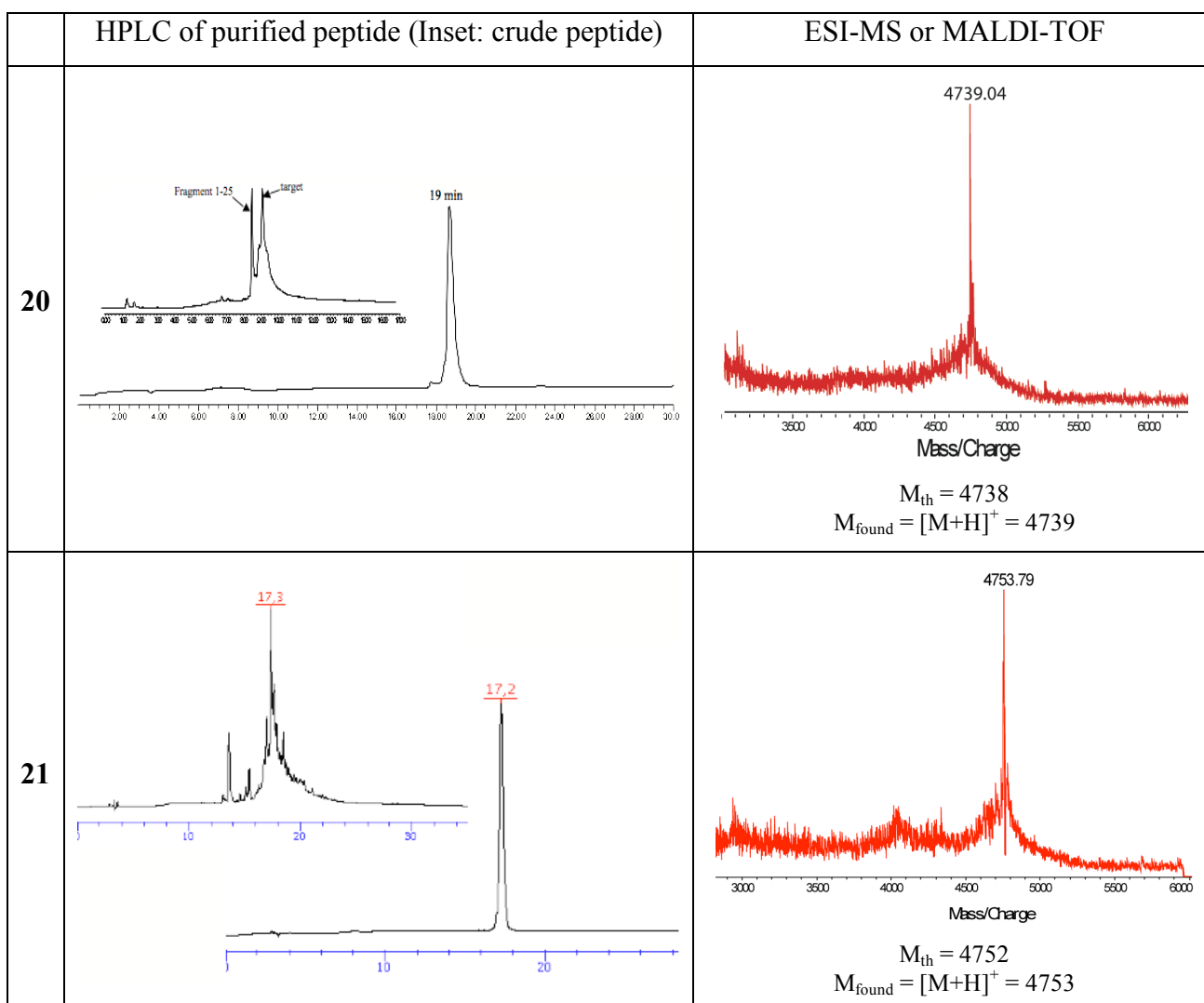


- peptide 23:



### 3.2. Synthesis and analytical data

The A $\beta$  derived switch-peptides were synthesized by solid phase peptide synthesis using the Fmoc/tBu strategy on a preloaded NovaSyn TGA resin based on tentagel with a low capacity (loading 0.23 mmol/g) (see experimental part). Cleavage of the peptides from the resin was achieved by using a mixture of TFA/TIS/EDT/H<sub>2</sub>O 94:2:2:2 (one hour, twice). Precipitation in cold ether gave the crude switch-peptides (Figure 29, insets). The peptides were well soluble in water and were purified by semi-preparative HPLC using a C<sub>8</sub> column. The obtained peptides were analyzed by analytical HPLC (> 95% purity) and mass spectroscopy. The HPLC chromatograms and mass spectra of the purified compounds are depicted in Figure 29:





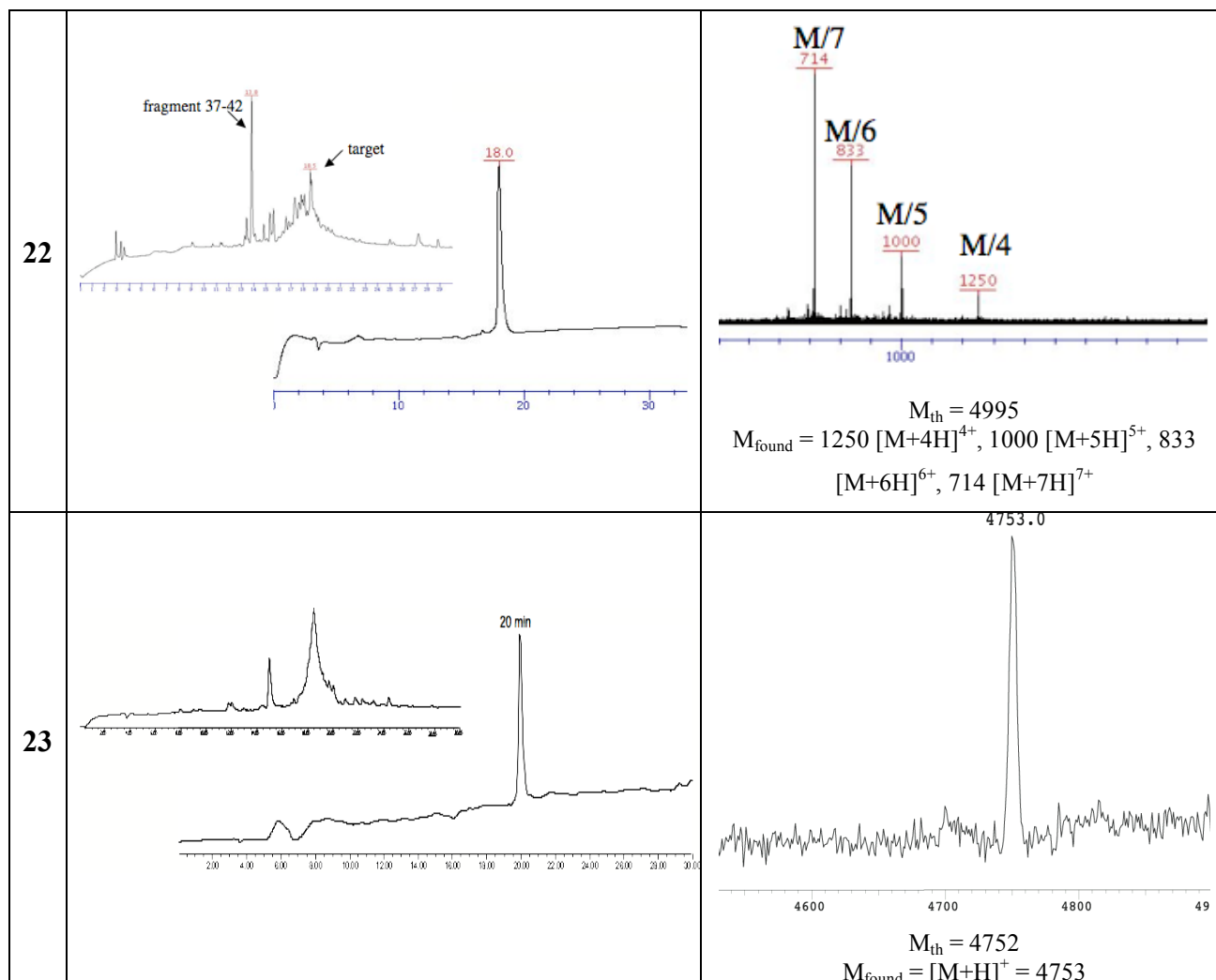


**Figure 29.** Characterization of A $\beta$  analogs by HPLC ( $C_8$  column, gradient 0-100% A in 30 min) and Mass Spectroscopy (ESI/MS or MALDI-TOF).

### 3.3. Stability studies

To assess the stability of the different amyloid derived switch-peptides towards aggregation, they were incubated at 37°C for two to three days in their  $S_{off}$  states. Electron microscopy, ThT fluorescence and CD spectroscopy were used to measure and control the morphology of the peptide after each incubation period.

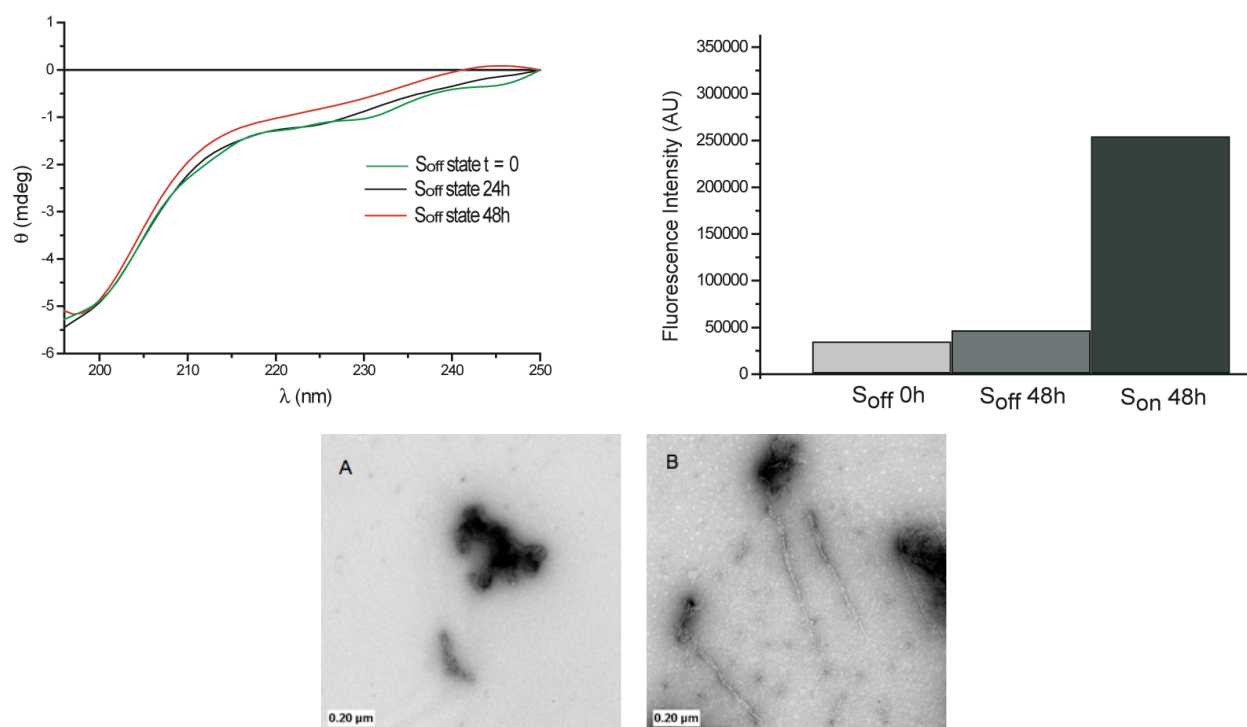


**Figure 30.** CD profile of peptide **23** ( $S_{off}$  state) after 24h and 48h at 37°C in Tris buffer pH 7.4 (upper left). ThT fluorescence intensity of peptide **23** in  $S_{off}$  and  $S_{on}$  states after 48h incubation at pH 7.4, 37°C (upper right). EM images of the peptide in the  $S_{off}$  state after 24h (A) and 48h (B) at pH 7.4, 37°C (bottom).

CD studies of peptide **23** ( $S_{off}$  state) demonstrate that the peptide remains in a flexible random coil conformation after 48 hours at 37°C in pH 7.4 Tris buffer. Moreover, ThT fluorescence level after 48h was as low as at time zero; EM images revealed the presence of only minor oligomeric structures under these conditions, confirming that peptide **23** in its  $S_{off}$  state does not form amyloid-like fibrils even after a long incubation period (Figure 30).

Stability towards aggregation of peptides **20** and **22** was assessed by incubating them at 37°C in  $H_2O$  at 200  $\mu$ M and in pH 7.4 Tris buffer at 25  $\mu$ M for two to three days. EM studies revealed that peptide **22** comprising 2 switch elements did not form fibrils after 3 days in  $H_2O$  but showed a diminished stability at physiological conditions (oligomeric structures were observed after 24h) (Figure 31).

EM studies of peptide **20** comprising only one switch at position 26 of its sequence showed fibril-like structures after two days of incubation in  $H_2O$ ; nevertheless, the peptide was stable under these conditions for 24h. Moreover, as for peptide **22**, the stability towards aggregation of peptide **20** was diminished at pH 7.4, EM images revealed a significant amount of oligomers after 24h and short fibrils after 48h (Figure 31).

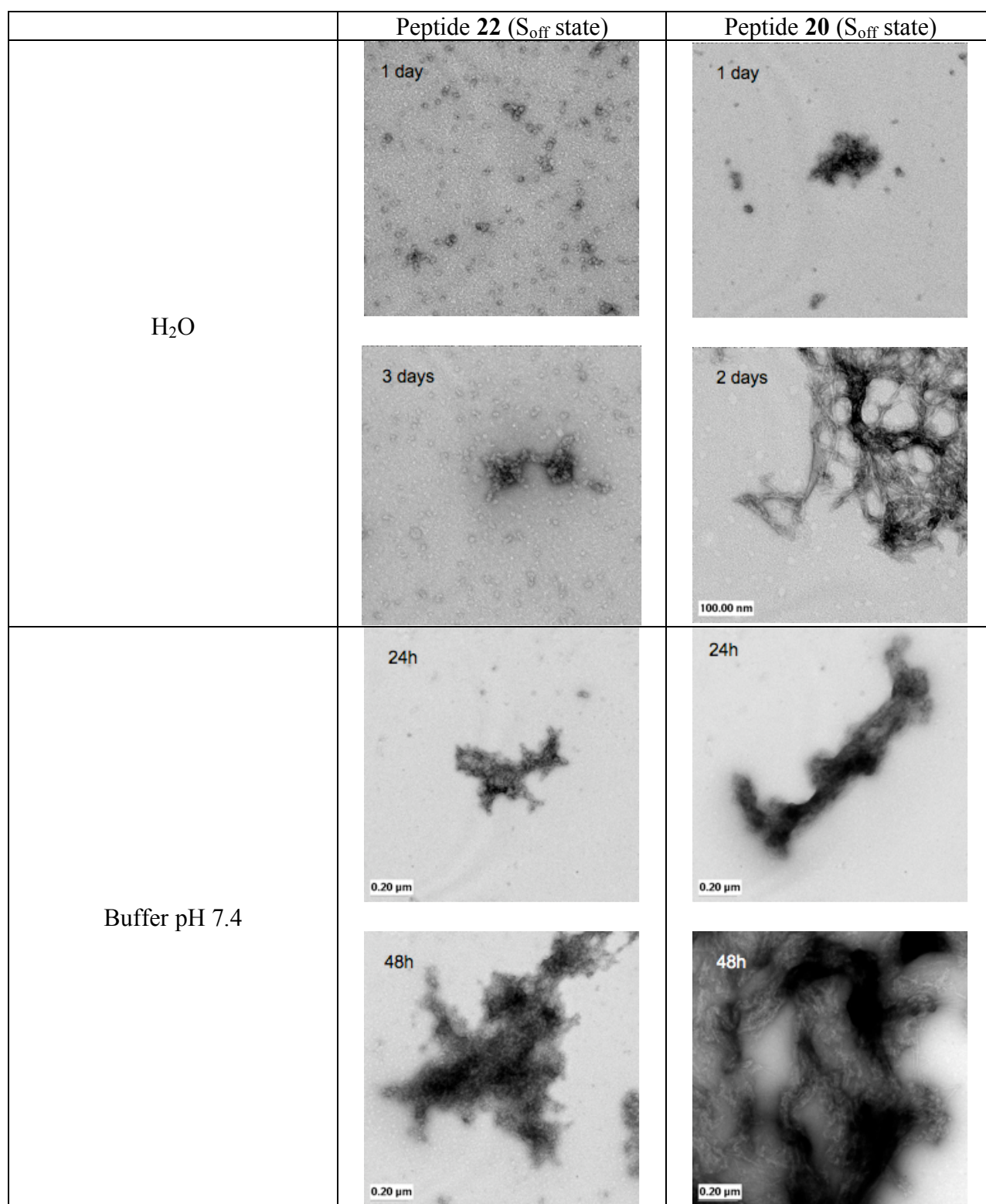


**Figure 31.** Electron Microscopy of peptide 20 and 22 in their  $S_{off}$  state after 24h, 48h or three days incubation at 37°C in H<sub>2</sub>O (peptide concentration = 200 μM) and in Tris buffer pH 7.4 (peptide concentration = 25 μM).

### 3.4. Folding and aggregation studies

The folding and aggregation process of the amyloid  $\beta$ -derived switch-peptides **20-23** were investigated by analytical HPLC, CD spectroscopy, EM and ThT fluorescence. The results are depicted below.

#### Peptide **20**

Switch-peptide **20** possesses one S element at position 26, which can be triggered by the enzyme DPPIV. To study the enzyme-induced acyl transfer, peptide **20** was dissolved in a solution of H<sub>2</sub>O/Tris pH 7.4 (30 mM) (1:3) and 150 mM NaCl at a concentration of 200  $\mu$ M, 20  $\mu$ L of DPPIV (0.02 unit) were added to the mixture prior to incubation at 37°C. At various intervals, 20  $\mu$ L aliquots were taken from the sample and injected to analytical HPLC. Figure 32 shows the HPLC chromatograms of the chemical conversion of switch-peptide **20** from its S<sub>off</sub> to its S<sub>on</sub> state. However, monitoring of the conversion resulted in broadening and eventual vanishing of the S<sub>off</sub> peak, which was due to the rapid precipitation of the peptide, accompanied by an increase in solution turbidity observed in the vial. As precipitation occurs before the completion of O to N acyl migration, monitoring the conversion by HPLC is difficult (see Figure 32).

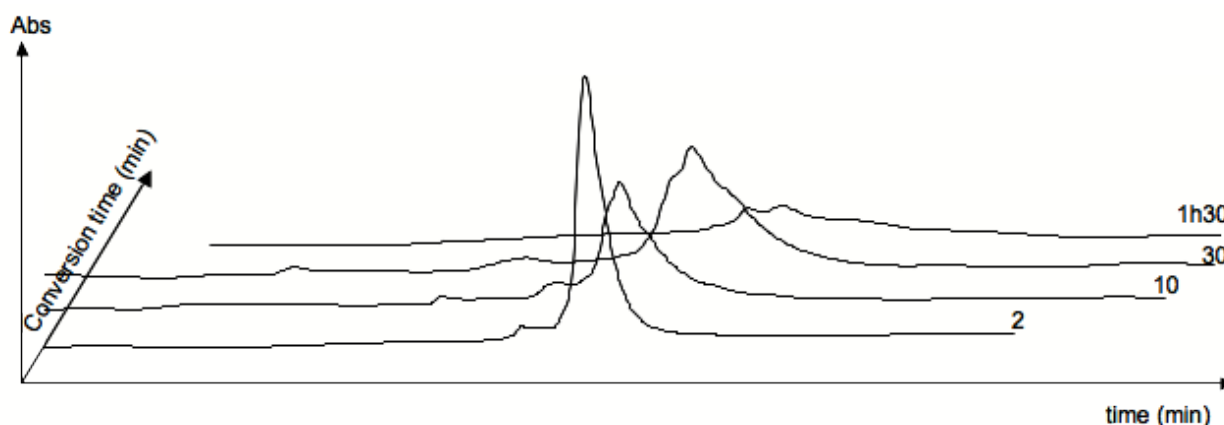


**Figure 32.** HPLC chromatograms of peptide **20** obtained for the DPPIV-triggered acyl transfer at S<sup>26</sup>.

However, we attempted to further investigate conformational transitions and fibril formation of peptide **20** by circular dichroism, electron microscopy and ThT fluorescence. To this end, the peptide was first dissolved in a solution of H<sub>2</sub>O/Tris pH 7.4/TFE 35:60:5 ( $c = 25 \mu$ M); TFE was added to favor the solubility after the transition from rc to  $\beta$ -sheet. Unexpectedly, we observe at time zero a CD spectrum characteristic for a  $\beta$ -sheet with a strong negative cotton effect at  $\lambda =$

218 nm (Figure 33, red curve). Obviously, the content of TFE (5%) promoted  $\beta$ -sheet formation in the  $S_{\text{off}}$  state. To overcome this problem, a mixture containing 2.5% TFE was prepared and at time zero, the spectrum was characteristic of a random coil with a negative cotton effect at  $\lambda = 198$  nm (Figure 33, black curve).

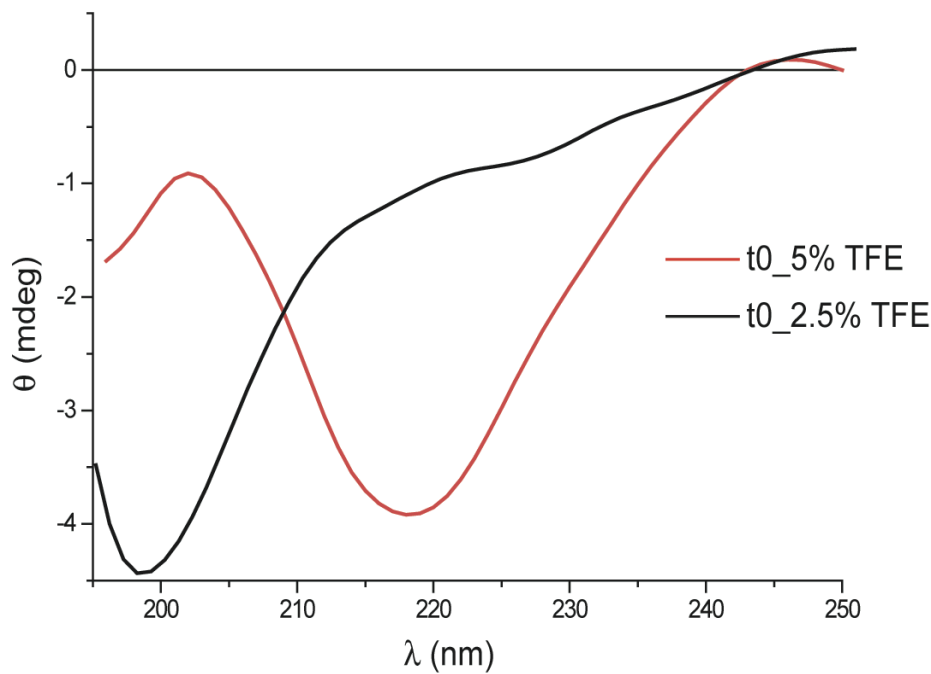


**Figure 33.** CD spectra of peptide **20** in the  $S_{\text{off}}$  state at pH 7.4 with 5% or 2.5% TFE.

Subsequently, acyl migration was triggered in the sample with 2.5% TFE by the addition of 2  $\mu\text{L}$  DPPIV enzyme (0.002 unit) and the sample was incubated at 37°C. The conformational transition was relatively slow, showing a transformation from rc to  $\beta$ -sheet after 24h. The  $\beta$ -sheet transition was accompanied by a significant decrease in negative cotton effect at  $\lambda = 218$  nm ( Figure 34, green curve), further demonstrating the high propensity of the peptide for precipitation. EM images revealed the presence of oligomeric structures after 24 and 48h of incubation and, short fibrillar morphology of the peptide was only observed after 4 days of incubation. A low remaining concentration of peptide in solution may have accounted for the slow onset of fibrillogenesis found with this peptide. It is indeed well-known that fibrillogenesis is concentration dependent.

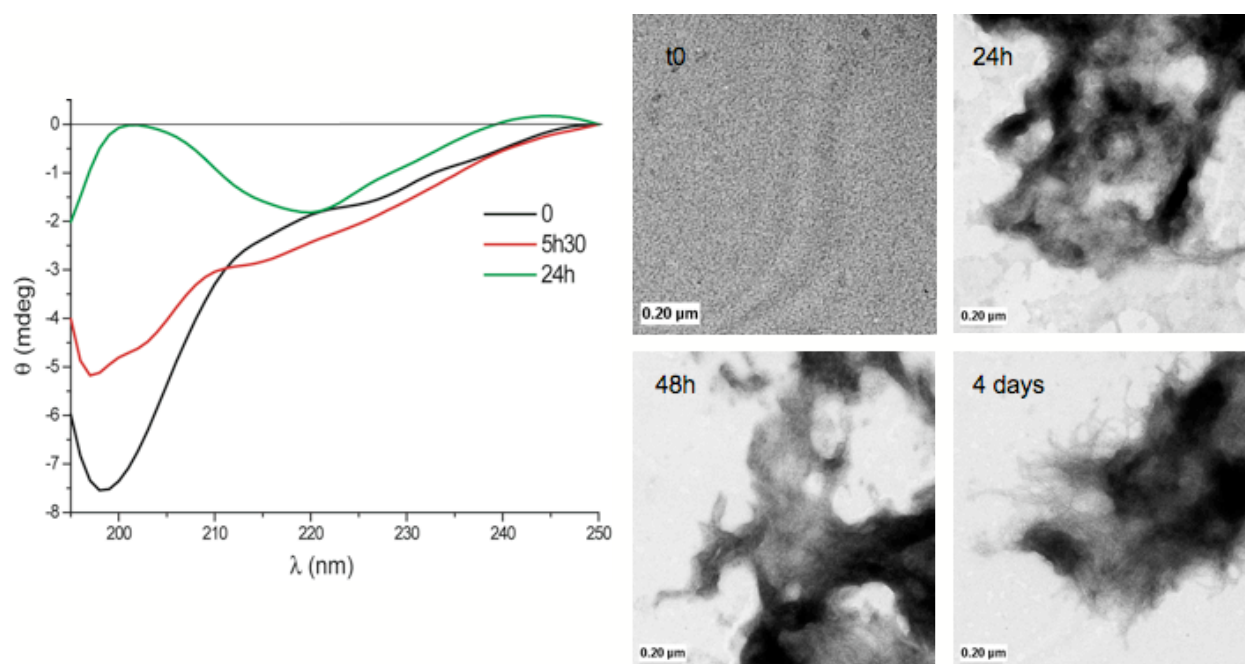


**Figure 34.** Conformational transition upon O to N acyl migration of peptide **20** monitored by CD in Tris buffer pH 7.4/ 2.5% TFE at 37°C (left). Fibril formation followed by EM over a period of 4 days (right).

Because peptide **20** was difficult to investigate due to its instability towards precipitation (see stability studies above) and its rapid precipitation during acyl migration, a new generation of amyloid  $\beta$ -derived switch-peptides (peptides **21** and **22**) comprising a second switch element at the C-terminus of the sequence (position 37) was designed.

### Peptide **21**

In switch-peptide **21**, the central  $S^{26}$  is triggered by adjusting the pH to physiological pH. To study the pH-induced acyl transfer, switch-peptide **21** (200  $\mu\text{M}$ ) was dissolved in a solution of  $\text{H}_2\text{O}$ /Tris pH 7.4 (30 mM) (1:3) and 150 mM NaCl. At various intervals, 20  $\mu\text{L}$  aliquots were taken, quenched with 10  $\mu\text{L}$  HCl 1M and injected to analytical HPLC. Figure 35 represents the acyl migration after triggering  $S^{26}$ , restoring native  $\text{A}\beta(1-36)$ . The chromatogram shows a gradual decrease in absorbance of the  $S_{\text{off}}$  peak and concomitant increase in absorbance of the  $S_{\text{on}}$  peak. This time no precipitation was associated with the activation of  $S^{26}$  suggesting that  $\text{A}\beta(1-36)$  has no tendency for spontaneous aggregation. EM imaging confirmed a substantial stability found in peptide **21** after 48h, showing that the additional switch at  $S^{37}$  prevents it from undergoing fibrillogenesis.

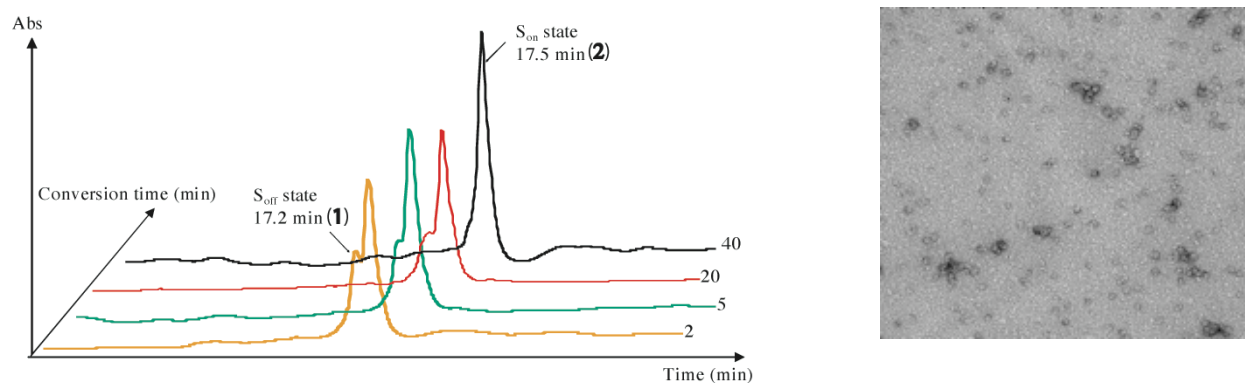


**Figure 35.** Overlay of chromatograms obtained for the pH-induced acyl transfer at switch  $S^{26}$  in peptide **21**. Triggering of  $S^{26}$  restores the regular amide bond  $A\beta(1-36)$  (left). EM image of peptide **21**  $S^{26}_{on}/S^{37}_{off}$  after 24h.

To trigger switch element  $S^{37}$ , enzyme DPPIV (0.002 unit) was added to the solution; O,N-acyl migration was again monitored by analytical HPLC by injecting 20  $\mu$ L aliquots at various time points (Figure 36). Here, we observe a gradual decrease in absorbance of peak 2 ( $S^{26}_{on}, S^{37}_{off}$ ) and the increase in absorbance of a new peak (3) corresponding to  $S^{26}_{on}, S^{37}_{on}$ . Interestingly, by the subsequent enzymatic switching on of the C-terminal segment (37-42), the characteristic phenomena observed for native  $A\beta(1-42)$ , *i.e.* aggregation and precipitation are initiated as monitored by a drastic decrease in absorbance of peak 3 and its complete disappearance after a few hours.

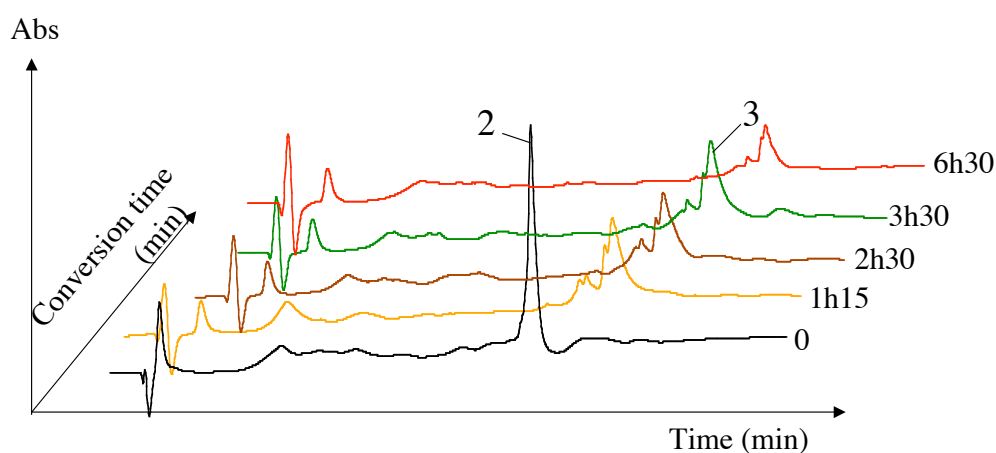


**Figure 36.** Overlay of the HPLC chromatograms obtained for the DPPIV-triggered O,N-acyl transfer at  $S^{37}$  in switch-peptide **21**. At time zero,  $S^{26}$  is on and  $S^{37}$  is off, after 1h15, two peaks are observed corresponding to  $S^{26}_{on}, S^{37}_{off}$  (peak 2) and after restoring the complete  $A\beta(1-42)$  sequence, peak 3 ( $S^{26}_{on}, S^{37}_{on}$ ).

In parallel, the conformational transition was monitored by CD and EM at 25  $\mu\text{M}$ , 37°C in Tris buffer pH 7.4 / 5% TFE. At time zero, the curve corresponding to  $S^{26}_{\text{on}}$ ,  $S^{37}_{\text{off}}$  was characteristic of a random coil, which evolved to a  $\beta$ -sheet conformation after addition of DPPIV enzyme (Figure 37).

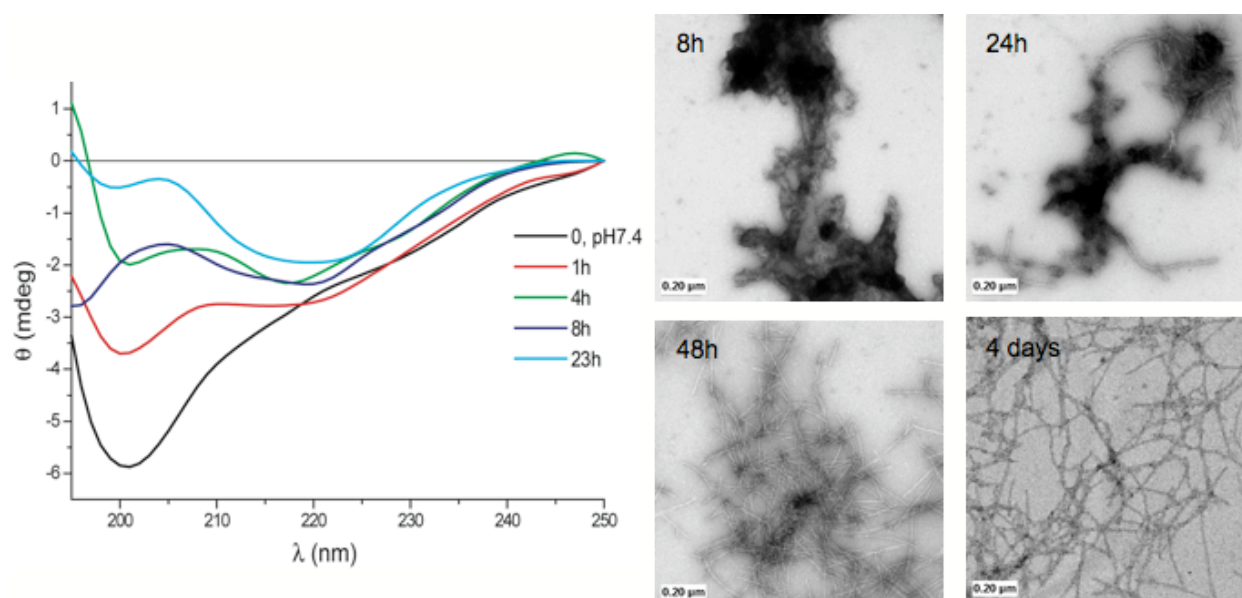


**Figure 37.** Conformational transition upon pH- and enzyme-triggered acyl migrations from a random coil ( $S_{\text{off}}$ ) to a  $\beta$ -sheet ( $S_{\text{on}}$ ) of switch-peptide **21** monitored by CD in Tris buffer pH 7.4/ 5% TFE at 37°C (left). Fibril formation followed by EM over a period of 4 days (right).

EM studies show that oligomers are formed after 8h and protofibrils start to grow after 24h, giving rise to amyloid-like fibrils after 2 days and reaching maturation after 4 days. These observations were confirmed by ThT fluorescence (Figure 41), where peptide **21** bound ThT dye and reached a plateau after 2 days.

With peptide **21**, the sequential triggering of the S elements was restricted to a particular order, i.e.  $S^{26}$  had to be switched on first by raising the pH to 7.4; in a second step the enzyme, only being active between pH 7 and 8, could be added to trigger  $S^{37}$  at the C-terminus of the peptide. Given this order of switching on the S-elements, it was thus not possible to study independently the impact of the C-terminal part on the folding of A $\beta$ ; therefore, peptide **22**, containing two orthogonal switches (at position 26 and 37 as well) was designed. Peptide **22** possesses one switch protected by NVoc group (photolytic cleavable group) at  $S^{26}$  and one switch at  $S^{37}$



cleavable by the enzyme DPPIV. In this particular case, we do not have to follow a specific order, i.e. we can trigger either  $S^{37}$  first or vice versa.

### Peptide 22

To follow O to N acyl migration, peptide **22** was subjected to HPLC analysis under the same conditions as previously for peptide **20** and **21**. Here,  $S^{37}$  was triggered first ( $S^{26}$  remained in the  $S_{\text{off}}$  state). From HPLC monitoring, we can see the disappearance of peak 1 ( $S^{26}_{\text{off}}, S^{37}_{\text{off}}$ ) and the appearance of the peak 2 ( $S^{26}_{\text{off}}, S^{37}_{\text{on}}$ ) over time. Interestingly, by triggering first  $S^{37}$  and letting  $S^{26}$  off, i.e. switching on the C-terminal segment (37-42), we already observe a significant decrease in absorbance and complete disappearance of the  $S_{\text{on}}$  peak after a few hours, indicating that precipitation and aggregation were already initiated. This gives a first experimental proof of the importance of A $\beta$  C-terminal part for folding and aggregation of A $\beta$ (1-42).

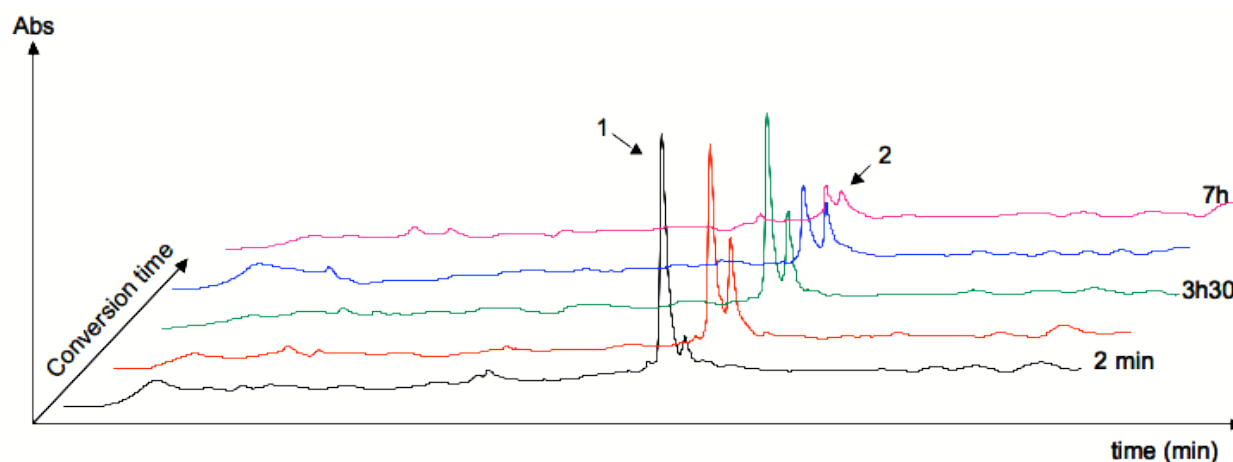


**Figure 38.** HPLC chromatograms of acyl migration of  $S^{37}$  in peptide **22**. Peak 1 corresponds to switch-peptide **22** in the  $S_{\text{off}}$  state, peak 2 (more hydrophobic) represents the peptide after acyl migration at switch  $S^{37}$ .

To further examine the importance of the C-terminus on folding and aggregation, peptide **22** was subjected to CD, EM and ThT studies. The peptide was dissolved in H<sub>2</sub>O/Tris buffer pH 7.4/ 2.5% TFE to a final concentration of 25  $\mu$ M. The switch at position  $S^{37}$  was triggered by the addition of 2  $\mu$ L enzyme DPPIV (0.002 unit) at 37°C. At time zero, a strong negative cotton effect at  $\lambda = 198$  nm characteristic of a random coil is observed (Figure 39, black curve). The signal evolves over time towards a spectrum corresponding to a  $\beta$ -sheet structure and after 7h30 the transformation is nearly complete (Figure 40, blue curve). Moreover, EM images revealed

that significant amounts of oligomers were formed after 6 hours and amyloid-like fibrils were found after two days. This result confirms that the C-terminus part of A $\beta$ (1-42) represents a nucleation site for folding and aggregation and that even by letting the position S<sup>26</sup> off, aggregation occurred and was as fast as observed for peptide **21**.

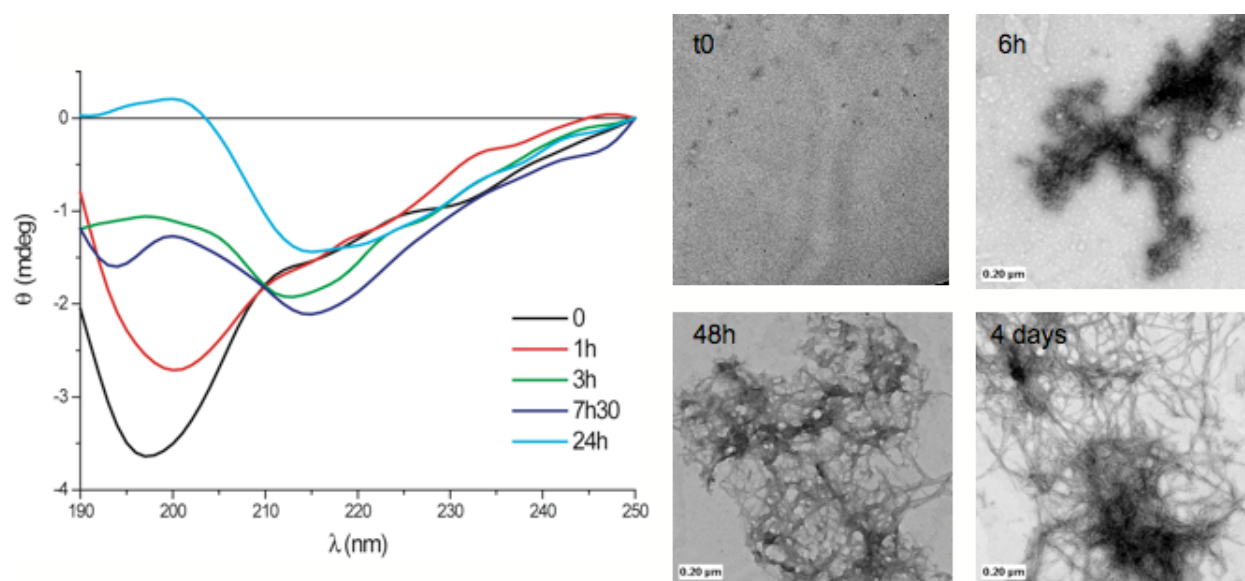


**Figure 39.** Conformational transition upon enzyme-triggered acyl migration from a random coil ( $S_{off}$ ) to a  $\beta$ -sheet ( $S_{on}^{37}$ ) of switch-peptide **22** monitored by CD in Tris buffer pH 7.4/ 2.5% TFE at 37°C (left). Fibril formation followed by EM over a period of 4 days (right).

As we have demonstrated that the switch element at position 26 did not seem to have a big impact on folding and aggregation of A $\beta$ (1-42) compared to switch element at position 37, the design of a peptide containing a single switch element at position 37 (peptide **23**) seemed to be the most challenging for elucidating folding and aggregation in comparison to previous peptides.

### Peptide **23**

As before, peptide **23** was subjected to CD, EM and ThT studies to evaluate its folding process at physiological conditions and at a concentration of 25  $\mu$ M. To follow the transition from random coil to  $\beta$ -sheet by CD, 5% of TFE was added to the solution. As already seen from the stability studies (Figure 30) peptide **23** adopts a random coil conformation for at least two days without fibril formation. Here, at time zero, the peptide shows a CD spectrum characteristic of a flexible random coil conformation. On triggering O,N-acyl migration by adding 2  $\mu$ L DPPiV, peptide **23**

undergoes a conformational transition to a  $\beta$ -sheet structure (negative cotton effect at  $\lambda = 220$  nm). EM studies revealed significant amounts of oligomers after 7h30 incubation and mature amyloid-like fibrils are formed after two days. These results clearly demonstrate that the C-terminus of A $\beta$ 1-42 plays a key role in the early step of misfolding.

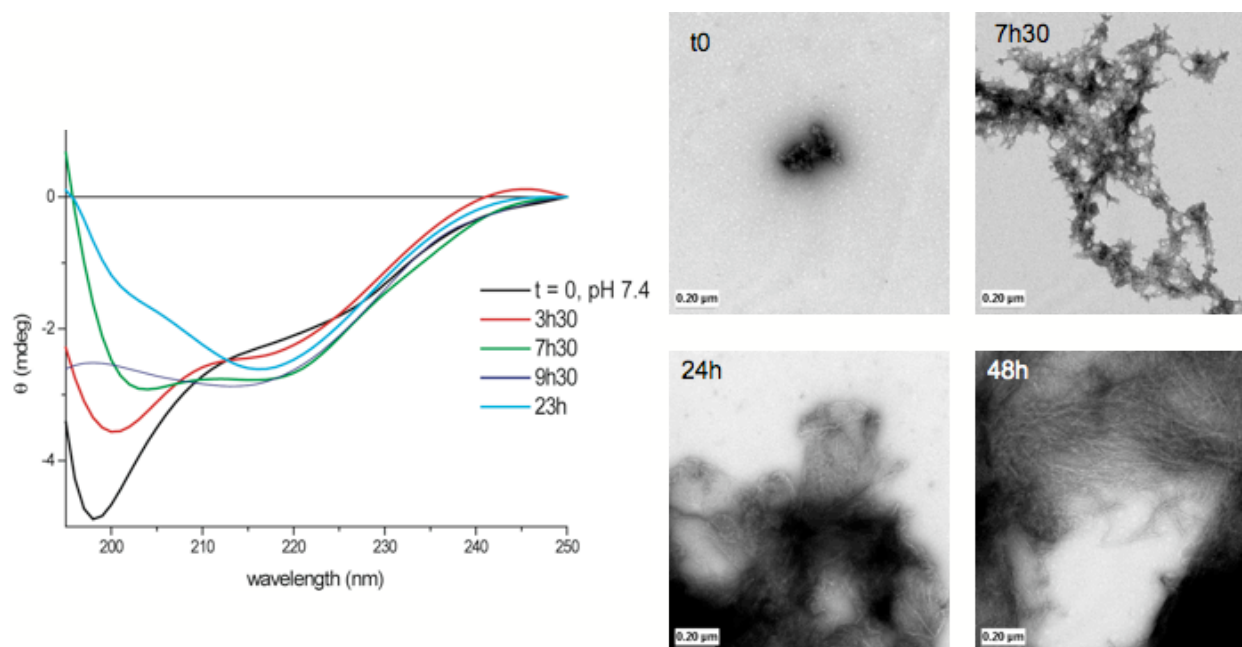


**Figure 40.** Conformational transition upon *O* to *N* acyl migration of peptide **23** (left) followed by CD in Tris buffer pH 7.4 at 37°C. Fibril formation followed by EM over a period of 4 days (right).

### 3.5. ThT kinetic comparison

In parallel to CD and TEM studies, the detection of fibril formation for the four A $\beta$ -derived switch-peptides was followed by ThT fluorescence. It is known that only multimeric fibrillar forms, not multiple  $\beta$ -sheet domains in native proteins, are fluorescent with ThT. Therefore, ThT is thought to interact specifically with amyloid fibrils; consequently, measuring the level of binding of ThT to fibrils is indicative for the kinetics of fibril formation.

In this experiment, the peptides were incubated under the same conditions as previously for the CD and EM studies.

We observe that peptide **20**, shown to have a high propensity for precipitation, does not show a strong fluorescent signal compared to peptides **21**, **22** & **23** (Figure 41), confirming our earlier finding that due to its rapid precipitation, the concentration of peptide **20** remaining in solution is too low to enable peptide for aggregation.

Figure 41 also shows that after triggering the two switch elements, peptide **21** binds ThT fluorescent dye in approximately the same degree as peptide **23** comprising one switch at position 37. For peptide **22**, in the state  $S_{\text{off}}^{26}$ ,  $S_{\text{on}}^{37}$ , we observe a lag phase to ThT binding but after two days a strong signal comparable to peptide **21**.

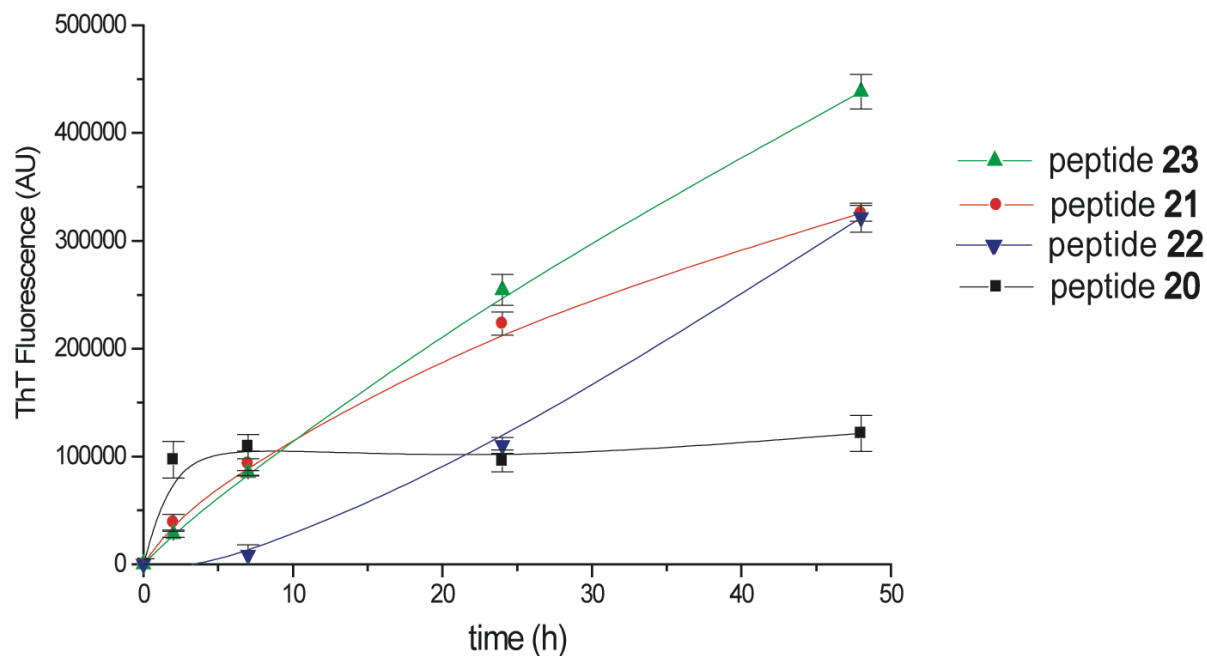


**Figure 41.** Kinetics of fibril formation for the four  $A\beta$ -derived switch-peptides monitored by ThT fluorescence.

### 3.6. Discussion

We have demonstrated that amyloid  $\beta$ -derived switch peptides are powerful tools to identify nucleation sites for fibril formation in A $\beta$  sequences and to follow its early aggregation steps.

The introduction of a single switch element at position 26 of A $\beta$  sequence facilitates the synthesis and the solvation of the peptide in aqueous media but is not sufficient to enable the investigation of O,N-acyl migration and the subsequent onset of  $\beta$ -structures and fibrillogenesis since the peptide precipitates immediately after triggering O,N-acyl migration. However, the incorporation of a second switch element at position S<sup>37</sup> allowed us to study in more detail the process of misfolding and thus to demonstrate that the C-terminal part of A $\beta$ (1-42), more particularly the segment A $\beta$ (37-42) is crucial for fibril formation and aggregation.

Moreover, we have demonstrated with peptide **23** that incorporating a single switch element at position 37 increases drastically the stability of A $\beta$  towards self-assembly, showing that disconnecting the C-terminal segment is sufficient to keep the peptide in an unfolded state.

These experimental results are in harmony with the 3D-structure of A $\beta$ (1-42) proposed by Lühns et al.<sup>54</sup> and confirm for the first time the important role of the C-terminus on the rate of fibril formation<sup>108</sup>.



#### ***4. Host-guest switch-peptides derived from A $\beta$ as a model for studying fibrillogenesis and for screening amyloid $\beta$ inhibitors in vitro.***

##### **4.1. Background**

Protein misfolding, such as found with A $\beta$  peptide in AD or  $\alpha$ -synuclein protein in PD, and its accompanying aspect in conformational transitions, has attracted a vast interest in various research fields.

For example, recent research suggests that conformational transitions of amyloid  $\beta$  precursor molecules into aggregated,  $\beta$ -sheet-type forms play a key role in the deposition of cerebral amyloid plaques characteristic of Alzheimer's disease.

It is also important to understand the mechanism of their formation starting from monomers because it is becoming increasingly clear that the nonfibrillar intermediates may be the toxic species in Alzheimer's disease<sup>40, 109-111</sup>.

It is thus of importance to find a method that could efficiently evaluate the influence of external factors such as temperature, pH, inhibitors or  $\beta$ -breakers on the propensity of a peptide to adopt a well-defined secondary structure. This method could then be applied to study the conformational transition of amyloid proteins from an unordered state into  $\beta$ -sheets.

This intrinsic problem of protein folding prompted Mutter et al. to apply the host-guest technique in combination with the concept of "switch-peptides" studying conformational transitions of peptide segments excised from their native sequence<sup>80, 112</sup>.

The host-guest approach was first introduced in peptide chemistry by Scheraga<sup>113</sup> in the early seventies. The method consists of incorporating guest residues into a host polypeptide sequence having the propensity to fold in an  $\alpha$ -helical structure to determine the helix-coil stability constants of the 20 naturally occurring amino acids. Few years later, Toniolo and Mutter et al.<sup>114-116</sup> used the host-guest technique to investigate the impact of guest amino acids (in particular Gly and Pro) on host peptide sequences having the potential to adopt both helical and  $\beta$ - structures. They were able to demonstrate that depending on the conformational preferences of the guest residue, the extension of an  $\alpha$ -helix forming host peptide could be blocked by a single guest

amino acid (notably Pro), or that a single guest amino acid inserted in to a  $\beta$ -sheet forming host peptide could destabilize the ordered conformation.

The hydrophobic A $\beta$ (16-20) sequence KLVFF of the A $\beta$  peptide is considered as a key region for nucleating self-assembly and oligomerization and therefore the formation of fibrils. However, the pentapeptide A $\beta$ (16-20) alone does not form fibrils by itself and thus, residues flanking this region are important for A $\beta$  fibril formation. Tjernberg et al.<sup>117</sup> identified the shortest fibril-forming A $\beta$  fragment as being the sequence HQKLVFFAED corresponding to the A $\beta$ (14-23). Even though this decapeptide forms fibrils, it does not give CD spectra characteristic for  $\beta$ -sheet formation probably due to its low overall propensity for the onset of  $\beta$ -sheets. To elucidate the role of this core region in  $\beta$ -sheet and fibril formation, we designed a host-guest system where A $\beta$ (14-24) is flanked between two  $\beta$ -sheet promoting (Leu-Ser)<sub>n</sub> oligomers as host sequences<sup>104, 118</sup>. Upon acyl migration i.e. in restoring the regular backbone of the host-guest peptide, it is possible to follow the ISN-induction of conformational transitions from random-coil to  $\beta$ -sheet. Consequently, host-guest switch-peptides may be used to study the early folding events of A $\beta$  as a tool for the screening of A $\beta$  inhibitors and  $\beta$ -breakers, bypassing, the difficulties of handling native A $\beta$ (1-42).

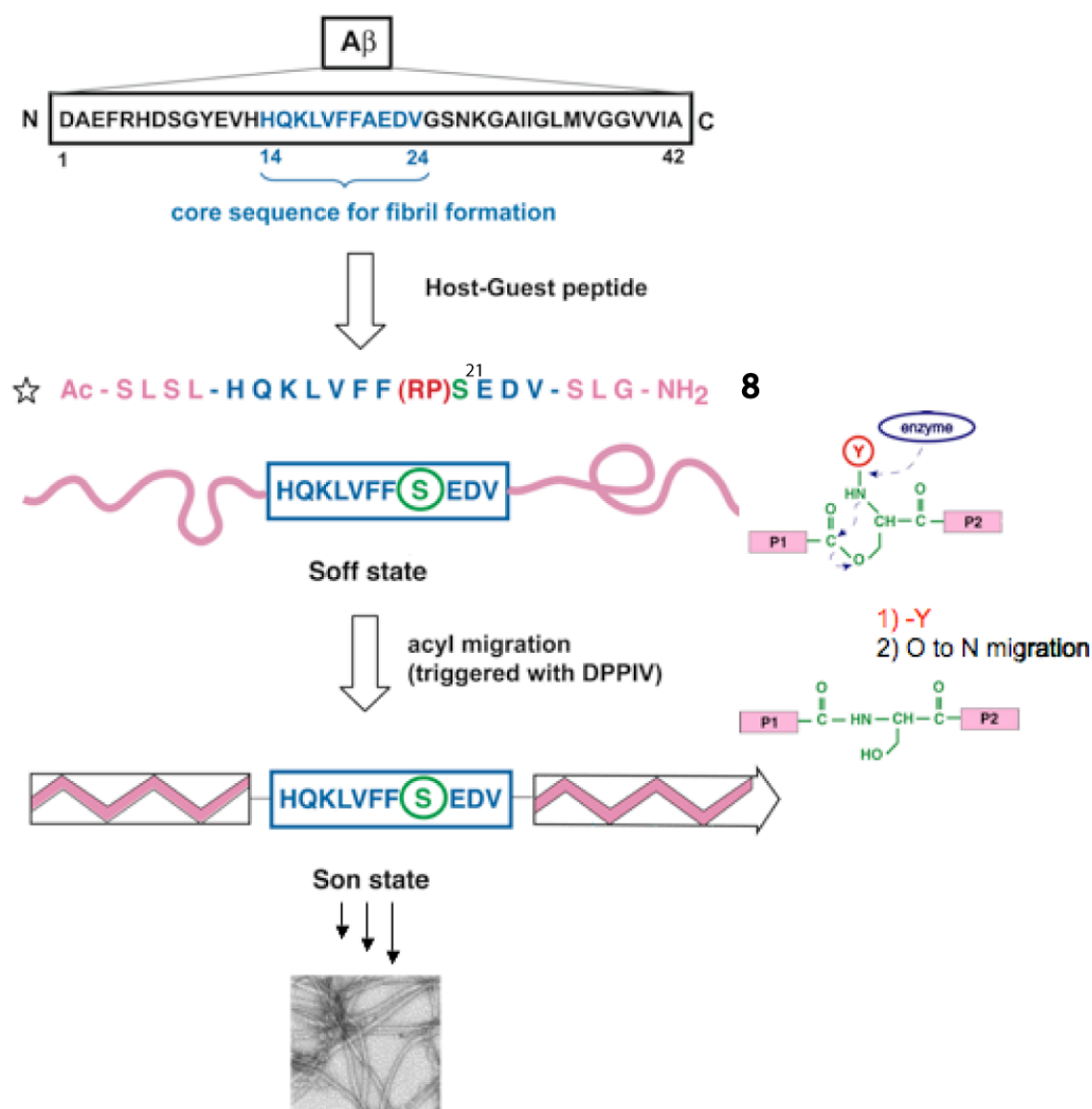
#### 4.2. Design of host-guest switch-peptides

Two amyloid  $\beta$ -derived host-guest switch-peptides are designed:

- Peptide **8** (Figure 42), containing a single switch at position 21 of [Ser<sup>21</sup>]A $\beta$ (14-24) that can be triggered by the enzyme DPPIV. To generate a switch element, Ala 21 has been replaced by a Ser residue.
- Peptide **9** (Figure 52) featuring two switch elements at the N- and the C- terminus of the guest sequence A $\beta$ (14-24).

Peptides **8** and **9** were subsequently used to investigate the spontaneous intramolecular O to N acyl migration as monitored by HPLC, the induction of folding events such as self-assembly,  $\beta$ -sheet (CD) and fibril formation (EM) of the molecule and their use as a screening kit system for A $\beta$  fibril inhibitors and  $\beta$ -sheet breakers.

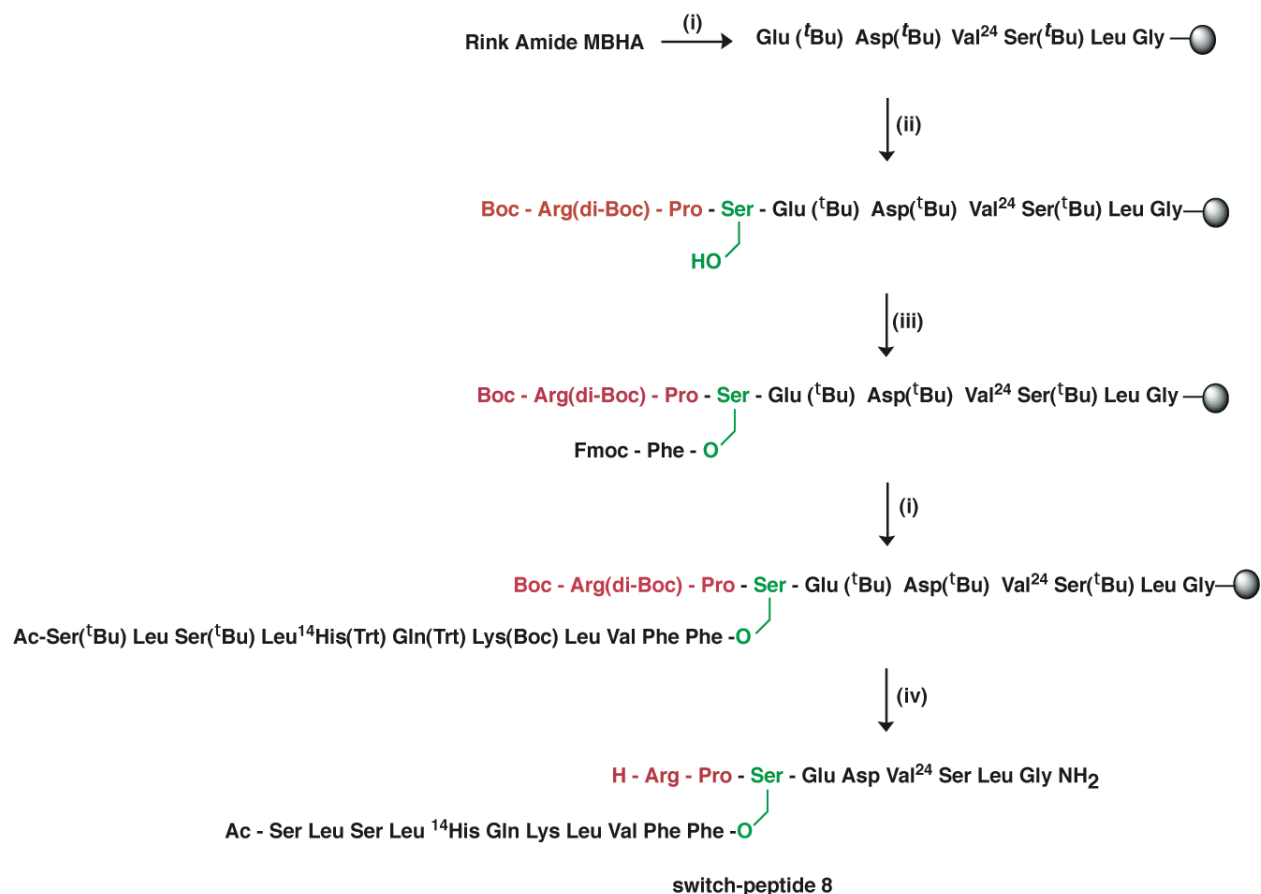


4.2.1. Host-guest switch-peptide **8** containing a single switch element S

**Figure 42.** Application of the concept of switch-peptides to host-guest peptide [ $\text{Ser}^{21}$ ] $\text{A}\beta(14-24)$  (**8**) with a single switch element at position 21. In the  $S_{\text{off}}$  state, the peptide is designed to adopt a random coil conformation; after addition of the enzyme DPPiV, the peptide undergoes O,N-acyl migration, inducing peptide folding and self-assembly.

### Synthesis

The synthesis of peptide **8** was performed in collaboration with S. Dos Santos (PhD thesis 2005, EPFL). The peptide was assembled on Rink amide MBHA resin applying the Fmoc/<sup>t</sup>Bu strategy as depicted in Scheme 3.



**Scheme 3.** Solid phase synthesis of switch-peptide **8**. (i) standard solid phase peptide synthesis according to the Fmoc/<sup>t</sup>Bu strategy, (ii) Fmoc-Ser(OH)-OH, Boc-Arg(di-Boc)-OH and Fmoc-Pro-OH (30 min); (iii) Fmoc-Phe-OH (3eq), DIC (3eq), DMAP (0.5eq), DCM/DMF (4:1), 2h; (iv) TFA/TIS/H<sub>2</sub>O 95:2.5:2.5, 2x1h.

The synthesis was straightforward and the HPLC revealed a major peak identified as the target peptide **8** (Figure 43). Some deletion sequences were observed. After purification by preparative HPLC, **8** was obtained in a yield of ca 30% (>95% purity).

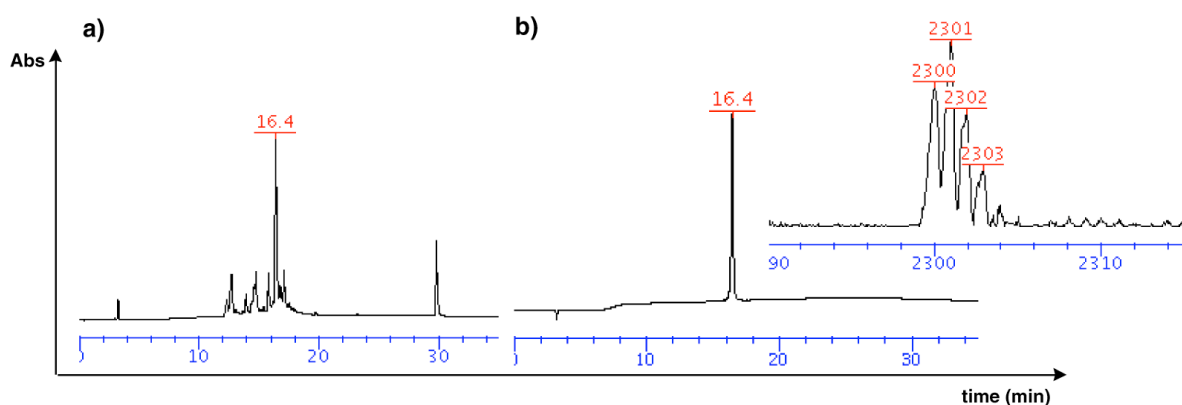


**Figure 43.** HPLC (C18, 0 to 100% A, 30 min) of crude and purified switch-peptide **8**, inset: MALDI-TOF of the purified compound ( $m/z = 2300 [M+H]^+$ ).

#### *Kinetic studies on folding and fibril formation by HPLC, CD, EM and ThT*

To follow the O to N acyl migration, peptide **8** was dissolved in Tris buffer pH 8 at a concentration of 400  $\mu$ M. Subsequently, enzyme DPPIV was added to the mixture. At various intervals, 20  $\mu$ L aliquots were taken and injected to analytical HPLC (Figure 44).

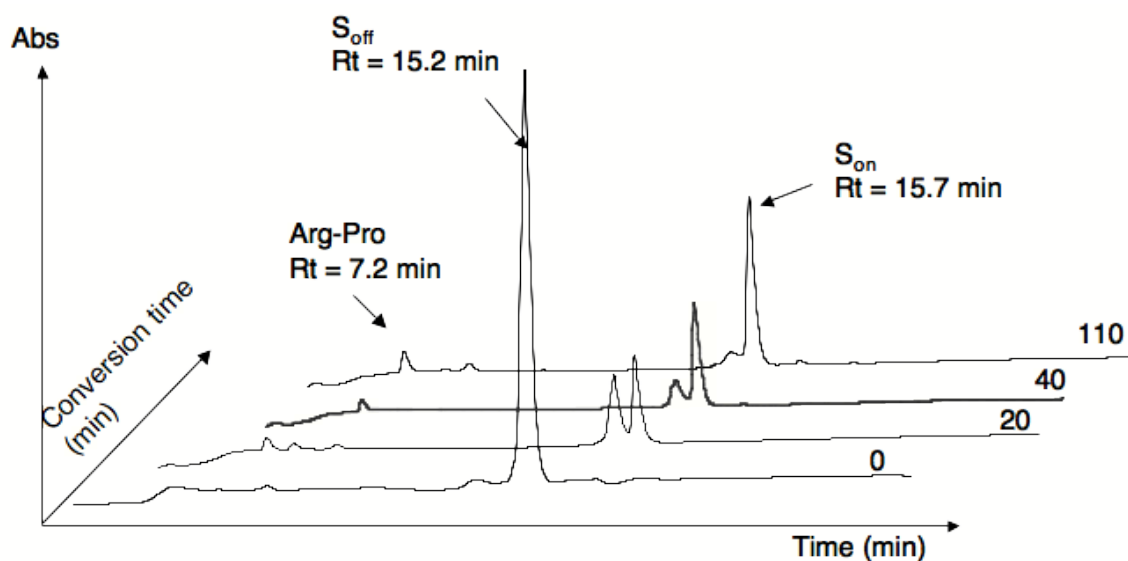


**Figure 44.** HPLC chromatograms of the enzymatic cleavage of dipeptide H-Arg-Pro-OH from switch-peptide **8** ( $S_{off}$ ) and subsequent acyl migration restoring the regular amide backbone (peptide **8** in the  $S_{on}$  state).

While triggering O,N-acyl migration by adding DPPIV enzyme, we observe by HPLC (Figure 44) the evolution of the cleaved dipeptide Arg-Pro (7.2min), the gradual disappearance of the  $S_{off}$  peak (15.2 min) and the onset of a new peak corresponding to the  $S_{on}$  state (peak at 15.7 min).

We can notice a decrease in absorbance of the  $S_{on}$  peak compared to the  $S_{off}$  peak. This corresponds to  $\beta$ -sheet formation and precipitation of the peptide.

In parallel, the conformational transition was monitored by CD and EM at 50 and 20  $\mu$ M at 37°C and pH 8. At a concentration of 50  $\mu$ M (Figure 45), at time zero, the curve corresponding to the  $S_{off}$  state was characteristic of a random coil (rc) structure (blue) but after addition of DPPIV a dramatic change from rc to  $\beta$ -sheet conformation is observed. The time course of the process is relatively fast, the half-life of  $\beta$ -sheet formation or disappearance of the rc being ca 15 min (Figure 45). Similarly, EM studies (Figure 46) show that after restoring the peptide backbone, the onset of  $\beta$ -sheet formation results in spontaneous fibril formation. Protofibril formation is observed immediately after enzyme addition to the peptide and a large amount of fibrils comparable to amyloid  $\beta$  fibrils are observed after 20 minutes. Furthermore, the peptide binds ThT dye reaching a plateau at 10 min only. This finding suggests that the lag-time for fibril formation of peptide **8** is very fast and that amyloid-aggregates are formed reaching maturation after few a minutes.

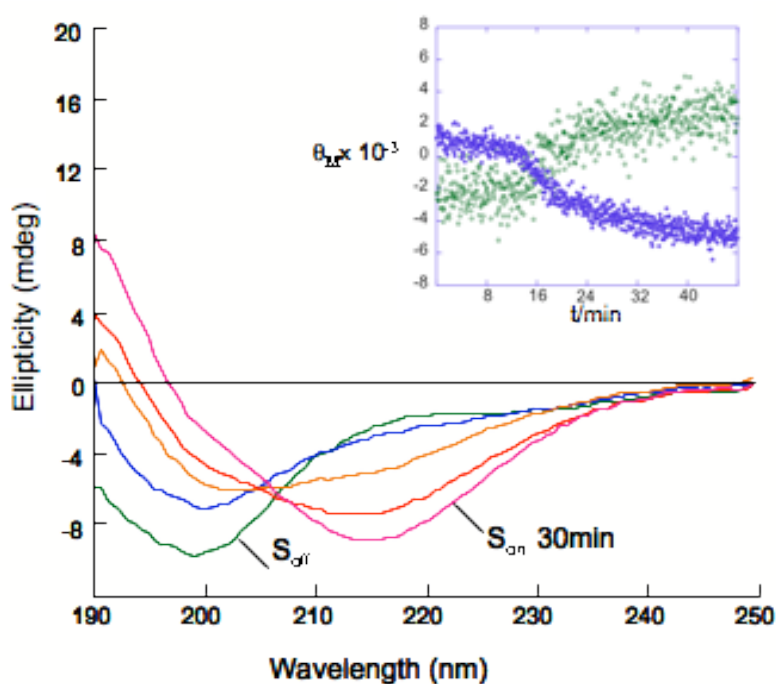


**Figure 45.** CD monitoring the conformational transition upon acyl migration from a random coil to a  $\beta$ -sheet conformation at 37°C in Tris buffer, pH 8 (500  $\mu$ M) + 10% MeOH and 2.5 mM NaCl (peptide concentration = 50  $\mu$ M). Inset: CD monitoring over time of  $\beta$ -sheet formation at 218 nm (green dots) and of random coil disappearance at 195 nm (blue dots).

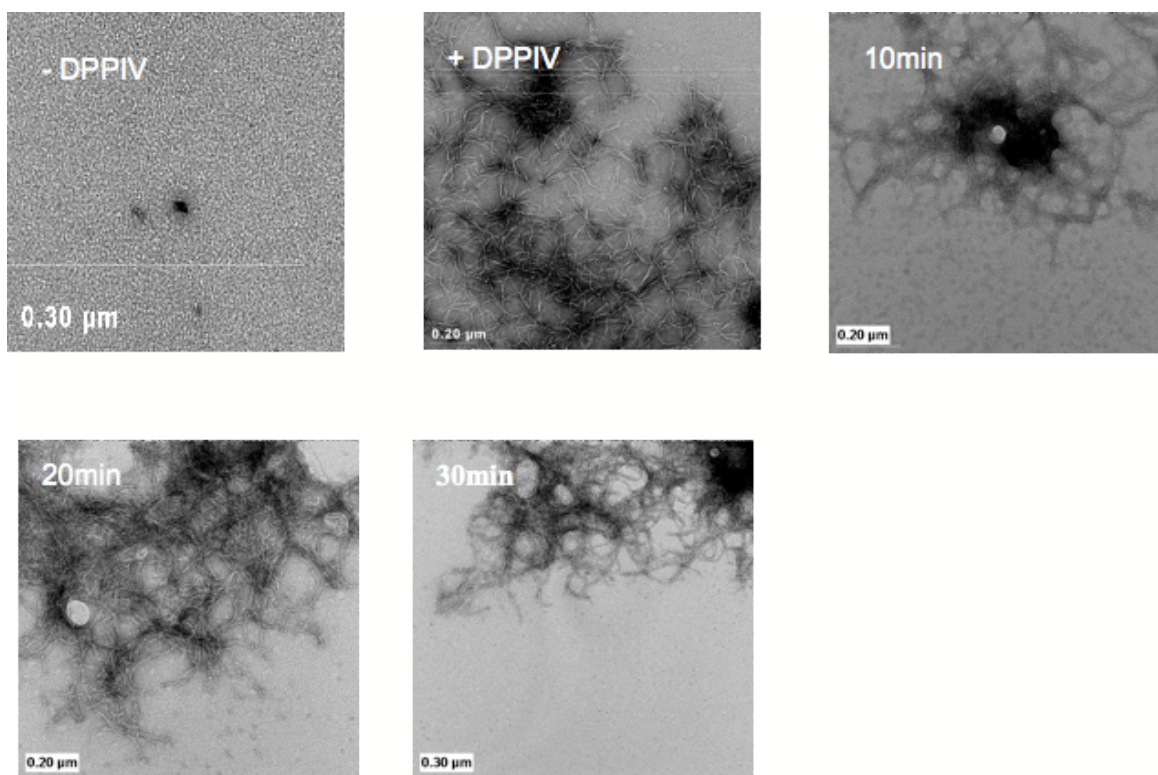


**Figure 46.** Conformational transition of peptide **8** followed by negatively stained electron microscopy in the absence of DPPIV and after its addition to the solution (see text).

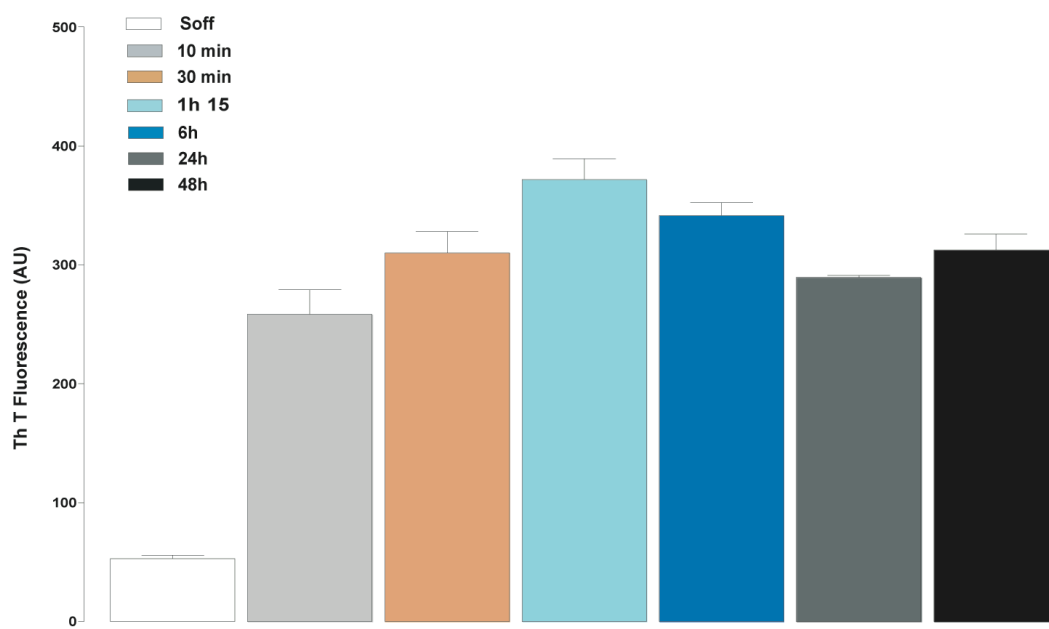


**Figure 47.** Thioflavin *T* fluorescence kinetics of peptide **8** at 50  $\mu\text{M}$  and 37°C.

In contrast, the folding of the peptide at 20  $\mu\text{M}$  (Figure 48 & Figure 49) was significantly slower (by factor of 8) compared to 50  $\mu\text{M}$  as shown by the CD spectra. A half-time value for the conformational transition from random coil to  $\beta$ -sheet of ca 120 min is observed, confirming that the folding and aggregation of peptide **8** strongly depends on the concentration.

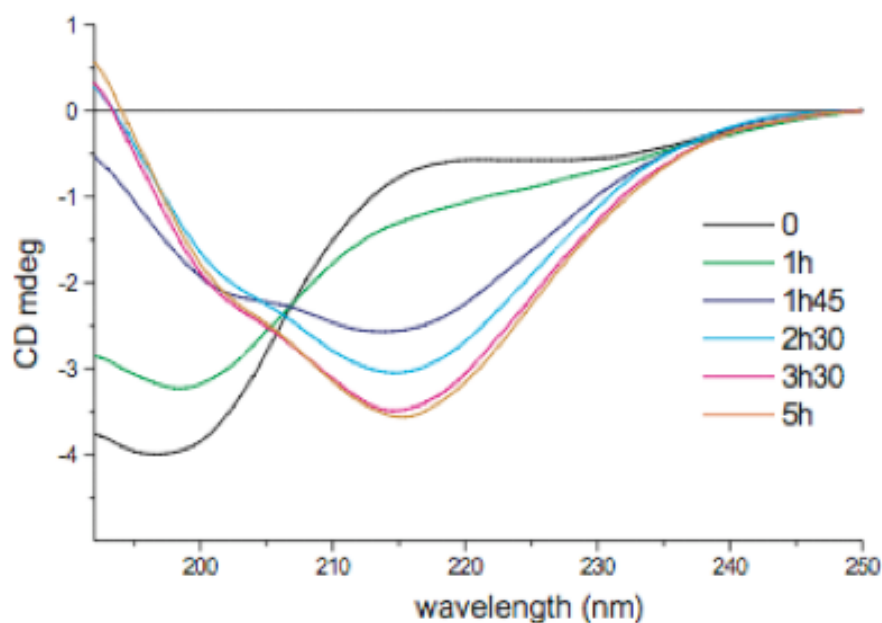


**Figure 48.** CD monitoring of the conformational transition upon acyl migration from a random coil to a  $\beta$ -sheet conformation at 37°C in Tris buffer pH 8 (500  $\mu\text{M}$ ) + 10% MeOH and 2.5 mM NaCl (peptide concentration = 20  $\mu\text{M}$ ).

The screening of CD samples by EM revealed the presence of short fibrillar-like structures after 1 hour (Figure 49). These morphological changes are in agreement with the changes in CD minima observed at 195 nm and 218 nm, indicating a slow transition from rc to  $\beta$ -sheet structure.  $\beta$ -sheet conversion appeared to be completed after 5 hours, as monitored by the negative cotton effect at 218 nm as well as the abundant presence of structurally mature fibrils. The first CD spectra (at  $t = 0$ , 1h and 1h45) converge in one point at  $\lambda = 208$  nm, the isosbestic point. This observation suggests that at this stage only two states contribute to the CD spectrum, i.e. that rc and  $\beta$ -sheet species are in equilibrium. However, after 2h30 the spectra do not converge into this point anymore, indicating the presence of multiple species in the solution, i.e. rc,  $\beta$ -sheet and soluble oligomeric structures and suggesting that aggregation started. Moreover, Th T fluorescence reached a plateau after 7 hours, which confirm our observations (Figure 50, black curve).

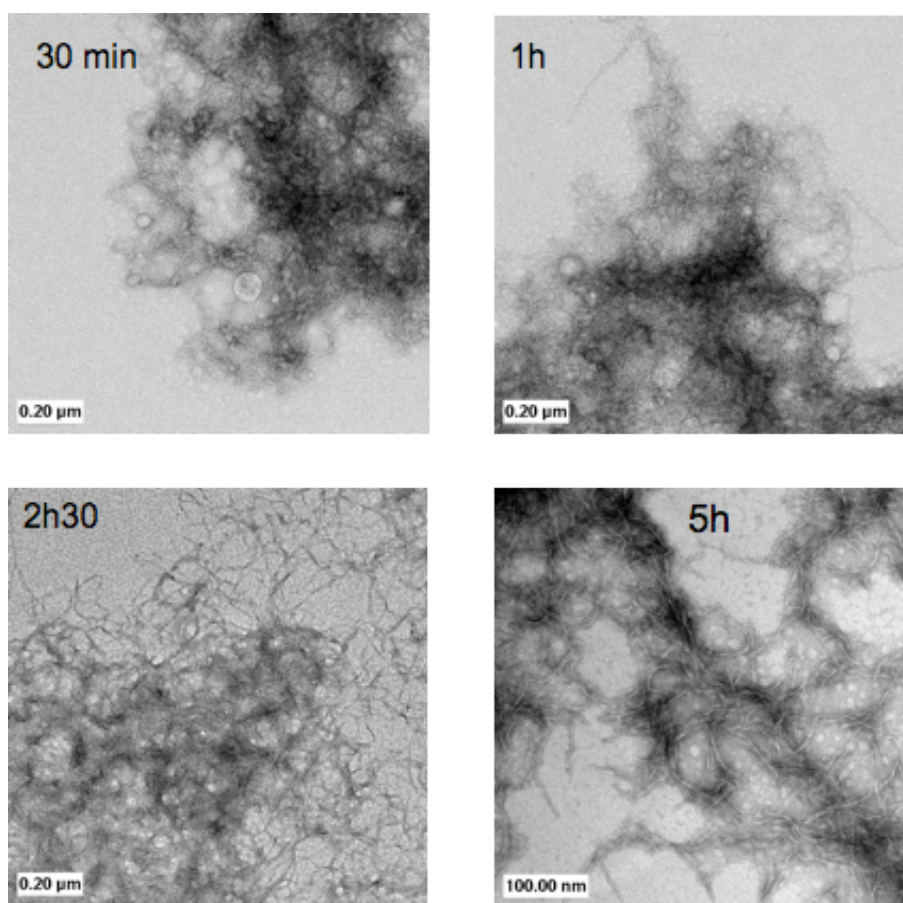


**Figure 49.** Electron micrographs of peptide **8** incubated at pH 8 and 37°C ( $c = 20 \mu\text{M}$ ).

#### *Screening of molecules of fibril-destabilizing activity*

After the establishment of the methodology, we further probed the potential of host-guest switch-peptide **8** for the investigation of the effect of molecules known for their A $\beta$  fibril destabilizing activity (taken from the literature) upon A $\beta$  fibril formation. For this purpose, we chose antioxidants such as tannic acid, wine-related polyphenols (myricetin) and the neurotransmitter dopamine<sup>119-122</sup> that have been demonstrated to protect the brain from in vitro A $\beta$  toxicity and to inhibit formation and extension of amyloid  $\beta$  1-40 and 1-42 in vitro.

#### *Experiments*

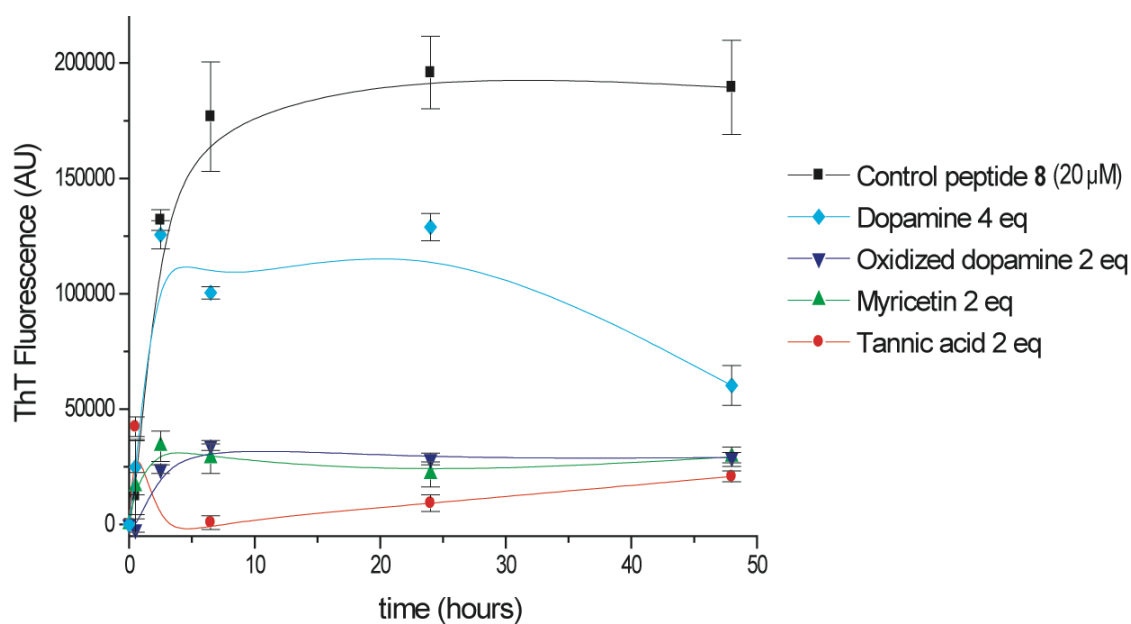
Peptide **8** was incubated for 48 hours under the following conditions: Peptide **8** was first dissolved in MeOH/H<sub>2</sub>O 50/50 to a final concentration of 400  $\mu\text{M}$  (stock solution). The solution was vortexed for 30 seconds and filtered through a 0.2  $\mu\text{m}$  filter by centrifugation for 5 min at

10'000 rpm. 50  $\mu\text{L}$  aliquots of the filtrate were transferred into autoclaved Eppendorf tubes. 750  $\mu\text{L}$  of Tris buffer pH 8 500  $\mu\text{M}$  + 2.5 mM NaCl and 100  $\mu\text{L}$  of MeOH were added to each tube. The inhibitors were dissolved in MeOH at concentrations of 400 to 800  $\mu\text{M}$  and 100  $\mu\text{L}$  of these stock solutions were added to the mixture to give the correct final concentration of inhibitor in the reaction mixture. 1.5  $\mu\text{L}$  (0.002 unit) of DPPIV enzyme was then added to each vial and placed in a water bath at 37°C for 48 hours. Aliquots of 160  $\mu\text{L}$  were removed from the incubated samples at different time points and stored at -18°C until further analysis.

### *Thioflavin T (ThT) and Electron microscopy (EM) analysis*

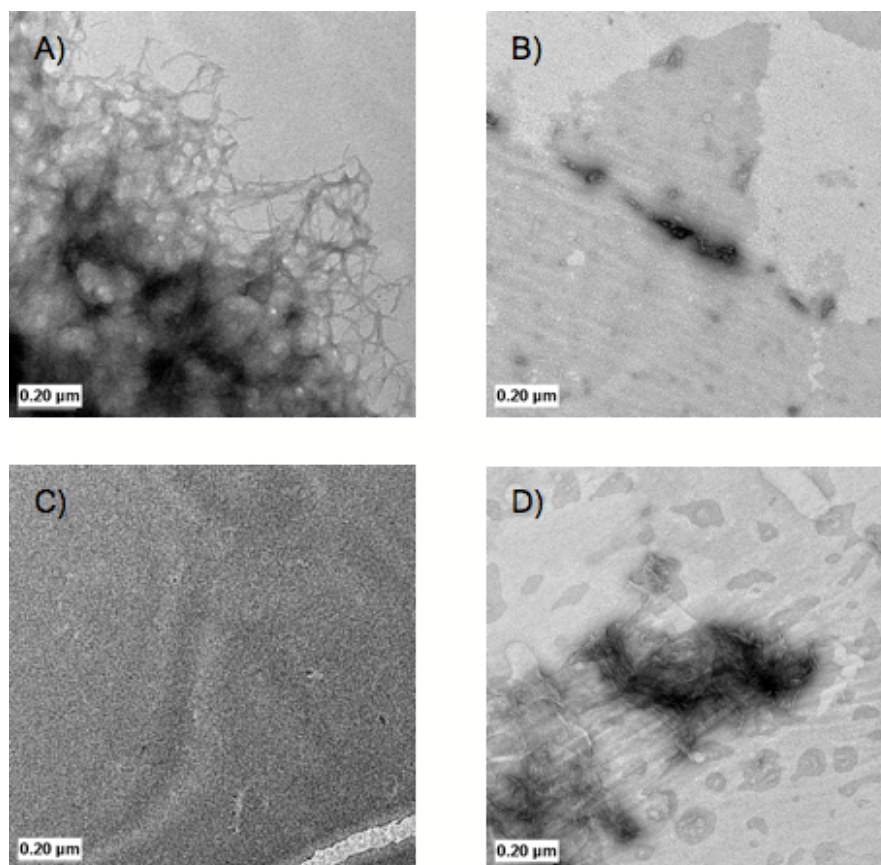
ThT is a fluorescent dye widely used for the detection of amyloid fibrils due to its relatively specific interaction.

The inhibitory effects on  $\beta$ -sheet formation of peptide **8** of tannic acid, myricetin and dopamine were tested using standard analytical techniques of ThT fluorescence and EM as described above.



**Figure 50.** Kinetics of fibril formation monitored by Th T fluorescence. Control (black); after addition of 80  $\mu\text{M}$  dopamine (cyan), 40  $\mu\text{M}$  oxidized dopamine (blue) and 40  $\mu\text{M}$  myricetin (green), 40  $\mu\text{M}$  tannic acid (red).



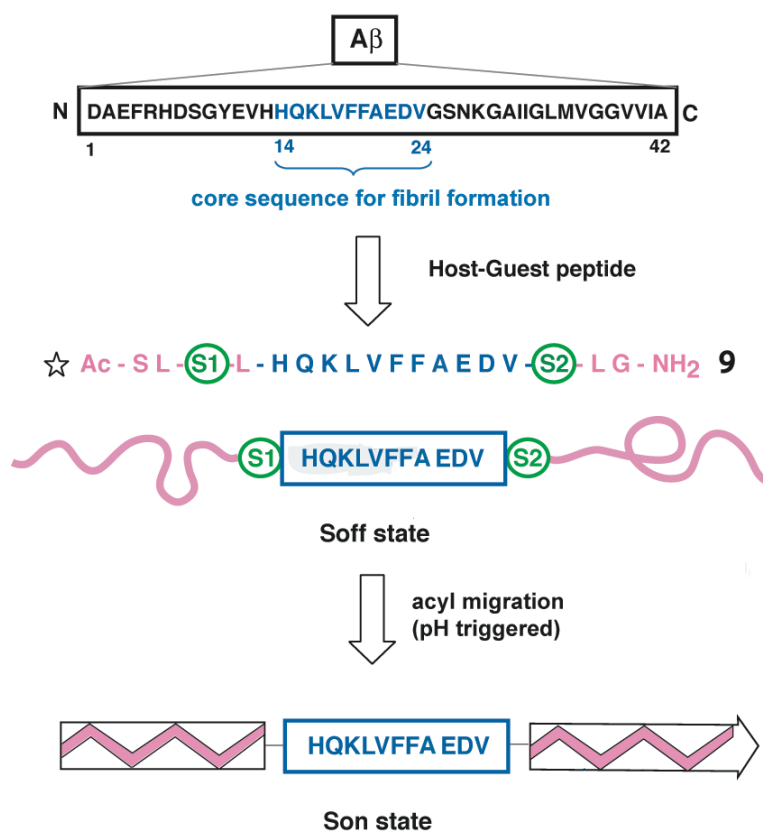


**Figure 51.** TEM images of peptide **8** fibrils A) after 48 h incubation at 37°C, and in presence of 2 eq of tannic acid (B), 2 eq of myricetin (C) and 4 eq of dopamine (D).

In the absence of inhibitors, peptide **8** (20 μM) forms fibrils within 5 hours upon enzymatic triggering, as can be seen by the fast increase in ThT fluorescence levels (Figure 50). ThT level-off after ca 6 h indicating saturation in ThT binding and fibril completion. The presence of mature fibrils observed by EM after 48 hours incubation time is in agreement with the kinetic of ThT binding (Figure 51; A).

Interestingly, secondary structure formation (rc to β-sheet) of peptide **8** was inhibited in the presence of tannic acid (40 μM), myricetin (40 μM) and oxidized dopamine (40 μM). Compared to the antioxidants the effect of dopamine (80 μM) is less pronounced within the first 2.5 hours of incubation. Nevertheless, significant inhibition was observed after 5 hours incubation incubation with dopamine, showing a gradual decline in ThT fluorescence. Most notably, fibrillogenesis was completely inhibited in samples co-incubated with the antioxidants tannic acid (Figure 51, B) or myricetin (Figure 51,C), as seen by the presence of some oligomeric

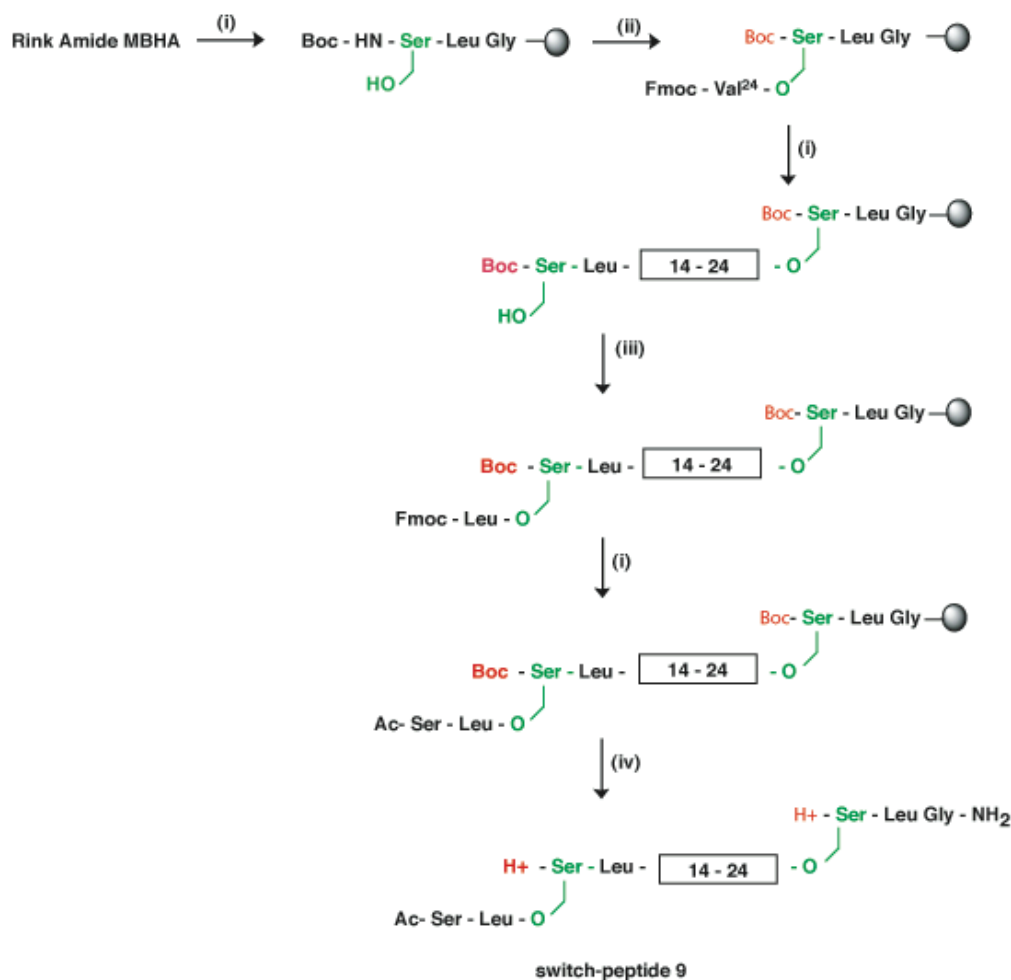
species, whereas residual amounts of short fibrillar structures could be observed in samples incubated with dopamine (Figure 51, D).

4.2.2. Host-guest switch-peptide **9** disposing two switch elements.

**Figure 52.** Host-guest switch-peptide **9**, containing two switch elements at the N- and C- terminus of the guest peptide  $\text{A}\beta(14-24)$ . In the  $S_{\text{off}}$  state, the peptide is designed to adopt a random coil conformation, after adjusting the pH to physiological conditions, spontaneous acyl migration occurs resulting in peptide folding.

*Synthesis*

The  $\text{A}\beta$ -derived host-guest switch-peptide **9** was assembled on 1 g of Rink amide MBHA resin (loading 0.66 mmol/g) according to the Fmoc/tBu strategy (Scheme 4).



**Scheme 4.** Solid phase synthesis (SPPS) of switch-peptide 9. (i) standard solid phase peptide synthesis according to the Fmoc/<sup>t</sup>Bu strategy, (ii) Fmoc-Val-OH (3 eq), DIC (3 eq), DMAP (0.5 eq), DCM/DMF (4:1); (iii) Fmoc-Leu-OH (3eq), DIC (3eq), DMAP (0.5eq), DCM/DMF (4:1), 2h; (iv) TFA/TIS/H<sub>2</sub>O 95:2.5:2.5, 2x1h.

The synthesis was straightforward and the HPLC revealed one major peak identified as the target peptide 9 (Figure 53). Only one deletion sequence was observed. After purification by preparative HPLC, 9 was obtained in a yield of ca 36% (> 95% purity).

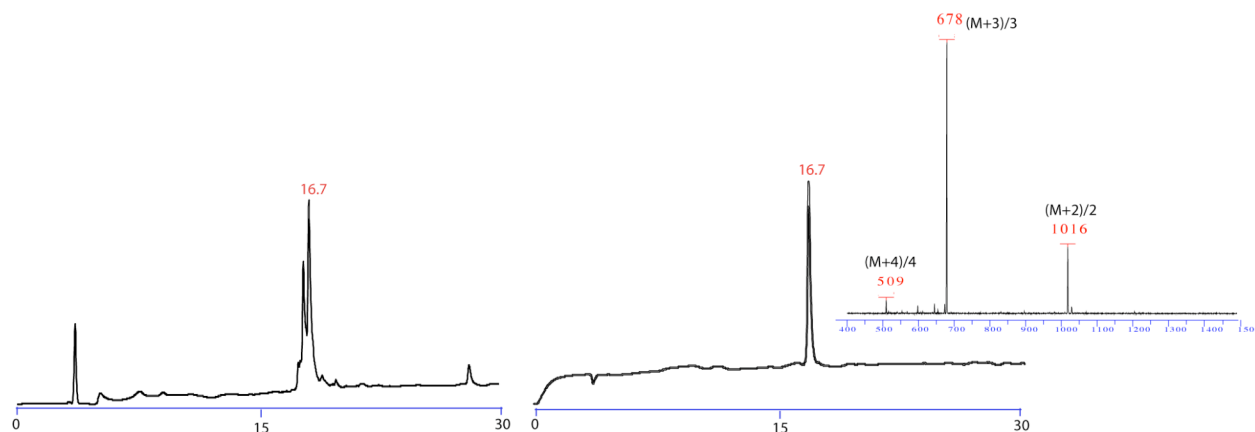


**Figure 53.** Analytical data of switch-peptide **9**, left: HPLC (C8, 0 to 100% A, 30 min) of crude compound, right: HPLC (0 to 100% A, 30 min) and ESI/MS ( $m/z$  1016  $[M + 2H]^{2+}$ , 678  $[M + 3H]^{3+}$ , 509  $[M + 4H]^{4+}$ ; inset) of purified compound.

#### Kinetic studies of folding and fibril formation

Conversion of peptide **9** from the  $S_{\text{off}}$  to the  $S_{\text{on}}$  state via O to N acyl migration was followed by HPLC. Peptide **9** was dissolved in acetate buffer, pH 4.6 (10 mM) at 400  $\mu\text{M}$ , 37°C. To trigger acyl migration, the pH was adjusted to 7.4 by adding 10% PBS buffer pH 7.4 (0.3 M + 150 mM NaCl). At various intervals, 20  $\mu\text{L}$  aliquots were taken and injected to analytical HPLC to follow the migration (Figure 54).

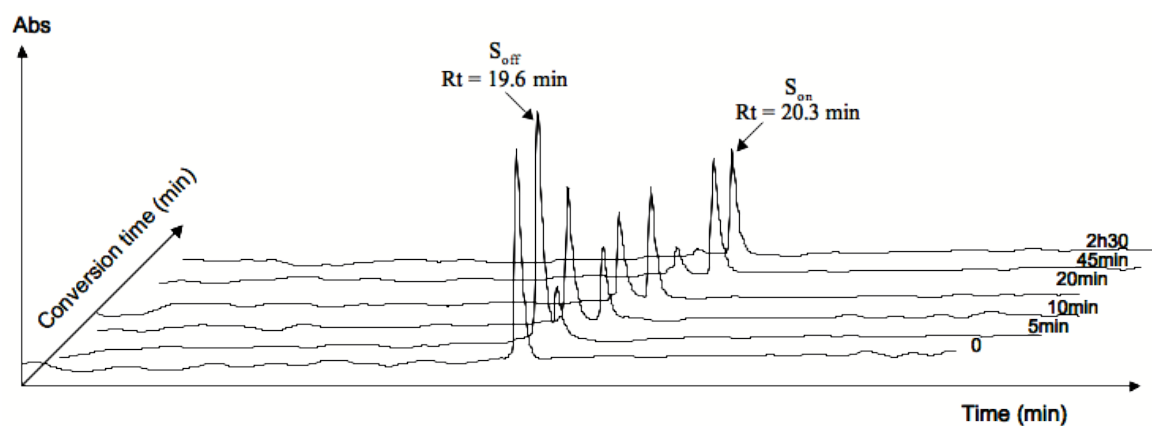


**Figure 54.** HPLC chromatograms of the O,N-acyl migration of peptide **9** at 37°C, pH 7.4.

The appearance of a new peak ( $S_{\text{on}}$ ) on the HPLC chromatogram is associated with triggering of both switches simultaneously. The half-time value for migration in peptide **9** (25 min) was found to be similar as in peptide **8**. However, unlike peptide **8**, pH triggering of peptide **9** at a concentration of 20  $\mu\text{M}$  did not result in the formation of fibrils, and CD spectra indicated a

predominant random coil structure after 5 hours of incubation at 37°C; in addition, only a weak Th T fluorescence signal was observed. This result prompted us to carry out the following experimental analyses at increased peptide concentrations; i.e.  $c = 40 \mu\text{M}$ .

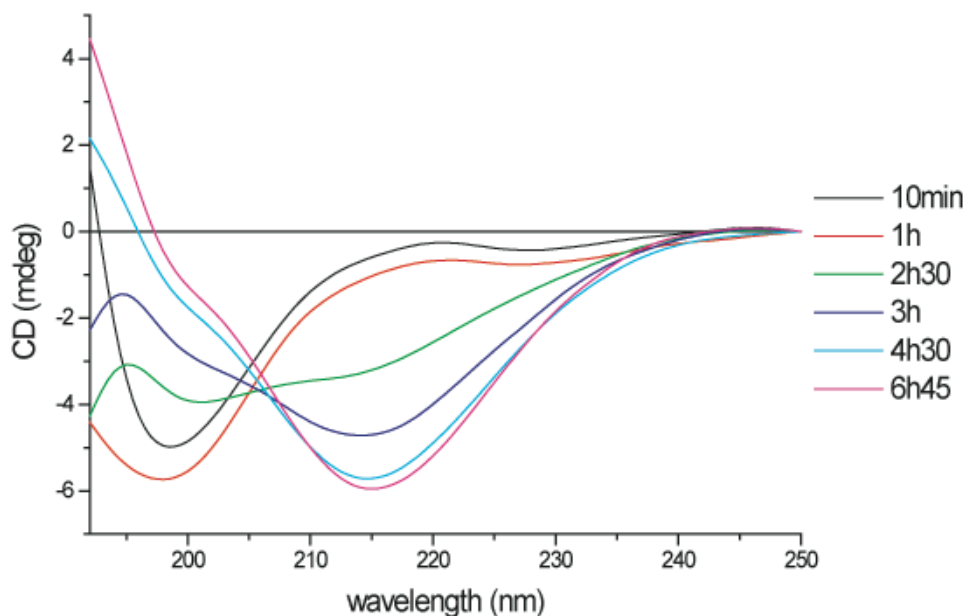


**Figure 55.** CD monitoring of the conformational transition of peptide **9** from random coil to  $\beta$ -sheet conformation at physiological conditions.

The CD spectra (Figure 55) show that incubation of peptide **9** ( $40\mu\text{M}$ ) at pH 7.4 results in a complete conversion from random coil to  $\beta$ -sheet structure within 4.5 hours. pH-induced changes in secondary structure of peptide **9** appeared slow within the first hour, showing a predominantly random coiled structure by CD, in agreement with the oligomeric morphology found by EM (Figure 56). The presence of fibrils and the onset in  $\beta$ -sheet formation was found after 2.5 hours of incubation, which seemed to be complete after 4.5 hours. A similar trend of increase in ThT fluorescence was observed, showing low levels ThT binding in peptide **9** within the first hour of incubation (Figure 57). The CD spectra revealed an isosbestic point for  $t = 1\text{h}$ ,  $2\text{h}30$ ,  $3\text{h}$ ,  $4\text{h}30$  suggesting a two-state transition within this time frame.

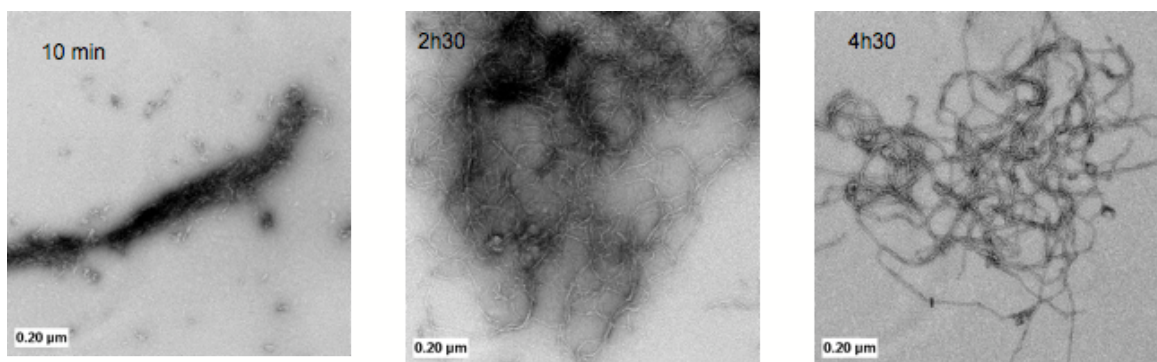


**Figure 56.** kinetic of fibril formation of peptide **9** followed by electron microscopy.

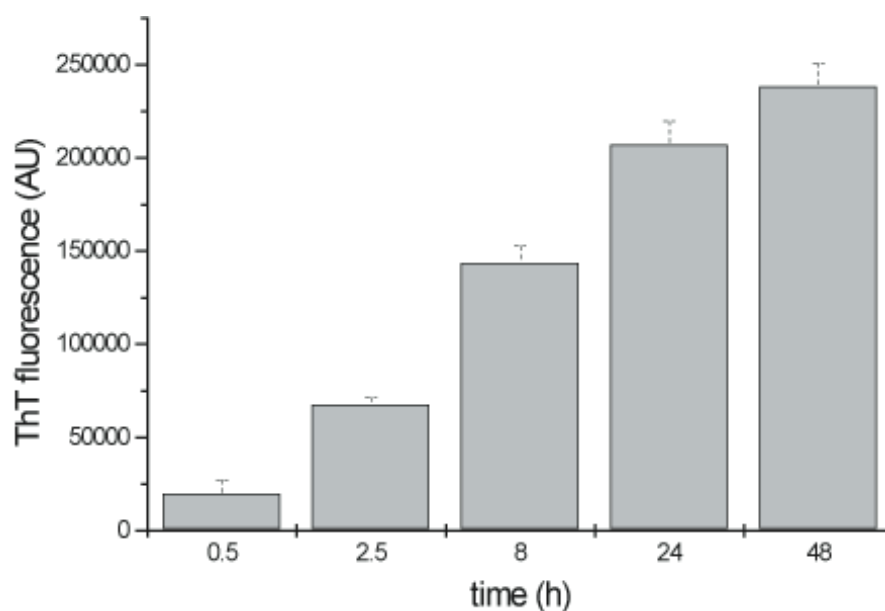


**Figure 57.** Bar chart representing the ThT values of peptide **9** incubated at 40 μM under physiological conditions.

In conclusion peptide **9** transforms from a soluble, flexible, unfolded state ( $S_{off}$ ) in situ to a  $\beta$ -sheet structure as monitored by CD spectroscopy, EM, and ThT fluorescence studies. Similar to peptide **8**, we further probed the potential of this model for mimicking A $\beta$  folding and aggregation and for examining the impact of three molecules well-known for their A $\beta$  fibril-destabilizing activity upon the onset of ordered conformations during the process of structure evolution (“in statu nascendi”).

*Screening of molecules of A $\beta$  fibril-destabilizing activity*

Aggregation kinetics in the presence of tannic acid, myricetin or dopamine were investigated using ThT fluorescence measurements and Electron Microscopy.

*Experiments*

Peptide **9** was dissolved in H<sub>2</sub>O to a final concentration of 800  $\mu$ M (stock solution). The solution was vortexed for 30 seconds and filtered through a 0.2  $\mu$ m filter by centrifugation (5 min at 10'000 rpm). 50  $\mu$ L aliquots of the filtrate were put into autoclaved Eppendorf tubes. 750  $\mu$ L of 100  $\mu$ M acetate buffer, pH 4.6 were added to each tube. The inhibitors were dissolved in MeOH at concentrations of 400 to 800  $\mu$ M and 100  $\mu$ L of these stock solutions were added to the mixture to give the correct final concentration of inhibitor in the reaction mixture. 100  $\mu$ L of Tris buffer pH 7.4 (0.3 M + 150 mM NaCl) were added to each vial to trigger the acyl migration and placed at 37°C for 48 hours. Aliquots of 90  $\mu$ L were removed from the incubated samples at different time points and stored at -18°C until further analysis.

*ThT and EM analysis*

By incubating peptide **9** at 37°C, ThT fluorescence followed a characteristic hyperbolic curve, pointing to a fast nucleation. This curve is consistent with a first-order kinetic model observed by Naiki and Nakakuki. When peptide **9** was incubated with 80  $\mu$ M tannic acid, myricetin or oxidized dopamine, the final equilibrium level decreased significantly indicating that no fibrils were present in the mixture. A low signal was also observed for the S<sub>off</sub> state of **9** (at 48h), indicating the presence of random coil conformation.



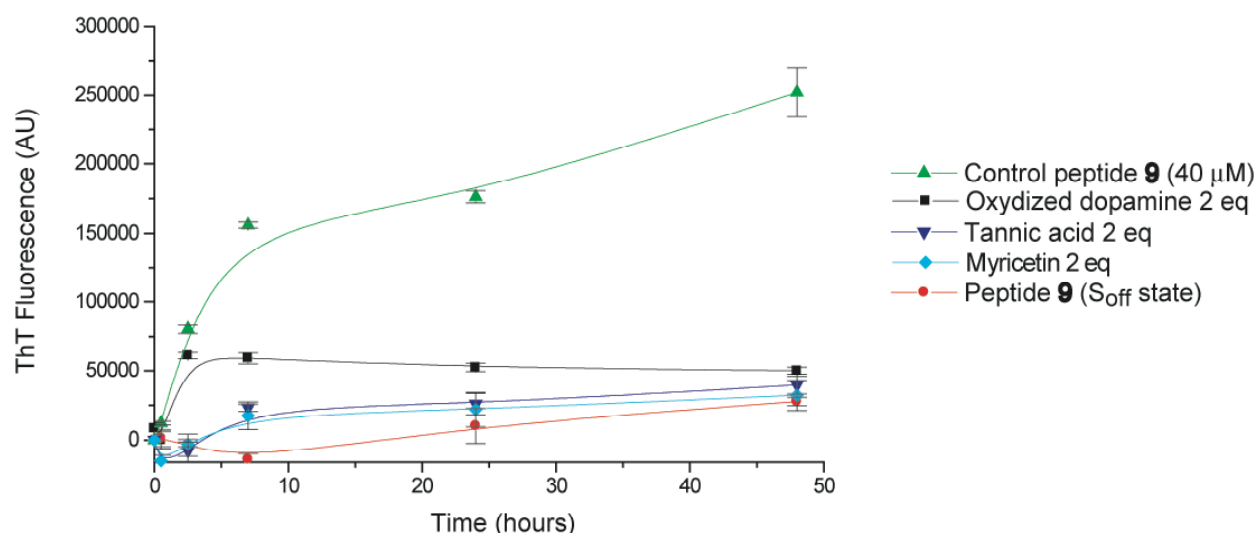


**Figure 58.** Kinetics of fibril formation monitored by Th T fluorescence. Control (green); after addition of 80 μM tannic acid (blue), 80 μM myricetin (cyan) and 80 μM dopamine (back), control peptide in the  $S_{\text{off}}$  state (red).

EM data are in support of the results obtained by ThT analysis. Most notably, we observe after two days incubation that peptide **9** forms mature amyloid-like fibrils (Figure 59, A), whereas when incubated in the presence of inhibitors no fibrils were present in the solution; only amorphous aggregates were observed by EM. In addition, incubation at pH 4.6 ( $S_{\text{off}}$  state) did not result in amyloid-like fibrils, in agreement with the adoption a soluble, unordered conformation in the  $S_{\text{off}}$  state over days at 37°C; short, non amyloid-like fibrils in the sample can be rationalized by ester bond hydrolysis (ca 5% after 48 h at 37°C, see Figure 22).

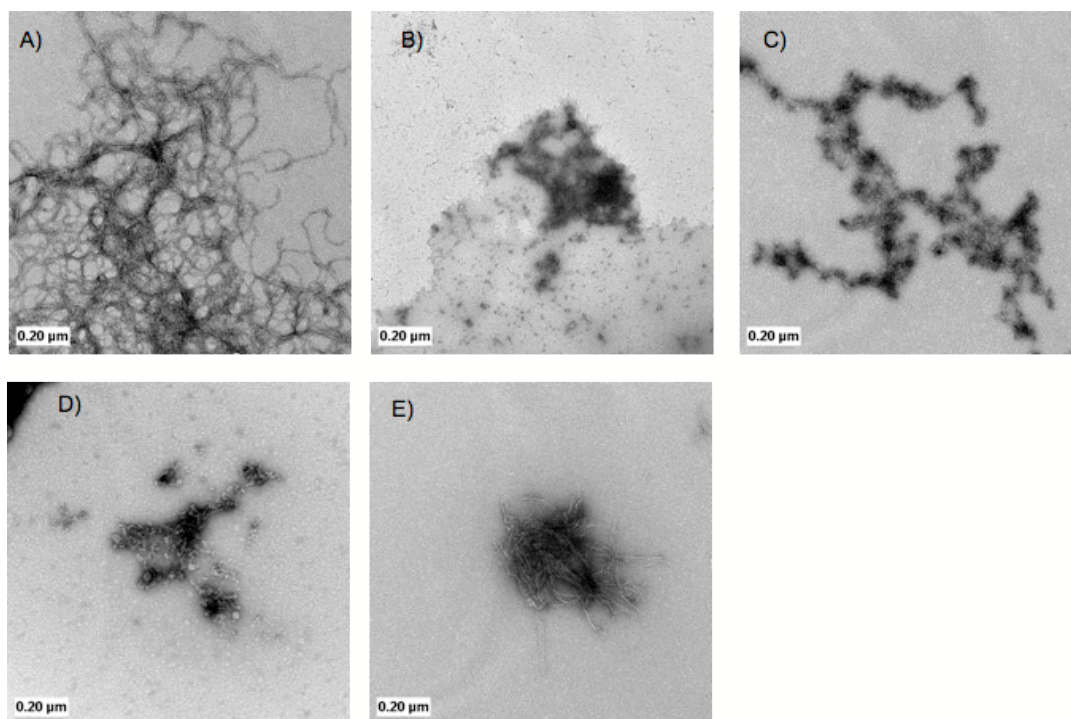


**Figure 59.** EM images of peptide **9** after 48 h at 37°C and pH 7.4 A) control  $S_{on}$  state, B) tannic acid 2 eq, C) myricetin 2 eq, D) oxidized dopamine 2 eq, E) control peptide **9** in the  $S_{off}$  state.

To probe the impact of an inhibitor upon the kinetics of acyl migration, peptide **9** was subject to O,N-acyl migration in the presence of tannic acid as monitored by HPLC. As shown in Figure 60 the migration occurs reaction proceeds without any disturbing effect by the inhibitor. The mass of the  $S_{off}$  and  $S_{on}$  peak being identical, the more hydrophilic peak ( $R_t = 18.1$  min) could be attributed (MALDI-TOF) to the peptide in the  $S_{off}$  state.

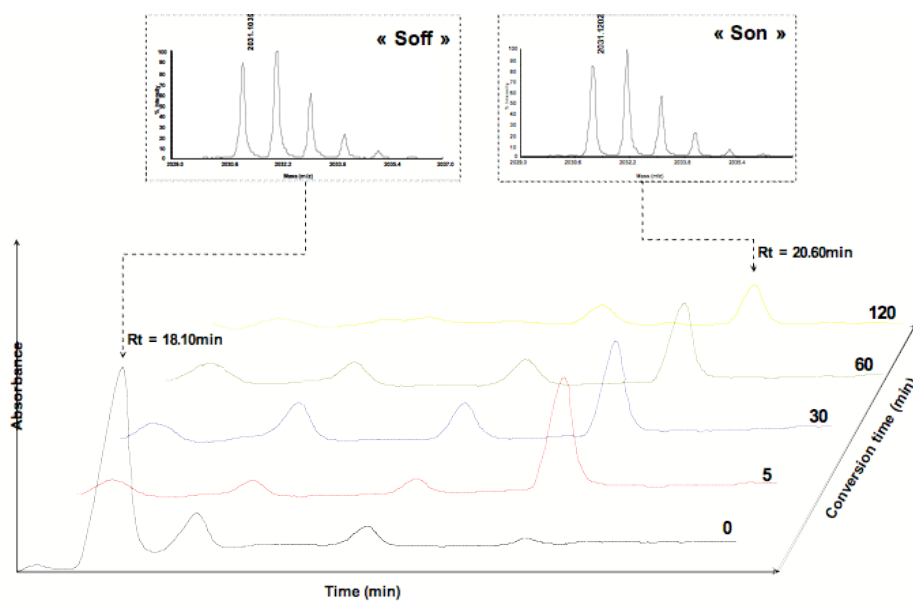


**Figure 60.** HPLC monitoring of the O to N acyl migration of peptide 9 ( $c = 40 \mu\text{M}$ ) in presence of 2 eq tannic acid inhibitor (see text).

### 4.3. Discussion

We have demonstrated that the host guest technique combined with the switch concept represent a versatile tool to follow the folding and aggregation of the sequence A $\beta$  (14-24), which plays a key role in  $\beta$ -sheet nucleation of full-length A $\beta$ . Our results suggest that starting from a stable, unfolded state ( $S_{\text{off}}$ ), the self-assembly and  $\beta$ -sheet formation as molecular origin of peptide fibrillogenesis can be studied in situ using specific nucleation sites of native A $\beta$  as guest segments within a host model peptide. EM and CD data indicate that the kinetics of the onset of fibril formation of both peptide **8** and **9** is fast and that the aggregates formed are similar to those by native A $\beta$ (1-42). The designed host guest systems, i.e. A $\beta$  (14-24) flanked N- and C-terminally by (Leu-Ser)<sub>n</sub> oligomers proved to be a versatile model of amyloid  $\beta$  for studying the onset of  $\beta$ -structures and subsequent fibrillogenesis.

Moreover, we have validated the host guest approach as a convenient and reliable screening system for the investigation of molecules of A $\beta$  fibril destabilizing activity.

## 5. Design and synthesis of Switch-peptides of amyloid $\beta$ fibril disrupting potential

### 5.1. Background

The main targets for therapeutic intervention of the A $\beta$  cascade include the inhibition of A $\beta$  production, the inhibition of A $\beta$  aggregation and fibril formation, in addition to the inhibition of the consequent inflammatory responses caused by the A $\beta$  deposition.

Soto *et al.*, Tjenberg *et al.* as well as Kapurniotu *et al.* proposed that short synthetic peptides capable of binding A $\beta$  but unable to become part of the  $\beta$ -sheet structure ( $\beta$ -sheet breaker peptides) may stabilize the amyloidogenic A $\beta$  conformer and hence preclude amyloid formation<sup>123-126</sup>. Thus, these peptides have the ability to interact specifically with A $\beta$  and block its  $\beta$ -sheet conformation, to disassemble preformed fibrils *in vitro*, to prevent neuronal death induced by fibrils in cell culture, to reduce amyloid  $\beta$ -protein deposition *in vivo* and to block the formation of amyloid fibrils in a rat brain model of amyloidosis. However, this hypothesis of  $\beta$ -breaking might have a counterproductive effect by transforming fibrils to oligomeric structures that are nowadays thought to be the most toxic species in the pathology of AD. At present, although some efficient drugs in slowing down the symptoms exist and huge progress are being made, there is still no effective treatment available for AD as well as for most of the protein folding disorders. However, the 5-residues peptides (Ac-LPFFD-NH<sub>2</sub> and Ac-LP(NMe)FFD-NH<sub>2</sub>) proposed by Soto protected at his N- and C-termini to prevent proteolytic degradation and to increase its blood-brain barrier permeability have shown the potential to be used as therapeutic agents to prevent or retard the progression of amyloidosis in AD<sup>125</sup>.

To further increase their stability and breaking effects, various pseudoproline ( $\Psi$ Pro) were substituted for Pro.  $\Psi$ -Pro are Ser, Thr or Cys-derived proline analogs. For example, the Pro-specific induction of the *cis*-geometry<sup>127</sup> of the Xaa- $\Psi$ Pro imide bond is pronounced and as a non-natural amino acid, it is more stable against proteolytic degradation.

The two pseudoproline-containing peptides investigated by Soto and Mutter *et al.* showed good enzymatic stability but a lower fibril inhibition activity compared to the Pro containing analogues<sup>72</sup>. The stabilization of the *cis*-configuration reduced the inhibition activity of the peptides suggesting, as the *cis*-Pro is the active conformation, that the *trans*-Pro is required for

binding to the target. It seems that conformational flexibility of the molecules is, at least in the recognition/binding step, crucial for activity. The process of fibrillogenesis inhibition can be delineated as two distinct steps: first, the peptides recognize a particular stretch of the A $\beta$  sequence and second, upon binding lead to a conformational destabilization of  $\beta$ -sheet structure formation. In the first step, the constraint (the *cis* amide bond) imposed by the pseudo-proline results in reduced binding to the A $\beta$  of the  $\beta$ -sheet breaker peptides. Consequently, it seemed reasonable to separate structure from function by using switch-peptides.

For this purpose, we have designed switch-peptides comprising a recognition element (P2) and a  $\Psi$ Pro-derived  $\beta$ -disrupting unit (P1) separated from each other by a switch element (S) (Figure 61). Upon introduction of a flexible ester-bond, the impact of the  $\Psi$ Pro-moiety is decoupled from the peptide chain and does not interfere with the bonding properties of the recognition sequence. After binding of the peptide to the A $\beta$  sequence, the switch can be triggered and the  $\beta$ -sheet destabilizing effect of the  $\Psi$ Pro is initiated. Thus, the modular character of switch-peptides is ideal to take into account the dual action of  $\beta$ -strand recognition/binding and  $\beta$ -sheet destabilization (Figure 61).

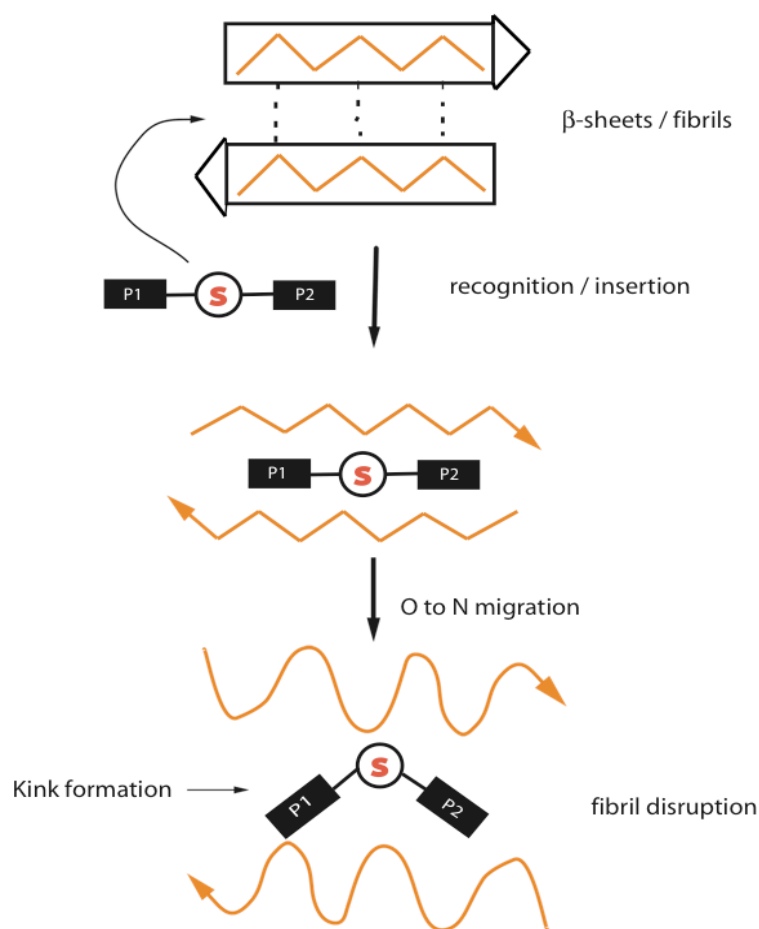
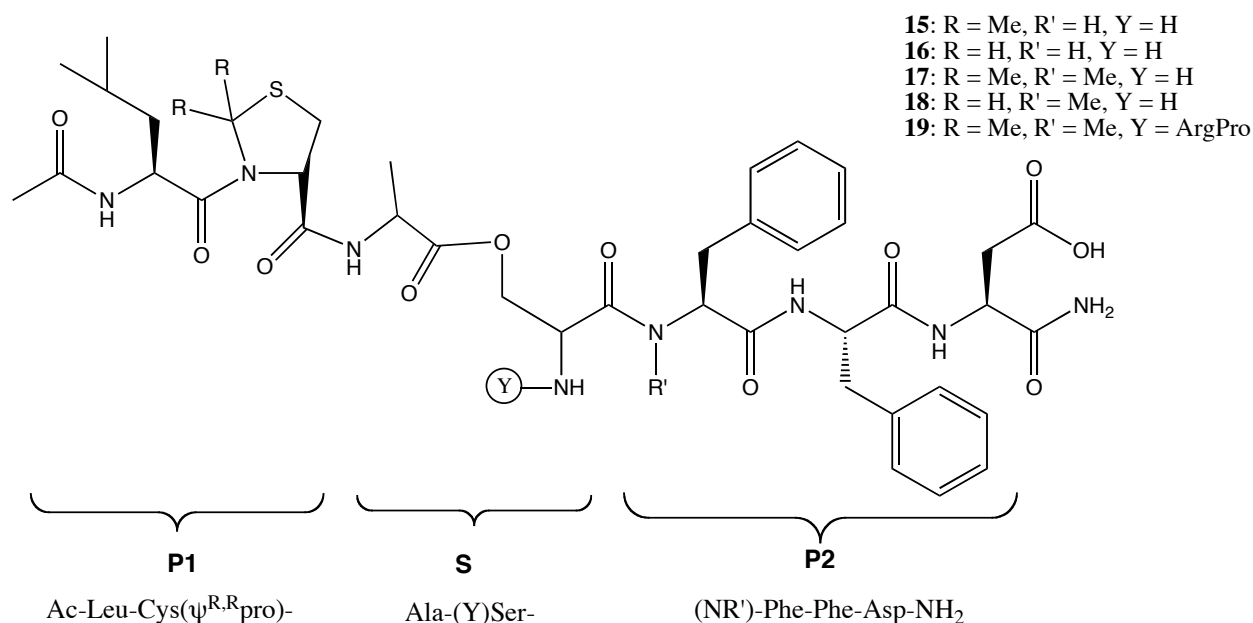


**Figure 61.** Disruption of  $\beta$ -sheets with kink-inducing switch-peptides.

## 5.2. Design and synthesis

Five different switch-peptides containing either the dimethyl-pseudo-proline or the dihydro-pseudo-proline in the  $\beta$ -sheet destabilization unit P1 were designed. The recognition sequence P2 was either H-Phe-Phe-Asp-NH<sub>2</sub> or H-MePhe-Phe-Asp-NH<sub>2</sub>. The switch element was protected either by a proton (H<sup>+</sup>) or a dipeptide (ArgPro), cleavable by the enzyme DPPIV. Scheme 5 gives a general overview of the different switch-peptides synthesized and further investigated.



**Scheme 5.** General scheme of Amyloid-derived switch-peptides (see text).

Firstly, pseudoproline derivatives were synthesized from cysteine hydrochloride and subsequently, the building block Ac-Leu-Cys( $\psi^{R,R}$ )pro-OH was prepared (see Figure 62) for further incorporation in solid phase peptide synthesis.

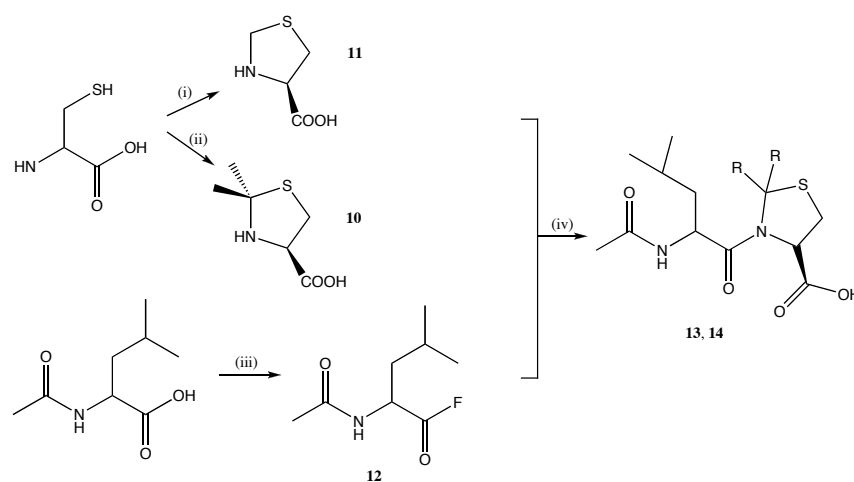
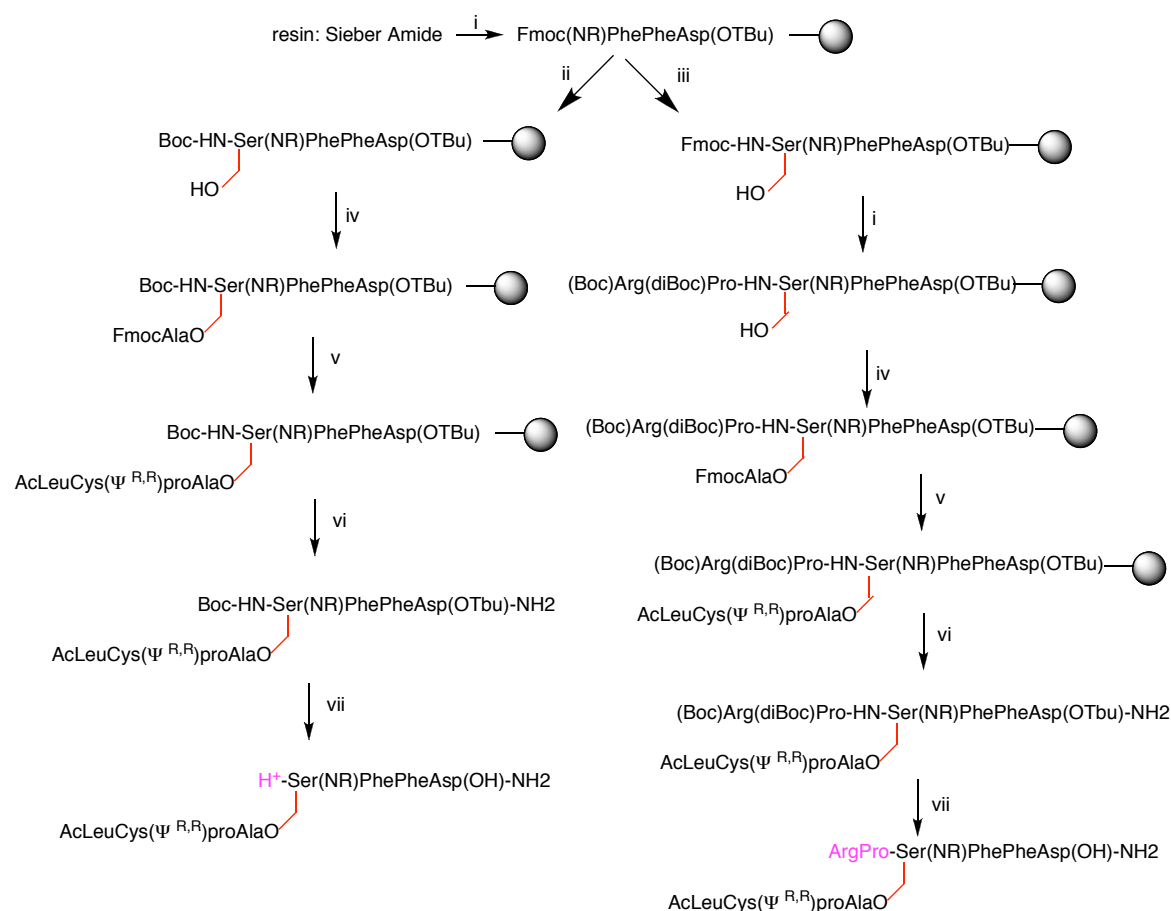


**Figure 62.** Synthesis of the dipeptide Ac-Leu-Cys( $\psi^{R,R}$ pro)-OH. (i) sol. HCHO 40% / H<sub>2</sub>O (4/10), overnight, RT, quantitative; (ii) acetone/dimethoxypropane (80/18), reflux, 2h, quantitative, (iii) DAST (1.2 eq), DCM, 15 min, (iv) Dipea (2 eq), DCM, 1h, 30%.

The synthesis of the five switch-peptides were performed on a Sieber amide resin (loading 0.71 mmol/g) following the Fmoc/tBu strategy as depicted in Scheme 6





**Scheme 6.** Solid phase synthesis of  $\beta$ -breaker switch-peptides **15** to **19**. Resin Sieber amide (0.71 mmole/g), (i) PyBop (2 eq), aa (2 eq), Dipea (4 eq), (ii) Boc-Ser-OH (2 eq), HATU (2 eq), Dipea (4 eq), (iii) Fmoc-Ser-OH (2 eq), HATU (2 eq), Dipea (4 eq), (iv) DIC (3 eq), DMAP (0.1 eq), Fmoc-Ala-OH (3 eq), (v) AcLeuCys( $\Psi^{R,R}$ )pro-OH (2 eq), HATU (2 eq), Dipea (4 eq), (vi) resin cleavage 1% TFA in DCM 2x20 min, (vii) Boc and tBu cleavage: 50% TFA in DCM, 2.5% TIS and 2.5% H<sub>2</sub>O.

The syntheses were straightforward and gave after purification by preparative HPLC a white powder with 15% to 20 % yield depending on the peptide (see experimental part). Here is the list of the switch-peptides synthesized followed by their analytical data:

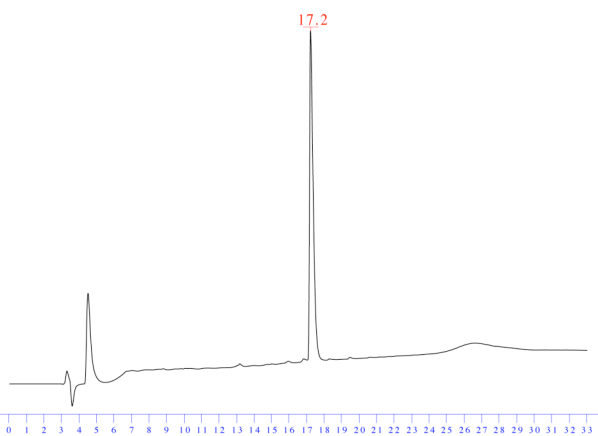
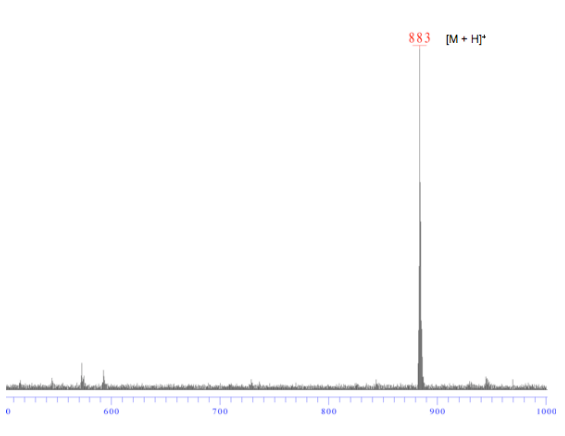
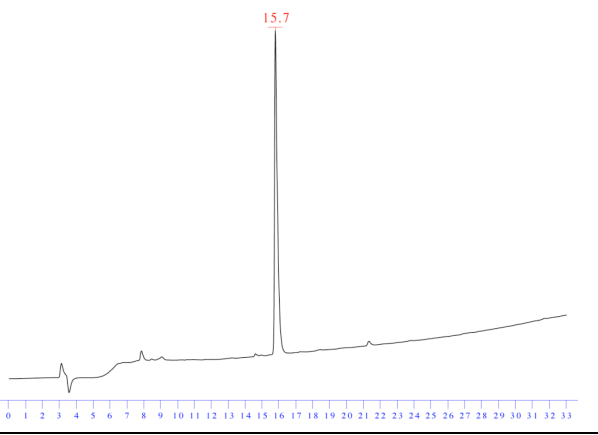
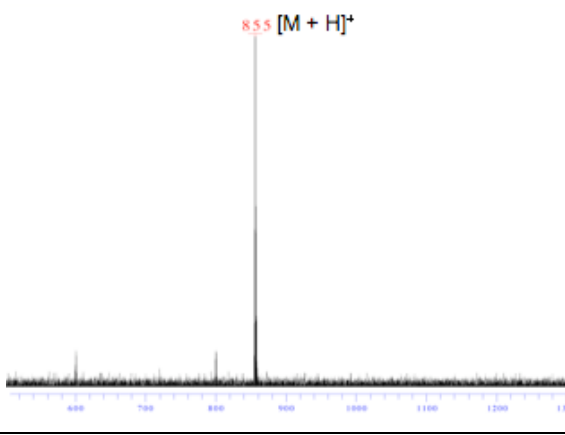
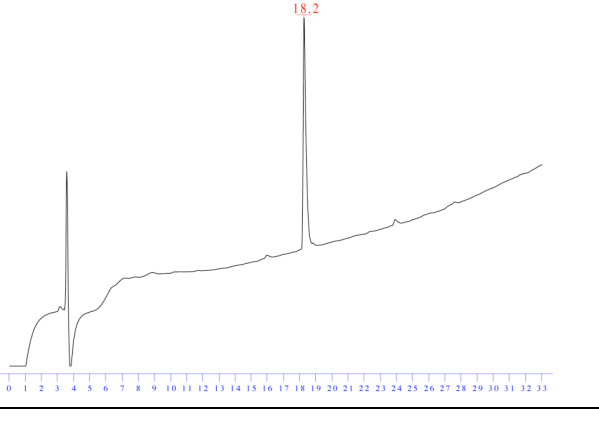
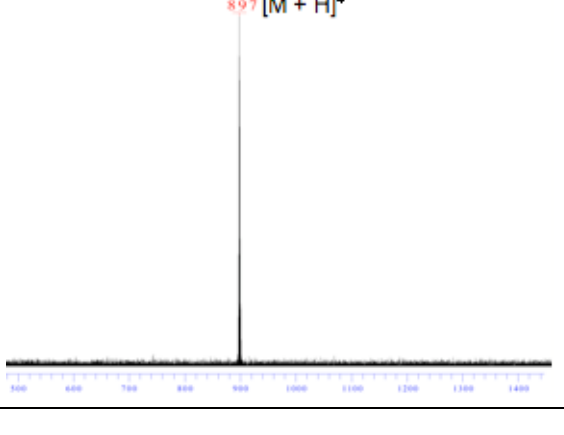
Peptide **15**: Ac-Leu-Cys( $\Psi^{Me, Me}$ pro)-Ala-(H<sup>+</sup>)Ser-Phe-Phe-Asp-NH<sub>2</sub>

Peptide **16**: Ac-Leu-Cys( $\Psi^{H, H}$ pro)-Ala-(H<sup>+</sup>)Ser-Phe-Phe-Asp-NH<sub>2</sub>

Peptide **17**: Ac-Leu-Cys( $\Psi^{Me, Me}$ pro)-Ala-(H<sup>+</sup>)Ser-(NMe)Phe-Phe-Asp-NH<sub>2</sub>

Peptide **18**: Ac-Leu-Cys( $\Psi^{H, H}$ pro)-Ala-(H<sup>+</sup>)Ser-(NMe)Phe-Phe-Asp-NH<sub>2</sub>

Peptide **19**: Ac-Leu-Cys( $\Psi^{Me, Me}$ pro)-Ala-(ArgPro)Ser-(NMe)Phe-Phe-Asp-NH<sub>2</sub>

	Analytical HPLC of purified compound	ES/MS of purified compound
15	 <p>HPLC chromatogram for compound 15. The x-axis represents time in minutes, ranging from 0 to 33. A major peak is observed at 17.2 minutes. There are smaller peaks at approximately 4.5 and 27 minutes.</p>	 <p>ES/MS mass spectrum for compound 15. The x-axis represents m/z, ranging from 0 to 1000. A major peak is observed at 883 m/z, labeled as <math>[M + H]^+</math>.</p>
16	 <p>HPLC chromatogram for compound 16. The x-axis represents time in minutes, ranging from 0 to 33. A major peak is observed at 15.7 minutes. There are smaller peaks at approximately 4.5 and 27 minutes.</p>	 <p>ES/MS mass spectrum for compound 16. The x-axis represents m/z, ranging from 0 to 1300. A major peak is observed at 855 m/z, labeled as <math>[M + H]^+</math>.</p>
17	 <p>HPLC chromatogram for compound 17. The x-axis represents time in minutes, ranging from 0 to 33. A major peak is observed at 18.2 minutes. There are smaller peaks at approximately 4.5 and 27 minutes.</p>	 <p>ES/MS mass spectrum for compound 17. The x-axis represents m/z, ranging from 0 to 1400. A major peak is observed at 897 m/z, labeled as <math>[M + H]^+</math>.</p>

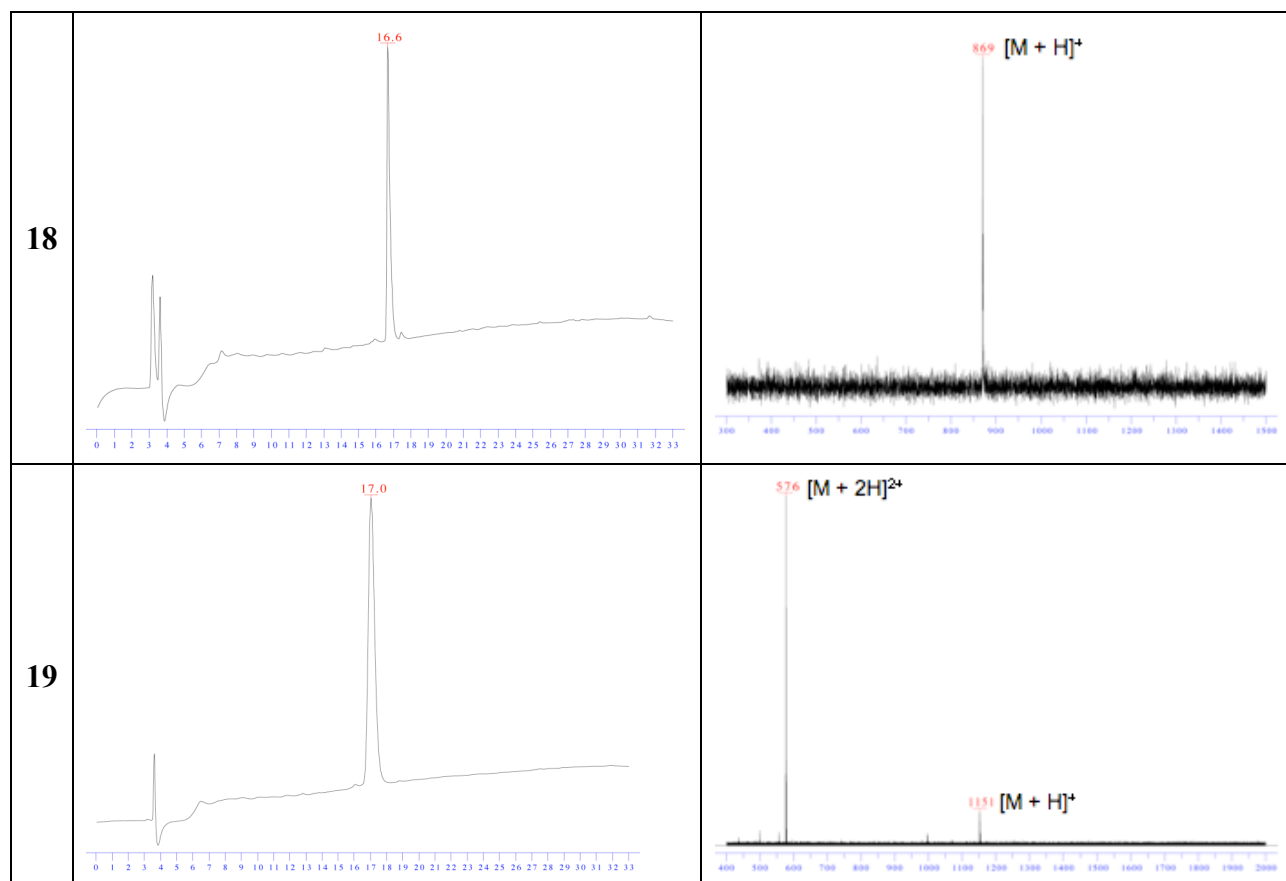


**Figure 63.** Analytical data of the purified compounds. HPLC (C18, gradient 0 to 100% A, 30 min); Mass spectroscopy ESI-MS.

### 5.3. Kinetic studies

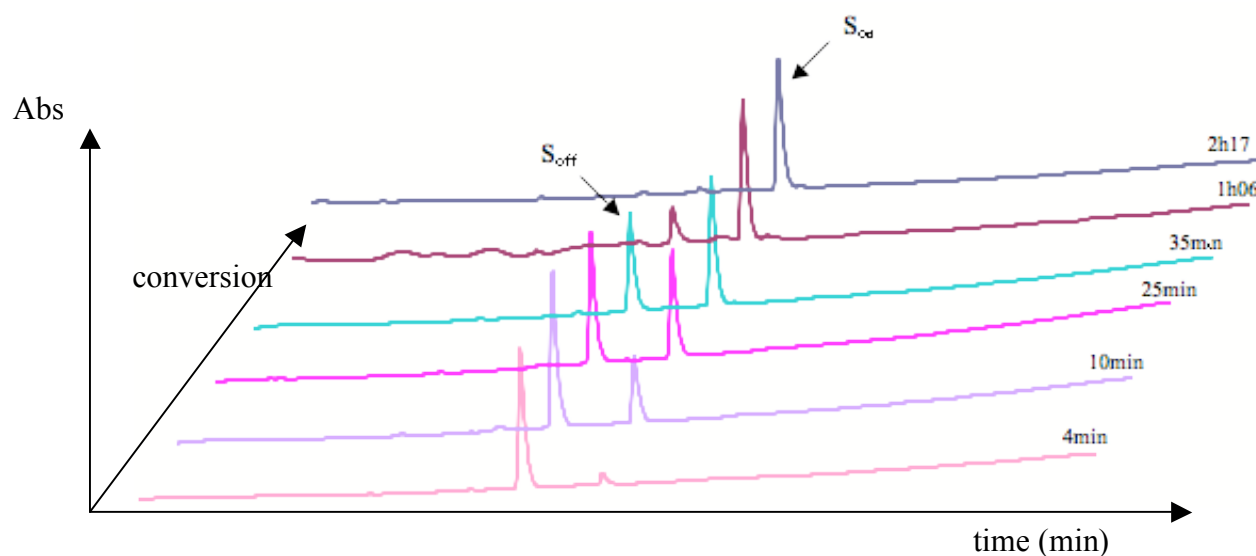
#### 5.3.1. pH-induced acyl migration

*Peptide 15:*  $Ac\text{-Leu-Cys}(\psi^{Me, Me}pro)\text{-Ala-(H}^+)\text{Ser-Phe-Phe-Asp-NH}_2$

To assess the influence of pH on the migration speed, the acyl migration of peptide **15** were triggered at three different pH (pH 6, 6.6 and 7.4). All experiments were done at 37°C, the peptide was dissolved in a mixture of acetonitrile/phosphate buffer of the desired pH (1:9) to a final concentration of 500  $\mu\text{M}$ . At different time points, 20  $\mu\text{L}$  aliquots were removed, quenched with 20  $\mu\text{L}$  HCl 1 M and injected to analytical HPLC.

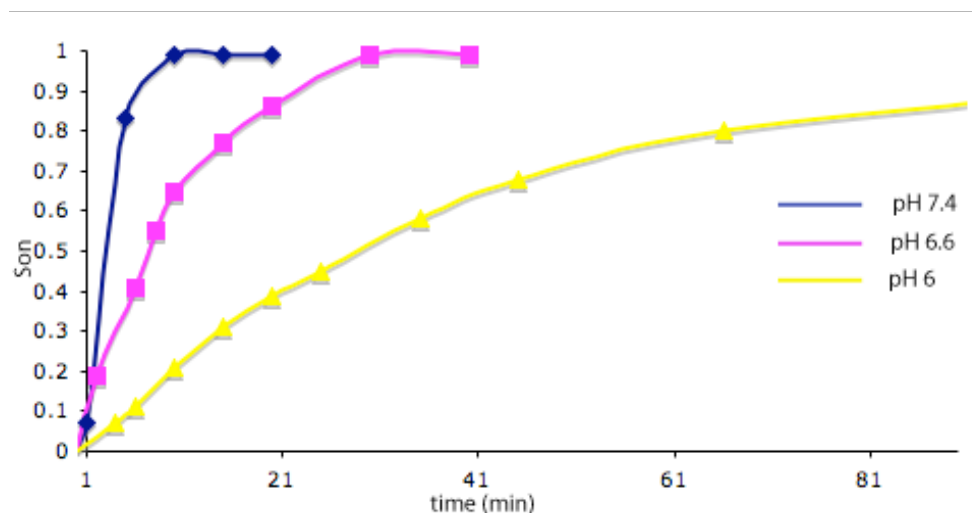
Figure 64 below shows the HPLC chromatograms of the migration at pH 6. The HPLC shows two peaks at  $R_t = 17$  min corresponding to the  $S_{\text{off}}$  state and  $R_t = 20$  min ( $S_{\text{on}}$  state after O to N migration). Upon migration, we observe the decrease in absorbance of the  $S_{\text{off}}$  peak and the

increase of the  $S_{on}$  peak; the migration is relatively rapid, even at pH 6 since the half-life value is about 25 min (see Figure 65).



**Figure 64.** HPLC chromatograms of the O to N acyl migration of peptide 15 in buffer pH 6/acetonitrile (9:1)

For the three different assays, the percent of peptide in the  $S_{on}$  state was plotted against time to compare the influence of the pH on acyl migration speed.



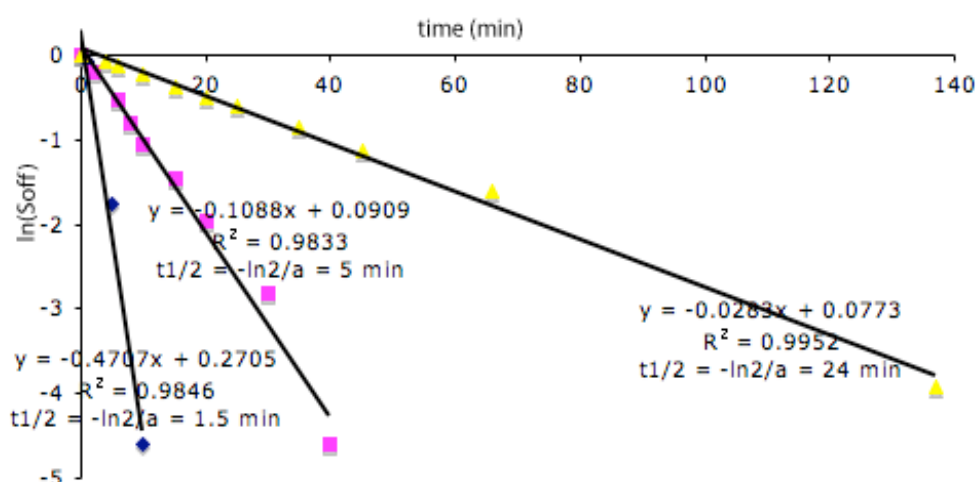


**Figure 65.** Overlay of time course and pseudo-first order kinetics of switch-peptide **15** subjected to different pH conditions.

The results obtained here at different pH show that the migration is extremely sensitive to pH. At pH 7.4 the half-life value was only of 1.5 min and at pH 6 was of 24 min, it is thus easier to follow the migration by HPLC at pH 6. Peptides **16**, **17** and **18** were therefore investigated at pH 6 under similar conditions.

*Peptide 16* :  $Ac-Leu-Cys(\psi^{H,H}pro)-Ala-(H^+)Ser-Phe-Phe-Asp-NH_2$

peptide **16** was dissolved in phosphate buffer pH 6 containing 10 % acetonitrile to a final concentration of 500  $\mu$ M. Figure 66 shows the chemical conversion of the peptide from its  $S_{off}$  state to its  $S_{on}$  state. In these conditions, the half-life value of the peptide ( $S_{off}$  state) is about 14 min (Figure 67). We also observe that the migration is complete after 90 min.

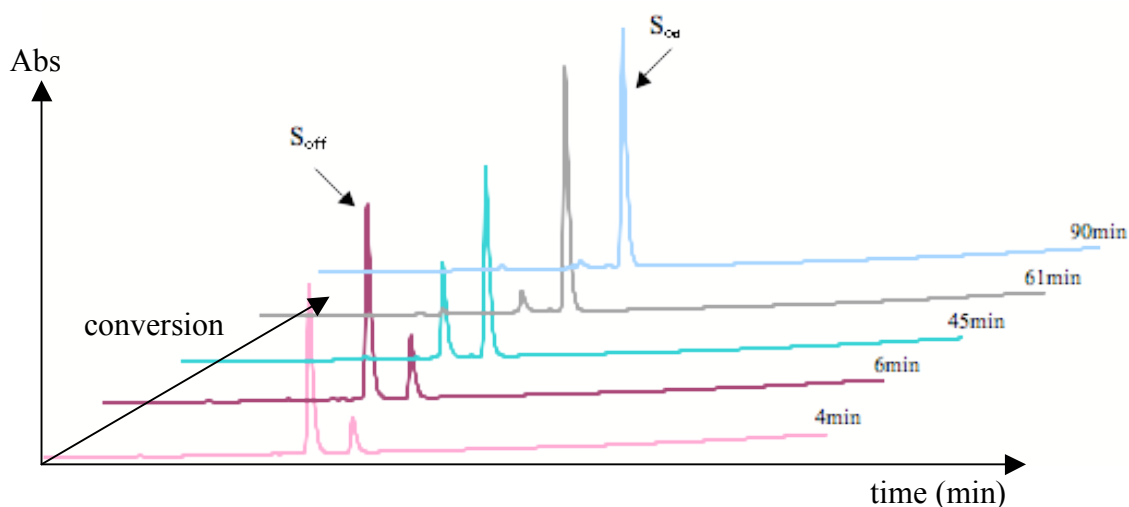


**Figure 66.** HPLC chromatograms of the O to N acyl migration of peptide **16** in buffer pH 6/acetonitrile.

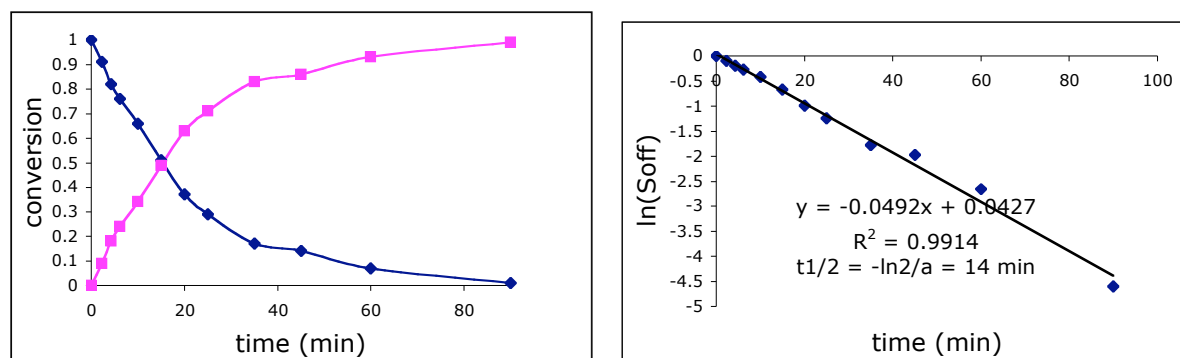


**Figure 67.** pH-induced acyl migration: time course (pink:  $S_{on}$ , blue:  $S_{off}$ ) and pseudo-first order kinetics of peptide **16**.

These results indicate that peptide **16** containing a dihydro-pseudoproline rearranges faster than peptide **15** containing a dimethyl-pseudoproline. This can be explained by the steric constraints imposed by the methyl groups of the dimethylpseudoproline and by the difference in electronegativity of the two pseudoprolines.

*Peptide 17: Ac-Leu-Cys( $\psi^{Me, Me}pro$ )-Ala-( $H^+$ )Ser-(NMe)Phe-Phe-Asp-NH<sub>2</sub>*

O to N acyl migration of peptide **17** was followed under similar conditions as previously. We observe here that the half-life value is about 19 min; it was of 25 min in the case of peptide **15** (Figure 68 & Figure 69). Compared to peptide **15**, peptide **17** also contains a dimethyl-pseudoproline but possesses an N-methylated phenylalanine after the S element. Interestingly, the constraint imposed by the methyl groups of the pseudo-proline has the effect of retarding the O,N-acyl migration (see results above) but on the contrary, the N-methylation of the residue Phe succeeding the switch element facilitates and accelerates the migration. One plausible explanation to this fact is that the methyl group of the N-methylated Phe residue, more electronegative than hydrogen, attracts electrons towards itself and speed up the migration by dislocating the electrons in the same direction as the O, N-acyl migration, contrary to dimethyl-pseudoproline (on the left side of the switch element) attracting the electrons on the opposite direction and hence having the effect of retarding the migration.

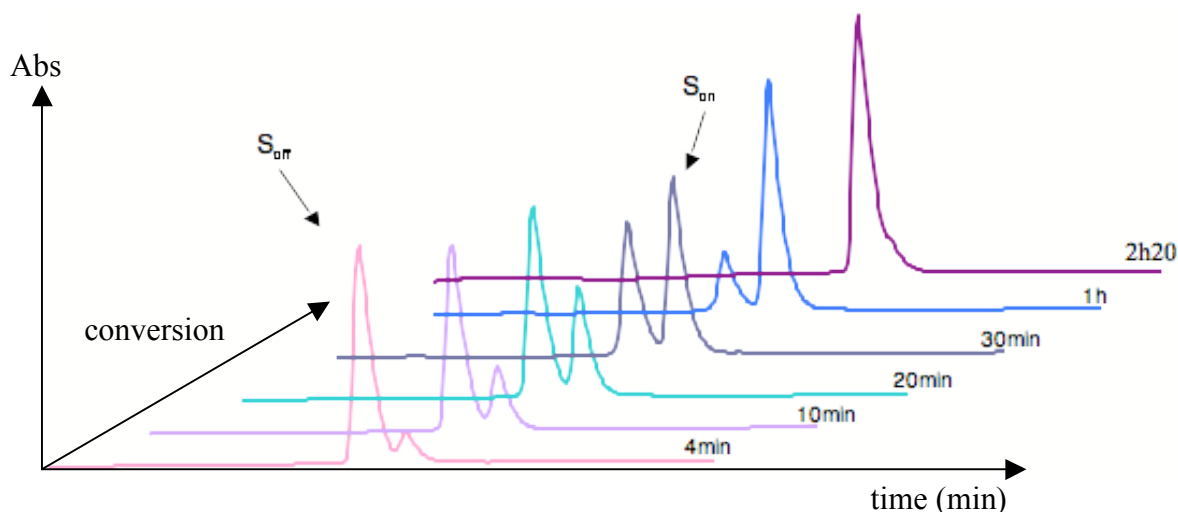


**Figure 68.** HPLC chromatograms of the O to N acyl migration of peptide 17 in buffer pH 6/acetonitrile.

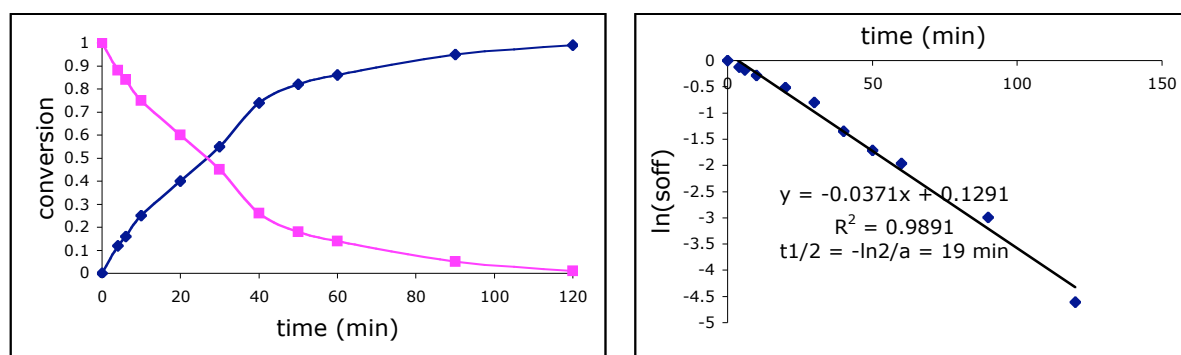


**Figure 69.** pH-induced acyl migration: time course (blue:  $S_{on}$ , pink:  $S_{off}$ ) and pseudo-first order kinetics of peptide 17.

**Peptide 18:**  $Ac\text{-Leu-Cys}(\psi^{H,H}pro)\text{-Ala-(H^+)Ser-(NMe)Phe-Phe-Asp-NH}_2$

Peptide **18** containing a dihydro-pseudoproline and a N-methylated phenylalanine after the switch element had the fastest rearrangement time under the conditions used for peptides **15**, **16** and **17**. Indeed, its half-life rearrangement value is of 8 min only (Figure 71), which is 3 times faster than peptide **15** having a dimethyl-pseudoproline and no N-methylation of the phenylalanine. This is easily explained by the reasons given earlier in this chapter.

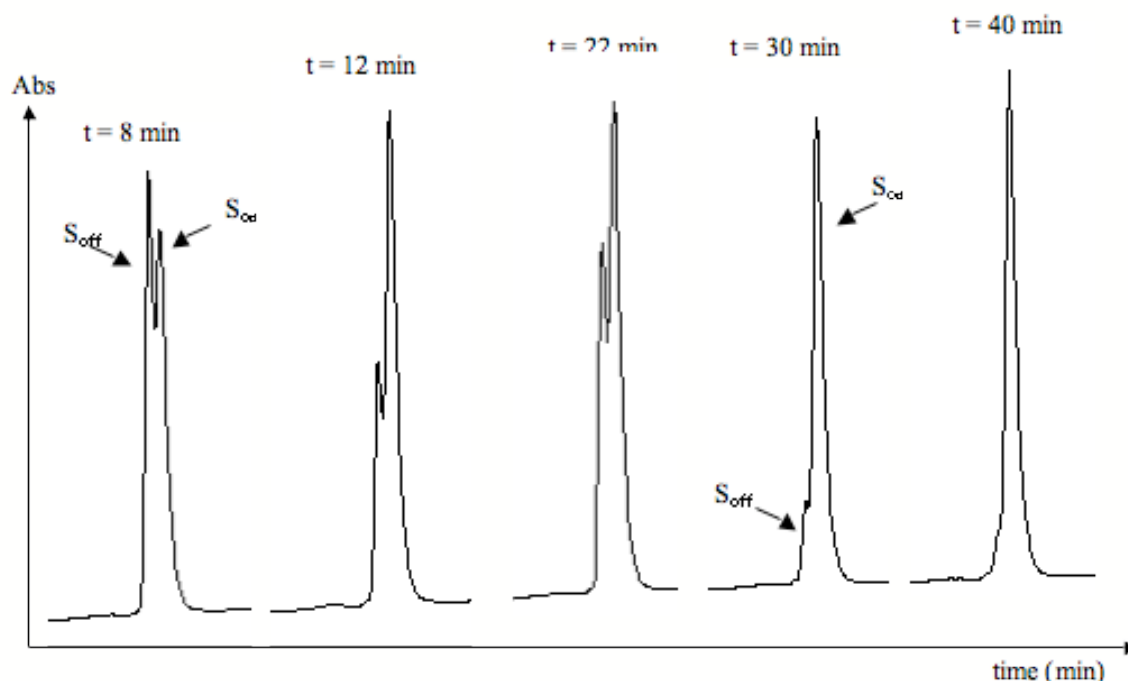


**Figure 70.** HPLC chromatograms of the pH induced acyl migration of peptide **18** at pH 6.

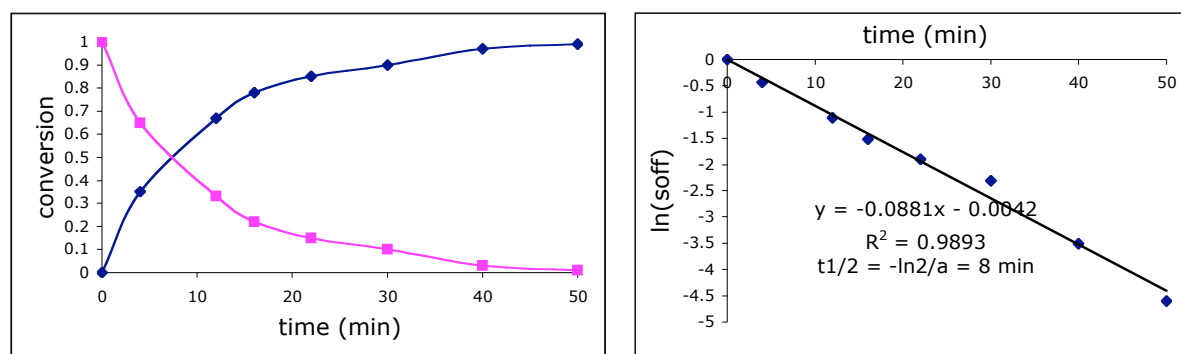


**Figure 71.** pH-induced acyl migration: time course and first order kinetics of switch-peptide **18**.

In summary, it emerges from these studies that O,N-acyl migration is greatly influenced by the pH. The half-life value can go from 1.5 min at pH 7.4 to 24 min at pH 6 (which means a factor of 12). The results obtained also point out that modifications brought to the molecule, even small, can have an impact on the kinetic of migration.

### 5.3.2. O to N acyl migration induced by enzymatic triggering

*Peptide 19:* Ac-Leu-Cys( $\psi^{Me, Me}pro$ )-Ala-(ArgPro)Ser-(NMe)Phe-Phe-Asp-NH<sub>2</sub>

The enzymatic conversion of peptide **19** was performed under physiological conditions. The peptide was dissolved in PBS pH 7.4 buffer at a concentration of 500  $\mu$ M and incubated at 37°



with DPPIV enzyme (ratio enzyme/substrat: 1/25 000). The enzymatic cleavage and the migration were monitored by analytical HPLC. At different time points, 20  $\mu$ L aliquots were withdrawn and injected to HPLC. Figure 72 shows the HPLC chromatograms of the enzymatic triggering of peptide **19**.

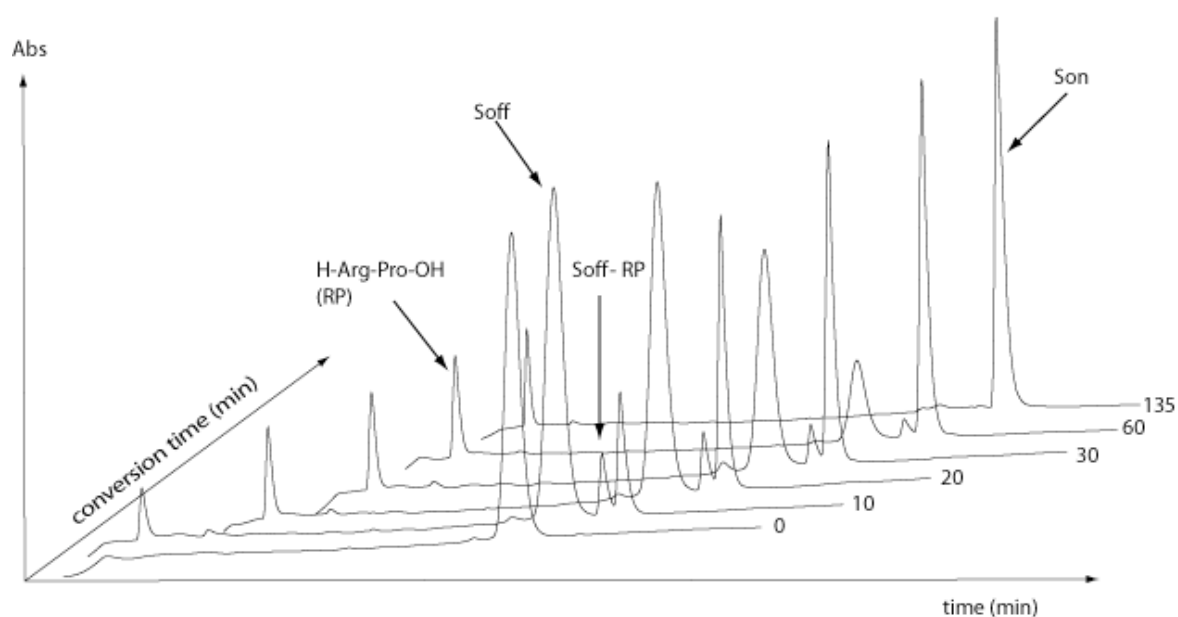


**Figure 72.** HPLC chromatograms of the enzymatic cleavage of dipeptide H-Arg-Pro-OH from switch-peptide **19** ( $S_{\text{off}}$ ), and subsequent acyl migration to give **19** in the  $S_{\text{on}}$  state.

HPLC overlay (Figure 72) shows the appearance of a first very hydrophilic peak corresponding to the cleavage of H-Arg-Pro-OH dipeptide by the enzyme. A second peak, decreasing with time, corresponds to the peptide in the  $S_{\text{off}}$  state. A third peak corresponding to the  $S_{\text{off}}$  state after Arg-Pro cleavage but before acyl migration is observed and eventually, a fourth peak corresponding to the peptide in its  $S_{\text{on}}$  conformation appears with a higher retention time. The enzymatic cleavage is relatively rapid; the conversion is complete after 2 hours 15 min at pH 7.4 ( $t_{1/2} \approx 20$  min). It is, however, slower than pH triggered acyl-migration for which a half-life value of 1.5 min was observed at pH 7.4.

#### 5.4. Study of the inhibition potential of Amyloid-derived switch-peptides

The inhibition potential of the five switch-peptides on fibrillogenesis was evaluated at physiological conditions by two different methods, electron microscopy and thioflavin T

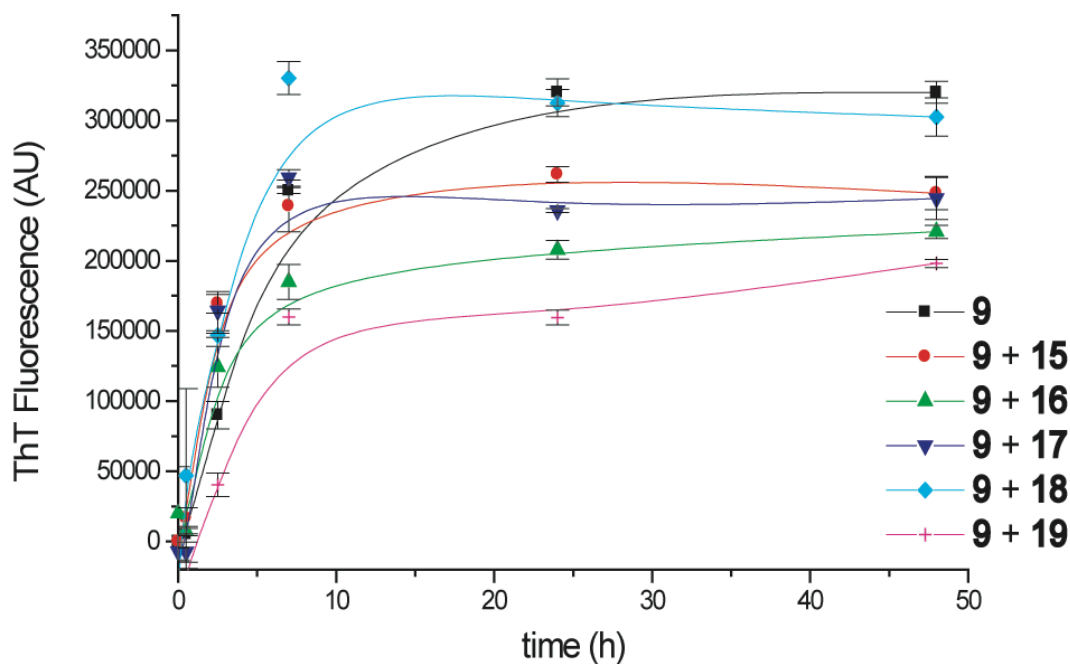
fluorescence on host-guest switch-peptide **9**, which proved to be a powerful tool for the screening of potential inhibitors of fibril formation in the previous section (see section 4).

#### *Experimental procedure*

Host-guest switch-peptide **9** was dissolved in H<sub>2</sub>O to a final concentration of 800  $\mu$ M (stock solution). The solution was vortexed for 30 seconds and filtered through a 0.2  $\mu$ m filter by centrifugation (5 min at 10'000 rpm). 50  $\mu$ L aliquots of the filtrate were put into autoclaved Eppendorf tubes. 750  $\mu$ L of acetate buffer pH 4.6 100  $\mu$ M were added to each tube. The inhibitors were dissolved in MeOH at concentrations of 1.6 mM and 100  $\mu$ L of these stock solutions were added to the mixture to give the correct final concentration of inhibitor in the reaction mixture. After 30 min (recognition lag time), 100  $\mu$ L of Tris buffer pH 7.4 (0.3 M) and 150 mM NaCl were added to each vial to trigger the switch. They were then placed in a 37°C water bath for 48 hours. Aliquots of 90  $\mu$ L were removed from the incubated samples at different time points and stored at -18°C until further analysis.

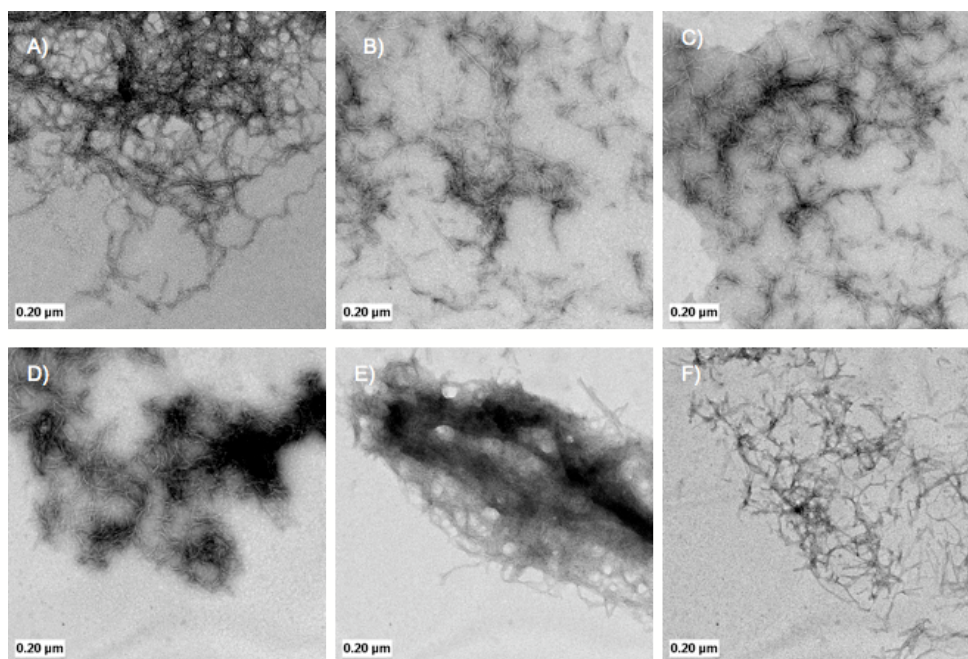
#### *ThT and EM analysis*

When peptide **9** was incubated alone at 37°C for 48 h, its ThT fluorescence curve (Figure 73, black curve) was similar to the ThT fluorescence curve of the full length A $\beta$ <sup>121</sup> (not shown). EM images taken after 2 days revealed amyloid-like fibril formation, confirming the results obtained from ThT measurements.



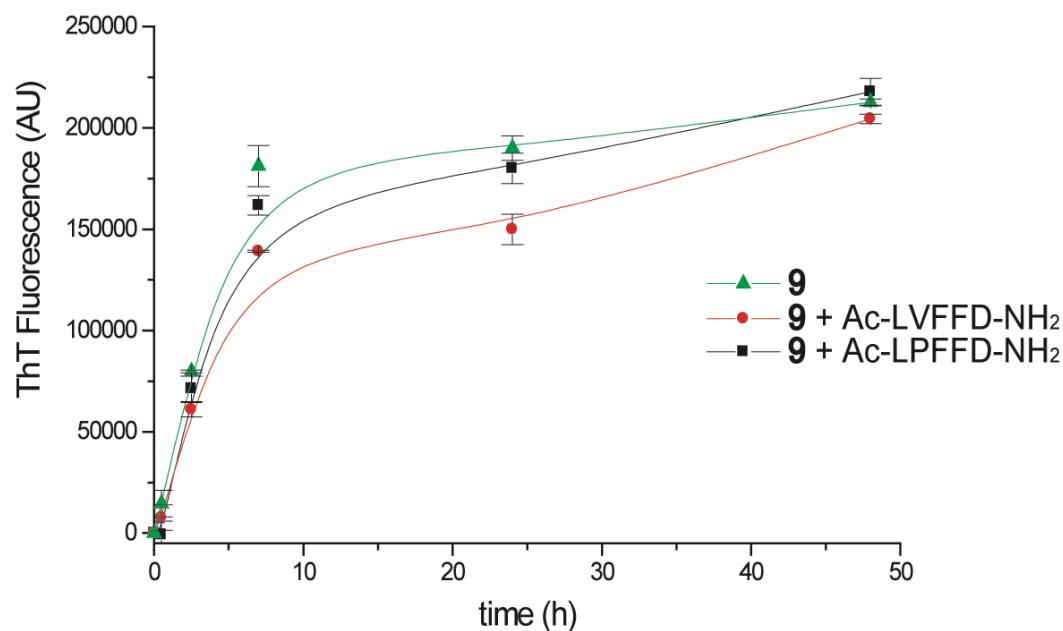
**Figure 73.** Kinetics of fibril formation of peptide **9** ( $40 \mu\text{M}$ ) monitored by ThT fluorescence. Control (black), with  $160 \mu\text{M}$  of peptides **15** (red), **16** (green), **17** (blue), **18** (cyan), and **19** (pink).

Figure 73 and Figure 74 (E) show that peptide **18** for which O,N-acyl migration was the fastest seems to have no inhibitory effect on fibril formation. Other inhibitors activated by pH with longer  $t_{1/2}$  half-life values showed a slightly increased inhibition (about 22% of inhibition by ThT after 48h). We can see by EM that the fibrils formed when peptide **9** is incubated in the presence of inhibitors **15**, **16**, **17** and **19** are shorter than fibrils of the control sample (see Figure 74). Interestingly, peptide **19**, which is activated by the enzyme DPPIV, exhibited a better inhibitory effect compared to the other investigated compounds (about 47% of inhibition after 48h). This phenomenon had previously been observed<sup>104,128</sup> and can be explained by the fact that O,N-acyl migration of peptides activated by enzymes is slower because enzyme triggering is the rate limiting step for acyl migration and not rearrangement. The results confirm previous observations that the switch-peptide in its  $S_{\text{off}}$  state where the recognition sequence of A $\beta$  is separated from the kink inducing unit should have time to first recognize A $\beta$  sequence before setting off the kink structure that stabilizes fibrils.



**Figure 74.** EM images of peptide **9** after 48 h at 37°C and pH 7.4, A) alone and in presence of 4 equivalents of B) peptide **15**, C) peptide **16**, D) peptide **17**, E) peptide **18** and F) peptide **19**.

To compare the inhibitory effect of our molecules with the well-known pentapeptide inhibitor iA $\beta$ 5 (Ac-LPFFD-NH<sub>2</sub>) and with Ac-LVFFD-NH<sub>2</sub>, their inhibitory effect was tested on peptide **9** under the same conditions as above. ThT fluorescence of peptide **9** with 4 eq of inhibitors did not show any decrease in fluorescence compared to the control.



**Figure 75.** Kinetics of fibril formation of peptide **9** (40  $\mu$ M) monitored by ThT fluorescence. Control (green), with 160  $\mu$ M of Ac-LVFFD-NH<sub>2</sub> (red), Ac-LPFFD-NH<sub>2</sub> (black).

However, although fibrils were observed by EM, they were shorter than the fibrils observed for the control. From these studies, we deduce that both molecules had a smaller inhibitory effect on peptide **9** fibrillogenesis than switch-peptides molecules investigated earlier. This confirms previous observations that the introduction of a switch element separating the  $\beta$ -sheet breaking unit from the recognition sequence enable a better recognition of the target before activating the switch, restoring the regular amide backbone and setting off the  $\beta$ -disrupting unit activity. This sequential process allows the peptide to be in closer contact with the target and have a stronger impact on fibril destabilization.

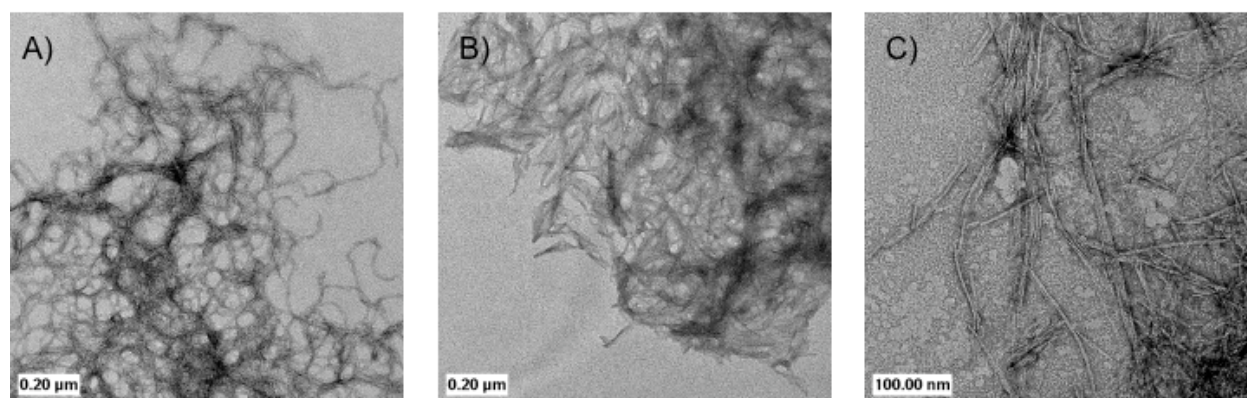


**Figure 76.** EM images of peptide **9** after 48 h at 37°C and pH 7.4, A) alone and in presence of 4 equivalents of B) Ac-LVFFD-NH<sub>2</sub>, C) Ac-LPFFD-NH<sub>2</sub>.

## 5.5. Discussion

The switch-peptides were successfully synthesized by SPPS in good yields. It emerges from these studies that O,N-acyl migration is greatly influenced by the pH. The half-life value can go from 1.5 min at pH 7.4 to 24 min at pH 6 (which means a factor of 12). The results obtained also point out that modifications brought to the molecule, even small, can have an impact on the kinetic of migration.

No significant differences in term of inhibition potential were noted between the switch-peptides triggered via pH, except for peptide **18** having the fastest rearrangement half-time value. The peptide did not show any inhibitory activity. The major reason might be that the peptide does not stay long enough in its recognition state ( $S_{\text{off}}$  state) before rearranging and thus, does not bind correctly to the target sequence to block its  $\beta$ -sheet and fibril formation.

Moreover, the rearrangement of switch-peptide **19** having a protecting group cleavable by an enzyme was slower and could be controlled easily. Peptide **19** was able to stay longer in the  $S_{\text{off}}$  state for better recognition, which was beneficial since it exhibited better inhibition activity compared to other peptides triggered via pH (47% inhibition vs. 22% inhibition).

Compared to the two pentapeptides Ac-LVFFD-NH<sub>2</sub> and Ac-LPFFD-NH<sub>2</sub> tested in the same manner, the switch-peptides had an enhanced inhibitory activity on the fibril formation of host-guest switch-peptide **9**.

These results open interesting perspective in the rational design of flexible peptides able to bind  $\beta$ -sheets in an efficient way before setting off the kink *in situ*, increasing the biological potential of inhibitors.

## **6. Disruption of Amyloid-Derived Peptide Assemblies through the Controlled Induction of a $\beta$ -sheet to $\alpha$ -Helix Transformation: Application of the Switch-Concept<sup>2</sup>**

Protein misfolding and self-assembly into highly ordered  $\beta$ -sheet rich fibrillar assemblies known as amyloid fibrils are common features of a growing class of systemic and neurodegenerative diseases, including Alzheimer's, Parkinson's, Huntington's disease, senile systemic amyloidoses, and type II diabetes<sup>129, 130</sup>. Although there is strong evidence implicating amyloid formation in the pathogenesis of these diseases, the precise mechanisms of amyloid formation and clearance *in vivo* as well as the structural basis of amyloid toxicity remain unknown. The lack of tools to monitor and/or control the initial structural transitions associated with protein misfolding, amyloid formation and/or dissociation is at the origin of this gap in knowledge. Significant efforts have been devoted to study proteins and small peptides that self-assemble into amyloid-like fibrillar structures as model systems to investigate amyloid formation or to generate materials with interesting physical properties. However, our knowledge of the mechanical and structural dynamics within  $\beta$ -sheet assemblies such as amyloid fibrils remains limited. Early assumptions<sup>131</sup> that  $\beta$ -sheet assemblies, including amyloid fibrils, occupy a global minimum of free energy that is lower than that of the native state led to greater emphasis on understanding and inhibiting amyloid formation, rather than amyloid dissociation and clearance. Despite the extreme stability of  $\beta$ -sheet rich amyloid fibrils to proteases, acid and chemical denaturants, increasing evidence from humans<sup>132</sup> and *in vitro* studies points to a dynamic structure within amyloid fibrils and suggests that the process of amyloid formation is reversible<sup>133, 134</sup>. These findings combined with the fact that strategies aimed at destabilizing amyloid and/or accelerating their clearance seem to reverse the disease phenotype<sup>135-137</sup> suggest that a detailed understanding of the stability and dynamic behavior of amyloid fibrils is of critical importance to developing therapeutic strategies for amyloid diseases.

Our laboratory has previously shown<sup>80, 100, 112</sup> that incorporation of molecular switches into polypeptides, based on O $\rightarrow$ N intramolecular acyl migration *in situ*<sup>105, 106, 138, 139</sup>, allows for

---

<sup>2</sup> This Chapter has been published in *Angew. Chem. Int. Ed.*, **2007**, 46, 2681-2684

controlled induction or reversal of secondary structural transitions<sup>140-142</sup> and self-assembly of small peptides.

Moreover, during his PhD Thesis<sup>143</sup>, R. Mimna, who worked mainly on the design and synthesis of helix-inducing N-cap compounds ( $\sigma$ )<sup>144</sup>, was able to demonstrate that in model switch-peptides, N-cap units prevented the formation of  $\beta$ -sheet by inducing a stable  $\alpha$ -helical structure. Subsequently, an amyloid-derived switch-peptide containing an N-cap as conformational induction unit ( $\sigma$ ) was designed. By triggering the switch, we could observed a transformation of type  $\beta$  to  $\alpha$  by Circular Dichroism (CD). Based on these primarily findings, the work presented in this chapter focuses on further investigating the feasablilty of disrupting amyloid formation through the controlled induced transformation form  $\beta$ -sheet to  $\alpha$ -helix structures of the self-assembled peptides within the amyloid structure (Figure 77).



## 6.1. Design

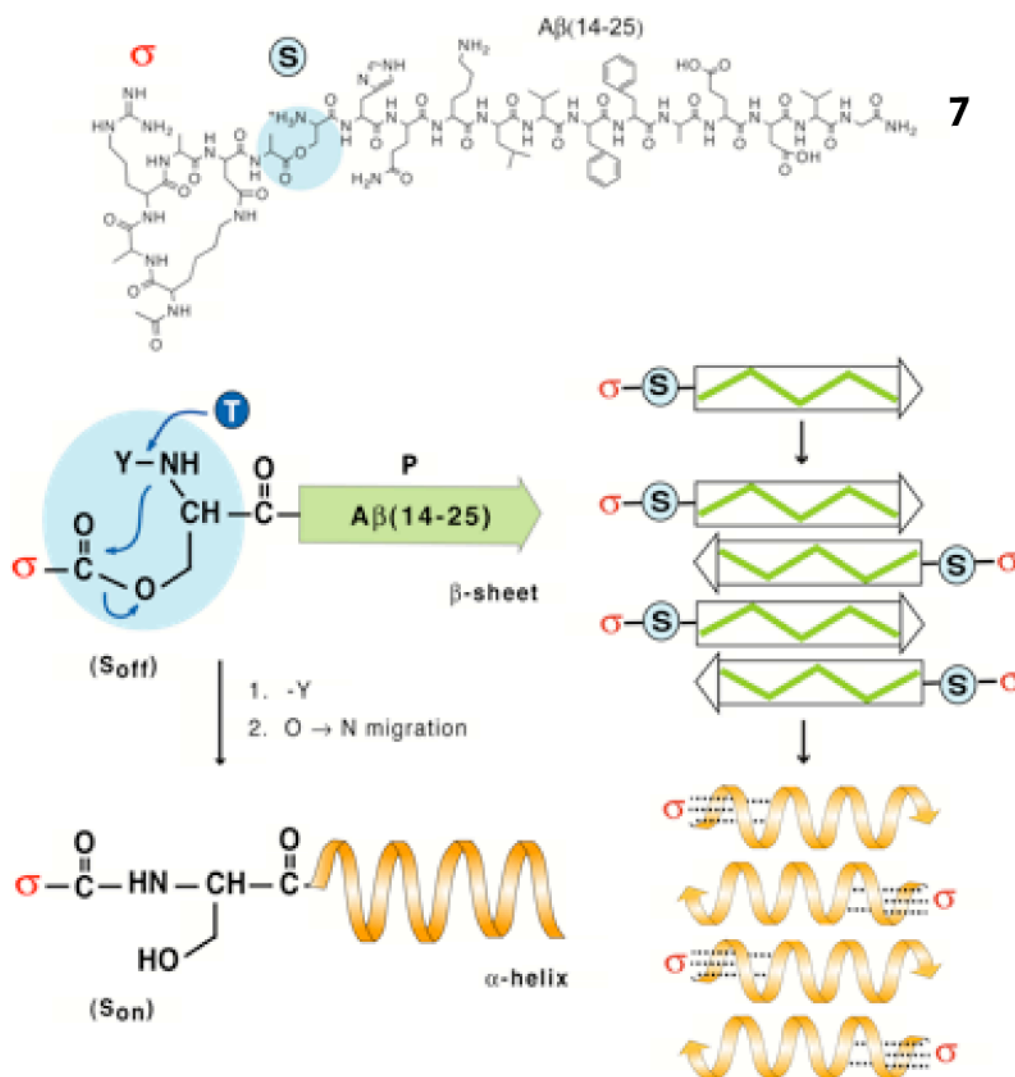


**Figure 77.**  $A\beta(14-25)$  is linked to a helix-inducing template  $\sigma$  ( $Ncap = Ac$ -[cyclo-1-5]-KARADA) through a Ser-derived switch-element  $S$  ( $O$ -acyl isopeptide unit,  $S_{off}$ -state). On removal of the  $N$ -protecting group  $Y$ , spontaneous  $O,N$ -acyl migration occurs ( $S_{on}$  state) resulting in the activation of  $\sigma$  and induction of a helix structure in peptide 7 (left). Under the right conditions, the helix-nucleating effect of  $\sigma$  is strong enough to induce a transformation from  $\beta$ -sheet (step 1) to  $\alpha$ -helix (step 2), along with disruption of the preformed  $A\beta(1-42)$ -derived  $\beta$ -sheet-rich assemblies within amyloid fibrils.

The amyloid-derived switch-peptide contains the shortest  $A\beta$  fibril-forming sequence HQKLVFFAEDVG, corresponding to  $A\beta(14-25)$ , connected to a helix nucleating  $Ncap^{144}$  ( $\sigma$ )



piperidine/DMF, 10 min x 2; Ac<sub>2</sub>O (10 eq), pyridine (10 eq), DMF, 30 min; (iv) TFA/TIS/H<sub>2</sub>O/DODT 95/2/2/1, 2h.

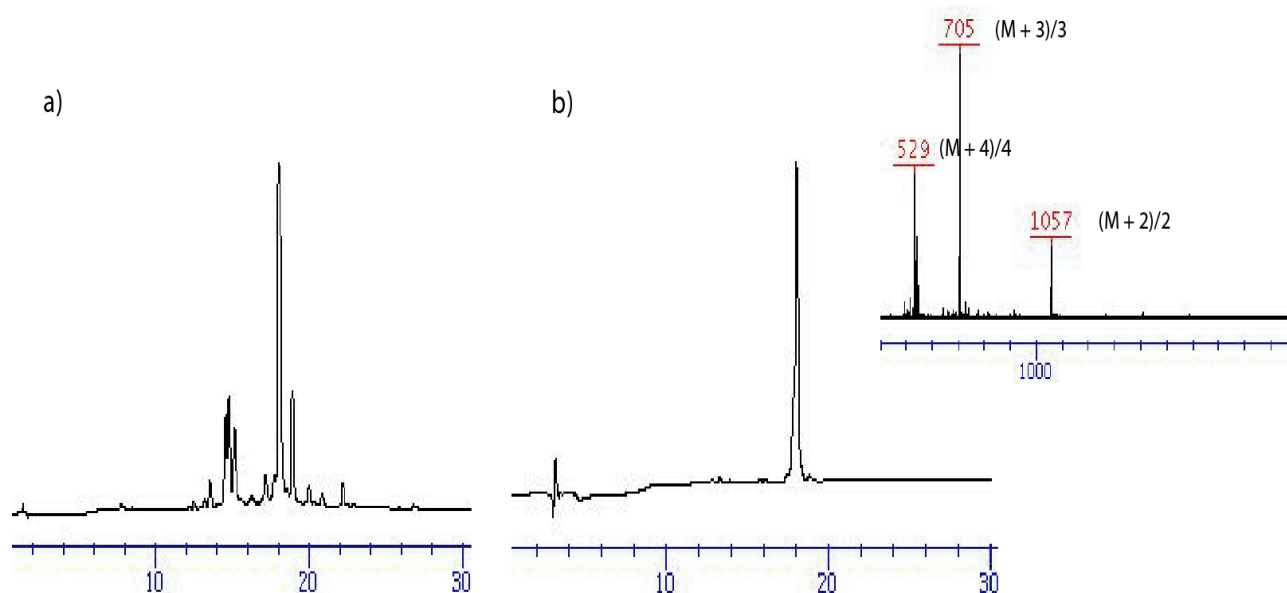


**Figure 78.** Analytical data of switch-peptide 7 a) HPLC chromatogram of crude compound, b) HPLC and ESI-MS (inset) of purified compound.

### 6.3. N-cap induced $\beta$ to $\alpha$ reversal of A $\beta$ (14-25)

#### CD and EM studies

To examine the solution properties of peptide 7 in the S<sub>off</sub> and S<sub>on</sub> states (Figure 77), the secondary structure and aggregation state of the peptide was probed by circular dichroism (CD) and electron microscopy (EM).

In the S<sub>off</sub> state (pH 4.5, 50 mM acetate, 150 mM NaCl) and at concentrations between 10-100  $\mu$ M, peptide 7 displays a CD spectra showing the typical cotton effect of a  $\beta$ -sheet structure (curve 1 in Figure 79). Activation of the helix-inducing Ncap (S<sub>on</sub>) via a pH-induced O,N-acyl migration<sup>80, 100, 105, 106, 138, 139</sup> is not sufficiently strong to overcome the intrinsic  $\beta$ -sheet propensity of A $\beta$ (14-24) resulting in identical CD spectra. However, when activated in the

presence of 25% TFE as  $\alpha$ -helix promoting cosolvent, an unprecedented structural transition from predominantly  $\beta$ -sheet in the  $S_{off}$  state with a strong negative cotton effect at  $\lambda = 218$  nm (curve 2) to an  $\alpha$ -helix in the  $S_{on}$  state with negative cotton effects at  $\lambda = 204$  nm and 222 nm (curve 3) is observed and is complete within less than 5 min at room temperature ( $t_{1/2}$  value = 150 sec, Figure 79, inset). This result demonstrates the strong nucleating effect of the Ncap and shows for the first time the possible reversibility of highly ordered  $\beta$ -sheet structures.

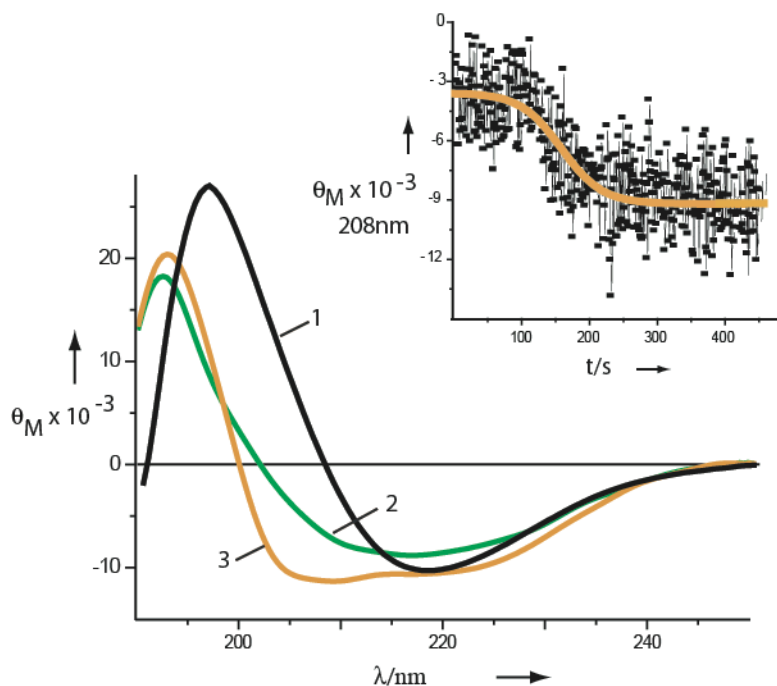


**Figure 79.** Conformational transitions of peptide 7 ( $c = 5 \times 10^{-5}$  M,  $T = 25^\circ\text{C}$ ): A) curve 1: pH 4.6 buffer ( $S_{off}$ ); curve 2: pH 4.6 buffer/TFE 75:25 ( $S_{off}$ ); curve 3: pH 7.0 buffer/TFE 75:25 ( $S_{on}$ ). Inset: the kinetics of the conformation from  $\beta$ -sheet ( $S_{off}$ ) to  $\alpha$ -helix ( $S_{on}$ ) structures as monitored by changes in the CD signal.

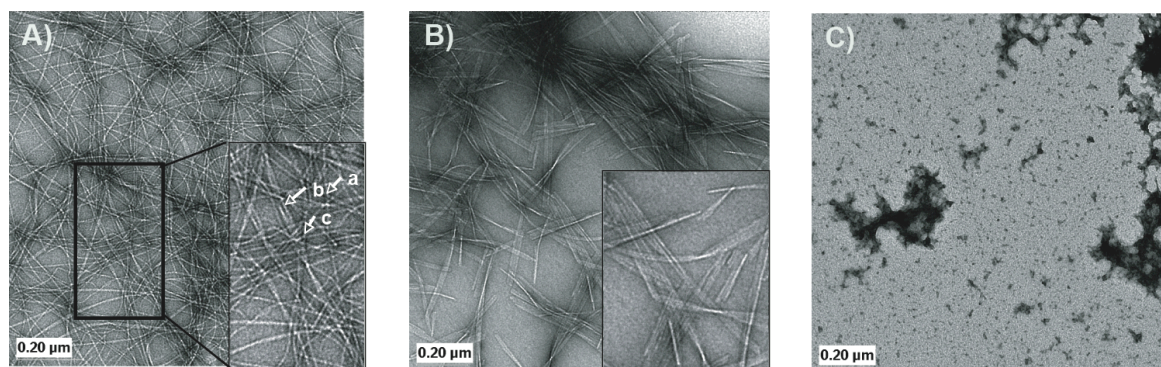


**Figure 80.** Negative electron micrographs of peptide 7 ( $c = 5 \times 10^{-5}$  M) in the  $S_{off}$  state (A) and  $S_{on}$  state 5min (B) and 12 h (C) after activation of the intramolecular O to N acyl migration.

Electron microscopy (EM) studies revealed that the transition from  $\beta$ -sheet to  $\alpha$ -helical structure is accompanied by a dramatic change in the morphology of the fibrils and subsequent dissociation. Figure 80 shows negatively stained micrographs of peptide 7 before ( $S_{\text{off}}$ , A) and after ( $S_{\text{on}}$ , B and C) triggering the switch element in the presence of 25% TFE. In the  $S_{\text{off}}$  state, peptide 7 self-assembles into long ( $> 2 \mu\text{m}$ ) unbranched fibrils with an average diameter of 3.3 nm (Figure 9A, inset: a). Lateral association of these thin fibrils results in the formation of twisted amyloid-like fibrils with an average diameter of 7.7 nm, 11 nm, and 20 nm, consistent with the 3.3 nm being the subunit “protofilament” of the wider fibrils (Figure 9A). Interestingly, upon triggering the O,N-acyl migration ( $S_{\text{on}}$  state), short ribbon-like structures (Figure 80B) are observed, but disappear quickly with time giving rise to predominantly soluble  $\alpha$ -helical structures of peptide 7. Filtration of peptide 7 solution ( $S_{\text{off}}$  state) through a  $0.22 \mu\text{m}$  membrane results in the loss of more than 80% of the peptide and disappearance of  $\beta$ -sheet structure (see Figure 80). In the  $S_{\text{on}}$  state, more than 95% of peptide 7 remains in solution after filtration through  $0.22 \mu\text{m}$  membrane, consistent with the transition from an aggregated  $\beta$ -sheet to soluble  $\alpha$ -helix structures (CD)(Figure 81) as evidenced by the disappearance of fibrillar assemblies (Figure 80C), and loss of ThT fluorescence upon activation of the O,N-acyl migration (Figure 82).

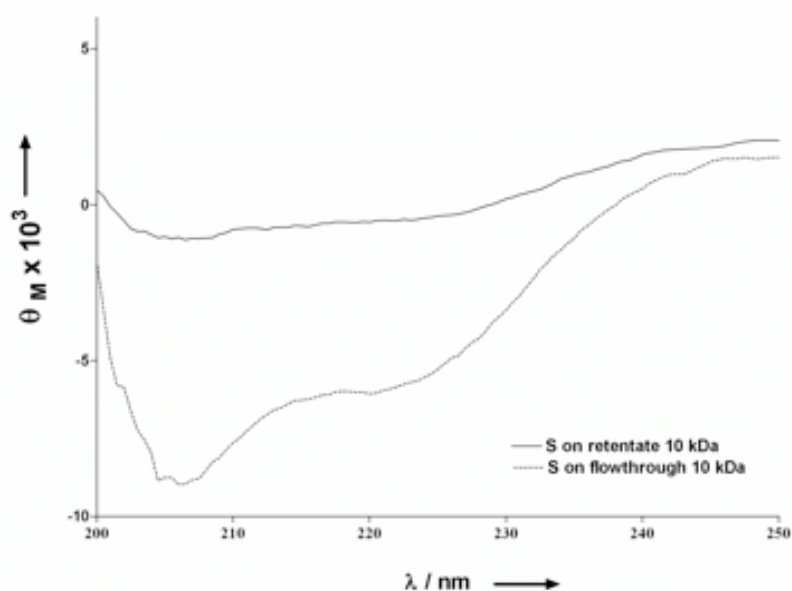


**Figure 81.** CD spectra of peptide 7 in the  $S_{\text{on}}$  state in 25% TFE at 25°C of the filtrate after filtration through a 10kDa membrane filter (dashed line), and of the retentate (continuous line).

*Thioflavin T (ThT) and Congo Red (CR) binding of peptide 7*

To confirm our results on the morphology of the fibrils, peptide **7** was mixed with amyloid specific dyes such as Congo Red (CR) and Thioflavin T (ThT) and its binding to these dyes was assessed by UV spectroscopy and fluorescence spectroscopy respectively (Figure 82).

The binding of peptide **7** to the amyloid specific dye Congo Red (CR) causes a red-shift in its absorbance spectrum, characteristic of amyloid fibrils. The left part of Figure 82 shows the absorbance spectra of Congo Red alone (full line), in the presence of peptide **7** in the  $S_{\text{off}}$ -state (dashed line) or preformed  $\alpha$ -synuclein fibrils (dotted line). The CR spectrum in the presence of peptide **7** resembles those previously published for  $A\beta$  and is virtually identical to that observed for preformed fibrillar assemblies of the amyloid forming protein  $\alpha$ -synuclein linked to Parkinson's disease. Amyloid fibrils of  $\alpha$ -synuclein were used because a freshly prepared fibrillar sample was available at the day the experiment with peptide **7** was carried out.

Furthermore, the peptide also binds Thioflavin T when it is in the  $S_{\text{off}}$  state, thus in a  $\beta$ -sheet conformation. This further confirms that the fibrils formed by the peptide are indeed amyloid-like fibrils (Figure 82, right).

The binding of peptide **7** in the  $S_{\text{on}}$  state to ThT was also examined and revealed that the peptide did not exhibit any fluorescence when it was in the  $S_{\text{on}}$  state, thus in an  $\alpha$ -helical conformation (Figure 82, right, orange bar). Therefore, we can conclude that a conformational transition from  $\beta$ -sheet to soluble  $\alpha$ -helical structure of the peptide has occurred and that amyloid fibrils have effectively been destabilized and cleared.

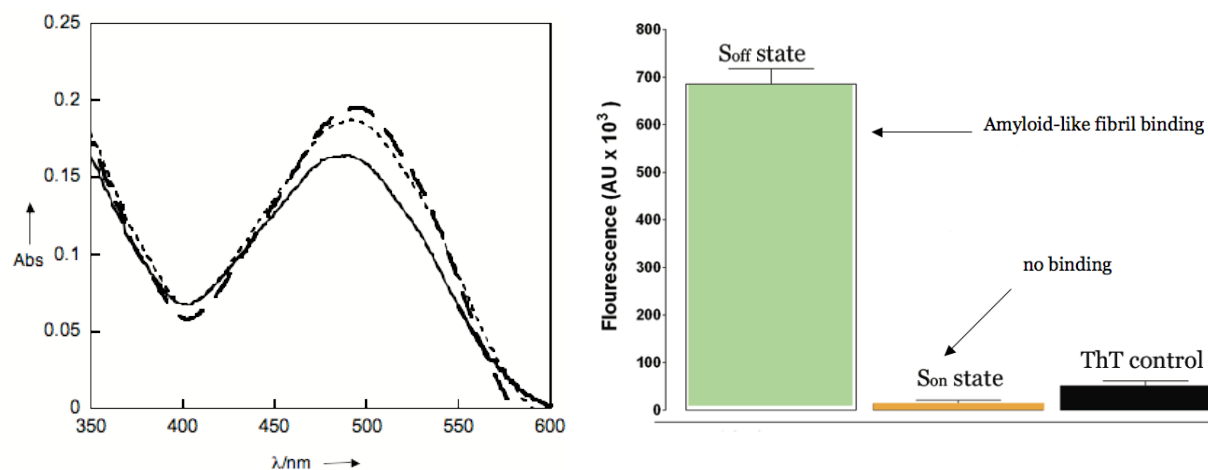


**Figure 82.** Left: Absorbance spectra of CR alone (full line), in the presence of peptide 7 in the  $S_{off}$  state (dashed line) and preformed  $\alpha$ -synuclein fibrils (dotted line). Right: ThT fluorescence of peptide 7 in 25% TFE in the  $S_{off}$  state (green), as well as after O to N acyl migration and filtration through a 10 kDa membrane filter (orange), ThT control (black).

#### Heat induced dissociation/denaturation

To better understand the structural properties of peptide 7, we probed its stability in the  $S_{on}$  and  $S_{off}$  state towards heat-induced dissociation/denaturation. To this end, the peptide solutions are heated gradually and the conformation of the peptide is monitored by CD (Figure 83). Heating of peptide 7 in the  $S_{off}$  state (pH 4.5, 25°C, green curve) to 95°C results in a transition from  $\beta$ -sheet to a predominantly unordered structure (black curve). Interestingly, upon cooling the sample to 25°C, the peptide does not return to its original  $\beta$ -sheet structure, but rather forms an  $\alpha$ -helical structure (orange curve), pointing to the onset of the helix-inducing effect of the Ncap at high temperature (due to temperature induced O,N-acyl migration and activation of the Ncap). Most notably, once the  $\beta$ -sheet is destabilized at high temperature, the helix-inducing effect of the Ncap is strong enough to overcome the intrinsic  $\beta$ -sheet potential of peptide 7, i.e. a Ncap-induced transition of type random-coil (95°C) to  $\alpha$ -helix (25°C) is observed.

Moreover, at pH 7 and in the absence of TFE, peptide 7 ( $S_{on}$  state) does not exhibit a clear  $\alpha$ -helical structure but when heated to 95°C and cooled back to 25°C the peptide undergoes a transformation similar to the one previously observed at pH 4.6.

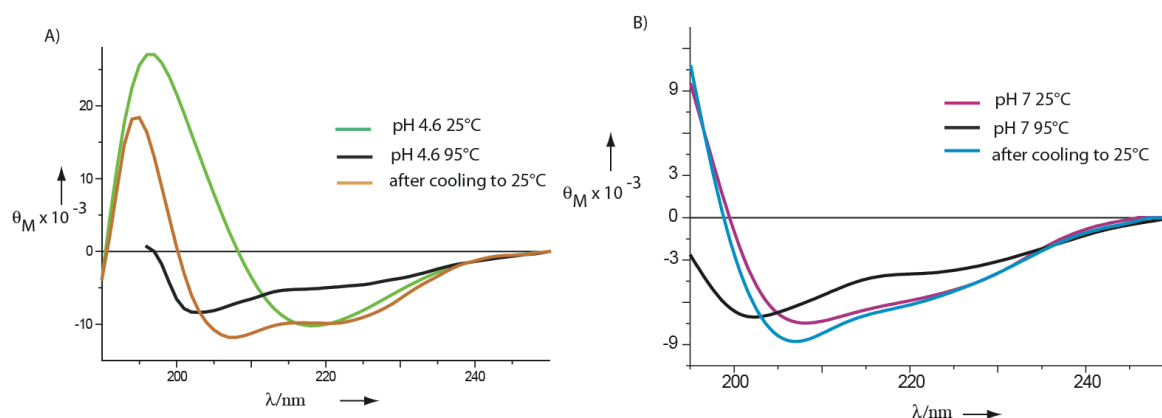


**Figure 83.** Monitoring conformational transition of peptide 7 by CD ( $c = 5 \times 10^{-5} \text{ M}$ ): A) in buffer pH 4.6 and B) in buffer pH 7.

#### Conformation of peptide 7 in the $S_{off}$ state in TFE

TFE is commonly used as a co-solvent in protein folding studies, this solvent can effectively solubilize both peptides and proteins and it is known that, depending upon its concentration, TFE can strongly affect the three-dimensional structure of proteins and facilitates helix formation by affecting hydrophobic interactions.

It is noteworthy that in the presence of TFE alone (20-100%), the conformation of peptide 7 is not affected and the peptide still forms predominantly  $\beta$ -sheet rich fibrillar aggregates (Figure 84).

It confirms that the helix nucleating template is necessary to enable peptide 7 to undergo a conformational transition from  $\beta$ -sheet to  $\alpha$ -helix.

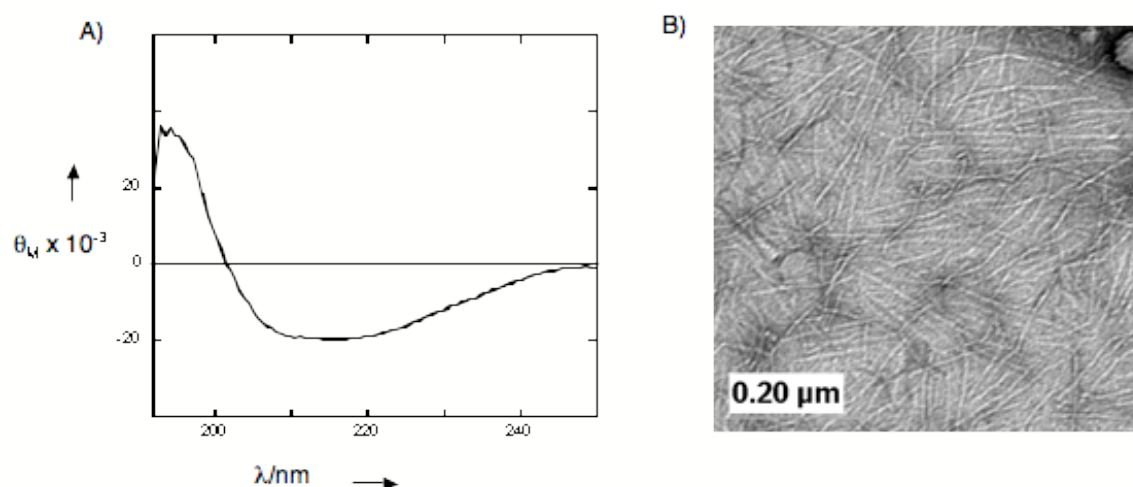


**Figure 84.** CD spectrum (A) and negatively stained electron micrograph (B) of peptide 7 dissolved directly in 100 % TFE



#### 6.4. Conclusion and perspective

Using peptide **7**, we were able to investigate the feasibility of disrupting amyloid formation through controlled induction of  $\beta$ -sheet to  $\alpha$ -helix transformation of the self-assembled peptides within the amyloid structure. The experimental data offer new insights into the stability and structural properties of amyloid fibrils.

Our studies support the dynamic structure of amyloid<sup>133, 134, 151</sup> and demonstrate that significant structural rearrangements can take place within the  $\beta$ -sheet structure of amyloid fibrils. Furthermore, these studies demonstrate for the first time that structural changes in polypeptide regions<sup>140</sup> that are not involved in amyloid formation could have significant impact on the stability and structural dynamics of amyloid fibrils.

Developing tools to disrupt and/or reverse  $\beta$ -sheet based self-assembly have important implications for understanding the mechanisms of protein aggregation and clearance *in vivo* and the development of therapeutic strategies aimed at preventing/reversing amyloid formation.

The ability to control the structure and morphology of the aggregates formed by peptide **7** suggest that engineering specific switch elements and/or structure templating motifs within amyloid forming proteins and peptides could provide the necessary means to correlate structural differences between the different amyloid morphologies with toxicity.



## Chapter III. Experimental part

### 1. Instrumentation and general methods

#### *Reagents and solvents*

Solvents and reagents were purchased from Fluka (Buchs, Switzerland), Sigma-Aldrich Chemie GmbH (Steinheim, Germany) or Acros (Geel, Belgium). Amino acids derivatives, resins and coupling reagents were obtained by Calbiochem-Novabiochem (Läufelfingen, Switzerland), Bachem Fine Chemicals (Bubendorf, Switzerland) or Alexis (Läufelfingen, Switzerland). DMF for peptide synthesis was purchased from SdS (Peypin, France) and degassed with nitrogen before use. Acetonitrile for analytical and preparative HPLC was obtained from Biosolve BV (Valkenswaard, Netherlands). Water used for HPLC was a Milli-Q quality, collected after passing through a Millipore Milli-Q purification system (Volketswil, Switzerland). Trifluoroacetic acid used for HPLC was purchased from Baker AG (Basel, Switzerland).

#### *Chromatography*

Analytical reversed-phase HPLC spectra were recorded on a Waters system (Waters Corporation, Milford, MA, USA) consisting of two Waters 600 pumps, a Waters 600 System Controller, a Waters 486 Tunable Absorbance Detector and a printer Waters 746, using columns packed with Vydac Nucleosil 218TP54 C<sub>18</sub> particles (250 x 4.6 mm), or 208TP54 C<sub>8</sub> particles (250 x 4.6 mm). Flow rates of 1 mL/min were used and the UV absorbance was monitored at 214 nm. All gradients were linear in eluent A (0.09% TFA in 90% aqueous acetonitrile) and eluent B (0.09% TFA in water).

Preparative HPLC purifications were performed on a Waters Delta Prep 3000 System, with a Waters 600E System Controller and a Waters 484 Absorbance Detector, with Vydac Nucleosil 218TP152050R C<sub>18</sub> particles (5 x 25 cm). Flow rates of 80 mL/min were used and the UV absorbance was monitored at 214 nm. All gradients were linear in eluent A (0.09% TFA in 90% aqueous acetonitrile) and eluent B (0.09% TFA in water).

Semi-Preparative HPLC purifications were performed on a Waters Delta Prep 3000 System, with a Waters 600E System Controller and a Waters 484 Absorbance Detector, with Vydac Nucleosil 218TP152050R C<sub>18</sub> particles (22mm), or 208TP1022 C<sub>8</sub> particles (2.2 x 25cm). Flow rates of 18 mL/min were used and the UV absorbance was monitored at 214 nm. All gradients were linear in eluent A (0.09% TFA in 90% aqueous acetonitrile) and eluent B (0.09% TFA in water).

For column chromatography, silica gel SiO<sub>2</sub> merck 60 (0.040 – 0.063 mm, 230 – 400 Mesh) was used.

#### *Mass spectroscopy*

Electrospray ionization (ESI-MS) mass spectra were recorded on a Finnigan MAT SSQ 710 C spectrometer equipped with an IBM PS1295XP486 (software Technivent Vector II) in positive ionization mode with CH<sub>3</sub>CN/H<sub>2</sub>O/CH<sub>3</sub>COOH 50:50:1 as solvent.

Whenever mass was higher than 2000 g/mol, mass was performed on a matrix-assisted laser desorption/ionization time of flight mass spectrometer MALDI-TOF Axima-CFR Shimadzu. All spectra were acquired in the reflectron mode or linear mode using  $\alpha$ -cyano matrix.

#### *Circular Dichroism (CD) spectroscopy*

CD spectra were recorded on a JASCO J-810 spectropolarimeter using a bandwidth of 1nm, a data pitch of 0.5 nm, step scanning mode, a response of 0.25 sec and an accumulation of 2. Spectra were recorded from 195 nm to 250 nm using Time course or Interval scan measurements and a 0.1 cm cuvette.

#### *Electron Microscopy (EM)*

5  $\mu$ L aliquots of switch-peptide solutions were adsorbed for two minutes on a carbon-coated 200-mesh copper grid and stained with a solution of 2% uranyl acetate for 1min. After removal of excess liquid by blotting with filter paper, specimens were examined in a JOEL 1210 electron microscope, operated at 100 kV. Digitized photographs were recorded with a slow scan CCD camera (Gatan, Model 679). Magnification calibration was performed using catalase crystals.

*Thioflavin T fluorescence assay (ThT)*

Fibril formation was monitored by a thioflavin T (ThT) (Sigma) fluorescence assay. Readings were carried out at a final protein and Th T concentration of 10 $\mu$ M, made up in a final volume of 100 $\mu$ l of 50mM Glycine-NaOH buffer (pH 8.5).

Th T fluorescence measurements were recorded on an Analyst Fluorescence instrument (LJL Biosystems, Sunnyvale CA, U.S.A) at an excitation and emission wavelength of 450 nm and 485 nm, respectively. The relative fluorescence at 485 nm was used as a measure of the amount of fibrillar aggregates formed in solution. All samples were analysed in triplicates and corrected for the fluorescence level of the studied peptide at time 0. Data were plotted using Microcal Origin.

## 2. Solid-Phase Peptide Synthesis

### *General*

The syntheses were carried out manually in a cylindrical vessel with a fritted disc and a removable lid equipped with a mechanical stirrer. Before each synthesis, silylation overnight of the glassware with a 25% solution of dichlorodimethylsilane in dry toluene is required to improve the surface hydrophobicity and prevents the beads from sticking to the wall of the vessel. The resin should be swollen with DCM for at least one hour and DMF degassed for at least 2 hours. Standard procedures of solid phase peptide synthesis using the Fmoc/<sup>t</sup>Bu strategy were performed using 2-chlorotrityl, Rink amide MBHA, pre-loaded NovasynTGA or Sieber amide resins.

### *Coupling reaction*

For a standard coupling, 2 eq of Fmoc-Xaa-OH and 2eq of PyBOP were first dissolved in degassed DMF and added to the resin, 4 eq of DIPEA were then added to the vessel. Coupling reaction time varied from 30 min to 60 min. Some other couplings were performed with HATU, and the number of equivalents increased to 4 eq.

### *Esterification method*

3 eq of Fmoc-Ala-OH, Fmoc-Phe-OH, Fmoc-Val-OH, Fmoc-Gly-OH or Fmoc-Leu-OH and 0.1 eq of DMAP were dissolved in a mixture of DCM/DMF (4:1) and added to the resin, 3 eq of DIC were then added to the vessel. After 2 hours, a cleavage test was performed and the extent of esterification controlled by HPLC. If completion was not achieved, a second or third esterification was performed.

### *Fmoc deprotection*

The Fmoc group was usually removed by treating the resin with a solution of 20% piperidine in DMF (2x10min). In switch-peptide **21** synthesis, a mixture of 2% DBU and 5% piperidine in DMF (2x5min) was sometimes used to avoid incomplete deprotection. When Rink amide

MBHA resin is used, the first Fmoc-group was removed with a solution of 20% piperidine in DMF for 5x2min and 1x10min.

#### *Colorimetric tests*

##### **Kaiser test**

Solution 1: 1 g ninhydrin in 20 mL of ethanol.

Solution 2: 80 g phenol in 20 mL of ethanol.

Solution 3: 2 mL 0.001 M aqueous KCN in 98 mL of pyridine.

A few resin beads were placed in a small test tube and 2 drops of each solution were added. The tube was then heated to 100°C for 3 min. A positive test is indicated by the presence of blue resin beads.

##### **Chloranil test**

Solution 1: 2% acetaldehyde in DMF.

Solution 2: 2% chloranil in DMF.

A few resin beads were placed in a small test tube and 2 drops of each solution were added. The mixture was then left at room temperature for 5 min and the beads inspected. A positive test is indicated by the presence of blue resin beads.

#### *Acetylation*

20 eq of acetic anhydride and 10 eq of pyridine in DMF were added to the resin and the reaction was carried out for 30 min.

#### *Cleavage of peptide from the resin*

The resin was treated with a solution of TFA/TIS/H<sub>2</sub>O 95:2.5:2.5 twice for 1 hour or, in the case of Sieber amide resin, with 1% TFA in DCM for 1 hour.

After washing with TFA and MeOH, the solvents were evaporated under high vacuum and the peptides were precipitated with cold diethyl ether. After centrifugation, the peptides were purified by preparative or semi-preparative HPLC.

Sieber amide resin was washed with DCM alone. Toluene was added to the solution in order to get rid of TFA via an azeotrope. The peptide was then precipitated with cold ether, centrifuged, and purified by preparative HPLC.

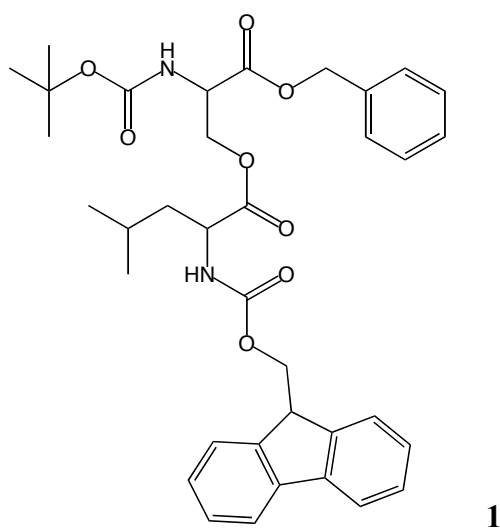
#### *Small cleavage assays*

Small cleavage assays were performed at different stages during solid phase synthesis in order to check the correct evolution of the synthesis. For this purpose, a few beads of resin were treated with a solution of TFA/TIS/H<sub>2</sub>O 95:2.5:2.5 for 30 min. After filtration through a Millex Syringe Driven Filter Unit 0.22 μm and precipitation in cold diethyl ether, the samples were analyzed by mass spectrometry and HPLC.

### 3. Synthesis

#### 3.1. Building block synthesis

##### **Fmoc-Leu-(Boc)Ser-OBzl<sup>1</sup> (1)**



Fmoc-Leu-OH (1 g, 2.83 mmol) and Boc-Ser-OH (0.84 g, 2.83 mmol) were dissolved in 25 mL DCM, DIC and DMAP were added to the solution. After stirring over night, the mixture was washed successively with 5% citric acid, 10% NaOH and brine and dried over CaCl<sub>2</sub>. After removal of the solvent, the colorless oil was purified by column chromatography

<sup>1</sup> We follow the proposed nomenclature for depsipeptides. See: S. V. Filip, F. Cavelier, *J. Pept. Sci.* **2004**, *10*, 115-118.



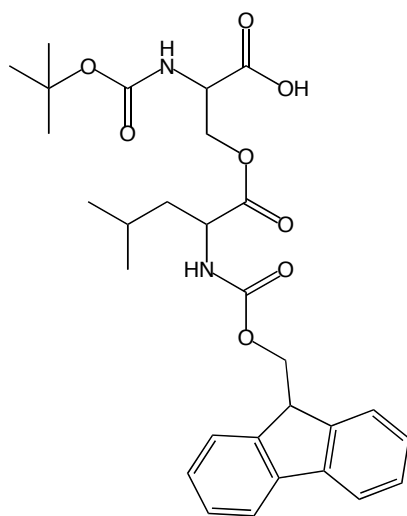
(Hexane/EtOAc 3:1) to give **1** as a white powder (1.55 g, 86%, C<sub>36</sub>H<sub>42</sub>N<sub>2</sub>O<sub>8</sub>, MW = 630.73 g/mol).

ESI MS: (m/z) 531.33 [M-Boc + H]<sup>+</sup>, 631.32 [M + H]<sup>+</sup>.

HPLC: Rt = 30 (C18 0 to 100 A in 30 min).

<sup>1</sup>H-NMR: (400MHz, CDCl<sub>3</sub>), δ (ppm) 0.94 (dd, 6H, 2CH<sub>3</sub>-Leu), 1.28 (t, 2H, CH<sub>2</sub>-Leu), 1.44 (s, 9H, (CH<sub>3</sub>)<sub>3</sub>-Boc), 1.58 (m, 1H, CH-Leu).

### Fmoc-Leu-(Boc)Ser-OH (**2**)

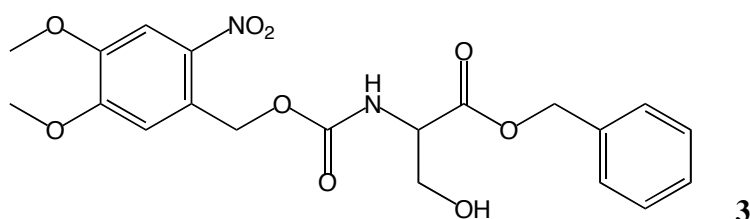


To a solution of Fmoc-Leu-(Boc)Ser-OBzl (500 mg, 0.79 mmol) in 30 mL MeOH was added 50 mg Pd on activated charcoal. A stream of H<sub>2</sub> mixed with N<sub>2</sub> was continuously bubbled through the mixture with stirring and after 2h at room temperature, the mixture was passed through celite, washed with MeOH, and evaporated under vacuum to give a white powder that was purified by preparative-HPLC and yielded **2** as a white powder (340 mg, 80%, C<sub>29</sub>H<sub>36</sub>N<sub>2</sub>O<sub>8</sub>, MW = 540.25 g/mol).

ESI MS: (m/z) 441.35 [M-Boc + H]<sup>+</sup>, 541.30 [M + H]<sup>+</sup>.

HPLC: Rt = 13.9 (C18 50 to 85 A in 20 min).

### NVOC-Ser-OBzl (**3**)

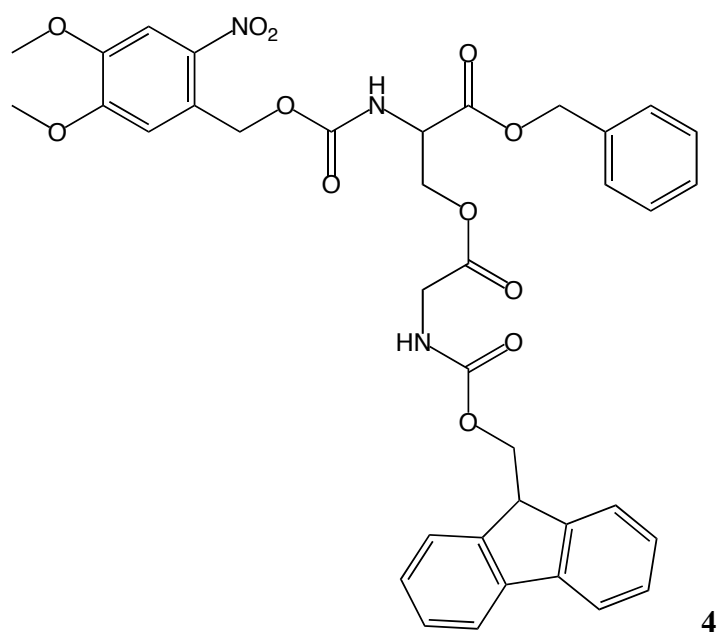


H-Ser-OBzl (1.18 g, 5.08 mmol) and DIEA (1.66 mL, 10.16 mmol, 2 eq) were dissolved in 20 mL DCM. NVocCl (1.2 g, 5.08 mmol) were added to the solution. After stirring 30 min, the mixture was diluted with 60 mL DCM, washed twice with 1N HCl, dried over MgSO<sub>4</sub>, filtered and dried under vacuum to give an orange solid that was pure by HPLC (1.78 g, 94%, C<sub>20</sub>H<sub>22</sub>N<sub>2</sub>O<sub>9</sub>, MW = 434.40 g/mol).

ESI-MS: (m/z) 435.17 [M + H]<sup>+</sup>.

HPLC: R<sub>t</sub> = 20.9 min (C<sub>18</sub>, 0 to 100% A in 30 min).

#### Fmoc-Gly-(NVOC)Ser-OBzl (4)

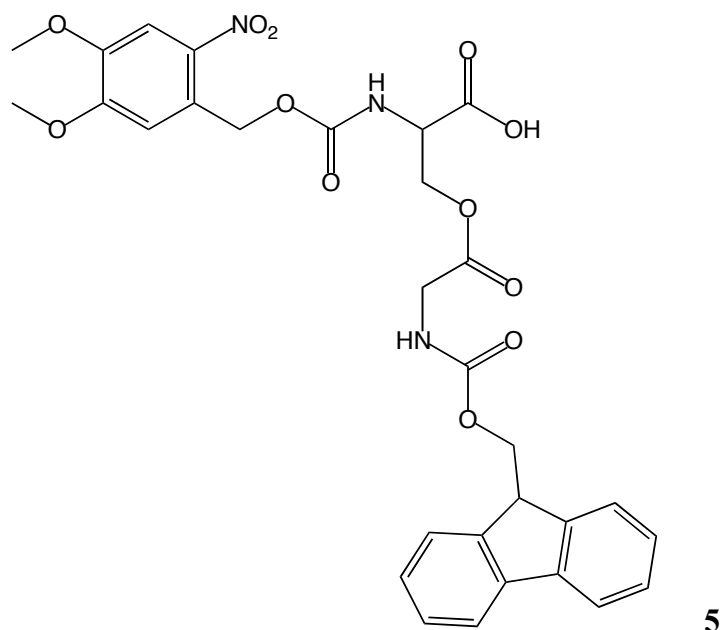


Fmoc-Gly-OH (1.16 g, 3.9 mmol), NVOC-Ser-OBzl (1.7 g, 3.9 mmol) and DMAP (47 mg, 0.39 mmol, 0.1 eq) were suspended in 15 mL DCM and EDCI (900 mg, 4.6 eq) was added and all contents fully dissolved. After stirring 1.5h, the mixture was chilled and filtered to remove the urea byproduct then diluted with DCM and washed successively with 5% citric acid, 5% NaHCO<sub>3</sub> and Brine. Drying over MgSO<sub>4</sub> and removal of solvent yielded **4** as an orange powder (2.7 g, quantitative, C<sub>37</sub>H<sub>35</sub>N<sub>3</sub>O<sub>12</sub>, MW = 713.22 g/mol).

ESI-MS: (m/z) 714.34 [M + H]<sup>+</sup>, 731.32 [M + H<sub>2</sub>O]<sup>+</sup>.

HPLC: R<sub>t</sub> = 28 (C<sub>18</sub> 0 to 100% A in 30 min)

#### Fmoc-Gly-(NVOC)Ser-OH (5)



Fmoc-Gly-(NVOC)Ser-OBzl (2 g, 2.8 mmol) was dissolved in 20 mL THF. N<sub>2</sub> atmosphere was applied for 15 min and then, 0.2 g Pd on activated charcoal were added to the solution. A stream of H<sub>2</sub> was continuously bubbled through the mixture with stirring and after 24h at room temperature, the mixture was flushed with N<sub>2</sub> for 5 min, passed through celite and evaporated under vacuum to give **5** as an orange powder that was pure by HPLC (1.56 g, 90%, C<sub>30</sub>H<sub>29</sub>N<sub>3</sub>O<sub>12</sub>, MW = 623.56 g/mol).

ESI-MS: (m/z) 624.52 [M + H]<sup>+</sup>, 641.56 [M + H<sub>2</sub>O]<sup>+</sup>.

HPLC: Rt = 22.8 (C<sub>18</sub> 0 to 100% A in 30 min)

### 3.2. Synthesis of switch-peptides of amyloid $\beta$ fibril disrupting potential

#### Synthesis of the dipeptides Ac-Leu-Cys( $\Psi^{\text{Me,Me}}\text{pro}$ )-OH and Ac-Leu-Cys( $\Psi^{\text{H,H}}\text{pro}$ )-OH

##### ➤ Pseudo-proline H-Cys( $\Psi^{\text{Me,Me}}\text{pro}$ )-OH (**10**)

L-cysteine hydrochloride (2 g, 11.4 mmol, 1eq) was suspended in 160 mL of acetone. After addition of 36 mL (318.8 mmol, 14eq) of dimethoxypropane, the suspension was stirred and heated to reflux for 2h. The reaction mixture was cooled down, filtered to yield **10** as a white powder (1.85 g, quantitative).

$^1\text{H}$  NMR (400 MHz, d6-DMSO):  $\delta$  (ppm) 1.74 (s, 6H,  $\text{CH}_3$ ); 3.40 (dd, 1H, Hb); 3.53 (dd, 1H, Hb'); 4.90 (t, 1H, Ha)

##### ➤ Pseudo-proline H-Cys( $\Psi^{\text{H,H}}\text{pro}$ )-OH (**11**)

L-cysteine hydrochloride (3.5 g, 20 mmol, 1eq) and 4 mL of 40% formaldehyde were left overnight at room temperature in 10 mL water. Addition of 10 mL of absolute EtOH and 6 mL of pyridine gave crystals which were collected, washed with EtOH and Et<sub>2</sub>O, and air-dried to give 1.9 g (72%) of **11** as a white powder.

$^1\text{H}$  NMR (400 MHz, d6-DMSO):  $\delta$  (ppm) 3.22 (dd, 1H, Hb1); 3.29 (dd, 1H, Hb2); 3.53 (dd, 1H, Hb'); 4.25 (t, 1H, Ha); 4.6 (s, 2H,  $\text{CH}_2$ )

#### Activated Ac-Leu-F (**12**)

To a suspension of Ac-Leu-OH (840 g, 4.85 mmol) in 20 mL DCM, was added dropwise under nitrogen, 720  $\mu\text{L}$  (5.81 mmol, 1.2 eq) of DAST. The reaction mixture was stirred for 15 min at room temperature. The solution was then extracted rapidly with iced water and the organic phase dried over  $\text{MgSO}_4$ . The resulting Ac-Leu-F was immediately used for the next coupling reaction.

#### Dipeptide Ac-Leu-Cys( $\Psi^{\text{Me,Me}}\text{pro}$ )-OH (**13**)

To the reactive Ac-Leu-F (4.85 mmol, 1eq) in DCM was added 790 mg of compound **10** (4.85 mmol) and 1.6 mL (9.7 mmol, 2 eq) of DIEA. The reaction was stirred at room temperature for one hour and the solvent was evaporated. The crude was then purified by preparative HPLC (C18, 0 to 100% A in 30 min) to yield **13** as a white powder (554 mg, 36%).

**Dipeptide Ac-Leu-Cys( $\Psi^{H,H}$ pro)-OH (14)**

To the reactive Ac-Leu-F (4.85 mmol, 1 eq) in DCM was added 645 mg of compound **11** (4.85 mmol) and 1.6 mL (9.7 mmol, 2 eq) of DIEA. The reaction was stirred at room temperature for one hour and the solvent was evaporated. The crude was then purified by preparative HPLC (C18, 10 to 30% A in 30 min) to yield **14** as a white powder (556 mg, 40%).

**Synthesis of  $\beta$ -breaker switch-peptides**

All  $\beta$ -breakers were synthesized on a Sieber amide MBHA resin (loading 0.71 mmol/g). Each coupling was performed with 2 eq of PyBop and 4 eq of DIEA, except for the last coupling where PyBop was replaced by HATU. After each coupling, the resin washed with DMF and DCM and Kaiser test was performed. Fmoc group was removed with a solution of 20% piperidine in DMF. The switch element was constructed by first coupling Boc-Ser-OH without side-chain protection. Fmoc-Ala-OH was then coupled via an ester bond to the free side-chain of Ser with DIC (46  $\mu$ L; 3 eq) and DMAP (6 mg; 0.5 eq).

After coupling of the dipeptide building block containing pseudoproline, the peptide was cleaved from the resin with a solution of 1% TFA in DCM (5\*10 min). After each cleavage cycle, the filtrate is collected in a flask containing 50 mL of toluene. After the last cycle, the solvent is evaporated and the peptide is precipitated with cold diethylether, centrifuged and washed 3 times with cold ether. The peptide was then redissolved in a mixture of water/acetonitrile and lyophilized.

**Synthesis of Ac-Leu-Cys( $\Psi^{Me,Me}$ pro)-Ala-(H<sup>+</sup>)Ser-Phe-Phe-Asp-NH<sub>2</sub> (15)**

Sieber amide resin: 0.10 mmol; 150 mg (loading 0.71 mmol/g)

Amino Acids	MW	Quantity (mg)	Coupling No.of equivalents	Coupling time (min)	Remarks
Fmoc-Asp( <i>t</i> -Bu)-OH	411.5	83/ 2 eq		60	Kaiser (-)
Fmoc-Phe-OH	387	78/ 2 eq		60	Kaiser (-)
Fmoc-Phe-OH	387	78/ 2 eq		60	Kaiser (-)
Boc-Ser-OH	474	41/ 2 eq		60	Kaiser (-)
Fmoc-Ala-OH	311	94/ 3 eq		2*120	esterification
Ac-Leu-Cys( $\Psi^{Me,Me}$ pro)-OH	316	50/ 2 eq		160	

## Cleavage of protecting groups

The crude peptide was suspended in a solution of TFA/DCM/TIS/H<sub>2</sub>O (50/40/5/5) 50 mL for 1h30. 50 mL of toluene was added to the reaction to facilitate the removal of TFA and thus prevent pseudoproline opening. After evaporation, few drops of DCM were added to the flask and the peptide was precipitated with diethylether. Purification by preparative HPLC (0 to 100% A in 30 min) yielded **15** as a white powder (13 mg; 15%).

ESI-MS: (m/z) 883.20 [M + H]<sup>+</sup>.

HPLC: Rt = 20.5 (C<sub>18</sub> 0 to 100% A in 30 min).

**Synthesis of Ac-Leu-Cys( $\Psi^{H,H}$ pro)-Ala-(H<sup>+</sup>)Ser-Phe-Phe-Asp-NH<sub>2</sub> (16)**

Sieber amide resin: 0.13 mmol; 240 mg (loading 0.55 mmol/g)

Amino Acids	MW	Quantity (mg) No. of equivalents	Coupling time (min)	Remarks
Fmoc-Asp( <i>t</i> -Bu)-OH	411.5	107/ 2 eq	60	Kaiser (-)
Fmoc-Phe-OH	387	100/ 2 eq	60	Kaiser (-)
Fmoc-Phe-OH	387	100/ 2 eq	60	Kaiser (-)
Boc-Ser-OH	474	53/ 2 eq	60	Kaiser (-)
Fmoc-Ala-OH	311	128/ 3 eq	2*120	esterification
Ac-Leu-Cys( $\Psi^{Me,Me}$ pro)-OH	288	74/ 2 eq	160	

## Cleavage of protecting groups

The crude peptide was suspended in a solution of TFA/DCM/TIS/H<sub>2</sub>O (60/30/5/5) 50 mL for 2h. 50 mL of toluene was added to the reaction to facilitate the removal of TFA and thus prevent pseudoproline opening. After evaporation, few drops of DCM were added to the flask and the peptide was precipitated with diethylether. Purification by preparative HPLC (0 to 100% A in 30 min) yielded **16** as a white powder.

ESI-MS: (m/z) 855.36 [M + H]<sup>+</sup>.

HPLC: Rt = 15.7 (C<sub>18</sub> 0 to 100% A in 30 min).

**Synthesis of Ac-Leu-Cys( $\Psi^{\text{Me,Me}}$ pro)-Ala-(H<sup>+</sup>)Ser-(NMe)Phe-Phe-Asp-NH<sub>2</sub> (17)**

Sieber amide resin: 0.23 mmol; 440 mg (loading 0.55 mmol/g)

Amino Acids	MW	Quantity (mg) No. of equivalents	Coupling time (min)	Remarks
Fmoc-Asp( <i>t</i> -Bu)-OH	411.5	189/ 2 eq	60	Kaiser (-)
Fmoc-Phe-OH	387	178/ 2 eq	60	Kaiser (-)
Fmoc-(NMe)Phe-OH	387	185/ 2 eq	60	HATU/ Kaiser (-)
Boc-Ser-OH	474	94/ 2 eq	60	HATU/ Kaiser (-)
Fmoc-Ala-OH	311	230/ 3 eq	2*120	esterification
Ac-Leu-Cys( $\Psi^{\text{Me,Me}}$ pro)-OH	316	145/ 2 eq	120	

## Cleavage of protecting groups

The crude peptide was suspended in a solution of TFA/DCM/TIS/H<sub>2</sub>O (50/40/5/5) 50 mL for 1h30. 50 mL of toluene was added to the reaction to facilitate the removal of TFA and thus prevent pseudoproline opening. After evaporation, few drops of DCM were added to the flask and the peptide was precipitated with diethylether. Purification by preparative HPLC (0 to 100% A in 30 min) yielded **17** as a white powder.

ESI-MS: (m/z) 897.80 [M + H]<sup>+</sup>.HPLC: Rt = 18.2 (C<sub>18</sub> 0 to 100% A in 30 min).**Synthesis of Ac-Leu-Cys( $\Psi^{\text{H,H}}$ pro)-Ala-(H<sup>+</sup>)Ser-(NMe)Phe-Phe-Asp-NH<sub>2</sub> (18)**

Sieber amide resin: 0.14 mmol; 255 mg (loading 0.55 mmol/g)

Amino Acids	MW	Quantity (mg) No. of equivalents	Coupling time (min)	Remarks
Fmoc-Asp( <i>t</i> -Bu)-OH	411.5	115/ 2 eq	60	Kaiser (-)
Fmoc-Phe-OH	387	108/ 2 eq	60	Kaiser (-)
Fmoc-(NMe)Phe-OH	387	112/ 2 eq	60	Kaiser (-)/ HATU
Boc-Ser-OH	474	58/ 2 eq	60	Kaiser (-)/ HATU
Fmoc-Ala-OH	311	138/ 3 eq	2*120	esterification

---

Ac-Leu-Cys( $\Psi^{\text{H,H}}$ pro)-OH	288	80/ 2 eq	120
---	-----	----------	-----

---

#### Cleavage of protecting groups

The crude peptide was suspended in a solution of TFA/DCM/TIS/H<sub>2</sub>O (60/30/5/5) 50 mL for 2h. 50 mL of toluene was added to the reaction to facilitate the removal of TFA and thus prevent pseudoproline opening. After evaporation, few drops of DCM were added to the flask and the peptide was precipitated with diethylether. Purification by preparative HPLC (0 to 100% A in 30 min) yielded **18** as a white powder (20 mg; 16%).

ESI-MS: (m/z) 869.37 [M + H]<sup>+</sup>.

HPLC: Rt = 16.5 (C<sub>18</sub> 0 to 100% A in 30 min).

#### Synthesis of Ac-Leu-Cys( $\Psi^{\text{Me,Me}}$ pro)-Ala-(Arg-Pro)Ser-(NMe)Phe-Phe-Asp-NH<sub>2</sub> (**19**)

Sieber amide resin: 0.23 mmol; 440 mg (loading 0.55 mmol/g)

Amino Acids	MW	Quantity (mg)	Coupling	Remarks
		No. of equivalents	time (min)	
Fmoc-Asp( <i>t</i> -Bu)-OH	411	189/ 2 eq	60	Kaiser (-)
Fmoc-Phe-OH	387	178/ 2 eq	60	Kaiser (-)
Fmoc-(NMe)Phe-OH	387	185/ 2 eq	60	Kaiser (-)/ HATU
Boc-Ser-OH	474	94/ 2 eq	60	Kaiser (-)/ HATU
Fmoc-Pro-OH	337	155/ 2 eq	60	
Boc-Arg(Boc) <sub>2</sub> -OH	474	218/ 2 eq	60	
Fmoc-Ala-OH	311	230/ 3 eq	2*120	esterification
Ac-Leu-Cys( $\Psi^{\text{Me,Me}}$ pro)-OH	316	145/ 2 eq	120	

---

#### Cleavage of protecting groups

The crude peptide was suspended in a solution of TFA/DCM/TIS/H<sub>2</sub>O (50/40/5/5) 50 mL for 1h30. 50 mL of toluene was added to the reaction to facilitate the removal of TFA and thus prevent pseudoproline opening. After evaporation, few drops of DCM were added to the flask



and the peptide was precipitated with diethylether. Purification by preparative HPLC (0 to 100% A in 30 min) yielded **19** as a white powder (42 mg; 18%).

ESI-MS: (m/z) 1150 [M + H]<sup>+</sup>, 576 [M + 2H]<sup>2+</sup>

HPLC: Rt = 17 (C<sub>18</sub> 0 to 100% A in 30 min).



**Fmoc-Ala-(Boc)Ser-OH:** To a solution of Fmoc-Ala-(Boc)Ser-OBzl (200 mg, 0.34 mmol) in 10 mL MeOH, 10 mg Pd on activated charcoal was added. A stream of H<sub>2</sub> mixed with N<sub>2</sub> was continuously bubbled through the mixture with stirring and after 1 h at room temperature, the mixture was passed through celite and evaporated under vacuum to yield a white powder that was pure by HPLC (168 mg, quant., C<sub>26</sub>H<sub>30</sub>N<sub>2</sub>O<sub>8</sub>, m/z calculated: 498.53).

ESI-MS: (m/z) 398.84 [M – Boc].

HPLC: R<sub>t</sub> = 24.0 (C<sub>18</sub>, 5 to 95% A in 30 min).

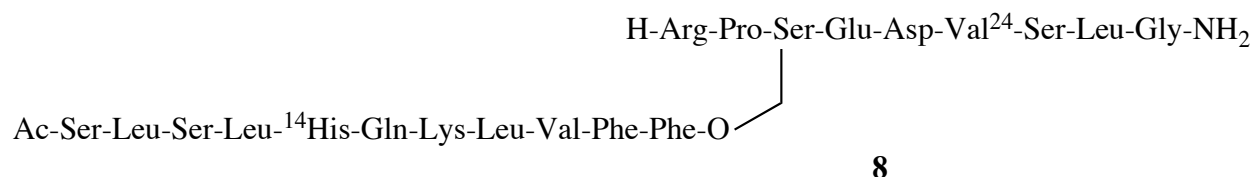
**Fmoc-[(cyclo-1-5)-Lys-Ala-Arg(Pbf)-Ala-Asp]-OH:** Synthesis of peptide **I** started by the preparation of the N-cap protected lactam-bridged pentapeptide that could be used as building block in SPPS. This was accomplished using the method developed by Shepherd et al.<sup>[15b]</sup>. The solid phase synthesis of a lactam-bridged peptide requires an orthogonal protection of the side chains to be cyclized. In Fmoc/tBu SPPS, this need is met by the use of Alloc/Allyl, which is removed by Pd<sup>0</sup> catalyzed reduction. The peptide is constructed and cyclized on a highly acid labile support. Cleavage can then be performed under mild acidic conditions to give a peptide fragment that is fully protected and contains a free acid at the C-terminus.

**Peptide 7:** The fibril-forming peptide HQKLVFFAEDVG was assembled on Rink amide resin (0.60 mmol/g, 0.30 g, 0.18 mmol), using automated synthesis, a glycine residue was included at the C-terminal end to serve as a spacer. The switch-element was introduced by manually coupling the depsidipeptide Fmoc-Ala-(Boc)Ser-OH. After Fmoc removal, the N-capping template Fmoc-(cyclo-1-5)-KARAD-OH was coupled manually to give Fmoc-[(cyclo-1-5)-KARAD]A-S<sub>1</sub>-HQKLVFFAEDVG-NH<sub>2</sub> where S<sub>1</sub> = (<sup>+</sup>H)Ser. As both the N-cap and the switch-element were introduced as building blocks, all couplings were PyBOP mediated amide couplings, and the synthesis was straightforward. Following Fmoc deprotection, the peptide was treated with an excess of Ac<sub>2</sub>O and pyridine in DMF for 1 h. Cleavage from the resin and purification by semi-preparative HPLC (C<sub>8</sub>, 10 to 60% A, 30 min) afforded the desired peptide **I** as a white powder with > 95% purity (12 mg, C<sub>95</sub>H<sub>146</sub>N<sub>28</sub>O<sub>27</sub>, m/z calculated: 2112.35).

ESI-MS: (m/z) 1056.86 [(M + 2H)/2]<sup>+</sup>, 704.81 [(M + 3H)/3]<sup>+</sup>, 529.31 [(M + 4H)/4]<sup>+</sup>.

HPLC: R<sub>t</sub> = 5.93 (C<sub>18</sub>, 0 to 30% A in 10 min).

Amino Acids	Coupling No.	Quantity (mg) No.of equivalents	Coupling time (min)	Remarks
Fmoc-Gly-OH	1	(134/ 2.5 eq)	2 x 30	
Fmoc-Val-OH	2	(153/ 2.5 eq)	2 x 30	
Fmoc-Asp(OtBu)-OH	3	(185/ 2.5 eq)	2 x 30	
Fmoc-Glu(OtBu)-OH	4	(200/ 2.5 eq)	2 x 30	
Fmoc-Ala-OH.H <sub>2</sub> O	5	(148/ 2.5 eq)	2 x 30	
Fmoc-Phe-OH	6	(174/ 2.5 eq)	2 x 30	
Fmoc-Phe-OH	7	(174/ 2.5 eq)	2 x 30	
Fmoc-Val-OH	8	(153/ 2.5 eq)	2 x 30	
Fmoc-Leu-OH	9	(159/ 2.5 eq)	2 x 30	
Fmoc-Lys(Boc)-OH	10	(211/ 2.5 eq)	2 x 30	
Fmoc-Gln(Trt)-OH	11	(275/ 2.5 eq)	2 x 30	
Fmoc-His(Trt)-OH	12	(279/ 2.5 eq)	2 x 30	Kaiser (-)
Fmoc-Ala-(Boc)Ser-OH	13	(302/ 3.0 eq)	90	manual coupling Kaiser (-)
Fmoc-[(cyclo-1-5)-Lys- Ala- Arg(Pbf)-Ala-Asp]-OH	14	(260/ 1.5 eq)	180	manual coupling Kaiser (-)

3.4. Host-Guest Switch-Peptide **8**

The amyloid derived host guest switch-peptide **8** was assembled on 500 mg of Rink amide MBHA resin (loading 0.64 mmol/g) by Dr. Sonia Dos Santos within her PhD Thesis.

Each coupling was performed with 2 eq of PyBop and 4 eq of DIEA. After each coupling, the resin was washed with DMF and DCM and a Kaiser test was performed after each step. Fmoc group was removed with a solution of 20% piperidine in DMF. The switch element was constructed by first coupling Fmoc-Ser-OH without side protection followed by Fmoc-Pro-OH and Boc-Arg(di-Boc)-OH which were coupled normally. Fmoc-Phe-OH was then coupled via an ester bond to the free side chain of the Ser<sup>21</sup> with DIC (3eq) and DMAP (0.5eq). Colorimetric tests were negative all along the synthesis and cleavage tests assays indicated the correct evolution of the synthesis.

After deprotection of the last Fmoc group and acetylation of the N-terminus, the peptide was cleaved from the resin with a solution of TFA/TIS/H<sub>2</sub>O (95/2.5/2.5) for 2 x 1h and thereafter, precipitated in cold diethylether. The crude peptide was purified by preparative HPLC (C<sub>18</sub>, 0 to 60% A in 30 min) to give in a white powder (220 mg, 30%).

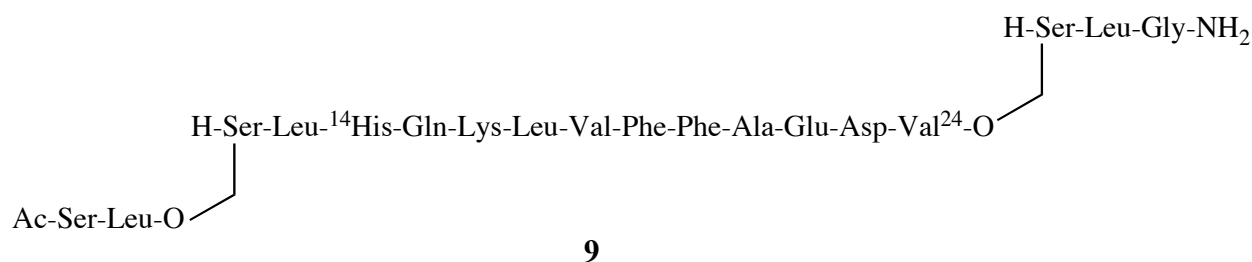
HPLC: Rt = 16.4 (C<sub>18</sub>, 0 to 100% A in 30 min)

MALDI-TOF: m/z = 2300 [M+H]<sup>+</sup>

Amino Acids	Quantity (mg), eq	Coupling time (min)	Test
Fmoc-Gly-OH	191/ 2eq	60	Kaiser (-)
Fmoc-Leu-OH	226/ 2eq	60	Kaiser (-)
Fmoc-Ser( <sup>t</sup> Bu)-OH	245/ 2eq	60	Kaiser (-)
Fmoc-Leu-OH	226/ 2eq	60	Kaiser (-)
Fmoc-Ser(OH)-OH	210/ 2eq	30	Kaiser (-)
Fmoc-Val-OH	217/ 2eq	60	Kaiser (-)
Fmoc-Asp( <sup>t</sup> Bu)-OH	264/ 2eq	60	Kaiser (-)
Fmoc-Glu( <sup>t</sup> Bu)-OH.H <sub>2</sub> O	284/ 2eq	60	Kaiser (-)
Fmoc-Ser(OH)-OH	210/ 2eq	30	Kaiser (-)

Fmoc-Pro-OH	228/ 2eq	30	Kaiser (-) Cleavage HPLC (C <sub>18</sub> , 0 → 100%A): R <sub>t</sub> = 12.2 min
Boc-Arg(di-Boc)-OH	304/ 2eq	30	ESI-MS : m/z = 958 [M+H] <sup>+</sup> , 480 [M+2H] <sup>2+</sup> Cleavage HPLC (C <sub>18</sub> , 0 → 100%A): R <sub>t</sub> = 20.9 min
Fmoc-Phe-OH	372/ 3eq	2x120	ESI-MS : m/z = 1327 [M+H] <sup>+</sup> , 664 [M+2H] <sup>2+</sup>
Fmoc-Phe-OH	248/ 2eq	60	Kaiser (-)
Fmoc-Val-OH	217/ 2eq	60	Kaiser (-)
Fmoc-Leu-OH	226/ 2eq	60	Kaiser (-)
Fmoc-Lys(Boc)-OH	300/ 2eq	60	Kaiser (-)
Fmoc-Gln(Trt)-OH	391/ 2eq	60	Kaiser (-)
Fmoc-His(Trt)-OH	397/ 2eq	60	Kaiser (-)
Fmoc-Leu-OH	226/ 2eq	60	Kaiser (-)
Fmoc-Ser( <sup>t</sup> Bu)-OH	245/ 2eq	60	Kaiser (-)
Fmoc-Leu-OH	226/ 2eq	60	Kaiser (-)
Fmoc-Ser( <sup>t</sup> Bu)-OH	245/ 2eq	60	Kaiser (-)

## 3.5. Host-Guest Switch-Peptide 9



The amyloid derived host guest switch-peptide **9** was assembled on 1 g of Rink amide MBHA resin (loading 0.66 mmol/g).

Each coupling was performed with 2 eq of PyBop and 4 eq of DIEA. After each coupling, the resin was washed with NMP and DCM and a Kaiser test was performed after each step. The four first Fmoc groups were removed with a solution of 2% DBU/ 5% piperidine in NMP and thereafter with 20 % piperidine in DMF. Switch elements were constructed by first coupling Boc-Ser-OH without side chain protection. The next amino acid was then coupled via an ester bond to the free side chain of the Ser with DIC 3eq and DMAP 0.5 eq. Colorimetric tests were negative all along the synthesis and cleavage tests assays indicated the correct evolution of the synthesis.

After deprotection of the last Fmoc group and acetylation of the N-terminus, the peptide was cleaved from the resin with a solution of TFA/TIS/H<sub>2</sub>O (95/2.5/2.5) for 2 x 1h and thereafter, precipitated in cold diethylether. The crude peptide was purified by preparative HPLC (C<sub>18</sub>, 30 to 50% A in 30 min) to give **9** as a white powder (500 mg, 36%).

HPLC: Rt = 16.7 (C<sub>18</sub>, 0 to 100% A in 30 min)

ESI-MS: (m/z) 1016.84 [(M + 2H)/2]<sup>+</sup>, 678.30 [(M + 3H)/3]<sup>+</sup>, 508.78 [(M + 4H)/4]<sup>+</sup>.

Amino Acids	Quantity (mg), eq	Coupling time (min)	Test
Fmoc-Gly-OH	500/ 2.5eq	30 x 2	Kaiser (-)
Fmoc-Leu-OH	580/ 2.5eq	30 x 2	Kaiser (-)
Boc-Ser-OH	339/ 2.5eq	30 x 2	Kaiser (-)
Fmoc-Val-OH	672/ 3eq	120 x 2	Kaiser (-)
Fmoc-Asp( <sup>t</sup> Bu)-OH	678/ 2.5eq	30 x 2	Kaiser (-)
Fmoc-Glu( <sup>t</sup> Bu)-OH.H <sub>2</sub> O	732/ 2.5eq	30 x 2	Kaiser (-)

---

Fmoc-Ala-OH	528/ 2.5eq	30 x 2	Kaiser (-)
Fmoc-Phe-OH	640/ 2.5eq	30 x 2	Kaiser (-)
Fmoc-Phe-OH	640/ 2.5eq	30 x 2	Kaiser (-)
Fmoc-Val-OH	560/ 2.5eq	30 x 2	Kaiser (-)
Fmoc-Leu-OH	580/ 2.5eq	30 x 2	Kaiser (-)
Fmoc-Lys(Boc)-OH	773/ 2.5eq	30 x 2	Kaiser (-)
Fmoc-Gln(Trt)-OH	1000/ 2.5eq	30 x 2	Kaiser (-)
Fmoc-His(Trt)-OH	1020/ 2.5eq	30 x 2	Kaiser (-)
Fmoc-Leu-OH	580/ 2.5eq	30 x 2	Kaiser (-)
Boc-Ser-OH	207/ 2eq	30 x 2	Kaiser (-)
Fmoc-Leu-OH	690/ 3eq	120 x 2	Kaiser (-)
Fmoc-Ser( <sup>t</sup> Bu)-OH	630/ 2.5eq	30 x 2	Kaiser (-)

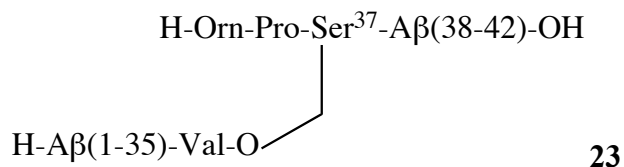
---





Boc-Orn(Boc)-OH	133	60min PyBOP, 2eq, 60min	R <sub>t</sub> = 13.1 min 756 [M+H] <sup>+</sup>	-
36 Fmoc-Val-OH	203	CDI, 3eq, 2x120min	R <sub>t</sub> = 21.4 min 1077 [M+H] <sup>+</sup> 539 [M+2H] <sup>2+</sup>	
35 Fmoc-Met-OH	149	HATU, 2eq, 60min	-	
34 Fmoc-Leu-OH	141	HATU, 2eq, 60min	R <sub>t</sub> = 22.3 min 1369 [M+H] <sup>+</sup> 683 [M+2H] <sup>2+</sup>	
33 Fmoc-Gly-OH	119	HATU, 2eq, 60min	-	
32 Fmoc-Ile-OH	141	HATU, 2eq, 60min	-	
31 Fmoc-Ile-OH	141	HATU, 2eq, 60min	-	
30 Fmoc-Ala-OH.H <sub>2</sub> O	124	HATU, 2eq, 60min	-	
29 Fmoc-Gly-OH	119	HATU, 2eq, 60min	-	
28 Fmoc-Lys(Boc)-OH	187	HATU, 2eq, 60min	-	
27 Fmoc-Asn(Trt)-OH	239	HATU, 2eq, 60min	R <sub>t</sub> = 20.2 min 988 [M+2H] <sup>2+</sup> 659 [M+3H] <sup>3+</sup>	
25-26 Fmoc-Gly-(NVoc)Ser-OH	374	HATU, 3eq, 90min	R <sub>t</sub> = 16.9 min 1180 [M+2H] <sup>2+</sup> 787 [M+3H] <sup>3+</sup>	-
24 Fmoc-Val-OH	137	HATU, 2eq, 60min	-	
23 Fmoc-Asp( <sup>t</sup> Bu)-OH	164	HATU, 4eq, 60min	R <sub>t</sub> = 19.9 min	
22 Fmoc-Glu( <sup>t</sup> Bu)-OH	170	HATU, 4eq, 60min	-	
21 Fmoc-Ala-OH.H <sub>2</sub> O	125	HATU, 4eq, 60min	-	
20 Fmoc-Phe-OH	155	HATU, 4eq, 60min		MS after Fmoc removal 1349 [M+2H] <sup>2+</sup> 900 [M+3H] <sup>3+</sup> 675 [M+4H] <sup>4+</sup>
19 Fmoc-Phe-OH	155	HATU, 4eq, 60min	-	
18 Fmoc-Val-OH	137	HATU, 4eq, 60min	1582 [M+2H] <sup>2+</sup> 1054 [M+3H] <sup>3+</sup> 791 [M+4H] <sup>4+</sup>	

17 Fmoc-Leu-OH	141	HATU, 4eq, 60min		
16 Fmoc-Lys(Boc)-OH	188	HATU, 4eq, 60min		
15 Fmoc-Gln(Trt)-OH	244	HATU, 4eq, 60min	1769 [M+2H] <sup>2+</sup> 1179 [M+3H] <sup>3+</sup> 884 [M+4H] <sup>4+</sup> -	
14 Fmoc-His(Trt)-OH	248	HATU, 4eq, 60min	-	
13 Fmoc-His(Trt)-OH	248	HATU, 4eq, 60min		
12 Fmoc-Val-OH	200	HATU, 4eq, 60min	-	
11 Fmoc-Glu( <sup>t</sup> Bu)-OH	200	HATU, 4eq, 60min	1347 [M+3H] <sup>3+</sup> 1010 [M+4H] <sup>4+</sup> 808 [M+5H] <sup>5+</sup> -	
10 Fmoc-Tyr( <sup>t</sup> Bu)-OH	184	HATU, 4eq, 60min	1051 [M+4H] <sup>4+</sup> 841 [M+5H] <sup>5+</sup> --	
9 Fmoc-Gly-OH	119	HATU, 4eq, 60min		
8 Fmoc-Ser( <sup>t</sup> Bu)-OH	153	HATU, 4eq, 60min	-	
7 Fmoc-Asp( <sup>t</sup> Bu)-OH	165	HATU, 4eq, 60min	-	
6 Fmoc-His(Trt)-OH	248	HATU, 4eq, 60min	-	
5 Fmoc-Arg(Pbf)-OH	260	HATU, 4eq, 60min	Maldi-TOF 4530 [M+H] <sup>+</sup>	small peak in maldi
4 Fmoc-Phe-OH	155	HATU, 4eq, 60min	-	
3 Fmoc-Glu( <sup>t</sup> Bu)-OH	200	HATU, 4eq, 60min	-	
2 Fmoc-Ala-OH.H <sub>2</sub> O	130	HATU, 4eq, 60min	-	
1 Boc-Asp( <sup>t</sup> Bu)-OH	116	HATU, 4eq, 60min	-	-

3.7. Synthesis of Amyloid- $\beta$  (1-42) derived switch-peptide 23

The synthesis was performed on 1 g of a pre-loaded Fmoc-Ala-NovaSyn TGA resin (loading 0.20 mmol/g).

The first Fmoc protecting group was removed with a solution of 20% piperidine in DMF (2x10 min) and the amino acids Fmoc-Ile-OH and Fmoc-Val-OH was coupled with 2 eq of PyBOP.

The Fmoc group was then removed with a solution of 2% DBU 5% piperidine in DMF until the 7<sup>th</sup> amino acid of the sequence (Aspartic acid) was reached. From 7<sup>th</sup> to 1<sup>st</sup> amino acid, Fmoc protecting group was removed with 20% piperidine in DMF to avoid aspartimide formation that can occur when strong basic conditions are used to remove Fmoc.

HATU was used as coupling reagent all along the synthesis (2 eq or 4 eq).

Switch element S at Ser<sup>37</sup> was constructed by first coupling Fmoc-Ser-OH without side chain protection followed by normal coupling of Fmoc-Pro-OH and Boc-Orn(Boc)-OH. Fmoc-Val<sup>36</sup>-OH was then coupled via an ester bond to the free side chain of the serine with DIC 3eq and DMAP 0.5 eq.

To facilitate the synthesis on the resin the pseudo-proline building block Fmoc-Gly<sup>25</sup>-Ser<sup>26</sup>( $\psi^{\text{Me,Me}}$ )pro-OH was used. During the final cleavage, the pseudo-proline opened and the normal sequence was restored.

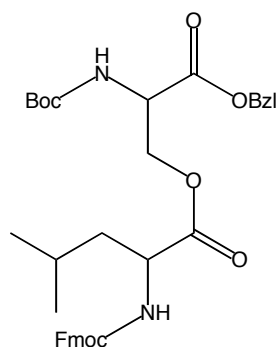
Cleavage test assays were performed during the synthesis and analyzed by HPLC, ESI-MS or MALDI-TOF to check the correct evolution of the synthesis.

Residue	Quantity (mg)	Coupling conditions	Cleavage test	remarks
41 Fmoc-Ile-OH	176	PyBOP, 2.5eq, 2 x 20min	-	20% piperidine
40 Fmoc-Val-OH	170	PyBOP, 2.5eq, 2 x 20min	525 [M+H] <sup>+</sup> -	
39 Fmoc-Val-OH	170	HATU, 2.5eq, 2 x 20min	-	

38 Fmoc-Gly-OH	150	HATU, 2.5eq, 2 x 20min	-	
37 Fmoc-Ser(OH)-OH	164	PyBOP, 2.5eq, 2 x 20min	-	
Fmoc-Pro-OH.H <sub>2</sub> O	169	PyBOP, 2.5eq, 2 x 20min		
Boc-Orn(Boc)-OH	166	PyBOP, 2.5eq, 2 x 20min	R <sub>t</sub> = 13.1 min 756 [M+H] <sup>+</sup>	-
36 Fmoc-Val-OH	170	CDI, 3eq, 2x120min	R <sub>t</sub> = 21.4 min 1077 [M+H] <sup>+</sup>	
35 Fmoc-Met-OH	186	HATU, 2.5eq, 2 x 20min	-	
34 Fmoc-Leu-OH	176	HATU, 2.5eq, 2 x 20min		
33 Fmoc-Gly-OH	150	HATU, 2.5eq, 2 x 20min	-	
32 Fmoc-Ile-OH	176	HATU, 2.5eq, 2 x 20min	1606 [M+H] <sup>+</sup> 803 [M+2H] <sup>2+</sup> -	
31 Fmoc-Ile-OH	176	HATU, 2.5eq, 2 x 20min	-	
30 Fmoc-Ala-OH.H <sub>2</sub> O	164	HATU, 2.5eq, 2 x 20min	-	
29 Fmoc-Gly-OH	150	HATU, 2.5eq, 2 x 20min	-	
28 Fmoc-Lys(Boc)-OH	235	HATU, 2.5eq, 2 x 20min	-	
27 Fmoc-Asn(Trt)-OH	300	HATU, 2.5eq, 2 x 20min		
25-26 Fmoc-Gly <sup>25</sup> - Ser <sup>26</sup> (ψ <sup>Me,Me</sup> )pro-OH	212	HATU, 2.5eq, 2 x 40min	R <sub>t</sub> = 16.9 min 1059 [M+2H] <sup>2+</sup> 706 [M+3H] <sup>3+</sup>	-
24 Fmoc-Val-OH	170	HATU, 2.5eq, 2 x 20min	-	
23 Fmoc-Asp( <sup>t</sup> Bu)-OH	205	HATU, 2.5eq, 2 x 20min		
22 Fmoc-Glu( <sup>t</sup> Bu)-OH	221	HATU, 2.5eq, 2 x 20min	-	
21 Fmoc-Ala-OH.H <sub>2</sub> O	164	HATU, 2.5eq, 2 x 20min	-	
20 Fmoc-Phe-OH	194	HATU, 2.5eq, 2 x 20min	1339 [M+2H] <sup>2+</sup> 893 [M+3H] <sup>3+</sup> 669 [M+4H] <sup>4+</sup>	
19 Fmoc-Phe-OH	194	HATU, 2.5eq, 2 x 20min	-	
18 Fmoc-Val-OH	170	HATU, 2.5eq, 2 x 20min		

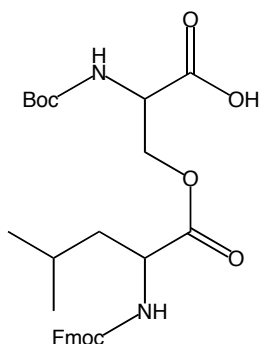
17 Fmoc-Leu-OH	176	HATU, 2.5eq, 2 x 20min		
16 Fmoc-Lys(Boc)-OH	235	HATU, 2.5eq, 2 x 20min		
15 Fmoc-Gln(Trt)-OH	305	HATU, 2.5eq, 2 x 20min	1647 [M+2H] <sup>2+</sup> 1098 [M+3H] <sup>3+</sup> 823 [M+4H] <sup>4+</sup> -	
14 Fmoc-His(Trt)-OH	310	HATU, 2.5eq, 2 x 20min	-	
13 Fmoc-His(Trt)-OH	310	HATU, 2.5eq, 2 x 20min		
12 Fmoc-Val-OH	170	HATU, 2.5eq, 2 x 20min	-	
11 Fmoc-Glu( <sup>t</sup> Bu)-OH	221	HATU, 2.5eq, 2 x 20min		
10 Fmoc-Tyr( <sup>t</sup> Bu)-OH	230	HATU, 2.5eq, 2 x 20min	--	
9 Fmoc-Gly-OH	150	HATU, 2.5eq, 2 x 20min	1339 [M+3H] <sup>3+</sup> 1004 [M+4H] <sup>4+</sup> - 803 [M+5H] <sup>5+</sup>	
8 Fmoc-Ser( <sup>t</sup> Bu)-OH	192	HATU, 2.5eq, 2 x 20min	-	
7 Fmoc-Asp( <sup>t</sup> Bu)-OH	205	HATU, 2.5eq, 60min	-	Deprotection with 20% piperidine
6 Fmoc-His(Trt)-OH	310	HATU, 2.5eq, 2 x 20min	-	
5 Fmoc-Arg(Pbf)-OH	324	HATU, 2.5eq, 2 x 20min		small signal in ESI/MS
4 Fmoc-Phe-OH	194	HATU, 2.5eq, 2 x 20min	-	
3 Fmoc-Glu( <sup>t</sup> Bu)-OH	221	HATU, 2.5eq, 2 x 20min	-	
2 Fmoc-Ala-OH.H <sub>2</sub> O	164	HATU, 2.5eq, 2 x 20min	-	
1 Boc-Asp( <sup>t</sup> Bu)-OH	145	HATU, 2.5eq, 2 x 20min	1584 [M+3H] <sup>3+</sup> 1188 [M+4H] <sup>4+</sup> - 905 [M+5H] <sup>5+</sup> -	-

**Product Index**



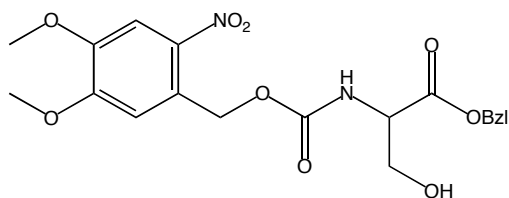
**Fmoc-Leu-(Boc)Ser-OBzl 1**

---



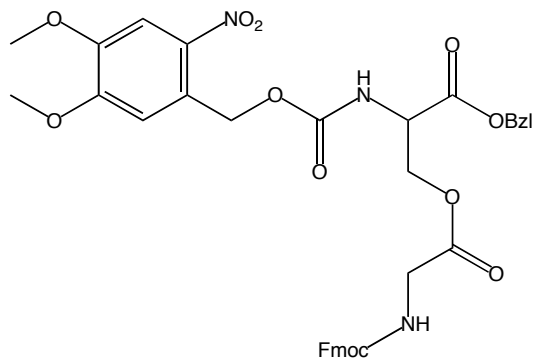
**Fmoc-Leu-(Boc)Ser-OH 2**

---



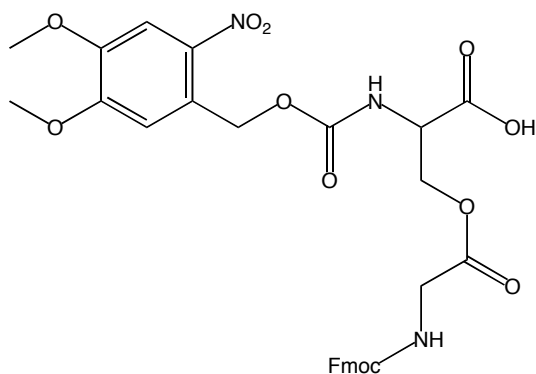
**NVOC-Ser-OBzl 3**

---



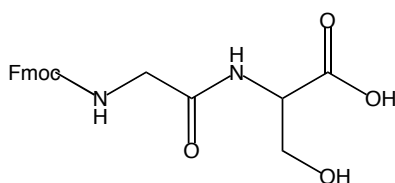
**Fmoc-Gly-(NVOC)Ser-OBzl 4**

---



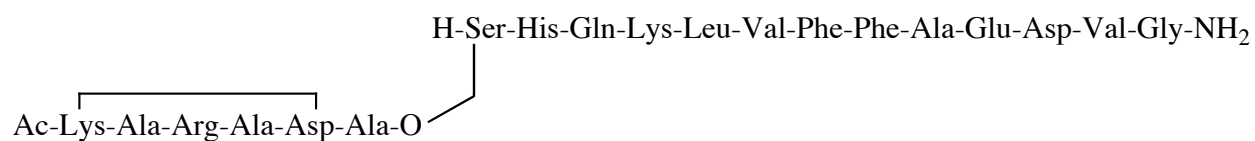
Fmoc-Gly-(NVOC)Ser-OH **5**

---



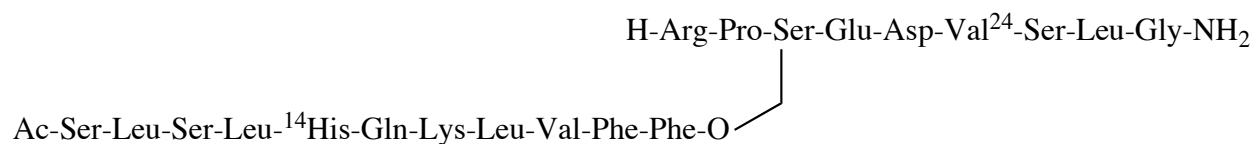
Fmoc-Gly-(NVOC)Ser-OH **6**

---



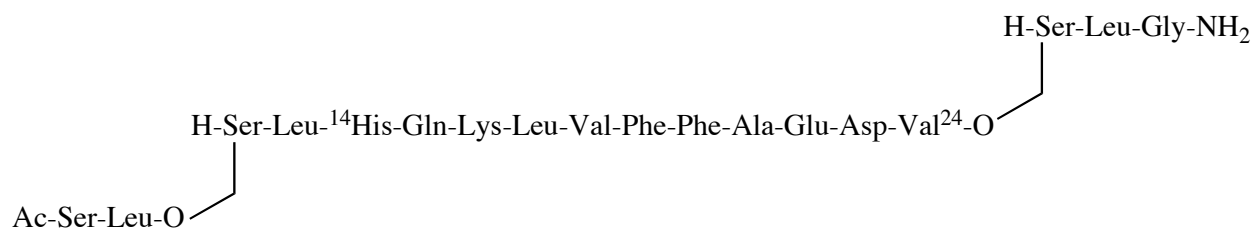
**7**

---



**8**

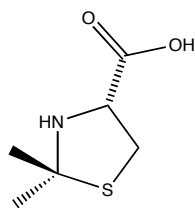
---



**9**

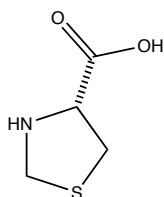
---





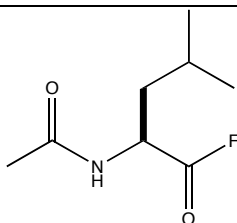
H-Cys( $\Psi^{\text{Me,Me}}$ pro)-OH **10**

---



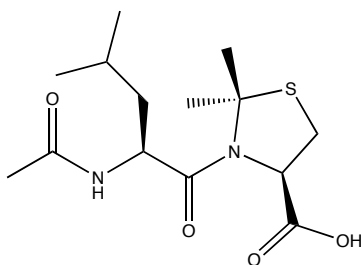
H-Cys( $\Psi^{\text{H,H}}$ pro)-OH **11**

---



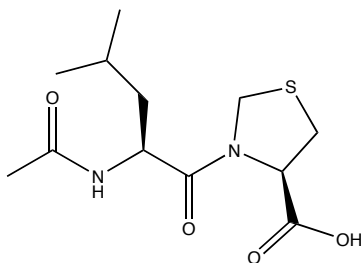
Ac-Leu-F **12**

---



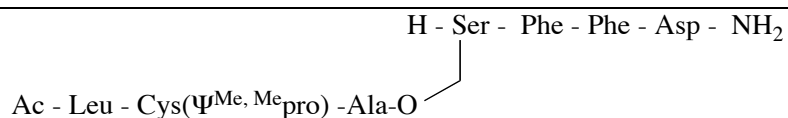
Ac-Leu-Cys( $\Psi^{\text{Me,Me}}$ pro)-OH **13**

---



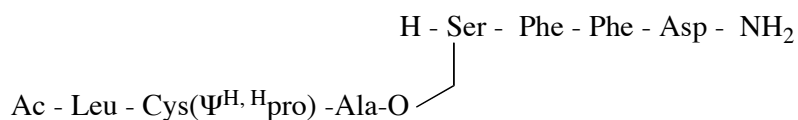
Ac-Leu-Cys( $\Psi^{\text{H,H}}$ pro)-OH **14**

---



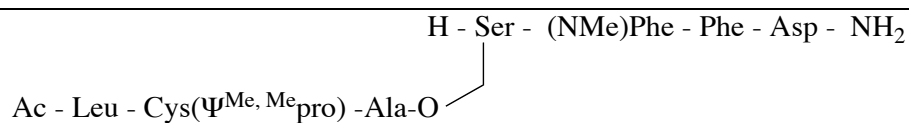
15

---



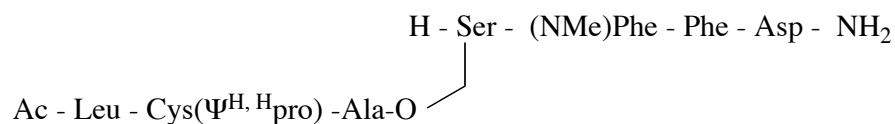
16

---



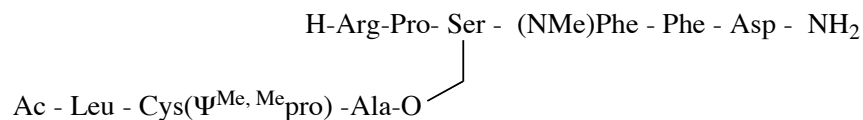
17

---



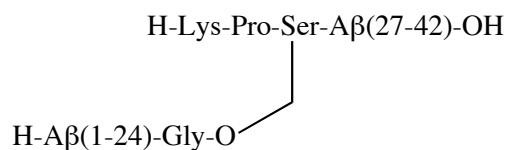
18

---



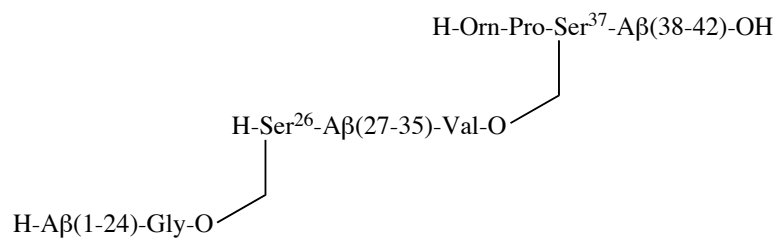
19

---



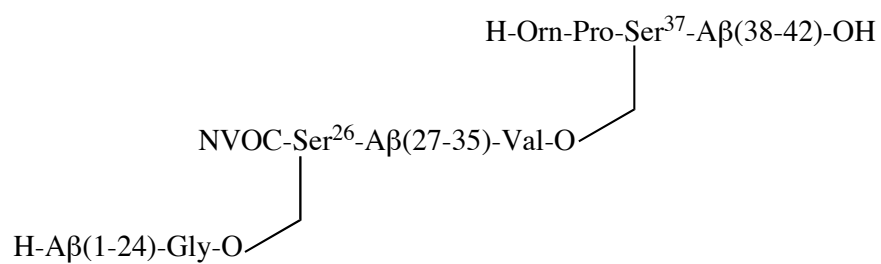
20

---

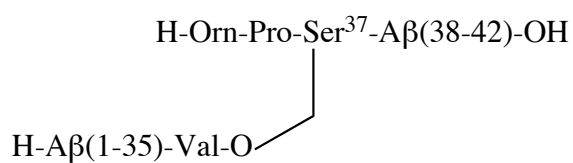


21

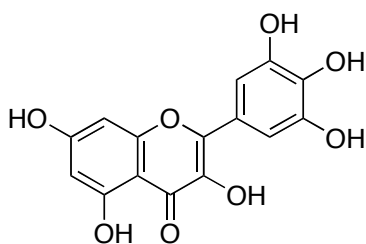
---



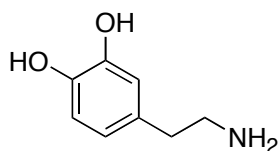
22



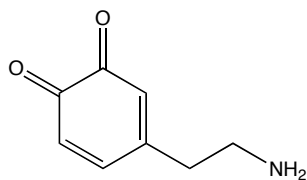
23



**Myricetin**

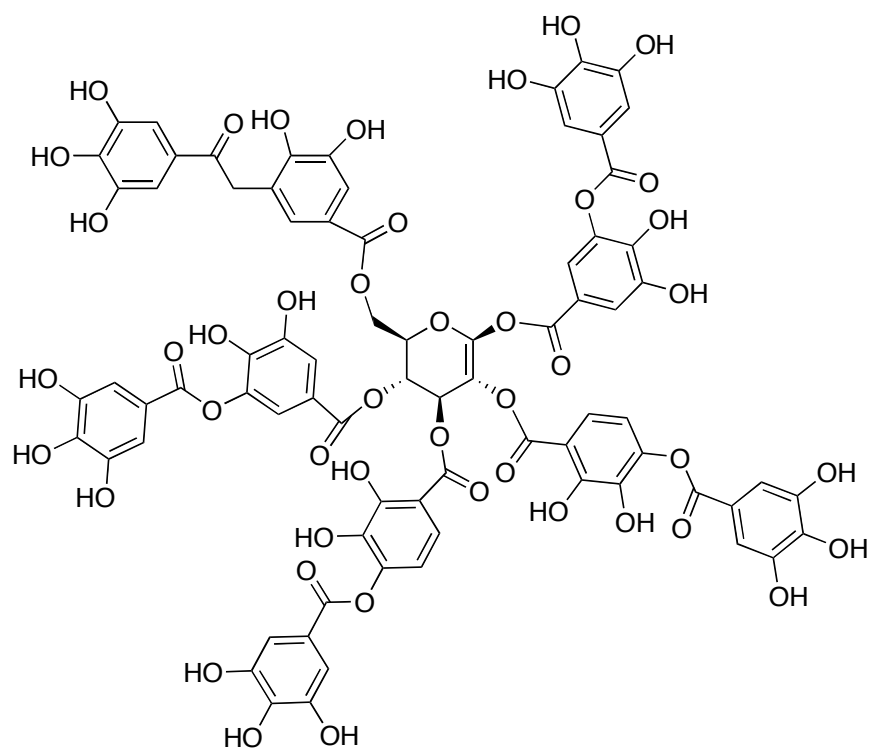


**Dopamine**



**Dopaquinone (oxidized dopamine)**

---



**Tannic acid**

---

## Bibliography

1. Pauling, L.; Corey, R. B.; Branson, H. R., The Structure of proteins: Two Hydrogen-Bonded Helical Configurations of the Polypeptide Chain. *PNAS* **1951**, 37, 205-211.
2. Ramachandran, G. N., Protein Structure and Crystallography. *Science* **1963**, 141, (3577), 288-291.
3. Branden, C.; Tooze, J., Introduction to protein structure. Garland Publishing, Inc.: **1991**.
4. Beck-Sickinger, A. G.; Jung, G., Structure-activity relationships of neuropeptide Y analogues with respect to Y1 and Y2 receptors. *Biopolymers* **1995**, 37, (2), 123-42.
5. Motta, A.; Morelli, M. A.; Goud, N.; Temussi, P. A., Sequential <sup>1</sup>H NMR assignment and secondary structure determination of salmon calcitonin in solution. *Biochemistry* **1989**, 28, (20), 7996-8002.
6. Ellenberger, T. E.; Brandl, C. J.; Struhl, K.; Harrison, S. C., The GCN4 basic region leucine zipper binds DNA as a dimer of uninterrupted alpha helices: crystal structure of the protein-DNA complex. *Cell* **1992**, 71, (7), 1223-37.
7. Bernheimer, A. W.; Rudy, B., Interactions between membranes and cytolytic peptides. *Biochim Biophys Acta* **1986**, 864, (1), 123-41.
8. Gani, D.; Lewis, A.; Rutherford, T.; Wilkie, J.; Stirling, I.; Jenn, T.; Ryan, M. D., Design, Synthesis, Structure and Properties of an  $\alpha$ -Helix Cap Template derived from N-[(2S)-2-chloropropionyl]-(2S)-Pro-(2R)-Ala-(2S,4R)-4-thioPro-OMe which Initiates  $\alpha$ -Helical Structures. *Tetrahedron* **1998**, 54, 15793-15819.
9. Zimm, B. H.; Bragg, J. K., Theory of the Phase Transition between Helix and Random Coil in Polypeptide Chains. *J. Chem. Phys.* **1959**, 31, 526-535.
10. Bierzynski, A.; Kim, P. S.; Baldwin, R. L., A salt bridge stabilizes the helix formed by isolated C-peptide of RNase A. *PNAS* **1982**, 79, 2470-2474.
11. Marqusee, S.; Baldwin, R. L., Helix stabilization by Glu-...Lys<sup>+</sup> salt bridges in short peptides of the de novo design. *PNAS* **1987**, 84, 8898-8902.
12. Shoemaker, K. R.; Kim, P. S.; Brems, D. N.; Marqusee, S.; York, E. J.; Chaiken, I. M.; Stewart, J. M.; Baldwin, R. L., Nature of the charged-group effect on the stability of the C-peptide helix. *PNAS* **1985**, 82, 2349-2353.
13. Kemp, D. S., Peptidomimetics and the template approach to nucleation of beta-sheets and alpha-helices in peptides. *Trends Biotechnol.* **1990**, 8(9), 249-255.

14. Wilson, R. S.; Scherr, P. A.; Hoganson, G.; Bienias, J. L.; Evans, D. A.; Bennett, D. A., Early life socioeconomic status and late life risk of Alzheimer's disease. *Neuroepidemiology* **2005**, 25, (1), 8-14.
15. Elgh, E.; Lindqvist Astot, A.; Fagerlund, M.; Eriksson, S.; Olsson, T.; Nasman, B., Cognitive dysfunction, hippocampal atrophy and glucocorticoid feedback in Alzheimer's disease. *Biol Psychiatry* **2006**, 59, (2), 155-61.
16. Dahm, R., Alzheimer's discovery. *Curr Biol* **2006**, 16, (21), R906-10.
17. Alzheimer, A., über eine eigenartige Erkrankung der Hirnrinde. *Allg. Z. Psychiatrie Psychisch-Gerichtl. Med.* **1907**, 64, 146-148.
18. Alzheimer, A., über einen eigenartigen schweren Erkrankungsprozeß der Hirnrinde. *Neurologisches Centralblatt* **1906**, 23, 1129-1136.
19. Alzheimer, A., über eigenartige Krankheitsfälle des späteren Alters. *Zeitschrift für die Gesamte Neurologie and Psychiatrie* **1911**, 4, 356-385.
20. Braak, H.; Braak, E., Neuropathological staging of Alzheimer-related changes. *Acta Neuropathol (Berl)* **1991**, 82, 239-259.
21. Mirra, S. S.; Heyman, A.; McKeel, D.; al., e., The consortium to establish a registry for Alzheimer's disease (CERAD). Part II. Standardization of the neuropathologic assessment of Alzheimer's disease. *Neurology* **1991**, 41, 479-486.
22. Cleveland, D. W.; Hwo, S. Y.; W., K. M., Physical and chemical properties of purified tau factor and the role of tau in microtubule assembly. *J. Mol. Biol.* **1977**, 116, 227-247.
23. Drubin, D. G.; Kirschner, M. W., Tau protein function in living cells. *J. Cell Biol.* **1986**, 103, 2739-2746.
24. Jenkins, S. M.; Johnson, G. V. W., Tau complexes with phospholipase C-gamma in situ. *Neuroreport* **1998**, 9, 67-71.
25. Biernat, J.; Mandelkow, E. M., The development of cell processes induced by tau protein requires phosphorylation of serine 262 and 356 in the repeat domain and is inhibited by phosphorylation in the proline-rich domains. *Mol Biol Cell* **1999**, 10, (3), 727-40.
26. Taniguchi, T.; Kawamata, T.; Mukai, H.; Hasegawa, H.; Isagawa, T.; Yasuda, M.; Hashimoto, T.; Terashima, A.; Nakai, M.; Mori, H.; Ono, Y.; Tanaka, C., Phosphorylation of tau is regulated by PKN. *J Biol Chem* **2001**, 276, (13), 10025-31.
27. Garcia, M. L.; Cleveland, D. W., Going new places using an old MAP: tau, microtubules and human neurodegenerative disease. *Curr Opin Cell Biol* **2001**, 13, (1), 41-8.

28. Stamer, K.; Vogel, R.; Thies, E.; Mandelkow, E.; Mandelkow, E. M., Tau blocks traffic of organelles, neurofilaments, and APP vesicles in neurons and enhances oxidative stress. *J Cell Biol* **2002**, 156, (6), 1051-63.
29. Gralle, M.; Ferreira, S. T., Structure and functions of the human amyloid precursor protein: the whole is more than the sum of its parts. *Prog Neurobiol* **2007**, 82, (1), 11-32.
30. Turner, P. R.; O'Connor, K.; Tate, W. P.; Abraham, W. C., Roles of amyloid precursor protein and its fragments in regulating neural activity, plasticity and memory. *Prog Neurobiol* **2003**, 70, (1), 1-32.
31. Schmid, A. An Electrophysiological and Biochemical Investigation of the effects of Beta Amyloid Peptide on Hippocampal Long-Term Potentiation in vivo. University College of Dublin, Dublin, 2004.
32. Haass, C.; Schlossmacher, M. G.; Hung, A. Y.; Vigo-Pelfrey, C.; Mellon, A.; Ostaszewski, B. L.; Lieberburg, I.; Koo, E. H.; Schenk, D.; Teplow, D. B.; et al., Amyloid beta-peptide is produced by cultured cells during normal metabolism. *Nature* **1992**, 359, (6393), 322-5.
33. Butterfield, D. A.; Kanski, J., Brain protein oxidation in age-related neurodegenerative disorders that are associated with aggregated proteins. *Mech Ageing Dev* **2001**, 122, (9), 945-62.
34. Stadtman, E. R.; Berlett, B. S., Reactive oxygen-mediated protein oxidation in aging and disease. *Chem Res Toxicol* **1997**, 10, (5), 485-94.
35. Butterfield, D. A.; Reed, T.; Newman, S. F.; Sultana, R., Roles of amyloid beta-peptide-associated oxidative stress and brain protein modifications in the pathogenesis of Alzheimer's disease and mild cognitive impairment. *Free Radic Biol Med* **2007**, 43, (5), 658-77.
36. Katzman, R., Alzheimer's disease. *N. Engl. J. Med* **1986**, 314, 964-973.
37. Terry, R. D.; Masliah, E.; Salmon, D. P.; Butters, N.; DeTeresa, R.; Hill, R.; Hansen, L. A.; Katzman, R., Physical basis of cognitive alterations in Alzheimer's disease: synapse loss is the major correlate of cognitive impairment. *Ann Neurol* **1991**, 30, (4), 572-80.
38. Dickson, D. W.; Crystal, H. A.; Bevona, C.; Honer, W.; Vincent, I.; Davies, P., Correlations of synaptic and pathological markers with cognition of the elderly. *Neurobiol Aging* **1995**, 16, (3), 285-98; discussion 298-304.
39. Dahlgren, K. N.; Manelli, A. M.; Stine, W. B., Jr.; Baker, L. K.; Krafft, G. A.; LaDu, M. J., Oligomeric and fibrillar species of amyloid-beta peptides differentially affect neuronal viability. *J Biol Chem* **2002**, 277, (35), 32046-53.

40. Hoshi, M.; Sato, M.; Matsumoto, S.; Noguchi, A.; Yasutake, K.; Yoshida, N.; Sato, K., Spherical aggregates of beta-amyloid (amylospheroid) show high neurotoxicity and activate tau protein kinase I/glycogen synthase kinase-3beta. *Proc Natl Acad Sci U S A* **2003**, 100, (11), 6370-5.
41. Kirkitadze, M. D.; Bitan, G.; Teplow, D. B., Paradigm shifts in Alzheimer's disease and other neurodegenerative disorders: the emerging role of oligomeric assemblies. *J Neurosci Res* **2002**, 69, (5), 567-77.
42. Haass, C.; Selkoe, D. J., Soluble protein oligomers in neurodegeneration: lessons from the Alzheimer's amyloid beta-peptide. *Nat Rev Mol Cell Biol* **2007**, 8, (2), 101-12.
43. Selkoe, D. J., Alzheimer disease: mechanistic understanding predicts novel therapies. *Ann Intern Med* **2004**, 140, (8), 627-38.
44. Walsh, D. M.; Klyubin, I.; Fadeeva, J. V.; Cullen, W. K.; Anwyl, R.; Wolfe, M. S.; Rowan, M. J.; Selkoe, D. J., Naturally secreted oligomers of amyloid beta protein potently inhibit hippocampal long-term potentiation in vivo. *Nature* **2002**, 416, (6880), 535-9.
45. Lambert, M. P.; Barlow, A. K.; Chromy, B. A.; Edwards, C.; Freed, R.; Liosatos, M.; Morgan, T. E.; Rozovsky, I.; Trommer, B.; Viola, K. L.; Wals, P.; Zhang, C.; Finch, C. E.; Krafft, G. A.; Klein, W. L., Diffusible, nonfibrillar ligands derived from Abeta1-42 are potent central nervous system neurotoxins. *Proc Natl Acad Sci U S A* **1998**, 95, (11), 6448-53.
46. Lashuel, H. A., Membrane permeabilization: a common mechanism in protein-misfolding diseases. *Sci Aging Knowledge Environ* **2005**, 2005, (38), pe28.
47. Walsh, D. M.; Lomakin, A.; Benedek, G. B.; Condron, M. M.; Teplow, D. B., Amyloid beta-protein fibrillogenesis. Detection of a protofibrillar intermediate. *J Biol Chem* **1997**, 272, (35), 22364-72.
48. Caughey, B.; Lansbury, P. T., Protofibrils, pores, fibrils, and neurodegeneration: separating the responsible protein aggregates from the innocent bystanders. *Annu Rev Neurosci* **2003**, 26, 267-98.
49. Serpell, L. C.; Blake, C. C.; Fraser, P. E., Molecular structure of a fibrillar Alzheimer's A beta fragment. *Biochemistry* **2000**, 39, (43), 13269-75.
50. Lansbury, P. T.; Lashuel, H. A., A century-old debate on protein aggregation and neurodegeneration enters the clinic. *Nature* **2006**, 443, (7113), 774-9.
51. Hardy, J.; Selkoe, D. J., The amyloid hypothesis of Alzheimer's disease: progress and problems on the road to therapeutics. *Science* **2002**, 297, (5580), 353-6.
52. Klunk, W. E.; Lopresti, B. J.; Ikonovic, M. D.; Lefterov, I. M.; Koldamova, R. P.; Abrahamson, E. E.; Debnath, M. L.; Holt, D. P.; Huang, G. F.; Shao, L.; DeKosky, S. T.;



Price, J. C.; Mathis, C. A., Binding of the positron emission tomography tracer Pittsburgh compound-B reflects the amount of amyloid-beta in Alzheimer's disease brain but not in transgenic mouse brain. *J Neurosci* **2005**, 25, (46), 10598-606.

53. Fagan, A. M.; Mintun, M. A.; Mach, R. H.; Lee, S. Y.; Dence, C. S.; Shah, A. R.; LaRossa, G. N.; Spinner, M. L.; Klunk, W. E.; Mathis, C. A.; DeKosky, S. T.; Morris, J. C.; Holtzman, D. M., Inverse relation between in vivo amyloid imaging load and cerebrospinal fluid Abeta42 in humans. *Ann Neurol* **2006**, 59, (3), 512-9.

54. Luhrs, T.; Ritter, C.; Adrian, M.; Riek-Loher, D.; Bohrmann, B.; Dobeli, H.; Schubert, D.; Riek, R., 3D structure of Alzheimer's amyloid-beta(1-42) fibrils. *Proc Natl Acad Sci U S A* **2005**, 102, (48), 17342-7.

55. Masters, C. L.; Beyreuther, K., Alzheimer's centennial legacy: prospects for rational therapeutic intervention targeting the Abeta amyloid pathway. *Brain* **2006**, 129, (Pt 11), 2823-39.

56. Tuszynski, M. H.; Thal, L.; U, H. S.; Pay, M. M.; Blesch, A.; Conner, J.; Vahlsing, H. L., Nerve growth factor gene therapy for Alzheimer's disease. *J Mol Neurosci* **2002**, 19, (1-2), 207.

57. Snyder, E. M.; Nong, Y.; Almeida, C. G.; Paul, S.; Moran, T.; Choi, E. Y.; Nairn, A. C.; Salter, M. W.; Lombroso, P. J.; Gouras, G. K.; Greengard, P., Regulation of NMDA receptor trafficking by amyloid-beta. *Nat Neurosci* **2005**, 8, (8), 1051-8.

58. Yamada, K.; Takayanagi, M.; Kamei, H.; Nagai, T.; Dohniwa, M.; Kobayashi, K.; Yoshida, S.; Ohhara, T.; Takuma, K.; Nabeshima, T., Effects of memantine and donepezil on amyloid beta-induced memory impairment in a delayed-matching to position task in rats. *Behav Brain Res* **2005**, 162, (2), 191-9.

59. Van Dam, D.; Abramowski, D.; Staufenbiel, M.; De Deyn, P. P., Symptomatic effect of donepezil, rivastigmine, galantamine and memantine on cognitive deficits in the APP23 model. *Psychopharmacology (Berl)* **2005**, 180, (1), 177-90.

60. Lesne, S.; Ali, C.; Gabriel, C.; Croci, N.; MacKenzie, E. T.; Glabe, C. G.; Plotkine, M.; Marchand-Verrecchia, C.; Vivien, D.; Buisson, A., NMDA receptor activation inhibits alpha-secretase and promotes neuronal amyloid-beta production. *J Neurosci* **2005**, 25, (41), 9367-77.

61. Masse, I.; Bordet, R.; Deplanque, D.; Al Khedr, A.; Richard, F.; Libersa, C.; Pasquier, F., Lipid lowering agents are associated with a slower cognitive decline in Alzheimer's disease. *J Neurol Neurosurg Psychiatry* **2005**, 76, (12), 1624-9.

62. Nathan, C.; Calingasan, N.; Nezezon, J.; Ding, A.; Lucia, M. S.; La Perle, K.; Fuortes, M.; Lin, M.; Ehrt, S.; Kwon, N. S.; Chen, J.; Vodovotz, Y.; Kipiani, K.; Beal, M. F., Protection from Alzheimer's-like disease in the mouse by genetic ablation of inducible nitric oxide synthase. *J Exp Med* **2005**, 202, (9), 1163-9.

63. Moreira, P. I.; Smith, M. A.; Zhu, X.; Nunomura, A.; Castellani, R. J.; Perry, G., Oxidative stress and neurodegeneration. *Ann N Y Acad Sci* **2005**, 1043, 545-52.
64. Perluigi, M.; Joshi, G.; Sultana, R.; Calabrese, V.; De Marco, C.; Coccia, R.; Butterfield, D. A., In vivo protection by the xanthate tricyclodecan-9-yl-xanthogenate against amyloid beta-peptide (1-42)-induced oxidative stress. *Neuroscience* **2006**, 138, (4), 1161-70.
65. Best, J. D.; Jay, M. T.; Otu, F.; Churcher, I.; Reilly, M.; Morentin-Gutierrez, P.; Pattison, C.; Harrison, T.; Shearman, M. S.; Atack, J. R., In vivo characterization of Abeta(40) changes in brain and cerebrospinal fluid using the novel gamma-secretase inhibitor N-[cis-4-[(4-chlorophenyl)sulfonyl]-4-(2,5-difluorophenyl)cyclohexyl]-1,1,1-trifluoromethanesulfonamide (MRK-560) in the rat. *J Pharmacol Exp Ther* **2006**, 317, (2), 786-90.
66. Peretto, I.; Radaelli, S.; Parini, C.; Zandi, M.; Raveglia, L. F.; Dondio, G.; Fontanella, L.; Misiano, P.; Bigogno, C.; Rizzi, A.; Riccardi, B.; Biscaioli, M.; Marchetti, S.; Puccini, P.; Catinella, S.; Rondelli, I.; Cenacchi, V.; Bolzoni, P. T.; Caruso, P.; Villetti, G.; Facchinetti, F.; Del Giudice, E.; Moretto, N.; Imbimbo, B. P., Synthesis and biological activity of flurbiprofen analogues as selective inhibitors of beta-amyloid(1)(-)(42) secretion. *J Med Chem* **2005**, 48, (18), 5705-20.
67. Brendza, R. P.; Bacskai, B. J.; Cirrito, J. R.; Simmons, K. A.; Skoch, J. M.; Klunk, W. E.; Mathis, C. A.; Bales, K. R.; Paul, S. M.; Hyman, B. T.; Holtzman, D. M., Anti-Abeta antibody treatment promotes the rapid recovery of amyloid-associated neuritic dystrophy in PDAPP transgenic mice. *J Clin Invest* **2005**, 115, (2), 428-33.
68. Gilman, S.; Koller, M.; Black, R. S.; Jenkins, L.; Griffith, S. G.; Fox, N. C.; Eisner, L.; Kirby, L.; Rovira, M. B.; Forette, F.; Orgogozo, J. M., Clinical effects of Abeta immunization (AN1792) in patients with AD in an interrupted trial. *Neurology* **2005**, 64, (9), 1553-62.
69. Lee, M.; Bard, F.; Johnson-Wood, K.; Lee, C.; Hu, K.; Griffith, S. G.; Black, R. S.; Schenk, D.; Seubert, P., Abeta42 immunization in Alzheimer's disease generates Abeta N-terminal antibodies. *Ann Neurol* **2005**, 58, (3), 430-5.
70. Lee, E. B.; Leng, L. Z.; Zhang, B.; Kwong, L.; Trojanowski, J. Q.; Abel, T.; Lee, V. M., Targeting amyloid-beta peptide (Abeta) oligomers by passive immunization with a conformation-selective monoclonal antibody improves learning and memory in Abeta precursor protein (APP) transgenic mice. *J Biol Chem* **2006**, 281, (7), 4292-9.
71. Findeis, M. A., Peptide inhibitors of beta amyloid aggregation. *Curr Top Med Chem* **2002**, 2, (4), 417-23.
72. Adessi, C.; Frossard, M. J.; Boissard, C.; Fraga, S.; Bieler, S.; Ruckle, T.; Vilbois, F.; Robinson, S. M.; Mutter, M.; Banks, W. A.; Soto, C., Pharmacological profiles of peptide drug candidates for the treatment of Alzheimer's disease. *J Biol Chem* **2003**, 278, (16), 13905-11.

73. Gervais, F.; Paquette, J.; Morissette, C.; Krzywkowski, P.; Yu, M.; Azzi, M.; Lacombe, D.; Kong, X.; Aman, A.; Laurin, J.; Szarek, W. A.; Tremblay, P., Targeting soluble Abeta peptide with Tramiprosate for the treatment of brain amyloidosis. *Neurobiol Aging* **2007**, 28, (4), 537-47.
74. Taniguchi, S.; Suzuki, N.; Masuda, M.; Hisanaga, S.; Iwatsubo, T.; Goedert, M.; Hasegawa, M., Inhibition of heparin-induced tau filament formation by phenothiazines, polyphenols, and porphyrins. *J Biol Chem* **2005**, 280, (9), 7614-23.
75. Necula, M.; Chirita, C. N.; Kuret, J., Cyanine dye N744 inhibits tau fibrillization by blocking filament extension: implications for the treatment of tauopathic neurodegenerative diseases. *Biochemistry* **2005**, 44, (30), 10227-37.
76. Toniolo, C.; Bonora, G. M.; Mutter, M., Conformations of Poly(ethylene glycol) bound homooligo-L-alanines and L-valines in aqueous solution. *J. Am. Chem. Soc.* **1979**, 101, 450-454.
77. Gorman, P. M.; Chakrabartty, A., Alzheimer beta-amyloid peptides: structures of amyloid fibrils and alternate aggregation products. *Biopolymers* **2001**, 60, (5), 381-94.
78. Mutter, M.; Vuilleumier, S., A Chemical Approach to Protein Design - Template-Assembled Synthetic Proteins (TASP). *Angew Chem Int Ed Engl* **1989**, 28, 535-554.
79. Mutter, M., The Construction of New Proteins and Enzymes-a Prospect for the Future? *Angew Chem Int Ed Engl* **1985**, 24, (8), 639-653.
80. Mutter, M.; Chandravarkar, A.; Boyat, C.; Lopez, J.; Dos Santos, S.; Mandal, B.; Mimna, R.; Murat, K.; Patiny, L.; Saucedo, L.; Tuchscherer, G., Switch peptides in statu nascendi: induction of conformational transitions relevant to degenerative diseases. *Angew Chem Int Ed Engl* **2004**, 43, (32), 4172-8.
81. Tuchscherer, G.; Chandravarkar, A.; Camus, M. S.; Berard, J.; Murat, K.; Schmid, A.; Mimna, R.; Lashuel, H. A.; Mutter, M., Switch-peptides as folding precursors in self-assembling peptides and amyloid fibrillogenesis. *Biopolymers* **2007**, 88, (2), 239-52.
82. Ingwall, R. T.; Goodman, M., Polydepsipeptides. III. Theoretical conformational analysis of randomly coiling and ordered depsipeptide chains. *Macromolecules* **1974**, 7, (5), 598-605.
83. Arad, O.; Goodman, M., Depsipeptide analogues of elastin repeating sequences: conformational analysis. *Biopolymers* **1990**, 29, (12-13), 1652-68.
84. Silinski, P.; Fitzgerald, M. C., Comparative analysis of two different amide-to-ester bond mutations in the beta-sheet of 4-oxalocrotonate tautomerase. *Biochemistry* **2003**, 42, (21), 6620-30.

85. Arnett, E. N.; Mitchell, E. J.; Murty, T. S. S. R., Basicity. Comparison of hydrogen bonding proton transfer to some Lewis bases. *J. Am. Chem. Soc.* **1974**, *96*, 3875-3891.
86. Yang, X.; Wang, M.; Fitzgerald, M. C., Analysis of protein folding and function using backbone modified proteins. *Bioorg Chem* **2004**, *32*, (5), 438-49.
87. Koh, J. T.; Cornish, V. W.; Schultz, P. G., An experimental approach to evaluating the role of backbone interactions in proteins using unnatural amino acid mutagenesis. *Biochemistry* **1997**, *36*, (38), 11314-22.
88. Deechongkit, S.; Nguyen, H.; Powers, E. T.; Dawson, P. E.; Gruebele, M.; Kelly, J. W., Context-dependent contributions of backbone hydrogen bonding to beta-sheet folding energetics. *Nature* **2004**, *430*, (6995), 101-5.
89. DeGrado, W. F.; Schneider, J. P.; Hamuro, Y., The twists and turns of beta-peptides. *J Pept Res* **1999**, *54*, (3), 206-17.
90. Chou, P. Y.; Fasman, G. D., Empirical predictions of protein conformation. *Annu Rev Biochem* **1978**, *47*, 251-76.
91. Bergmann, M.; Brand, E.; Weinmann, F., Rearrangements of peptide-like substances. Derivatives of  $\alpha$ -amino- $\beta$ -hydroxybutyric acid. *Z. Physiol. Chem.* **1923**, *131*, 1-17.
92. Iwai, K.; Ando, T., N to O acyl rearrangement. *Methods Enzymol.* **1967**, *11*, 263-282.
93. Phillips, A. P.; Baltzly, R., Rearrangements between primary ethanolamides of carboxylic acids and the corresponding aminoethylesters. *J. Am. Chem. Soc.* **1947**, *69*, 200-204.
94. Kazmierski, W. M.; Bevans, P.; Furfine, E.; Spaltenstein, A.; Yang, H., Novel prodrug approach to amprenavir-based HIV-1 protease inhibitors via O $\rightarrow$ N acyloxy migration of P1 moiety. *Bioorg Med Chem Lett* **2003**, *13*, (15), 2523-6.
95. Gopin, A.; Pessah, N.; Shamis, M.; Rader, C.; Shabat, D., A chemical adaptor system designed to link a tumor-targeting device with a prodrug and an enzymatic trigger. *Angew Chem Int Ed Engl* **2003**, *42*, (3), 327-32.
96. Grether, U.; Waldman, H., An enzyme-labile safety catch linker for synthesis on a soluble polymeric support. *Chem. Eur. J.* **2001**, *7*, 959-971.
97. Buur, A.; Bundgaard, H.; Lee, V. H. L., Prodrugs of propranolol: hydrolysis and intramolecular aminolysis of various propranolol esters and an oxazolidin-2-one derivative. *International Journal of pharmaceuticals* **1988**, *42*, 51-60.
98. Durrer, A.; Wernly-Chung, G. N.; Boss, G.; Testa, B., Enzymatic hydrolysis of nicotinate esters: comparison between plasma and liver catalysis. *Xenobiotica* **1992**, *22*, 273-282.

99. Hsu, C.-H.; Jay, M.; Bummer, P. M.; Lehmler, H.-J., Chemical Stability of Esters of Nicotinic Acid Intended for Pulmonary Administration by Liquid Ventilation. *Pharmaceutical Research* **2003**, 20, (6), 918-925.
100. Saucède, L.; Santos, S. D.; Arunan, C.; Mandal, B.; Mimna, R.; Murat, K.; Camus, M.-S.; Bérard, J.; Grouzmann, E.; Adrian, M.; Dubochet, J.; Lopez, J.; Lashuel, H.; Tuchscherer, G.; Mutter, M., Switch-Peptides: From Conformational Studies to Alzheimer's Disease. *Chimia* **2006**, 60, 199-202.
101. Snow, C. D.; Nguyen, H.; Pande, V. S.; Gruebele, M., Absolute comparison of simulated and experimental protein-folding dynamics. *Nature* **2002**, 420, (6911), 102-6.
102. Mayor, U.; Johnson, C. M.; Daggett, V.; Fersht, A. R., Protein folding and unfolding in microseconds to nanoseconds by experiment and simulation. *Proc Natl Acad Sci U S A* **2000**, 97, (25), 13518-22.
103. Mayor, U.; Guydosh, N. R.; Johnson, C. M.; Grossmann, J. G.; Sato, S.; Jas, G. S.; Freund, S. M.; Alonso, D. O.; Daggett, V.; Fersht, A. R., The complete folding pathway of a protein from nanoseconds to microseconds. *Nature* **2003**, 421, (6925), 863-7.
104. DosSantos, S. Switch-peptides: Controlling Biological Function and Self-Assembly of Amyloid  $\beta$ -derived Peptides using Enzyme-Triggered Acyl Migrations. PhD Thesis, EPFL, Lausanne, 2005.
105. Sohma, Y.; Hayashi, Y.; Skwarczynski, M.; Hamada, Y.; Sasaki, M.; Kimura, T.; Kiso, Y., O-N intramolecular acyl migration reaction in the development of prodrugs and the synthesis of difficult sequence-containing bioactive peptides. *Biopolymers* **2004**, 76, (4), 344-56.
106. Carpino, L. A.; Krause, E.; Sferdean, C. D.; Schuemann, M.; Fabian, H.; Bienert, M.; Beyermann, M., Synthesis of 'difficult' peptide sequences: application of a depsipeptide technique to the Jung-Redemann 10- and 26-mers and the amyloid peptide A $\beta$ (1-42). *Tetrahedron lett.* **2004**, 45, (40), 7519-7523.
107. Lazo, N. D.; Grant, M. A.; Condrón, M. C.; Rigby, A. C.; Telpow, D. B., On the nucleation of amyloid  $\beta$ -protein monomer folding. *Protein Sci.* **2005**, 14, 1581-1596.
108. Jarrett, J. T.; Berger, E. P.; Lansbury, P. T., Jr., The carboxy terminus of the beta amyloid protein is critical for the seeding of amyloid formation: implications for the pathogenesis of Alzheimer's disease. *Biochemistry* **1993**, 32, (18), 4693-7.
109. Walsh, D. M.; Selkoe, D. J., Deciphering the molecular basis of memory failure in Alzheimer's disease. *Neuron* **2004**, 44, (1), 181-93.
110. Walsh, D. M.; Selkoe, D. J., A beta oligomers - a decade of discovery. *J Neurochem* **2007**, 101, (5), 1172-84.

111. Maloney, M. T.; Minamide, L. S.; Kinley, A. W.; Boyle, J. A.; Bamberg, J. R., Beta-secretase-cleaved amyloid precursor protein accumulates at actin inclusions induced in neurons by stress or amyloid beta: a feedforward mechanism for Alzheimer's disease. *J Neurosci* **2005**, 25, (49), 11313-21.
112. Dos Santos, S.; Chandravarkar, A.; Mandal, B.; Mimna, R.; Murat, K.; Saucedo, L.; Tella, P.; Tuchscherer, G.; Mutter, M., Switch-peptides: controlling self-assembly of amyloid beta-derived peptides in vitro by consecutive triggering of acyl migrations. *J Am Chem Soc* **2005**, 127, (34), 11888-9.
113. Dreele, P. H. v.; Poland, D.; Scheraga, H. A., Helix-Coil Stability Constants for the Naturally Occurring Amino Acids in Water. I. Properties of Copolymers and Approximate Theories. *Macromolecules* **1971**, 4, (4), 396-407.
114. Mutter, M.; Maser, F.; Altmann, K. H.; Toniolo, C.; Bonora, G. M., Sequence-dependence of secondary structure formation: conformational studies of host-guest peptides in alpha-helix and beta-structure supporting media. *Biopolymers* **1985**, 24, (6), 1057-74.
115. Bonora, G. M.; Moretto, V.; Toniolo, C.; Anzinger, H.; Mutter, M., Conformational characteristics of homo-oligopeptides of O-benzyl-L-tyrosine. *Int J Pept Protein Res* **1983**, 21, (4), 336-43.
116. Toniolo, C.; Bonora, G. M.; Mutter, M.; Pillai, V. N. R., The Effect of the Insertion of a Proline Residue on the Solution Conformation of Host Peptides. *Makromol. Chem.* **1981**, 182, 2007-2014.
117. Tjernberg, L. O.; Callaway, D. J.; Tjernberg, A.; Hahne, S.; Lilliehook, C.; Terenius, L.; Thyberg, J.; Nordstedt, C., A molecular model of Alzheimer amyloid beta-peptide fibril formation. *J Biol Chem* **1999**, 274, (18), 12619-25.
118. Mandal, B. Switch-Peptides: a new tool for the study of  $\beta$ -sheet aggregation and the design of novel b-breakers. PhD Thesis, EPFL, Lausanne, 2006.
119. Porat, Y.; Abramowitz, A.; Gazit, E., Inhibition of amyloid fibril formation by polyphenols: structural similarity and aromatic interactions as a common inhibition mechanism. *Chem Biol Drug Des* **2006**, 67, (1), 27-37.
120. Pu, F.; Mishima, K.; Irie, K.; Motohashi, K.; Tanaka, Y.; Orito, K.; Egawa, T.; Kitamura, Y.; Egashira, N.; Iwasaki, K.; Fujiwara, M., Neuroprotective effects of Quercetin and Rutin on Spatial Memory Impairment in an 8-Arm Radial Maze Task and Neuronal Death Induced by Repeated Cerebral Ischemia in Rats. *J. Pharmacol. Sci.* **2007**, (Uncorrected Proof).
121. Ono, K.; Hasegawa, K.; Naiki, H.; Yamada, M., Anti-amyloidogenic activity of tannic acid and its activity to destabilize Alzheimer's beta-amyloid fibrils in vitro. *Biochim Biophys Acta* **2004**, 1690, (3), 193-202.

122. Ono, K.; Yoshiike, Y.; Takashima, A.; Hasegawa, K.; Naiki, H.; Yamada, M., Potent anti-amyloidogenic and fibril-destabilizing effects of polyphenols in vitro: implications for the prevention and therapeutics of Alzheimer's disease. *J Neurochem* **2003**, *87*, (1), 172-81.
123. Kapurniotu, A.; Schmauder, A.; Tenidis, K., Structure-based design and study of non-amyloidogenic, double N-methylated IAPP amyloid core sequences as inhibitors of IAPP amyloid formation and cytotoxicity. *J Mol Biol* **2002**, *315*, (3), 339-50.
124. Adessi, C.; Soto, C., Converting a peptide into a drug: strategies to improve stability and bioavailability. *Curr Med Chem* **2002**, *9*, (9), 963-78.
125. Poduslo, J. F.; Curran, G. L.; Kumar, A.; Frangione, B.; Soto, C., Beta-sheet breaker peptide inhibitor of Alzheimer's amyloidogenesis with increased blood-brain barrier permeability and resistance to proteolytic degradation in plasma. *J Neurobiol* **1999**, *39*, (3), 371-82.
126. Tjernberg, L. O.; Naslund, J.; Lindqvist, F.; Johansson, J.; Karlstrom, A. R.; Thyberg, J.; Terenius, L.; Nordstedt, C., Arrest of beta-amyloid fibril formation by a pentapeptide ligand. *J Biol Chem* **1996**, *271*, (15), 8545-8.
127. Mutter, M.; Wöhr, T.; Gioria, S.; Keller, M., Pseudo-prolines: induction of cis/trans-conformational interconversion by decreased transition state barriers. *Biopolymers* **1999**, *51*, (2), 121-8.
128. Murat, K. Le Concept "Switch-peptides": Le potentiel de la migration S,N acylique dans l'induction de l'activité biologique et la rupture de structures secondaire in situ. PhD Thesis, EPFL, Lausanne, 2006.
129. Stefani, M.; Dobson, C. M., Protein aggregation and aggregate toxicity: new insights into protein folding, misfolding diseases and biological evolution. *J Mol Med* **2003**, *81*, (11), 678-99.
130. Soto, C.; Estrada, L.; Castilla, J., Amyloids, prions and the inherent infectious nature of misfolded protein aggregates. *Trends Biochem Sci* **2006**, *31*, (3), 150-5.
131. Jager, M.; Nguyen, H.; Crane, J. C.; Kelly, J. W.; Gruebele, M., The folding mechanism of a beta-sheet: the WW domain. *J Mol Biol* **2001**, *311*, (2), 373-93.
132. Gillmore, J. D.; Stangou, A. J.; Tennent, G. A.; Booth, D. R.; O'Grady, J.; Rela, M.; Heaton, N. D.; Wall, C. A.; Keogh, J. A.; Hawkins, P. N., Clinical and biochemical outcome of hepatorenal transplantation for hereditary systemic amyloidosis associated with apolipoprotein AI Gly26Arg. *Transplantation* **2001**, *71*, (7), 986-92.
133. Carulla, N.; Caddy, G. L.; Hall, D. R.; Zurdo, J.; Gairi, M.; Feliz, M.; Giralt, E.; Robinson, C. V.; Dobson, C. M., Molecular recycling within amyloid fibrils. *Nature* **2005**, *436*, (7050), 554-8.

134. Kheterpal, I.; Lashuel, H. A.; Hartley, D. M.; Walz, T.; Lansbury, P. T., Jr.; Wetzel, R., Abeta protofibrils possess a stable core structure resistant to hydrogen exchange. *Biochemistry* **2003**, 42, (48), 14092-8.
135. Pepys, M. B.; Herbert, J.; Hutchinson, W. L.; Tennent, G. A.; Lachmann, H. J.; Gallimore, J. R.; Lovat, L. B.; Bartfai, T.; Alanine, A.; Hertel, C.; Hoffmann, T.; Jakob-Roetne, R.; Norcross, R. D.; Kemp, J. A.; Yamamura, K.; Suzuki, M.; Taylor, G. W.; Murray, S.; Thompson, D.; Purvis, A.; Kolstoe, S.; Wood, S. P.; Hawkins, P. N., Targeted pharmacological depletion of serum amyloid P component for treatment of human amyloidosis. *Nature* **2002**, 417, (6886), 254-9.
136. Janus, C.; Chishti, M. A.; Westaway, D., Transgenic mouse models of Alzheimer's disease. *Biochim Biophys Acta* **2000**, 1502, (1), 63-75.
137. Morgan, D.; Diamond, D. M.; Gottschall, P. E.; Ugen, K. E.; Dickey, C.; Hardy, J.; Duff, K.; Jantzen, P.; DiCarlo, G.; Wilcock, D.; Connor, K.; Hatcher, J.; Hope, C.; Gordon, M.; Arendash, G. W., A beta peptide vaccination prevents memory loss in an animal model of Alzheimer's disease. *Nature* **2000**, 408, (6815), 982-5.
138. Taniguchi, A.; Sohma, Y.; Kimura, M.; Okada, T.; Ikeda, K.; Hayashi, Y.; Kimura, T.; Hirota, S.; Matsuzaki, K.; Kiso, Y., "Click peptide" based on the "o-acyl isopeptide method": control of A beta1-42 production from a photo-triggered A beta1-42 analogue. *J Am Chem Soc* **2006**, 128, (3), 696-7.
139. Coin, I.; Dolling, R.; Krause, E.; Bienert, M.; Beyermann, M.; Sferdean, C. D.; Carpino, L. A., Depsipeptide methodology for solid-phase peptide synthesis: circumventing side reactions and development of an automated technique via depsipeptide units. *J. Org. Chem.* **2006**, 71, 6171-6177.
140. Pagel, K.; Vagt, T.; Kokschi, B., Directing the secondary structure of polypeptides at will: from helices to amyloids and back again? *Org. Biomol. Chem.* **2005**, 3, 3843-3850.
141. Mutter, M.; Gassmann, R.; Buttkus, U.; Altmann, K.-H., Switch-peptides: pH-induced  $\alpha$ -helix to  $\beta$ -sheet transitions of bis-amphiphilic oligopeptides. *Angew. Chem. Int. Ed.* **1991**, 30, 1514-1516.
142. Mutter, M.; Hersperger, R., Peptides as conformational switch : medium-induced conformational transitions of designed peptides. *Angew. Chem. Int. Ed.* **1990**, 29, 185-187.
143. Mimna, R. Switch-Peptides: In Situ Nucleation of Conformational Transitions Relevant to Protein Misfolding Diseases. EPFL, CH-Lausanne, 2005.
144. Mimna, R.; Tuchscherer, G.; Mutter, M., Toward the Design of the Highly Efficient, Readily Accessible Peptide N-caps for the Induction of Helical Conformations. *International Journal of Peptide Research and Therapeutics* **2007**, 13, 237-244.



145. Tjernberg, L. O.; Tjernberg, A.; Bark, N.; Shi, Y.; Ruzsicska, B. P.; Bu, Z.; Thyberg, J.; Callaway, D. J., Assembling amyloid fibrils from designed structures containing a significant amyloid beta-peptide fragment. *Biochem J* **2002**, 366, (Pt 1), 343-51.
146. Castano, E. M.; Prelli, F.; Wisniewski, T.; Golabek, A.; Kumar, R. A.; Soto, C.; Frangione, B., Fibrillogenesis in Alzheimer's disease of amyloid beta peptides and apolipoprotein E. *Biochem J* **1995**, 306 ( Pt 2), 599-604.
147. Shepherd, N. E.; Hoang, H. N.; Abbenante, G.; Fairlie, D. P., Single turn peptide alpha helices with exceptional stability in water. *J Am Chem Soc* **2005**, 127, (9), 2974-83.
148. Felix, A. M.; Heimer, E. P.; Wang, C. T.; Lambros, T. J.; Fournier, A.; Mowles, T. F.; Maines, S.; Campbell, R. M.; Wegrzynski, B. B.; Toome, V.; et al., Synthesis, biological activity and conformational analysis of cyclic GRF analogs. *Int J Pept Protein Res* **1988**, 32, (6), 441-54.
149. Chan, W. C.; White, P. D., *Fmoc Solid Phase Peptide Synthesis-A practical Approach*. Oxford University Press: New York, 2000.
150. Filip, S. V.; Cavelier, F., A contribution to the nomenclature of depsipeptides. *J. Pept. Sci* **2004**, 10, 115-118.
151. Plakoutsi, G.; Bemporad, F.; Calamai, M.; Taddei, N.; Dobson, C. M.; Chiti, F., Evidence for a mechanism of amyloid formation involving molecular reorganisation within native-like precursor aggregates. *J Mol Biol* **2005**, 351, (4), 910-22.



**Marie-Stéphanie CAMUS**

Chemin des Fleurettes 20

1007 Lausanne

+41 76 547 31 25

[marie.camus@gmail.com](mailto:marie.camus@gmail.com)

Date of Birth: 25.08.1980

Nationality: French

**Education**

---

- 2004- present      **PhD thesis in Bioorganic Chemistry** in collaboration with life sciences; Laboratory of Biomimetic and Peptide Chemistry, Ecole Polytechnique Fédérale de Lausanne (EPFL) – Lausanne, Switzerland
- 2000-2003      **Master of Science in Chemistry and Chemical Engineering**  
Royal Institute of Technology (KTH) – Stockholm, Sweden
- 1998-2000      Diplôme Universitaire de Technologie (DUT)  
Chemical Institute of Technology at Université Claude Bernard-Lyon, France

**Languages**

---

French: mother tongue;  
English: fluent;  
Swedish: fluent;  
German: good;  
Swiss German: good understanding.

**Professional Experience**

---

- 2004- present      **Research Assistant** in Peptide Chemistry, EPFL, Lausanne, Switzerland  
Design and investigation of amyloid  $\beta$  derived switch peptides, known to play a key role in Alzheimer's disease. Switch peptides have been designed as a general tool to study the onset and inhibition in polypeptide folding, self-assembly and aggregation.
- 2003 (6 months)      **Research Assistant** in Organic Chemistry at Helsinki University of Technology (HUT) – Finland  
Synthesis of 4-substituted prolines and their incorporation into peptide sequences. Study of their impact on peptide conformation.

Two internships in industry (SICPA and FILAB) during my studies and summer work in a hospital as an assistant in a physical therapy facility (3\* 8 weeks).

**Others Skills and Competences**

---

**Management**

- Member of the organizing committee of Forum EPFL 2007, Public Relations representative and organized the conference held during the manifestation.
- Teaching Assistant for EPFL students and training of a student during his semester project in a chemistry laboratory.
- Attended modules on Management of Biotech, Medtech and Pharma ventures (MoT, EPFL).

**Computer** Office, Illustrator, Photoshop, ChemDraw, SciFinder, Origin.

## Hobbies

---

Outdoor activities (hiking, cycling, ski), swimming, travels, cooking, photography.

## Publications, Posters and Oral Communications

---

“Disruption of amyloid-derived peptide assemblies through the controlled induction of a  $\beta$ -sheet to  $\alpha$ -helix transformation: application of the switch concept”, M.-S. Camus, R. Mimna, A. Schmid, G. Tuchscherer, H.A. Lashuel, M. Mutter, *Angew. Chem. Int Ed*, **2007**, 6(15): 2681-4.

“Switch-peptides as folding precursors in self-assembling peptides and amyloid fibrillogenesis”, G. Tuchscherer, A. Chandravarkar, M.-S. Camus, J. Bérard, K. Murat, A. Schmid, H. A. Lashuel, M. Mutter, *Biopolymers (Peptide Science)*, **2007**;88(2):239-52.

“Switch-peptides: From conformational studies to Alzheimer’s disease”, L. Saucède, S. Dos Santos, A. Chandravarkar, B. Mandal, R. Mimna, K. Murat, M.-S. Camus, J. Bérard, E. Grouzmann, M. Adrian, J. Dubochet, J. Lopez, H. A. Lashuel, G. Tuchscherer, M. Mutter, *Chimia*, **2006**, 60, 199-202.

“Switch on Amyloid  $\beta$  peptide self-assembly by acyl migrations”, S. Dos Santos, A. Chandravarkar, B. Mandal, R. Mimna, K. Murat, M.-S. Camus, G. Tuchscherer, M. Mutter, *Biopolymers (Peptide Science)*, **2005**, 80, 4, 568 and Proceedings of the 19<sup>th</sup> American Peptide Symposium, San Diego, June 18-23, **2005**.

“Host-Guest switch-peptides derived from A $\beta$  as a model for studying fibrillogenesis and for screening amyloid  $\beta$  inhibitors in vitro”, M.-S. Camus, A. Schmid, S. Dos Santos, A. Chandravarkar, B. Mandal, G. Tuchscherer, H. A. Lashuel, M. Mutter, *in preparation*.

“Studying the folding mechanism of the full length amyloid  $\beta$  peptide using switch-peptides”, M.-S. Camus, A. Schmid, S. Dos Santos, A. Chandravarkar, G. Tuchscherer, H. A. Lashuel, M. Mutter, *in preparation*.

“Disruption of amyloid-derived peptide assemblies through the controlled induction of a  $\beta$ -sheet to  $\alpha$ -helix transformation: application of the switch concept”, M.-S. Camus, R. Mimna, A. Schmid, G. Tuchscherer, H.A. Lashuel, M. Mutter. Poster, 7<sup>th</sup> German Peptide Symposium, **2007**, Heidelberg, Germany.

“Switch-Peptides: Folding Precursors in Self-Assembling Peptides and Amyloid Fibrillogenesis and In Situ Induction of Conformational Transitions”, M.-S. Camus, R. Mimna, A. Chandravarkar, A. Schmid, G. Tuchscherer, H.A. Lashuel, M. Mutter. Oral communication, *Swiss Chemical Society fall meeting*, **2007**, Lausanne, Switzerland and 20<sup>th</sup> American Peptide Symposium, **2007**, Montreal, Canada.